School of Pharmacy

Targeted topical delivery of peptides and small molecules to the skin

Mohammed Yousuf Hussain

This thesis is presented for the Degree of
Doctor of Philosophy
of
Curtin University

July 2012

Declaration

To the best of my knowledge and belief this thesis contains no material previously published by any other person except where due acknowledgment has been made.

This thesis contains no material which has been accepted for the award of any other degree or diploma in any university.

Signature: …….

Date: ……

Dedicated to

Her dream

In loving memories of my Late aunt Razia Sarfaraz Hussain

To

My parents

My Family

Acknowledgements

Acknowledgements are due to all the people who have helped, encouraged and supported me throughout my PhD.

Firstly, I would like to offer my sincerest gratefulness to my supervisor, Dr Heather Benson, who has supported me throughout my project and thesis with her patience and knowledge. I would like to thank her for having undeterred faith in my ability. I would also like to thank her for many insightful conversations during the conception and development of this thesis, and for helpful comments on the text. She provided me constant encouragement and support in various ways. Without her encouragement, effort and belief in me, this thesis could not have been compiled. I undoubtedly consider myself very lucky, to have worked under her able guidance.

I am hugely indebted to Dr Tarl Prow for his support, patience and knowledge. I only wish I could have learnt more from him.

I earnestly thank Dr Yan Chen for her understanding, insight and valuable advice.

To the School of Pharmacy, Curtin University for providing me the support and equipment I have needed to produce and complete my thesis. I would also like to thank the School of Pharmacy and the head of the School Prof. Jeffery Hughes for organising and supporting my stay at University of Queensland for the later part of my project.

To the School of Medicine and therein Therapeutics Research Centre and Dermatology Research Centre at the P A Hospital, University of Queensland.

I am gratefully thankful to Mr Mike Boddy, for his assistance in the laboratory for the entire duration of my work at Curtin. I would also like to acknowledge Mr Mike Stack, our laboratory manager.

I am gratified to acknowledge Prof. Michael Roberts and Dr Jeffery Grice for their valuable inputs throughout my time at the University of Queensland.

I am also grateful to Miss Jenny Lisette Ordóñez, for her assistance in the laboratory for the entire duration of my work at University of Queensland.

My heartfelt thanks are due to Mr Richard Parsons for his patience and assistance with statistical analysis of my results.

I am particularly obliged to thank Prof. Ernest Giralt and Dr Meritxell Teixidó of the University of Barcelona for providing me with the Cell Penetrating peptides and for answering all the questions I put forth regarding the project.

My sincerest thanks to OBJ Ltd for providing with the transdermal delivery magnets used in this research project.

I am grateful to the Australian Government and Curtin University for providing the financial support during my PhD through APA and CRS scholarships.

I convey special thanks to Ms. Kathleen Whiteman, Ms. Jennifer Ramsay and Ms. Charmaine D'Costa for their crucial help with ordering of chemicals and consumables so that I could carry out my research without the need to worry about anything.

I would like to specially thank Sarika for her constant support, motivation and patience throughout the duration of my studies.

To Rafi, Gayathri, David, Li Lin and Klinteen for always being there for me. Your friendship and patience has gone a long way to ensure me during times of fun and need.

I would also like to thank Alexander Ansaldo and Anthony Raphael for their help with image analysis and research.

Most importantly, I would like to thank my parents and my siblings for their inseparable support. They have motivated me throughout my life to strive for better. My mother has always been the hidden strength without which, no accomplishment would be fulfilling. My father has always managed to convey the most in saying the least.

Finally, I would like to thank everybody who was important to the successful realization of this thesis, as well as expressing my apology that I could not mention personally one by one.

TABLE OF CONTENTS

TABLE OF CONTENTS I

List of Figures IX

List of Tables XIV

List of Abbreviations……XV

Abstract XVIII

Chapter 1

Introduction 1

1.1 Structure of human skin 3

1.1.1 Stratum corneum 4

1.1.2 Stratum Granulosum 5

1.1.3 Stratum spinosum 6

1.1.4 Stratum basale 7

1.2 Fick's law and delivery routes of peptides through skin 7

1.3 Strategies to enhance transdermal delivery of peptides 9

1.3.1 Formulation optimisation/permeant modification approaches 9

1.3.1.1 Pro-drugs 9

1.3.1.2 Encapsulation 10

1.3.1.3 Nanoparticles 11

1.3.1.4 Chemical conjugation 12

1.3.1.5 Cell-penetrating peptides 14

1.3.2 Chemical penetration enhancers 22

1.3.3 Active penetration enhancement techniques 23

1.3.3.1 Iontophoresis 23

1.3.3.2 Electroporation 26
1.3.3.3 Magnetophoresis 28
1.3.3.4 Ultrasound 31
1.3.3.5 Jet applicators 33
1.3.3.6 Photomechanical waves 34
1.3.3.7 Microneedles 35
1.3.4 Stratum corneum ablation 40
1.3.4.1 Radio frequency ablation (RF) 40
1.3.4.2 Laser ablation 41
1.3.4.3 Suction blister ablation 42
1.3.4.4 Thermal poration 42
1.3.5 Peptides as potential therapeutic and cosmetic agents 43
1.3.5.1 Bioactive peptides as cosmeceuticals 43
1.3.5.2 Bioactive peptides as dermatologicals (in skin diseases) 45
1.4 Significance 48
1.5 Objectives 49
Chapter 2
Permeation of Cell Penetrating Peptides and their Influence on the Permeation of Diclofenac and a Dipeptide through Human Skin 50
2.1 Introduction 51
2.2 Aims of the project 52
2.3 Materials and Methods 52
2.3.1 Chemicals 52
2.3.2 Synthesis of DKP and DKP-diclofenac 53
2.3.3 Synthesis of TAT and TAT-diclofenac 55
2.3.4 HPLC instrumentation and conditions 56

2.3.4.1 DKP *56*
2.3.4.2 DKP-diclofenac *56*
2.3.4.3 Ala-Trp *56*
2.3.4.4 Diclofenac *57*
2.3.4.5 TAT *57*
2.3.4.6 TAT-diclofenac *57*
2.3.5 HPLC analysis and validation **57**
2.3.5.1 Linearity *57*
2.3.5.2 Precision *58*
2.3.5.3 Intra-day repeatability *58*
2.3.5.4 Inter-day repeatability *58*
2.3.5.5 Lower limit of detection (LOD) *58*
2.3.5.6 Lower limit of quantification (LOQ) *58*
2.3.6 Human skin preparation **59**
2.3.7 Skin permeation experiments to determine effect of cell penetrating peptides **59**
2.3.7.1 Skin hydration *59*
2.3.7.2 In-vitro skin diffusion studies *59*
2.3.8 Mass balance and recovery **61**
2.3.9 Cyclooxygenase (COX) inhibition assays **61**
2.3.9.1 Dilution of assay buffer *62*
2.3.9.2 Heme *62*
2.3.9.3 COX-2 (human recombinant) *62*
2.3.9.4 Arachidonic acid *62*
2.3.9.5 Preparation of the fluorimeteric substrate, ADHP (10-acetyl-3,7 dihydroxyphenoxazine) *63*
2.3.9.6 Preparation of standard concentration of the Inhibitors *63*
2.3.9.7 Reaction mixture *63*
2.3.10 Statistical analysis **64**
2.4 Results and discussion **64**
2.4.1 Chromatography **64**

2.4.1.1 DKP 64
2.4.1.2 Ala-Trp 65
2.4.1.3 Diclofenac 66
2.4.1.4 DKP and Ala-Trp physical mixture 67
2.4.1.5 DKP- diclofenac physical admixture 68
2.4.1.6 TAT and TAT-diclofenac conjugate 69
2.4.1.7 DKP-diclofenac conjugate 71
2.4.2 Human epidermal penetration and accumulation: preliminary experiments 74
2.4.2.1 Choice of donor vehicle 74
2.4.2.2 Determination of donor concentration 74
2.4.2.3 Pre-hydration of epidermal membrane 75
2.4.2.4 Stability of DKP/study duration of permeability experiments 75
2.4.2.5 Final experimental protocol 77
2.4.3 Permeation of cell penetrating peptides, admixtures of cell penetrating peptide and active, and conjugated cell penetrating peptide-actives across human epidermis *in vitro* 77
2.4.3.1 Influence of DKP on skin permeation of diclofenac and Ala-Trp 78
2.4.3.1.1 DKP 78
2.4.3.1.2 Ala-Trp 80
2.4.3.1.3 DKP-Ala-Trp (physical admixture) 81
2.4.3.1.4 Diclofenac 82
2.4.3.1.5 DKP-diclofenac (physical admixture) 84
2.4.3.1.6 DKP-diclofenac conjugate 85
2.4.3.2 Skin permeation of TAT and TAT-diclofenac conjugate 87
2.4.4 Recovery from and retention of cell penetrating peptide and cell penetrating peptide conjugates in the skin 89
2.4.5 Inhibition of Cyclooxygenase (COX) by diclofenac and DKP-diclofenac conjugate 92
2.5 Conclusions 93

Chapter 3

Microneedle Based Skin Penetration Studies on Fluorescent Peptides.....94

3.1 Introduction..... 95

3.2 Aims 95

3.3 Materials and methods..... 96

3.3.1 Peptides and other chemicals 96

3.3.2 Instrumentation and techniques 96

3.3.2.1 Reflectance confocal microscopy and florescence imaging..... 96

3.3.2.2 Microneedles and Microneedle applicator..... 97

3.3.2.3 Transepidermal water loss (TEWL) 98

3.3.3 Skin preparation for permeation studies 99

3.3.4 Study design..... 99

3.3.4.1 Studies on sodium fluorescein..... 99

3.3.4.2 Studies on fluorescent peptides 101

3.3.4.3 Standard curves for sodium fluorescein and fluorescent peptides….. 102

3.3.5 Imaging and analysis of images 102

3.3.6 Statistical analysis 105

3.4 Results and Discussion 106

3.4.1 Preliminary studies 106

3.4.1.1 Preliminary studies on Sodium fluorescein 106

3.4.1.1.1 Effect of concentration of Sodium fluorescein (NaFsc) on its lateral diffusion….....106

3.4.1.1.2 Effect of time.....107

3.4.1.1.3 RCM settings- Auto power control.....108

3.4.1.1.4 Effect of microneedle size/ design and impact velocity of the applicator…….108

3.4.1.2 Preliminary studies on fluorescent peptides 110
3.4.1.2.1 Effect of concentration 110
3.4.1.2.2 Effect of time 111
3.4.1.2.3 Effect of vehicle for peptide dissolution 111
3.4.2 Imaging protocol for MN based delivery studies 112
3.4.3 MN based delivery studies on Sodium Fluorescein (NaFsc) 114
3.4.4 Standard curves and fluorescence quantification of NaFsc and fluorescent peptides 122
3.4.5 MN based delivery studies on fluorescent peptides 124
3.4.5.1 Melanostatin 124
3.4.5.2 Rigin 128
3.4.5.3 Pal-KTTKS 131
3.5 Future directions 134
3.6 Conclusions 135
Chapter 4
Effect of low field strength magnets on the skin permeation of peptides and small molecules. Assessment of potential synergistic enhancement with microneedle pretreatment. 136
4.1 Introduction 137
4.2 Aims 138
4.3 Materials and Methods 138
4.3.1 Chemicals 138
4.3.2 Instrumentation 139
4.3.2.1 Magnetic film arrays (ETP) 139
4.3.2.2 Microneedles and Microneedle applicator 139
4.3.2.3 Reflectance confocal microscopy and imaging parameters 140

4.3.2.4 UV spectrophotometry 140

4.3.2.5 HPLC instrumentation and conditions 140

4.3.2.6 HPLC analysis and validation 141

4.3.2.6.1 Linearity 141

4.3.2.6.2 Precision, Intra and Inter-day repeatability 141

4.3.2.6.3 Lower limit of detection (LOD) 141

4.3.2.6.4 Lower limit of quantification (LOQ) 141

4.3.2.7 Multi photon tomography 141

4.3.3 Study design 142

4.3.3.1 Studies on permeation of brilliant blue dye in Agar gel syringes…. 143

4.3.3.2 Studies on permeation of diclofenac gel through human skin 144

4.3.3.2.1 Preparation of diclofenac gel 144

4.3.3.2.2 Human skin preparation 144

4.3.3.2.3 Skin permeation of diclofenac sodium across human skin 145

4.3.3.2.4 Data Analysis 146

4.3.3.3 Studies on permeation of Curcumin through human volunteer skin……..... 146

4.3.3.4 Studies on florscent tagged Melanostatin 149

4.3.4 Statistical analysis 150

4.4 Results and Discussion 151

4.4.1 Studies on agar gel 151

4.4.2 *In vitro* studies on excised human skin/ Magnetophoretic delivery of diclofenac sodium in carbopol gel formulation. 152

4.4.2.1 Chromatography 152

4.4.2.2 Permeation of diclofenac sodium through human epidermis with ETP and Dermaportation. 153

4.4.3 *In vivo* studies on a model fluorescent compound (Curcumin) 156

4.4.4 Ex-vivo studies on a fluorescent peptide (Melanostatin) 161

4.5 Conclusions and future directions 164

Chapter 5

Summary and future directions 166

Chapter 6

References.....172

List of Figures

Figure 1.1 Typical structure of mammalian skin[14] 3

Figure 1.3 Multiphoton microscope image of stratum granulosum in human volunteer skin 6

Figure 1.4 Multiphoton microscope image of stratum spinosum in human volunteer skin 6

Figure 1.5 Multiphoton microscope image of stratum basale in human volunteer skin 7

Figure 1.6 Drug penetration across the stratum corneum[28] 8

Figure 1.7 Typical permeation profile for an infinite dose application to human skin membranes[29] 8

Figure 1.8 Chemical structure of human calcitonin 13

Figure 1.9 Illustration of the possible interactions of the peptides with the phospholipid membranes, and different mechanisms for translocation of CPPs.[68] 16

Figure 1.10 Schematic of an iontophoretic device[121] 24

Figure 1.11 Schematic representation of PEMF Dermaportation waveform..... 30

Figure 1.12 SonoPrep skin permeation device: rapid local anaesthesia by ultrasound enhanced delivery of lidocaine (Sontra Medical Corp, Franklin, MA)..... 32

Figure 1.13 PowderMed jet propulsion delivery system 33

Figure 1.14 Types of microneedles A) and D) Hollow; B) solid and C) coated microneedles[186-188] 35

Figure 1.15 Viaderm radiofrequency thermal ablation (TransPharma Medical Ltd) 41

Figure 2.1 Synthesis of DKP library (scheme 1)..... 53

Figure 2.2 Chemical structure of DKP-2Nal-N-MePhe 54

Figure 2.3 Synthesis of DKP-diclofenac (scheme 2) 55

Figure 2.4 Chemical structure of DKP-diclofenac 55

Figure 2.6 Chromatogram of 100 µg/mL standard of DKP 65

Figure 2.8 Chromatogram of 15.7 µg/mL standard of diclofenac 67

Figure 2.10 Chromatogram of 125 µg/mL standard of DKP-diclofenac (physical admixture) ... 69

Figure 2.12 Chromatogram of 250 µg/mL standard of TAT-diclofenac conjugate 70

Figure 2.14 Permeation profile of cumulative amount vs. time of DKP-diclofenac conjugate (300µL donor volume i.e. 1.5 mg and 150 µg) across human epidermis. Results are expressed as mean (±SEM), n=5..... 75

Figure 2.16 Passive permeation of DKP over 24 h, Amount in donor - 150 µg, Results are expressed as mean (±SEM: n=7). 78

Figure 2.17 Passive permeation of Ala-Trp over 24 h, Amount in donor - 150 µg. Results are expressed as mean (±SEM: n=4). 80

Figure 2.19 Passive permeation of diclofenac over 24 h, Amount in donor - 150 µg, Results are expressed as mean (±SEM: n=5). 83

Figure 2.20 Passive permeation of DKP-diclofenac (physical admixture) over 24 h, Amount in donor - 150 µg, Results are expressed as mean (±SEM: n=5). 84

Figure 2.21 Passive permeation of DKP-diclofenac conjugate over 24 h, Amount in donor - 150 µg, Results are expressed as mean (±SEM: n=4). 86

Figure 2.22 Passive permeation of TAT over 24 h, Amount in donor - 150 µg, Results are expressed as mean (±SEM: n=6). 88

Figure 2.23 Passive permeation of TAT-diclofenac conjugate over 24 h, Amount in donor - 150 µg, Results are expressed as mean (±SEM: n=6). 88

Figure 2.24 Amount of DKP in the skin after the permeation experiments (Donor amount of 150 µg, 300 µg and 1500 µg). Results are expressed as mean (±SEM: n=4) 90

Figure 2.26 Percent inhibition of COX-2 by diclofenac and DKP-diclofenac conjugate (n=1) ... 92

Figure 3.1 VivaScope 2500 96

Figure 3.2 Motorised sample placement stage - VivaScope 2500..... 97

Figure 3.3 MN plate with three 700 µm length × 250 µm width MN..... 98

Figure 3.4 Skin setup for MN application..... 98

Figure 3.5 AquaFlux AF200 TEWL meter. 99

Figure 3.6 Sodium fluorescein imaged 5 min after treatment application. 100

Figure 3.7 Samples prepared for standard curve. 102

Figure 3.8 a) Image with line plot, b) Plot of the intensities measured..... 103

Figure 3.9 a) High intensity area, b) Outline of the area of high intensity. 104

Figure 3.10 a) Circular area around the microneedle hole, b) Integrated intensity vs. radius plot..... 104

Figure 3. 11 a) NaFsc diffusion (passive) in viable epidermis, b) NaFsc diffusion (active-MN) in viable epidermis. 107

Figure 3.12 NaFsc at 4 h after MN application. 108

Figure 3.13 a) Stainless steel MN plate with a row of 5 MN, b) Stainless steel MN plate with a row of 3 1mm MN, c) Cured epoxy adhesive MN plate with a row of 3 MN, d)) Stainless steel MN plate with a row of 3 MN..... 110

Figure 3.14 Images from the viable epidermis taken during a pilot study a) Water as solvent b) DMSO as solvent..... 112

Figure3.15 a) 'Z' stack image of MN hole in reflectance mode and b) 'Z' stack image in fluorescence mode..... 113

Figure 3.16 Penetration of NaFsc in stratum corneum, viable epidermis and dermis from 5-120 min after microneedle mediated skin delivery (Donor 1)..... 115

Figure 3.17 Penetration of NaFsc in stratum corneum, viable epidermis and dermis from 5-120 min after microneedle mediated skin delivery (Donor 2)..... 116

Figure 3.18 Penetration of NaFsc in stratum corneum, viable epidermis and dermis from 5-120 min after microneedle mediated skin delivery (Donor 3)..... 116

Figure 3.19 Image from the 40 min time point a) selected intensity threshold range of 54-255 AU b) selected intensity threshold range of 14-255 AU. 117

Figure 3.20 Average area of NaFsc penetration in skin strata (n=3, results expressed as mean ± SD)..... 118

Figure 3.21 3D view of the area of penetration-5 min 119

Figure 3.22 Fluorescence plane divided in 4 Zones 120

Figure 3.23 Average integrated density in all layers of the skin a) Stratum corneum (SC) b) Viable epidermis (VE) c) Dermis (DER) and d) Total ID (n= 4, results are expressed as mean ± SD)..... 121

Figure 3.24 Average intensity in the three layers of the skin across the four compartments (n=3, results are expressed as mean ± SEM)..... 122

Figure 3.25 Standard curves of NaFsc at different power levels 123

Figure 3.26 Mosaic images of the 8 study groups..... 125

Figure 3.27 Melanostatin penetration at 1 and 24 h (n=3, results expressed as ± SEM) 126

Figure 3.28 1 h and 24 h penetration of melanostatin after MN based delivery in three different skin donors..... 127

Figure 3.29 Images of rigin with and without MN at 1 h 129

Figure 3.30 Images from rigin treated skin after MN application..... 129

Figure 3.31 Penetration of rigin through human skin (n=3, results are expressed as ± SEM) .. 130

Figure 3.32 Pal-KTTKS penetration after MN application in excised human skin over 24 h (n=3, results expressed as mean ± SEM) 132

Figure 3.33 Images from Pal-KTTKS treated skin after MN application (n=3, results expressed as ± SEM) **133**

Figure 4.1 a) ETP 008 magnetic field and b) ETP 012 magnetic field as observed on a metal dust polymer strip **139**

Figure 4.2 A microneedle plate on finger tip **140**

Figure 4.3 Schematic showing a typical MPT set-up **142**

Figure 4.4 Overview of experimentation **143**

Figure 4.5 Study setup for Agar gel pilot studies **144**

Figure 4.6 Set-up for diclofenac gel studies **146**

Figure 4.7 a) Structure and b) fluorescence spectrum of curcumin in different solvents[386] **147**

Figure 4.8 a) Volunteer arm with ETP treatment b) Volunteer during the MPT imaging **148**

Figure 4.9 Set-up for studies on Melanostatin **150**

Figure 4.10 Permeation of Brilliant blue dye in the agar gel (n=4). Results are expressed as mean ± SEM **151**

Figure 4.11 HPLC chromatogram of diclofenac sodium at 31.25 µg/mL **153**

Figure 4.12 Skin permeation of diclofenac sodium. Results are expressed as mean ±SEM (n=8) **155**

Figure 4.13 ETP 008 induced skin penetration enhancement of curcumin **157**

Figure 4.14 ETP 012 induced skin penetration enhancement of curcumin **157**

Figure 4.15 TEWL readings before and after the treatment **159**

Figure 4.16 Average TEWL across subjects (n=6). Results are expressed as mean ± SD **159**

Figure 4.17 Pseudo coloured images from channel 1 and channel 3 –Negative control (MO) and positive control (TS + CUR) **160**

Figure 4.18 Pseudo coloured images from channel 1 and channel 3 – Passive (CUR) and active treatments (ETP 008, ETP 012) **160**

Figure 4.19 Net fluorescence intensity (δ) of curcumin following treatment with ETP 008, ETP 012 and tape stripping **161**

Figure 4.20 Average penetration area and average integrated density of melanostatin after 1 h post treatment with MN and ETP magnets **162**

Figure 4.21 Width and fluorescence intensity signal analysis within skin furrows (mean ± SD, n=3) **164**

Figure 5.1 Skin penetration enhancement strategies used in this project **166**

Figure 5.2 Comparison of penetration area of peptides after microneedle (MN) based application. Mean ±SEM (n=3) 169

Figure 5.3 3M - Microchannel Skin System..... 169

List of Tables

Table 2.1 HPLC summary data for analysis of cell penetrating peptides, actives, physical admixtures and conjugates 72

Table 2. 2 Overview of the research plan 77

Table 2.3 Summary of DKP and active drugs permeation 87

Table 2.4 Summary of TAT and active compounds permeation 89

Table 4.1 Skin permeation results for diclofenac sodium post magnetophoretic treatment (n=8) 154

Table 4.2 Penetration area and fluorescence integrated density of melanostatin after MN and ETP treatment 162

List of abbreviations

CPP	Cell penetrating peptide	**AMPs**	Antimicrobial peptides
DKP	Diketopiperazine	**AD**	Atopic dermatitis
TAT	HIV-1Trans-Activator of Transcription	**Pal-KVK**	Palmitoyl tripeptide
COX	cyclooxygenase	**ADHP**	10-acetyl-3,7-dihydroxyphenoxazine
MN	Microneedles	**HPLC**	High performance liquid chromatography
CLSM	Confocal laser scanning microscopy	**LOD**	Limit of detection
ETP	Enhanced transdermal polymer	**LOQ**	Limit of quantification
SC	Stratum corneum	**PG**	Propylene glycol
SG	Stratum granulosum	**rhVEGF**	Recombinant human vascular endothelial growth factor
SS	Stratum spinosum	**MEL**	Melanostatin
TEWL	Trans epidermal water loss	**FITC**	Fluorescein isothiocyanate
DMA	Dimethylacitamide	**NaFsc**	Sodium Fluorescein
NP	Nanoparticles	**ID**	Integrated density
PEG	Polyethylene glycol	**DMSO**	Dimethylsulfoxide
LHRH	Luteinizing hormone	**VE**	Viable epidermis

	rereleasing hormone		
TRH	Thyrotropin releasing hormone	**DER**	Dermis
CTL	Cytotoxic T lymphocytes	**DHEA**	Dehydroepiandrosterone
BBB	Blood brain barrier	**PBS**	Phosphate buffered saline
PAMPA	Parallel Artificial Membrane Permeability Assay	**PIH**	Post inflammatory hyperpigmentation
SOD	Superoxide dismutase	**DP**	Dermaportation
CAT	Superoxide catalase	**TS**	Tape stripping
MPM	Multi photon microscopy	**5-ALA**	5-aminolevulinic acid
MPT	Multi photon tomography	**dNPs**	Dissolving nanopatches
AVP	Arginine vasopressin	**HIF**	High intensity fluorescence
TEM	Transmission electron microscopy	**FLIM**	Fluorescence-lifetime imaging microscopy
MT-DDS	Magnetically targeted-drug delivery system	**RCM**	Reflectance confocal microscopy
PEMF	Pulsed electromagnetic fields	**EGF**	Epidermal growth factor
ATR-FTIR	Attenuated total reflectance Fourier transform infra-red spectrometry	**OCT**	Optical coherence tomography
LIF	Low intensity	**hGH**	Human growth hormone

	fluorescence		
ECM	Extracellular matrix	**Pal-KTTKS**	Palmitoyl pentapeptide
P.L.E.A.S.E	Painless Laser Epidermal System		
GI tract	Gastro intestinal tract	**TGF-α**	Transforming growth factor-α

Abstract

Developing new treatment options, particularly for chronic skin diseases that are often poorly controlled by available therapeutics, is a priority in dermatological research.[1,2] Peptides possess enormous potential for the treatment of varied diseases and in improving skin aesthetics. The increasing number of new molecules of biotechnological origin such as monoclonal antibodies, hormones and vaccines make peptide and protein delivery an important area of research.[3] The current PhD project explores the enhanced transdermal delivery of peptides and other small model molecules through the use of three techniques.

Firstly, permeation enhancement of a dipeptide and the anti-inflammatory drug, diclofenac with the use of novel cell penetrating peptides (CPPs)–diketopiperazines (DKP) is explored. CPPs are peptides with a maximum of 30 amino acids, which are able to enter cells in a seemingly energy-independent manner.[4] To be effective drug delivery tools, CPPs need to be very specific in targeting their desired location. Two strategies involving CPPs have been described to date; the first one requires chemical linkage between the drug and the carrier for cellular drug internalization, and the second is based on the formation of stable complexes with drugs, depending on their chemical nature.

Physical admixture of DKP with the dipeptide Ala-Trp and with diclofenac increased the epidermal permeation of Ala-Trp by 9 fold and diclofenac by 2 fold. Conjugation of DKP with diclofenac enhanced the transdermal flux by 9 fold. DKP was found to be a more effective permeation enhancer than the well-established CPP, HIV-1-Trans-Activator of Transcription (TAT), which when conjugated to diclofenac increased its permeation by only 1.9-fold. Further, the amount of DKP-diclofenac conjugate present in the skin was at least 6-fold greater than TAT-diclofenac conjugate and at least 14 times greater than diclofenac alone.

Enzyme assay results demonstrated COX inhibition by the DKP-diclofenac conjugate, showing the anti-inflammatory activity was retained. This demonstrated the potential of the diketopiperazines as CPPs for the enhancement of skin permeation.

The second study in this project explored the enhanced delivery of three peptides by microneedle pre-treatment of the skin. Microneedles (MN) have been shown to substantially enhance skin penetration and may offer a painless and effective delivery method.[5] Confocal laser scanning microscopy (CLSM) was used to visualise and quantify the penetration of the peptides studied in this project in a rapid and efficient manner. The peptides selected for these studies were 3, 4 and 5 amino acids in length (melanostatin, rigin and palmitoyl pentapeptide). These peptides were primarily selected as cosmeceutical agents to better understand their diffusion and distribution within the different layers of the human skin, rather than their role in systemic delivery.

All peptides showed enhanced penetration with microneedle pre-treatment, although the enhancement varied considerably between the peptides. Melanostatin (Pro-Lue-Gly) showed a 10-fold enhancement in penetration area in the viable epidermis at 1 h and a 22-fold increase in area in the dermis with microneedle pre-treatment at 24 h. Melanostatin has been used in specific hyperpigmentary conditions and as a skin-lightening agent in cosmetic products.

Rigin (Gly-Gln-Pro-Arg), the tetrapeptide commonly used in cosmetic industry as palmitoyl tetrapeptide-7 showed a 1.8-fold increase in penetration area at 1 h and no difference at 24 h with microneedle pre-treatment. Similarly, palmitoyl pentapeptide (Pal-KTTKS) showed no difference in penetration area in the viable epidermis with the use of microneedles, but over 24 h the passive permeation of Pal-KTTKS was increased 2.6-fold when compared to microneedle pre-treatment. Both rigin and Pal-KTTKS are used in skin firming and anti-aging products, though studies describing their transdermal and topical penetration or intradermal accumulation have not been reported to date.

Successful application of microneedles depends on various factors and it is very important to choose the right type of microneedle for efficient delivery of medical and cosmeceutical products. The imaging technique used to evaluate the outcomes of these experiments allows for non-invasive monitoring of the skin with microscopic resolution second only to histological analysis.

A recent skin penetration enhancement technique- magnetophoresis was investigated for the transdermal penetration of small model molecules, a fluorescent natural

molecule and a fluorescent tripeptide. Magnetophoresis is the enhancement of drug permeation across biological barriers by application of a magnetic field, and is thought to act predominantly by diamagnetic forces.[6,7] Different diffusion and skin permeation models were used to assess the role of magnetophoresis as a potential transdermal delivery enhancement tool. Further, a possible synergistic interaction with application of microneedles was also investigated. In a non-membrane model study, utilizing agar gel syringes to examine the diffusion of dye molecules in the influence of diamagnetic repulsion, the diffusion of brilliant blue dye was enhanced by 33%. A study with prepared human epidermis showed a 2.4-fold increase in diclofenac permeation *in vitro* across human epidermis with magnetic film array (ETP 012) when compared to passive treatment.

A volunteer study was done in order to assess the penetration of a naturally fluorescent compound curcumin. The results showed a 200% increase in the net fluorescence intensity generated by curcumin when compared to passive (dummy non-magnetic strips of similar material). When investigated for their use in combination with microneedles, the magnetic film array (ETP 012) showed a 5-fold increase in skin diffusion of melanostatin in full thickness human skin *ex vivo* when compared to microneedles alone. The ETP 012 magnets also showed a 7-fold increase in the area of penetration when compared to dummy strips without the microneedles. Though, the total area was much smaller when compared to the area of penetration with the use of microneedles.

This work demonstrates the importance of minimally invasive (MN) and non-invasive (CPPs and ETP) transdermal delivery techniques in optimising transdermal delivery of peptides and small molecules.

Chapter 1

Introduction

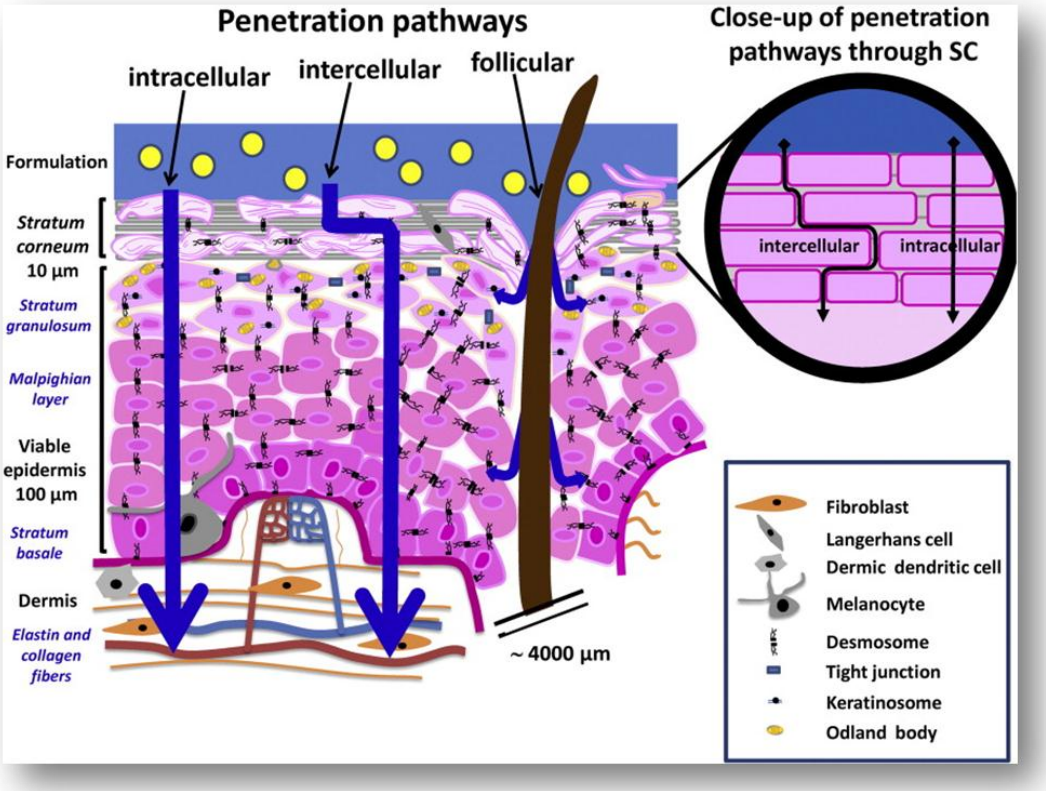

"Research on the penetration of drugs through the skin merits renewed attention as a result of concerns such as transdermal therapies, safety of cosmetic products and skin decontamination."[8]

Peptides are considered the new generation of biologically active pharmaceuticals because they are key regulators in cellular and intercellular physiological responses. These macromolecules possess enormous potential for the treatment of disease. The increasing number of new molecules of biotechnological origin such as monoclonal antibodies, hormones and vaccines make peptide and protein delivery an important area of research.[3] Research has also led to peptides being important tools for understanding protein structure and function. A large number of new and potentially potent peptide and protein drugs have been developed in the past few decades, with several finding success in prior areas of unmet need by providing therapeutics based on enzyme inhibition and activation.[9]

Developing new treatment options, particularly for chronic skin diseases that are often poorly controlled by available therapeutics, is a priority in dermatological research.[1,2] Most proteins and peptides range in molecular weight from 100 to greater than 1000,000 Da. Due to their large molecular size and primary structure proteins and peptides are vulnerable to proteolytic attack, and are subject to extensive "first pass" metabolism and thus are unsuitable for oral administration. They have short plasma half-lives and require frequent injection to maintain therapeutic levels.

Over the years, much research has been directed towards alternate administration routes, other than parenteral injections, for effective peptide and protein drug delivery, resulting in fewer side effects as well as better patient compliance.[1,10,11] Transdermal delivery is a potential delivery route. However, due to the hydrophilic nature and presence of charge at physiological pH, skin permeation of peptides is poor and despite generally having high potency, they are ineffective if administered transdermally because they do not permeate into the skin. In addition to the inherent properties of the peptides, the biggest barrier for the transdermal transport resides in the outermost layer of the skin, the stratum corneum (SC).[3,12] Despite these challenges the transdermal route is worthy of investigation due to the potential advantages to be realised if the challenges can be overcome.

1.1 Structure of human skin

The skin is the largest and the most readily accessible organ of the human body with at least five different cell types contributing to its structure, and other cell types from circulatory and immune systems being transient residents.[1] Its primary function is protection, including physical, chemical, immune, pathogen, UV radiation and free radical. For the purpose of transdermal drug delivery, human skin can be categorised into four main layers: the innermost hypodermis or subcutaneous fat layer, the overlying dermis, the viable epidermis and the outermost stratum corneum. (Figure 1.1)[13,14]

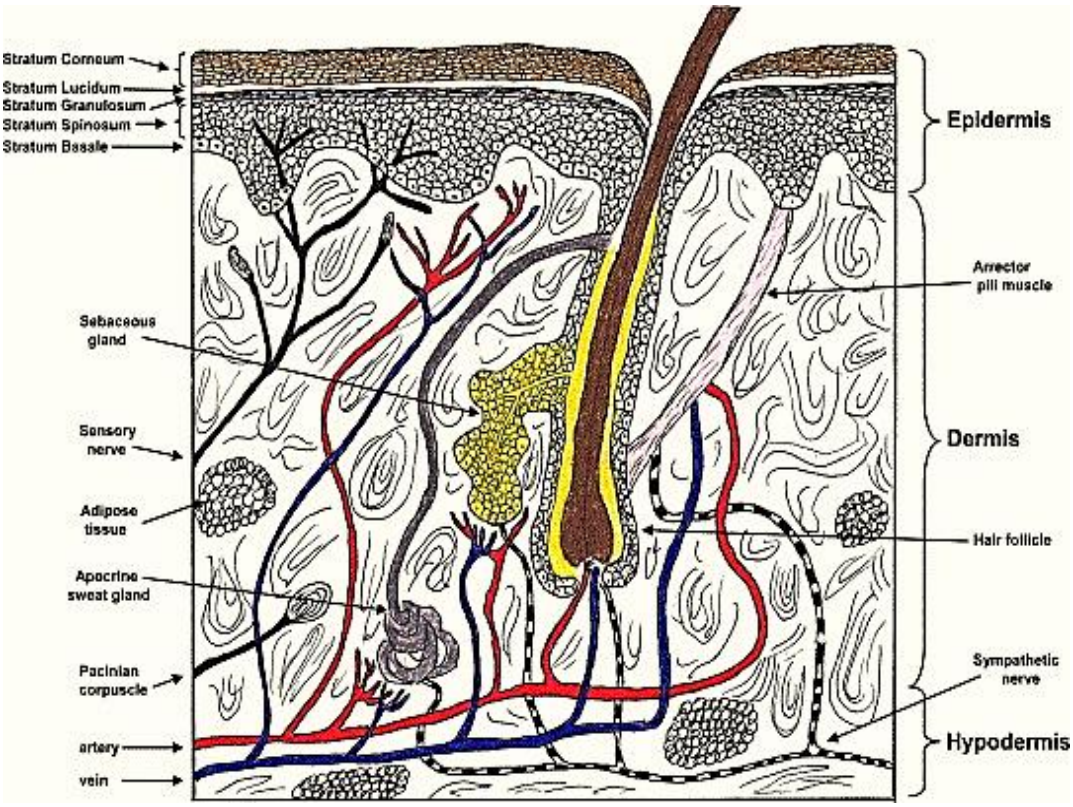

Figure 1.1 Typical structure of mammalian skin[14]

The hypodermis or subcutaneous fat layer lies between the dermis and the underlying body constituents. This layer of adipose tissue provides a store for high energy molecules and insulates the body to provide protection against mechanical shock.[13] The dermis is 3 – 5 mm thick and is composed of a network of connective tissue, predominantly collagen fibrils, which provide support and flexibility.[15] Blood and lymphatic vessels, nerve endings, pilosebaceous units (hair follicles and sebaceous glands), and sweat glands (eccrine and apocrine) are found in the dermal tissue. In terms of transdermal drug delivery, this layer is often viewed as essentially gelled

water, and thus provides a minimal barrier to the delivery of most polar drugs.[13] For transport across the skin the dermal blood supply maintains a concentration gradient between the applied formulation and the vasculature across the skin. It is this concentration gradient that provides the driving force for drug permeation.[13]

The epidermis is a complex, multilayered membrane which varies in thickness from around 0.06 mm on the eyelids to around 0.8 mm on the palms and soles of the feet. The epidermis is differentiated into 5 layers: stratum corneum, stratum granulosum, stratum spinosum, stratum lucidum and stratum basale.[13]

1.1.1 Stratum corneum

The barrier function of the epidermis resides primarily in the stratum corneum (SC), which consists of anucleate cells called corneocytes and varies in thickness from approximately 10 -15 µm in the dry state to 40 µm when hydrated.[16] The corneocytes are arranged in a "brick and mortar" like structure where the keratin rich corneocyte-bricks are embedded in an intercellular matrix-mortar, which is essentially composed of long chain ceramides, free fatty acids, cholesterol, cholesterol sulfate and sterol/wax esters.[17,18] The ceramides are covalently bound to the surface of the corneocytes.[19] These bound lipids have alkyl chain lengths of 30 – 34 carbons and contain no cholesterol.[20] The lipid chains are arranged into regions of crystalline, lamellar gel and lamellar liquid crystal phases thereby creating various domains within the lipid bilayer.[21] The crystalline nature and the presence of a 13 nm lamellar phase are considered to be crucial for the barrier function of the skin. (Figure 1.2 a and 1.2 b) Penetrating molecules have to traverse a highly convoluted tortuous lipid pathway for diffusion. Consequently, penetrant molecules must migrate over larger distances than the membrane thickness.[20] The lipid content in the stratum corneum differs between individuals and body site.[22] The stratum corneum has been recognised as the main barrier to transdermal penetration for centuries and there have been wide ranging ways to overcome it for therapeutic advantage. From ancient medical knowledge it is evident that not all medicaments are active orally, and by disrupting the top most skin layer medications could be sent inside the human body. The first documented application of epicutaneous drug delivery consisted of a vaccine, dating back more than 3000 years.[23] Indeed, the first immunization against smallpox was practiced in India by administrating dry scabs of smallpox lesions onto

the scarified skin of healthy individuals using sharp needle-like objects, a procedure called 'variolation'.[23] Conversely if the stratum corneum is disrupted or dysfunctional it leads to loss of hydration out of the skin and access of certain irritant allergens into the body.[24] Psoriasis and atopic dermatitis are common examples of dysfunctional skin conditions. Researchers have used parameters such as transepidermal water loss (TEWL), tape stripping and instruments such as photo acoustic spectrometry to establish the relationship between disrupted barrier function of the stratum corneum and increased permeation.[25]

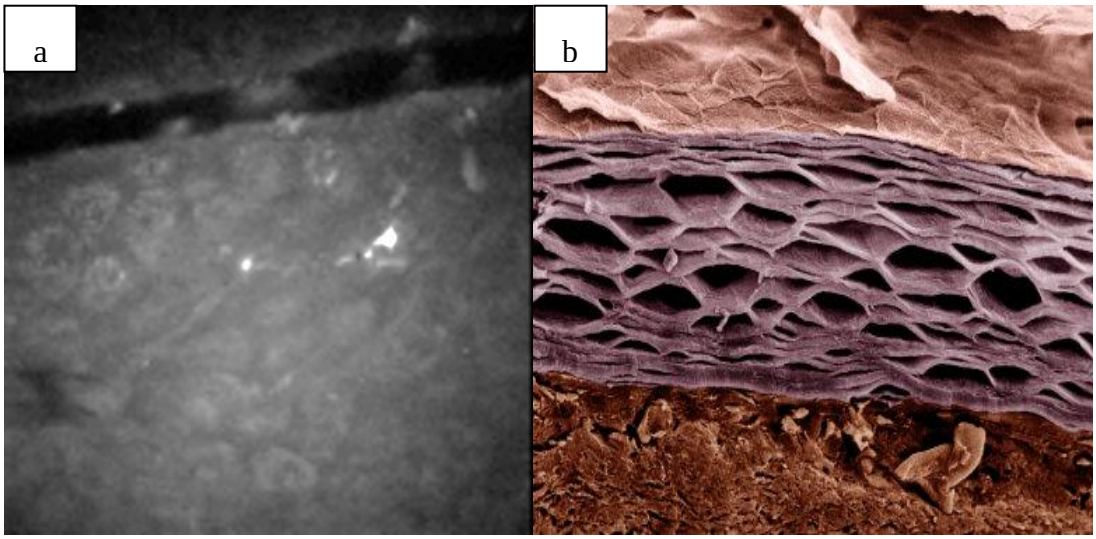

Figure 1.2 (a) Multiphoton microscope image of stratum corneum in human volunteer skin (b) Cross section image of human stratum corneum

1.1.2 Stratum Granulosum

The stratum granulosum is a thin granular layer of cells in the epidermis. These cells contain keratohyalin granules, protein structures that promote hydration and crosslinking of keratin.[2] Keratinocytes in the stratum granulosum continue to differentiate. Figure 1.3 below shows a multiphoton image of stratum granulosum captured from human volunteer skin during the project.

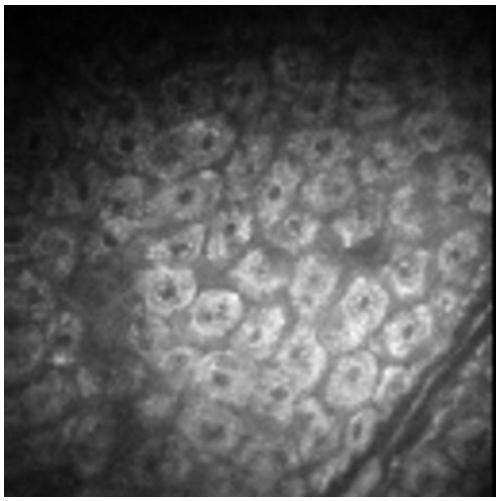

Figure 1.3 Multiphoton microscope image of stratum granulosum in human volunteer skin

1.1.3 Stratum spinosum

The stratum spinosum, also called the pickle layer, is comprised of two to six cell layers.[2] It lies just above the basal layer and together with the basal layer it is referred to as the Malpighian layer. Figure 1.4 illustrates an image of stratum spinosum captured during a volunteer study. The keratinocytes in this layer differentiate to form keratin, which aggregates to form tonofilaments. The condensation of these tonofilaments leads to the formation of desmosomes which maintain a distance of almost 20 nm between the cells and are vital to the structural integrity of the epidermis.[13]

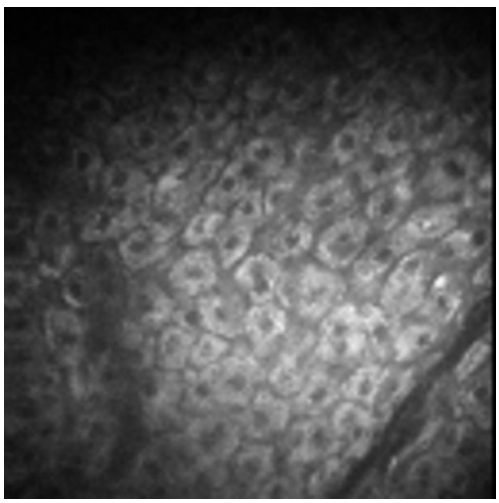

Figure 1.4 Multiphoton microscope image of stratum spinosum in human volunteer skin

1.1.4 Stratum basale

The keratinocytes present in the basal layer undergo mitotic cell division. The resulting daughter cells migrate upwards towards the skin surface. In addition to the structural precursor cells that produce the stratum corneum, there are three types of specialized cells[13], namely the melanocytes, the immunogenic Langerhans' cells and the Merkel's cells associated with nerve endings found on the dermal side of the basement membrane.[26] Unlike the upper layers of the epidermis nuclei are less visible in the basale as seen in figure 1.5.

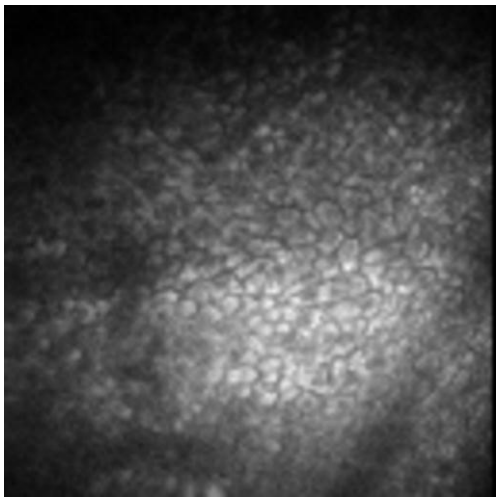

Figure 1.5 Multiphoton microscope image of stratum basale in human volunteer skin

1.2 Fick's law and delivery routes of peptides through skin

There are three principal routes of entry from the skin surface to the sub-epidermal tissue and systemic circulation: through the hair follicles with their associated sebaceous glands called the shunt or appendageal route, the transcellular route through the densely packed keratinocytes, or the intercellular route across the continuous stratum corneum between the appendages (Figure 1.6).[27,28]

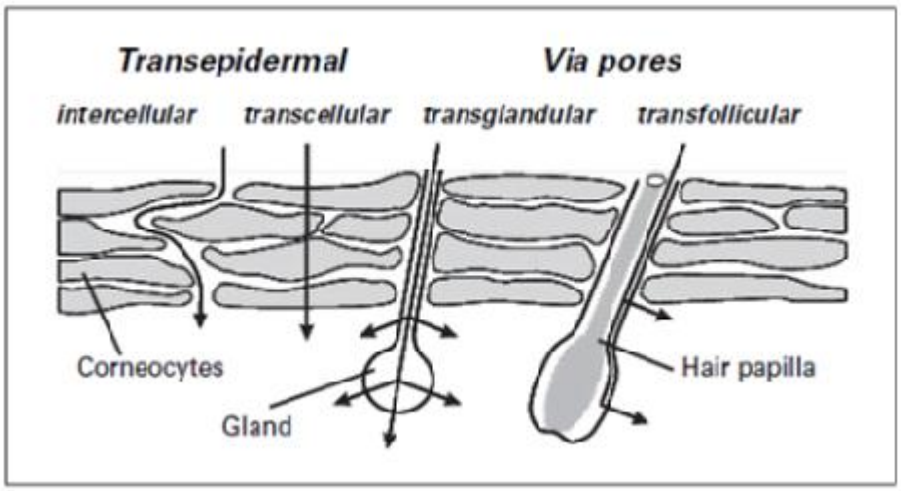

Figure 1.6 Drug penetration across the stratum corneum[28]

Favourable candidates for transdermal delivery are small molecules with good water and lipid solubility, and typically with a logP of ≅ 3. Fick's first law of diffusion states that the rate of transfer of diffusing substances through unit area of a section is proportional to the concentration gradient measured normal to the section and can be used to analyse permeation data predictively.[29]

$$J = -D\, dc/dx \qquad (1)$$

Where J is the flux of the permeant, D is the diffusion coefficient and dc/dx is the concentration gradient.

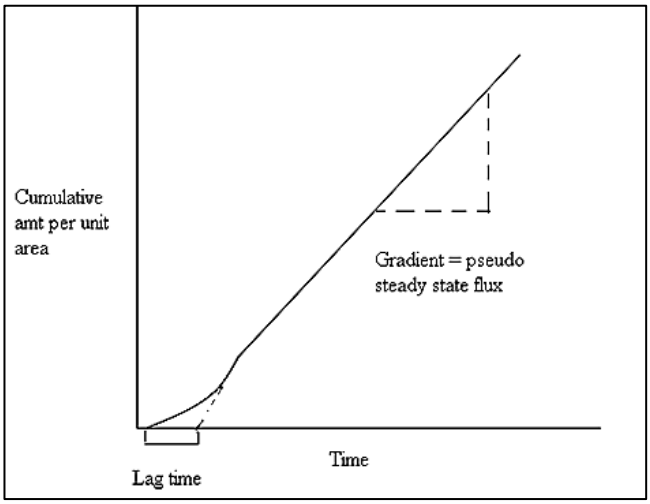

Figure 1.7 Typical permeation profile for an infinite dose application to human skin membranes[29]

Fick's second law can be derived from the first equation:

$$\delta c/\delta t = D\ \delta^2 c/\delta x^2 \qquad (2)$$

Thus the flux is obtained as the gradient of the linear portion of the permeation profile Figure 1.7.[29]

Skin permeation enhancement strategies may be postulated based on Fick's first law: (i) increase the diffusion of the drug across the membrane; (ii) increase drug partitioning into the membrane; and (iii) increase the degree of saturation of the drug in the vehicle.[30]

1.3 Strategies to enhance transdermal delivery of peptides

Several penetration enhancement techniques have been developed to overcome the skin barrier and facilitate the permeation of peptides and proteins through the skin. The various enhancement strategies have been broadly classified into formulation optimisation/permeant modification approaches, chemical penetration enhancement and application of active techniques.

1.3.1 Formulation optimisation/permeant modification approaches

1.3.1.1 Pro-drugs

The major hindrance to transdermal drug penetration is the low partition coefficient of the drug molecule.[30] Prodrugs are designed with lipophilic moieties attached to the parent compound to increase the partitioning of parent polar solutes across the stratum corneum. Upon reaching the viable epidermis the prodrug is hydrolysed by esterases to release the parent drug.[31] Lipophilic ion pairs can be formed by adding oppositely charged molecules to increase penetration across the stratum corneum. After partitioning into the stratum corneum lipids the complex dissociates releasing the ion pair into aqueous viable epidermis from where it diffuses onwards.[32]

Larsen et al. esterified a model dipeptide (Gly-Phe) at the C-terminal carboxylic acid group to convert it into a lipophilic prodrug. Their work indicates that sufficient oil solubility might only be obtained for relatively small peptides by using the prodrug approach and therefore a combination with other solubility enhancing organic solvents like dimethylacitamide (DMA) would be required to achive sufficient permeation.[33]

1.3.1.2 Encapsulation

Encapsulation is a general term used to describe the entrapment of the drug within particulate delivery systems such as microspheres, liposomes, or nanoparticles. Liposomes are phospholipid based vesicles which have been extensively investigated in transdermal delivery. They have been widely used for local delivery but there is no evidence that they penetrate the epidermis intact. A number of other liposome-like vesicles with increased structural flexibility have been developed including transfersomes, niosomes and ethosomes.[3]

In a study by Touitou et al., *in vivo* transdermal absorption of the steroid hormone, testosterone was enhanced 2.2-2.4 times through rabbit pinna skin using an ethosomal patch (vesicles with ethanol in their structure).[34] Niosomes are vesicles composed of non-ionic surfactants that have been evaluated as carriers for a number of cosmetic and drug applications. Gupta et al.[35] studied the relative potential of transfersomes, niosomes and liposomes in non-invasive delivery of tetanus toxoid (TT). Transfersomes are composed of phospholipids such as phosphatidylcholine, but also contain surfactant which acts as an 'edge activator' conferring deformability on the vesicle.[3,36] *In vivo* study revealed that topically administered tetanus toxoid containing transfersomes, after secondary immunization elicited immune response (anti-TT-IgG) equivalent to one that was produced following intramuscular alum-adsorbed TT-based immunization. In comparison to transfersomes, niosomes and liposomes elicited weaker immune response.

They observed that the entrapment efficiency, elasticity and topical effect with these encapsulated forms were higher than intramuscular administration of alum-adsorbed tetanus toxoid.[35] In another study, conducted on trans-retinoic acid or tretinoin, the potential of niosomes as topical delivery systems capable of improving the cutaneous delivery of tretinoin was assessed. Tretinoin cutaneous delivery was strongly affected by vesicle composition and thermodynamic activity of the drug, with negatively charged niosomal formulations showing higher cutaneous drug retention than both liposomes and commercial formulations.[37,3,36] However in all cases, scale up of these delivery systems to provide therapeutic peptide levels in humans is yet to be demonstrated.

1.3.1.3 Nanoparticles

Controlled release of drugs from nanoparticles is attracting increasing attention because of its potential for targeted delivery in cancer therapy and other ailments.[38] Compared to liposomes or micelles, polymeric nanoparticles are much simpler to prepare and to scale-up, as a low number of excipients are required.[39] Nanoparticles may be composed of metal oxides such as zinc oxide and titanium dioxide[40] (common sunscreens), polymer blends and lipids (solid lipid nanoparticles). There is considerable controversy regarding the safety of nanoparticles when used transdermally. It is generally agreed that non-biodegradable nanoparticles if taken up through the skin can be potentially dangerous[41,42] and caution needs to be exercised concerning topical exposure to formulations that have characteristics enabling some skin penetration or nanoparticles consisting of inherently toxic constituents.[43] Studies have shown that most commercially available nanoparticles present in sunscreens do not penetrate intact stratum corneum.[40,41]

Nanoparticles such as therapeutic or cosmetic solid lipid nanoparticles for topical application have already reached the market (NanoRepair Q10® by Dr. Rimpler uses Coenzyme Q10 an endogenous, vitamin-like substance)[44, 45] The main concern during the loading of nanoparticles with peptides or proteins is the chemical stability at conditions such as elevated temperatures, shear force, surfactants, presence of free radicals and UV radiation.[46, 47]

Recently, Ailhas et al.[48] designed a novel type of functional nanoparticle, 22 nm diameter self-assembled from single polypeptide chains. The open ended design of the peptide chain can be modified to attach targeting peptides, cell penetration peptides, certain drugs or molecular markers.[48] A study by Lee et al. reported successful preparation of nanoparticles encapsulated with a plasmid DNA containing a reporter gene (CS/g-PGA/DNA). Currently gold micro/nanoparticles are used as DNA carriers for transdermal gene delivery.[49] The authors suggested that the reporter genes tested in this study could replace gold nanoparticles.[50] Coulman et al.[51] investigated the influence of surface charge and pore size on the penetration of a colloidal fluorescent polymeric nanoparticle formulation through well-defined micro-channels generated by the application of a microneedle array to the skin. A significant impact of these parameters was observed on the permeation and subsequent distribution of the nanoparticle formulation within the skin but further

work is required to better understand the interaction of nanoparticle formulations with the skin layers following disruption of the barrier with a microneedle array.[51] Similarly Lee et al. fabricated microneedle projections which had nanoparticles attached to the tip. Nanoparticles when used with microneedle arrays have tremendous potential as an alternative method to deliver cosmetic or pharmaceutical materials into human skin locally without the need for professional procedures.[52]

1.3.1.4 Chemical conjugation

Novel drug-delivery systems for the oral administration of drugs and peptides have been developed by combining a peptide or drug with a lipophilic chain, then encapsulating within liposomes and polyethylene glycol (PEG) conjugates which can act as a carrier.[53] The chemical modification approach may protect peptides against degradation by peptidases and other enzymes and render the peptides and proteins more lipophilic, resulting in increased permeability.

In a study conducted by Setoh et al., the *in vitro* permeability of chemically modified tetragastrin with fatty acids was assessed through rat skin. The flux of these acyl derivatives was in the order of acetyl > butyroyl > caproyl. The stability of tetragastrin in skin homogenate was also significantly improved by chemical modification with fatty acids. These results suggested that chemical modification of tetragastrin with fatty acids increases its lipophilicity, which makes it more permeable across the skin. Moreover, it also reduced the degradation in the viable skin, resulting in increase in permeation of tetragastrin across the stratum corneum.[54]

In another study luteinizing hormone rereleasing hormone (LHRH) and thyrotropin releasing hormone (TRH) were chemically modified by conjugation to a novel class of compounds: lipidic amino acids and their homo-oligomers, the lipidic peptides. Conjugation to lipidic peptides increased the half-life of LHRH and TRH, with the peptides subsequently being released from Caco-2 cell homogenates. The released LHRH or TRH demonstrated a longer half-life than when present alone in the incubation mixture, suggesting that the cleaved lipidic amino acid is capable of inhibiting enzymes.[55] Naturally occurring Thymogen dipeptide (L-Glu-L-Trp-OH), which possesses immunomodulating and anti-angiogenic properties, exhibited higher intestinal permeability across Caco-2 cell layers for all lipid and glycoside conjugates when compared to the dipeptide alone.[56]

Lipophilic derivatives of Phe-Gly have also been synthesized by chemical modification with butyric acid (C4), caproic acid (C6) and octanoic acid (C8).[57] The *in vitro* stability, permeability and accumulation of this peptide were investigated in rat skin. The native peptide rapidly degraded in the skin homogenates but the acyl-Phe-Gly derivatives were more stable than the parent peptide. After 1 h approximately 15% of the native peptide was present in comparison to almost 100% of the acyl derivatives. All three conjugates permeated across the skin with the permeation of the C6 acyl derivative being the greatest. No permeation of the parent peptide was observed.

Similar lipidation strategies were undertaken with carnosine (β-Ala-His) and human calcitonin. To improve the intestinal absorption of human calcitonin (hCT) (Figure 1.8), novel lipophilic derivatives of hCT were synthesized by chemical modification with short-chain length fatty acids such as acetic acid and caproic acid, and the intestinal absorption and stability of these derivatives were examined in rats.

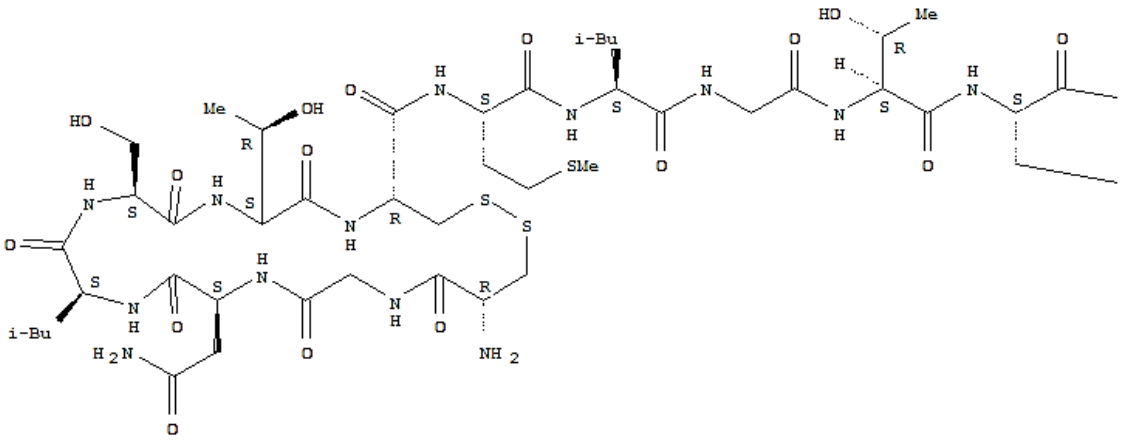

Figure 1.8 Chemical structure of human calcitonin

The effect of absorption enhancers on the absorption of the synthesized derivatives was also investigated. The intestinal absorption of hCT was enhanced by chemical modification with fatty acids and it was further promoted by the combination of acylation and absorption enhancers.[58] Carnosine is very water soluble and was therefore conjugated with a longer chain palmitoyl acid. The parent molecule had very low affinity for the skin and did not permeate beyond the first layer of the

stratum corneum. The lipophilic derivative on the other hand, diffused into the stratum corneum and into the epidermal and dermal layers. Having shown that modified peptide can penetrate into the skin but not through it, Linter et al.[59] applied the concept to the tripeptide glycyl-L-histidyl-L-lysine. They synthesized palmitoyl Gly-L-His-L-Lys and studied the stimulation of collagen synthesis in human fibroblast culture. Histological examination of skin samples (human biopsies from plastic surgery, abdominal tissue) that had been irradiated with daily doses of UVA light for a week showed a strong degradation of dermal collagen. Treatment of skin samples after irradiation with retinoic acid or with palmitoyl-Gly-His-Lys during the same week showed almost total preservation and/or renewal of tissue collagen.[59]

Lipid conjugation of peptide sequences holds promise in modifying the properties of peptides by increasing their stability and permeability across biological membranes thus enhancing their activity and potential for therapeutic and cosmetic significance.

1.3.1.5 Cell-penetrating peptides

In 1988, two independent research groups discovered that a trans-activating transcription factor, TAT, from the human immunodeficiency virus (HIV) was able to freely internalize into cultured cells.[60,61] Since then more than 100 cell-penetrating peptide (CPPs) have been described,[60-63] but it is the TAT peptide that has been most successfully used to deliver therapeutic molecules into cells. In a 2004 review of the literature, Dietz et al.[64] described over 300 different applications of CPPs, with TAT being used in 50% of the cases, this trend has continued and more recent reviews describe a similar proportion of TAT usage.[64,65] CPPs are defined as peptides with a maximum of 30 amino acids, which are able to enter cells in a seemingly energy-independent manner; this can be postulated as they internalize even when cells were incubated at 4ºC or when inhibitors of endocytosis were present.[4] CPPs thus were believed to translocate across membranes in a non-endocytotic fashion, although several other modes of transport have been described.

CPPs can be broadly divided into two classes based on their net charge. The first class consists of amphipathic (i.e. containing both hydrophobic and hydrophilic parts) helical peptides where Lys is the main contributor to the positive charge. These CPPs deliver more cargo into the cells than the second class, the Arg rich TAT and penetratin, which are non-amphipathic. The peptide-induced membrane leakage

is thought to be proportional to amphipaticity.[4,62] CPPs derived from proteins are often referred to as protein transduction domains. Hansen et al.[66] described the current practice and tools used to predict what features in a peptide can lead to it being termed as a CPP. Though trial and error seemed to be the most frequent way of CPP discovery, bioinformatics and z-descriptors derived from Sandberg's[67] expanded z-scales can be informative.[66]

There is considerable debate about what specific peptide sequences contribute to the ability to translocate across biological membranes, though a high content of basic amino acids, resulting in a net positive charge.[68] Alain et al.[69] observed that replacement of the arginine amino acid by lysine in the basic region reduces the cell penetrating ability, thus suggesting that the arginine residues have specific properties beyond an interaction with negative charges at the cell surface.[69] Whilst endocytosis is not required for translocation of some CPPs, for others, such as TAT and penetratin, endocytosis is the main mode of transport.[70] TAT is non-amphipathic with a high content of cationic amino acids (arginine) and binds to the lipid membrane with a high amount of anionic lipids. Membrane leakage is not observed at low micro molar concentrations. Whilst endocytosis is important, other active modes of transport have also been suggested for TAT. For example, Tyagi et al.[71] suggested that heparan sulfate proteoglycans, which are expressed in most cell types, could be responsible for the internalization of the full-length TAT protein.[71] Wender et al.[72] further showed that the TAT peptide, comprising amino residues 48-60 from the full length TAT protein, showed an elevated internalization efficacy over the parent protein.[72] Proposed mechanisms for the direct membrane transduction included pore formation, carpet-like perturbations and inverted micelles (Figure 1.9).[65,73] These different processes demonstrate that peptide mediated membrane translocation is mediated by several different pathways simultaneously and different peptides utilize diverse uptake mechanisms depending on their cargo and biophysical properties.[74] The penetration of CPPs into cells is rapid and initially governed by first-order kinetics, with half-times from 5 to 20 mins. Smaller cargoes usually do not affect the rate of internalization, but as the size of the cargoes is increased, the rate is substantially decreased.[63]

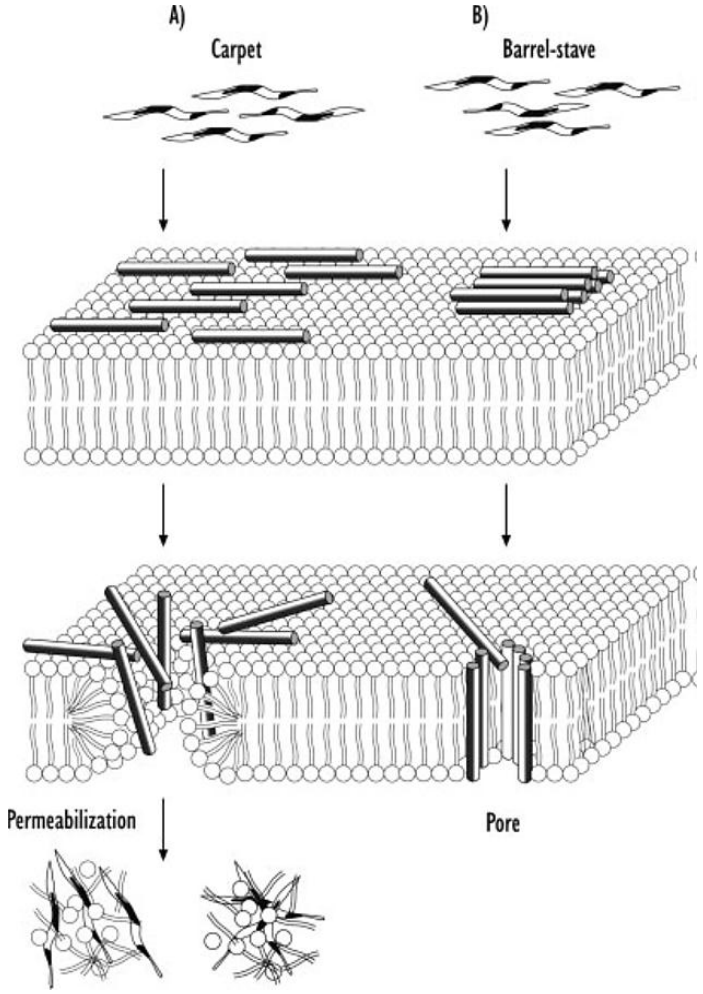

Figure 1.9 Illustration of the possible interactions of the peptides with the phospholipid membranes, and different mechanisms for translocation of CPPs.[68]

The kinetics of CPP mediated transport has been extensively investigated. Pooga et al.[75] visualized biotinylated transportan in Bowe's melanoma cells using confocal microscopy and suggested it could be used to transport hydrophilic macromolecules into the cell to regulate finely tuned cellular processes.[75] Zorko et al.[63] specifically identified that the concentration of internalized CPP as a function of time, can be more reliable and informative if the concentration equilibrium between external and internalized CPP is determinable.[63] Hällbrink et al.[4] quantitatively characterized the yield and kinetics of cellular cargo delivery of different CPPs.[4] The difference in cargo delivery efficiency between the amphipathic peptides and non-amphipathic peptides is due to the ability of the amphipathic peptides to enter and exit cells, in contrast to the non-amphipathic peptides which are trapped in the cells as they bind to the lipid membrane with a high amount of anionic lipids. In terms of the cellular uptake and cargo delivery kinetics, model amphipathic peptide (MAP) has the fastest

uptake, followed by transportan, TAT (48–60), and penetratin. Similarly, MAP has the highest cargo delivery efficiency, followed by transportan, TAT (48–60), and penetratin.[76]

The ability of these peptides to translocate through cell membranes can be accompanied by toxic effects resulting from membrane perturbation at higher peptide concentrations. This can be attributed to the resemblance of CPPs to the antimicrobial lytic peptides that kill microbial cells by disrupting their cell membrane.[63] CPPs have been subjected to a high degree of scrutiny regarding the highly controversial issue of direct permeation of the strongly cationic peptide across negatively charged lipid membranes. Barany-Wallje et al.[77] used confocal laser scanning microscopy on rhodamine labelled giant vesicles incubated with carboxyfluorescein labelled penetratin to show no evidence of trans bilayer movement. The studies conducted on charged black lipid membranes were backed by additional results from confocal fluorescence spectroscopy.[77] A study by Saar et al.[78] assessed the toxicity of popular CPPs in leukaemia cells and erythrocytes. The amphipatic CPPs-MAP and transportan were shown to cause membrane leakage at lower concentrations in the leukaemia cells; conversely the non-amphipathic CPPs like TAT (48-60) and penetratin showed low membrane damage.[78,68] When the minimal membrane-translocating TAT domain was discovered by Vives et al.[79], no toxicity was found in very extreme conditions on HeLa cells with a 24 h incubation at 100 μM concentration.[79,80] In addition, it is noteworthy that peptide concentrations used in toxicity tests are often far above the concentrations used for delivering various drugs into cells.[81] However, it needs to be mentioned that most of the well-described CPPs are derived from non-human proteins and could potentially induce an immune response when injected into the human body, at least when bearing a large size cargo.[82]

To be effective drug delivery tools, CPPs need to be very specific in targeting their desired location. This can be achieved by conjugating a CPP to T cell epitope peptides or proteins for direct immunization. These conjugates can then be applied to several sites by simultaneous intradermal administration and will enter any cell without the need for specific receptor targeting of the dendritic cells for immunotherapy. Targeting has also been achieved with receptor-specific antibody antigen conjugates, carbohydrate–antigen complexes, or nanoparticles. However,

CPP-mediated delivery can overcome complexities associated with the manufacture of these agents.[83] The discovery of cancer-specific peptides, for instance, can be facilitated by phage display technology, where a library of bacteriophages exposing a different peptide sequence on their capsule are intravenously injected into animals bearing the tumour to be targeted. The phages displaying the "correct" sequence bind specifically to the tumour and are afterwards collected, amplified and their exposed sequence identified as the tumour targeting sequence. These "tumour homing sequences" have been applied successfully *in vivo*, demonstrating an accumulation of the vector drug complexes into the tumour.[84,85]

The dual ability of CPPs to covalently and non-covalently bind to a cargo complex of much bigger size than their own and translocate it across the plasma membrane, and the ability to act as nuclear localization signal, has demonstrated potential to revolutionize the field of cell biotechnology.[86] The ideal cargo for peptide-mediated delivery should have a large impact at low concentrations. Therapeutics such as recombinases and small interfering RNA-siRNA are prime candidates for an ideal CPP cargo. CPP technology is peptide-based, so it is easily modified with the addition of specific functional units. Increased retention in specific tissues can be obtained by attaching homing peptide sequences or other targeting motifs to CPPs.[87] The indiscriminate transduction of CPPs is a drawback if targeted delivery is preferred.[25] Translocation of a CPP from cytoplasm to the nucleus is mediated by a signal or localization sequence. There are a variety of sub-cellular localization sequences. Each of these signal sequences has a distinct property that targets a cytosolic protein to a specific organelle. The nuclear pore complexes which are responsible for the uptake of CPPs along with their attached cargo, are capable of dilating to 10–25 nm in diameter to facilitate the active transport of large molecules.[86] Laakkonen et al.[88] showed that a 9 amino acid peptide LyP-1 selected from a phage-displayed peptide library specifically binds to tumour and endothelial cells of tumour lymphatics in certain tumours. The peptide preferentially localizes in hypoxic areas within the tumours. They also showed that systemically administered LyP-1 causes tumour cell apoptosis, reduces the number of tumour lymphatics, and inhibits tumour growth in mice bearing breast cancer xenografts.[88]

CPPs can be used to internalise molecules and selectively interfere with diverse cellular mechanisms. Gius et al.[89] used TAT for intracellular delivery of cyclin-

dependent kinase inhibiting peptide, to enable the arrest of cell proliferation. Ward et al.[90] developed a cell-permeant peptide inhibitor of mitogen-activated protein kinase-activated protein kinase 2 (MK2). It was observed that the CPPs alone inhibited varying amounts of MK2 activity and the conjugation of CPP to the MK2 inhibition sequence enhanced the efficacy of the therapeutic domain showing synergism.[90] An interesting application of the CPPs is the design of cytotoxic T lymphocytes (CTL). CLTs and vaccines for the treatment or prevention of infectious and malignant conditions were shown to rapidly internalize into cells. Furthermore, the use of the conjugates as immunogens resulted in considerably enhanced antigen specific CTL responses in mice.[91]

Proteins and peptide delivery with the use of CPPs has gained a lot of attention. The major obstacles for *in vivo* clinical applications of peptides is their poor permeability through plasma membrane and their sensitivity to enzymatic degradation.[92] Nucleic acid delivery in cells is commonly carried out using cationic lipids or viruses; however, both have several drawbacks. Cationic lipids are restricted to *in vitro* applications, whereas the latter are sometimes immunogenic *in vivo*.[93] Based on the principal purpose of the cargo molecule, the peptide and protein cargoes can be categorized into two distinct subclasses: reporter peptides/proteins (giving simply a positive read-out upon effective delivery) and functional peptides/proteins (allowing the detection of any alteration in the cellular processes).[84,94] Protein and peptide cargoes do not behave the same when applied using CPPs. Mark et al.[95] observed that, compared to CPP–protein conjugates, substantially greater concentrations of CPP–peptide conjugates (>10 μM) were required for biological activity. The proteins are likely to have a greater affinity, resulting from their secondary and tertiary structure.[95]

Myou et al.[96] demonstrated that blockade of Ras protein by administration of TAT-dominant negative-dnRas blocks nonspecific airway hyper-responsiveness to methacholine.[96] Fujimoto et al.[97] demonstrated the growth inhibitory effects of a p16-derived peptide ($P16^{INK4A}$).[97] Snyder et al.[98] used peritoneal carcinomatosis mouse model that more closely resembles metastatic human disease to demonstrate a selective activation of the p53 protein in cancer cells, but not normal cells. To circumvent the problem of proteolytic degradation, the researchers synthesized a

retro-inverso version of the parental p53C′ peptide-RI-TATp53C′ and showed it to be therapeutically effective in preclinical models of terminal human malignancy.[98]

Effective drug delivery to the brain is required in neurodegenerative diseases, such as Parkinson and Alzheimer disease and central nervous system (CNS) diseases, such as schizophrenia, epilepsy, and bipolar disorder.[99] Neuropharmaceutics is the largest potential growth sector of the pharmaceutical industry. Many promising neuropharmaceutical compounds do not become successful therapeutics due to blood-brain barrier (BBB) transport problems, >98% of these potential agents do not reach the drug development stage.[100] The BBB consists of a monolayer of polarized endothelial cells connected by complex tight junctions that separate the blood compartment from the extracellular fluid compartment of the brain parenchyma and poses a formidable obstacle to drug therapy to the CNS.[91] Effective brain delivery requires that the CPP and its cargo are not trapped within the epithelial cells but escape into the brain parenchyma or the other side of the interstitial barrier.[69] Kumar et al.[101] conjugated a small peptide derived from the rabies virus glycoprotein (RVG) with nine arginine molecules. This conjugate was shown to carry siRNA into the CNS and bind the acetylcholine receptor resulting in specific gene silencing.[101] Rousselle et al.[102] showed increased brain delivery of doxorubicin when conjugated with penetratin, with higher brain concentrations of CPP-doxorubicin (2.14±0.23 μL/s/g) compared to free doxorubicin (0.25±0.09 μL/s/g). CPP-doxorubicin was found at lower levels in the heart, significantly reducing cardiotoxicity, which is the main side effect of doxorubicin.[102]

In 2007 a research group from Barcelona introduced the concept of using small cyclic peptides, diketopiperazines (DKPs) as shuttles for brain delivery. They illustrated transport of dopamine and baicalin across an *in vitro* BBB model using the Parallel Artificial Membrane Permeability Assay (PAMPA).[99] DKPs represent an important class of biologically active natural products but the advent of combinatorial chemistry has revived interest in DKPs for two reasons: firstly, they are simple heterocyclic scaffolds in which diversity can be introduced and stereochemically controlled at up to four positions; secondly, they can be prepared from readily available α-amino acids using very robust chemistry.[103]

DKPs have been isolated and identified from a variety of natural sources including marine sponges, lichens and herbs. Bolognesi et al.[104] reported the identification of a

novel bifunctional DKP derivative 1D, which exhibits activity in the low micro molar range against prion replication in ScGT1 cells, while showing low cytotoxicity. Martins et al.[105] reviewed the biological activities of DKPs and described that most of their biological properties are related to the inhibition of plasminogen activator inhibitor and alteration of cardiovascular and blood-clotting functions. DKPs have antitumor, antiviral, antifungal, antibacterial, and antihyperglycaemic activities.[105] Malakoutikhah et al.[106] described the influence of the terminal groups of a DKP peptide on its permeability. The peptide with acetyl and amide groups as N-terminus and C-terminus respectively showed the best permeation.[106] The Barcelona group have synthesised a library of 15 DKPs with distinct side chains using a solid-phase synthetic methodology for systematic testing.[99] Chapter 2 of the thesis describes our collaboration with the Barcelona group in the investigation of DKP as a potential carrier for transdermal delivery.

CPPs have been investigated for transdermal delivery. Rothbard et al.[107] investigated the mechanism of transport of oligoarginine conjugates into the cutaneous barrier and demonstrated that the conjugates penetrate intact skin and enter into the cells by active transport across lipid cellular membrane. Thus CPPs enter the layers of cells, accumulate there, and then enter the adjacent layers presumably by forming a concentration gradient.[107] Hou et al.[108] proposed the involvement of macropinocytosis and actin reorganization in transdermal delivery of CPPs into the skin.[108] Jin et al.[109] described the synthesis and CPP conjugation of an antioxidant peptide superoxide catalase-CAT. Immunohistochemistry and specific enzyme activity showed efficient penetration into the epidermis and dermis when the TAT-CAT and 9Arg-CAT fusion proteins were sprayed on animal skin. Antioxidant enzymes like superoxide dismutase (SOD) and catalase (CAT) are very effective against diseases mediated by reactive oxygen species such as skin inflammation, skin cancer, cutaneous autoimmune diseases, phototoxicity and skin ageing.[109] Wender et al.[110] showed that biotin peptide can effectively penetrate across the stratum corneum when applied topically as a biotin-transporter-9 conjugate. Intense nuclear localization was observed in the epidermal cells showing that it translocated into the cells faster than even 9Arg and TAT.[110]

Lim et al.[111] showed enhanced penetration of Glycine-Lysine-Histidine tripeptide (GKH) derived from parathyroid hormone. TAT conjugated GKH penetrated 36

times more efficiently than GKH into excised hairless mice skin. TAT-GKH can be used as a cosmetic ingredient in slimming products, with both penetration enhancement and lipolytic effect without cytotoxicity.[111] In a recent study, Hsu et al. synthesized a novel CPP-skin penetrating and cell entering peptide (SPACE). Conjugation of the peptide to siRNA led to their enhanced absorption into full thickness porcine skin and knockdown of corresponding protein targets. The ability of the SPACE peptide to deliver Interleukin- 10 (IL-10) siRNA and reduce the overall level of the cytokine may offer unique therapeutic opportunities in the treatment of atopic dermatitis and other dermatological diseases.[112]

1.3.2 Chemical penetration enhancers

Chemical enhancers, such as fatty acids, surfactants, esters and alcohols exert their action via a temporary alteration of barrier properties of the stratum corneum. The various mechanisms involved in skin perturbation include stratum corneum partitioning, fluidization of the crystalline structure, increased solubility by enhancing thermodynamic activity in the formulation and dissolution of stratum corneum lipids leading to enhanced drug flux.

Lee et al.[113] and Tsai et al.[114] demonstrated the disruption of intracellular keratin networks and intercellular cohesion of corneocytes by penetration enhancers present in a depilatory cream using multi photon microscopy (MPM visualization).[113, 114] Pretreatment with depilatory cream, which contains potassium thioglycolate or calcium thioglycolate in the base, can detach corneocytes from the stratum corneum and can also generate intracellular pores in the remaining corenocytes by disrupting the intracellular keratin, providing shunts for drug penetration. However, due to low permeability coefficients of macromolecules such as peptides, the enhancement effects required to ensure delivery of therapeutically effective concentrations are likely to be beyond the capability of chemical enhancers at concentrations tolerated by the skin.[115] Peptides require substantially greater enhancement due to their hydrophilicity and molecular weight. Magnusson et al.[116] reported 3 to 5 fold enhancement of M-TRH across human epidermis in vehicles combining terpene/ethanol and cineole/ethanol. As stated earlier substantial enhancement can be achieved for a small peptide but this approach is of limited value for larger peptides

and proteins, and moreover care needs to be taken that enhancer chemicals do not denature the peptide.[116]

The practical use of these enhancers in different formulations requires balancing their benefits and risks i.e. penetration enhancement effect and skin irritation. For example DMSO increases penetration of various drugs but is a powerful aprotic solvent and thus altered the biochemical and structural integrity of skin, as was observed during certain studies undertaken in chapter 3 in this thesis. The saturated and unsaturated fatty acids under occlusive conditions cause erythema and produce irritation. Thus, enhancers should be evaluated for potential irritancy under conditions of long term occlusion.[117]

1.3.3 Active penetration enhancement techniques

1.3.3.1 Iontophoresis

Iontophoresis is the application of a small electric potential ($\leq$ 0.5 mA/cm^2) to drive charged molecules into the skin.[118] The mode of enhancement of transdermal transport is principally by two mechanisms: electrostatic repulsion, whereby a solute with the same charge as an electrode placed on the skin surface is repelled into the skin[3] (Figure 1.10) and electroosmosis, where at neutral pH, the skin has a net negative charge and is permselective to cations and neutral molecules. This passage of cations induces a convective flow of water molecules from the anode which further enhances the permeability of cations while inhibiting that of anions.[119] An interesting feature of iontophoresis is that its primary action is on the peptide or drug molecule itself so it does not just involve passive diffusion and is not solely dependent on concentration gradient. By modulating the applied current, the delivery rate of peptides/small molecules can be adapted to individualise therapy thus offering the potential of pulsatile drug delivery.[120]

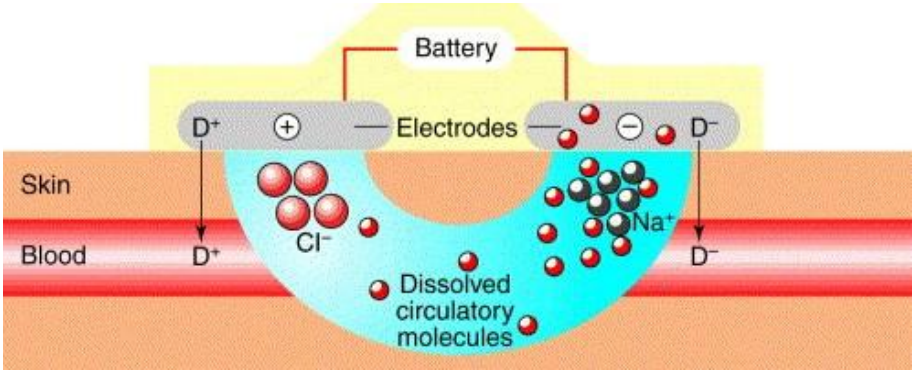

Figure 1.10 Schematic of an iontophoretic device[121]

Iontophoresis is the most extensively researched of the physical enhancer technologies and successful transdermal iontophoresis has been demonstrated for a number of peptides such as LHRH, TRH, cyclosporin, nafarelin, arginine vasopressin (AVP), octreotide, calcitonin and insulin.[3,122]

Many of the peptides mentioned above have been subject to mechanistic investigations and electroosmosis has been proposed to be the dominant mechanism in iontophoretic transport of large cationic peptides. Hirvonen et al.[122] designed and synthesized a series of cationic LHRH oligopeptides, three residues in length. They conserved the positively charged Arg residue in the oligopeptide and varied the degree of lipophilicity in the other two residues in an attempt to examine if the permselectivity of the membrane could be increased by augmenting the net negative charge. The results indicated that a combination of cationic and lipophilic residues, inhibited electroosmosis and in turn peptide flux. It is hypothesized that the cationic oligopeptide could interfere with electroosmotic transport by neutralizing the original charge of the skin and affecting its permselective properties.[122] Also, computational studies that generated 3D quantitative structure-permeation relationships predicted that iontophoresis was favoured by peptide hydrophilicity and hindered by voluminous, localized hydrophobicity.[123]

Leuprolide, a nonapeptide LHRH agonist was studied using constant current iontophoresis to explore methods for improving iontophoretic efficiency and determine the feasibility of delivery of therapeutic doses of the drug. It was found that in two different electrolyte systems and by varying current densities from 0.5 to 2.3 $\mu A/cm^2$, the fluxes could be extrapolated to show the delivery of therapeutically relevant doses of the drug.[124] Leuprolide containing D-Leu-Leu-Arg has been successfully delivered *in vivo* in humans to produce a peak leutinizing hormone

response similar to subcutaneous injection.[125] Electrically assisted transdermal delivery is rapid and plasma levels decline on termination of the applied current. For example, arginine vasopressin was pulsed across hairless rat skin in three discrete 1 $\mu g/cm^2$ spiked doses by application of three 60 min current pulses of 0.47 mA/cm^2.[126]

In addition to the use of iontophoresis as the sole enhancement technique, combinations of iontophoresis with chemical enhancers and formulation modifications have also been investigated.[127] Pillai et al.[128] investigated the *in vivo* and *in vitro* skin permeation of insulin in rats with chemical enhancer and/or iontophoresis. The study investigated the effect of pre-treatment with commonly used vehicles such as ethanol, propylene glycol, water and their binary combinations, dimethyl acetamide, 10% dimethyl acetamide in water, ethyl acetate and isopropyl myristate on insulin iontophoresis. Whilst increased skin penetration was achieved this was frequently associated with increased skin irritation.[128] The authors concluded that ethanol was the most useful solvent to combine with iontophoresis. Isopropyl myristate produced comparable enhancement but the high viscosity and relative incompatibility with other penetration enhancers are drawbacks. Marked decreases in blood glucose levels reflecting the increases in the plasma concentration of insulin in rats were also observed after combined electroporation/ iontophoretic administration, whilst no insulin penetration was detected by passive or iontophoresis alone. The results were attributable to the formation of an irreversible route in the stratum corneum, through which insulin could be absorbed.[129] Bhatia and co-workers investigated the effect of limonene/ethanol and iontophoresis on the *in vitro* percutaneous absorption of LHRH and on the ultrastructure of human epidermis by transmission electron microscopy (TEM). Limonene/ethanol at 5% concentration significantly enhanced the passive permeation of LHRH through human epidermis, and iontophoresis further increased the flux through enhancer treated epidermis. The combination of iontophoresis and enhancer treatment significantly enhanced LHRH delivery by disrupting keratin, and loosening and swelling of stratum corneum cell layers in comparison to controls with iontophoresis alone.[130] Boinpally et al.[131] reported that the *in vitro* transport of cyclosporine from lecithin vesicles under anodal iontophoresis was greater than when applied in combination with a microemulsion.[131]

As a result of this large body of research, the technology is now matured with many clinical applications in late stage clinical trials and some on the market. Examples are the LidoSite lidocaine delivery system for local anaesthesia (Vyteris, Inc., Fair Lawn, NJ), Iontopatch dexamethasone delivery system for musculoskeletal conditions (Travanti Pharma, Inc., Mendota Heights, MN) and the IONSYS fentanyl delivery system for patient controlled analgesia (Alza Corp/JNJ, Mountain View, CA) The IontoPatch is an extended time-released electronic transdermal drug delivery system. An innovative self-contained battery produces an electric current to carry drug molecules non-invasively across the skin and to underlying tissue. Drug delivery is shut off automatically when the prescribed dosage has been administered. IONSYS (fentanyl HCl) system is a needle-free, patient-controlled transdermal analgesic (PCTA), integrated system for on-demand dosing, delivering a nominal 40 μg fentanyl per on-demand dose from a hydrogel over ten minute dose duration. To date, iontophoretic transdermal delivery of large peptides and proteins sufficient to achieve therapeutic outcomes in humans has not been demonstrated. However the technique may be useful for local delivery of small peptides (less than 10 kDa) in the treatment of skin conditions or lesions.[53] Whilst the potential benefits are apparent, there are some limitations. Current densities up to 0.5 mA/cm^2 do not damage human skin, though iontophoresis at 1 mA/cm^2 has been shown to damage the membrane structure. The side effects of long term iontophoresis use are yet to be fully evaluated.[132]

1.3.3.2 Electroporation

Electroporation involves the application of an exponentially decaying high voltage (100–1000 V) for a very short time (micro or milli seconds) to produce transient changes in cell membranes or lipid bilayers.[133] It is hypothesized that electroporation destabilizes the lipid matrix of the cell membrane, resulting in the creation of transient hydrophilic pores that reduces skin resistance by up to three to four orders of magnitude for small and macromolecules.[134,135] Skin electroporation has been shown to be an effective method for enhancing transdermal delivery of peptides such as LHRH, heparin and oligonucleotides.[133,136-138] For example, Prausnitz et al. demonstrated *in vitro* skin permeation of heparin by electroporation at amounts equivalent to therapeutic levels (100–500 mg/cm^2/h). This was an order of magnitude greater than the heparin flux achieved with iontophoresis.[139] Electroporation has also

been used for DNA transfection in cells in culture, and *in vivo* electroporation in the presence of DNA plasmid can induce gene expression in several organs.[140] Wang et al.[141] assessed topical delivery of cyclosporin A (CSA) for treating psoriasis. Iontophoretic administration of a solution of cyclosporin A in 40% ethanol in phosphate buffered saline did not result in any significant increase in drug delivery. However electroporation applied as multiple pulses (25 pulses, 10 ms each) resulted in a 60-fold increase in the delivery of CSA to the skin compared to passive application.[141] Previous studies have shown that anionic lipids enhanced the electroporative transport of molecules up to 10 kDa in size. It was also shown that the charge and not the type of the phospholipid head group influenced the transdermal transport under electroporation. Moreover, phospholipids with saturated acyl chains enhanced the transport of larger molecules more as compared to those with unsaturated chains.

Sen et al.[142] reported a 20-fold increase in transport of fluorescence-labelled insulin in the presence of an anionic phospholipid (1,2-dimyristoyl-3-phosphatidylserine) with electroporation compared to electroporation alone, across porcine epidermis. They hypothesized that this permeation enhancement is due to the phospholipid stabilizing the aqueous pathways in the stratum corneum created by electroporation, thereby maintaining the pathways for a more prolonged period.[142] When iontophoresis was included in the experimental protocol it further increased insulin flux across the skin. A combination of electroporation and iontophoresis also led to increase in the transdermal flux of human parathyroid hormone (hPTH) up to 10 times greater than electroporation alone.[143] Therapeutic administration of macromolecules by skin electroporation could be clinically useful. The efficacy of transport depends on the drug physicochemical properties, the formulation and the electrical parameters.

The potency of the drug and safety concerns will be the critical issues to address.[144] The safety and efficacy of *in vivo* electroporation was assessed using histological and visual scores and bioengineering methods by Vanbever et al.[144]. The study yielded useful information on alterations of skin function following the application of high voltage pulses and the effects were shown to be dependent on the electrical parameters of the pulses. In conclusion they reported that improved electrode configuration might further improve tolerance and levels of sensation.[144] Whether

electroporation will be more efficient than other techniques used to enhance macromolecules delivery (e.g. liposomes or ultrasound) remains to be investigated.

1.3.3.3 Magnetophoresis

Magnetic energy has gained a lot of attention in the recent past, though the use of magnetic energy for healing dates back thousands of years. It has been described in most of the major ancient medical and philosophical records.[145] Also, biological, therapeutic and inductive effects of electromagnetic fields on biological tissues have been widely reported. These include enhanced healing of venous ulcers and bone fractures and effects on a range of cellular functions.[146,147] More recent advances in medicine have utilised magnetic energy ingeniously in drug targeting and healing itself.

Santini et al.[148] discussed the interesting idea of employing intelligent systems, based on a microchip technology activated by a magnetic impulse to deliver sodium fluorescein into a phosphate buffer saline well, and suggested that this system could be easily modified to release drugs in controlled-pulsatile mode.[148] Nishijima et al.[149] investigated a magnetically targeted-drug delivery system (MT-DDS), which involves binding a drug molecule to small biocompatible magnetic particles. When injected into the blood stream these drug-magnet nanoparticles can be pulled out of the suspension and moved to the target region using a high gradient magnetic field.[149] The study reported successful accumulation of ferromagnetic nanoparticles in an *in vitro* study. Ferromagnetic nanoparticles were separated in pig blood under a blood flow of 200 mm/sec using bulk superconducting magnets of 2.14 T magnetic flux density.[149]

In a previous work of similar nature, Grief et al.[150] described theoretical analysis of magnetically targeted drug delivery technique. A mathematical model tracking individual particles under the influence of Stokes drag and a magnetic force was derived. The authors also included interactions and collisions between moving red blood cells in the bloodstream in their calculations. The study concluded that, though it was possible to distribute the drug-magnet nanoparticles heterogeneously, magnetically targeted drug delivery with an externally applied field is only possible if targeted close to the surface of the body.[150]

Huang et al.[151] described a novel flexible drug delivery chip-like device which had a drug-carrying core-shell magnetic nanoparticle incorporated in a membrane. The chip was reported to be capable of delivering drugs with a fast and precise response over a wide variety of release patterns, including sustained release, step-wise release, and burst release. The chip was capable of eluting therapeutically effective amount of ethosuximide, an anti-epileptic drug by external magnetic stimulus in an animal model.[151] Magnetic drug delivery systems like MagNaGel®[32], FluidMAG® and TargetMAG® have already been commercialized and have been found satisfactory for use in patients under current regulations.[38]

Magnetophoresis is the enhancement of drug permeation across biological barriers by application of alternating magnetic field. Limited work has been undertaken to investigate the ability of magnetic fields to move diamagnetic substances through skin,[6] though this offers potential advantages, particularly in drug delivery into the skin. Magnetophoresis is a much recent development in the field of enhanced drug delivery.[2] The term diamagnetism was coined by Michael Faraday in 1845, when he realized that all materials in nature possessed some form of diamagnetic response to an applied magnetic field.[152] Drug molecules in a solution are particularly susceptible to diamagnetic repulsion due to the availability of localised electrons. The presence of large phospholipids in the skin, that with the aid of diamagnetic repulsion can be rearranged in hydrated skin further make for a case to magnetophoresis. Any rearrangement of the lipids in the skin will be very temporary and hence make magnetophoresis one of the most non-invasive techniques for transdermal drug delivery.[153]

Murthy et al. showed that magnetophoresis enhanced the transdermal drug delivery of lidocaine hydrochloride in *in vitro* and *in vivo* studies.[6,154] Sammeta et al.[155] reported lidocaine hydrochloride delivery flux of 3.07 ± 0.43 μg/cm^2/h from a magnetophoretic patch system across epidermis compared to 0.94 ± 0.13 μg/cm^2/h for passive permeation.[155] Krishnan et al. utilized an electromagnetic field to enhance drug permeation across the skin.[156] This study used the Dermaportation technology, a novel transdermal drug delivery system that uses pulsed electromagnetic fields (PEMF) to enhance the movement of diamagnetic substances through the skin. This technology utilizes a time varying electromagnetic field designed by OBJ Ltd, a

Perth-based biotechnology company. The Dermaportation system runs on a low-energy time varying electromagnetic pulse packet.

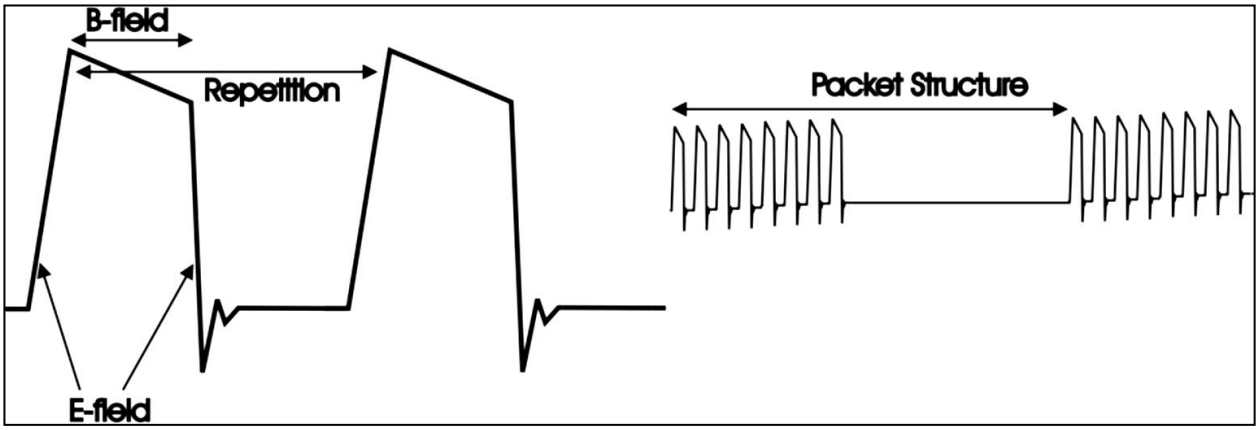

Figure 1.11 Schematic representation of PEMF Dermaportation waveform

Studies by our group using Dermaportation have demonstrated enhanced penetration of small molecules and peptides including 5-aminolevulinic acid, naltrexone, diclofenac, lidocaine and a model dipeptide Ala-Trp.[153,156-159] Dermaportation uses a low voltage (3V) and does not require direct physical contact with the skin to produce diffusion enhancement (Figure 1.11). This research was extended to investigate a fixed magnetic field derived from small flexible un-powered magnetic film array, termed ETP and also developed by OBJ Ltd. ETP is a thin flexible polymer matrix containing multiple magnetic elements arranged to produce complex 3-dimensional magnetic gradients. The peak magnetic field strength of these magnets is 40 mT. However the arrangement and distribution of alternating poles across the surface of the material results in a total magnetic gradient of 2 T/m^2. These small magnets were shown to enhance skin permeation of urea and increased hydration of the skin.[7]

Benson et al.[7] reported that the potential mechanism for magnetophoresis was modulation of the permeability of the stratum corneum.[7] This has however been strongly debated by Murthy et al. who believe that an electromagnetic field of 5 mT strength is insufficient to cause a change in the stratum corneum membrane lipid integrity. Murthy et al.[154] suggested that the predominant mechanism for drug permeation enhancement is magnetokinesis and enhanced partitioning of drug into the stratum corneum. Their hypothesis was based on assessment of skin changes by attenuated total reflectance Fourier transform infra-red spectrometry (ATR-FTIR) in

which they did not show changes in the skin spectrum. Murthy et al. used magnets of much greater strength of 450 mT at the skin surface. Thus the magnetophoretic devices used by these groups are not comparable and the mechanism of enhancement may be different.

In this PhD project I have investigated the permeation of curcumin (a small molecular weight model drug) using ETP (Chapter 4). The penetration of curcumin in volunteer skin was assessed using multiphoton tomography (MPT) and fluorescence lifetime imaging microscopy (FLIM). This along with other experiments on magnetophoresis will be discussed in Chapter 4.

1.3.3.4 Ultrasound

Low-frequency ultrasound (or sonophoresis) has been shown to increase the permeability of human skin by several orders of magnitude to many low molecular weight drugs (<500) as well as high molecular weight proteins such as insulin.[160] Therapeutic frequencies in the range of 1–3 MHz was first applied to enhance the skin penetration of small drugs in the 1980s. More recently low frequency ultrasound (<100 kHz) has been used to provide greater enhancement and has been extended to the delivery of macromolecules across intact skin.[161] It is hypothesized that ultrasound application induces growth and oscillations of air pockets present in the keratinocytes of the stratum corneum by a phenomenon known as cavitation. This leads to perturbation of the lipid bilayers thereby enhancing transdermal transport.[162] *In vitro* studies have shown increases in skin permeability of macromolecules such as insulin (6,000 Da), β-interferon (17,000 Da) and erythropoietin (48,000 Da) using low frequency 20 kHz sonicators with wave intensities of 12.5-225 mW/cm^2.[163] Mitragotri et al.[162] showed that low frequency ultrasound was much more effective in inducing significant transdermal transport of the above mentioned macromolecules due to the proposed inverse relationship between ultrasound frequency and cavitational effects.[162,164] In addition to cavitation as the primary mechanism of action, it has also been reported that ultrasound causes stratum corneum lipid extraction, which contributes to increased permeability.[165] Tezel at al.[166] investigated the transdermal transport pathways of hydrophilic solutes including peptides, in the range 180–70000 Da, under low-frequency ultrasound. Based on a modified porous pathway model, they concluded that skin porosity could be enhanced by up to 4100-fold by the application of low-frequency ultrasound.[166]

Sonophoresis has also been used in combination with other skin permeation enhancement techniques such as chemical enhancers and electroporation. Liu et al.[167] recently assessed the permeation of cyclosporin A into and across rat skin when applied with low frequency ultrasound in combination with chemical penetration enhancers and electroporation. Permeation into the skin was enhanced with the ultrasound and chemical enhancer combination, but the transdermal delivery across the skin only occurred when applied in combination with electroporation.[167] Transdermal heparin delivery has been achieved by combining low frequency ultrasound with iontophoresis and electroporation. Sonophoretic enhancement of 56-fold was reported when used in combination compared to 15-fold by iontophoresis and 13-fold by ultrasound alone.[168]

Sonophoresis offers promising potential for non-invasive drug administration and commercial sonophoretic units have been developed. The SonoPrep system (Figure 1.12) (Sontra Medical Corp, Franklin, MA) which accelerates skin delivery of lidocaine has been introduced for rapid local anaesthesia. This company is also developing the system for other small and macromolecule applications including vaccine delivery.

Figure 1.12 SonoPrep skin permeation device: rapid local anaesthesia by ultrasound enhanced delivery of lidocaine (Sontra Medical Corp, Franklin, MA)

Another commercially available ultrasound system is the Sonopulse II system which uses ultrasound frequencies of 1.0 MHz - 3.0 MHz. It also allows the possibility of combined therapy, that is, ultrasound associated with electro stimulation. Sonopulse

II Combined Therapy was developed to be used in physical rehabilitation and aesthetics in conditions such as inflammatory rheumatic diseases, inflammatory diseases of superficial skin area, tissue healing etc. In aesthetics, the equipment is indicated for cellulite treatment, localized fat, flaccidity, lymphatic drainage and analgesia.

1.3.3.5 Jet applicators

Jet injectors or needle-less injectors are claimed to be a pain free method of administering drugs to the skin. A number of devices are commercially available to propel powders and liquids into the skin at high velocity. These examples include Ped-O-Jet®, Iject®, Biojector2000®, Medi-jector® and Intraject® for liquids. The Vitajet (Bioject), Biojector (Bioject) and Medi- Jector (Antares Pharma, Ewing, NJ) systems and their associated versions deliver jet injections of proteins in liquid form.[3,169] The PowderMed system, initially known as Powderject® injector, uses a high velocity jet to carry the drug particles to the skin surface (Figure 1.13). The Powderject injector has been reported to successfully deliver testosterone, lidocaine hydrochloride and macromolecules such as calcitonin and insulin[169] The physical properties of the device, velocity of the carrier gas, discharge pressure and particle size dictate the penetration depth achieved by the injector.[170]

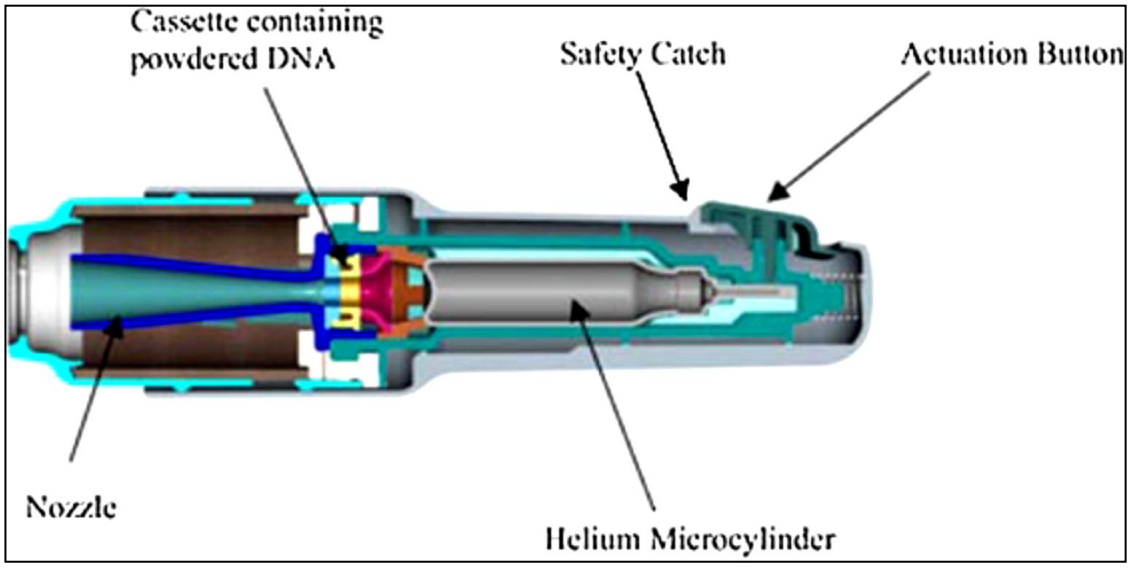

Figure 1.13 PowderMed jet propulsion delivery system

The acceptance of conventional jet injectors has been mixed due to variable reactions in the level of pain experienced at the administration site, with some people experiencing the same level of pain compared to hypodermic needles. In addition,

post injection symptoms have been reported to develop quickly after administration and include mild erythema, hyper-pigmentation, flaking and discoloration at the injection site.[171-173] Other issues faced by needle less injector systems include high developmental costs of both the device and dosage form and the difficulty of controlling drug delivery to compensate for inter subject differences. These devices could be very useful in vaccine delivery to the epidermis where frequent dosing is not required and a much higher level of immune stimulation could be achieved than a traditional injection[174,175]

1.3.3.6 Photomechanical waves

Photomechanical stress waves are generated by impact of high power pulse lasers – LSW on a target material such as polystyrene that is then directed towards the skin surface.[3,176] The waves are broadband (fast rise time), unipolar, compressive and interact with cells and tissue in ways that are different from those of ultrasound. The action of ultrasound is primarily mediated by heat and cavitation[177] whereas photomechanical wave effects are caused by mechanical forces.[178] Studies have shown that photomechanical waves can induce or enhance delivery of molecules across the plasma membrane of cells *in vitro* without loss of viability. It is thought that these waves form a continuous or hydrophilic pathway across the skin.[179] Lee and co-workers[180] assessed the topical transport of a peptide like small molecule 5-aminolevulinic acid (5-ALA) with a single photomechanical wave in humans, to investigate the impact of the wave on the stratum corneum barrier and its recovery *in vivo*. The results showed that a single 110 nano second photomechanical wave increased the permeation of 5-ALA across the stratum corneum *in vivo* and the barrier function recovered within minutes. Lee et al.[181] also demonstrated that a photomechanical wave can facilitate the transport of macromolecules such as dextran and fluorescent latex particles through the stratum corneum into the viable epidermis and dermis in a rat model.[181] Delivery of insulin through the skin of diabetic rats resulted in 80 ± 3% reduction in blood glucose, with the level maintained below 200 mg/dL for 3 h.[182] A design concept for a transdermal drug delivery patch based on the use of photomechanical waves has been proposed by Doukas and Kollias.[183]

1.3.3.7 Microneedles

Transdermal penetration enhancement techniques discussed so far have all dealt with finding ways to alter the stratum corneum temporarily or modify the formulation characteristics. An alternative approach involves creating larger transport pathways of a few µm in dimension using arrays of sub-millimeter needles. These pathways are orders of magnitude higher than the molecular dimensions of most drugs and therefore should readily permit the transport of macromolecules, as well as possibly supra-molecular complexes and microparticles. The microneedle concept of reducing the needle size to only a few hundred microns was proposed in the 1970s[184] and it was demonstrated experimentally only in the early 1990s.[185]

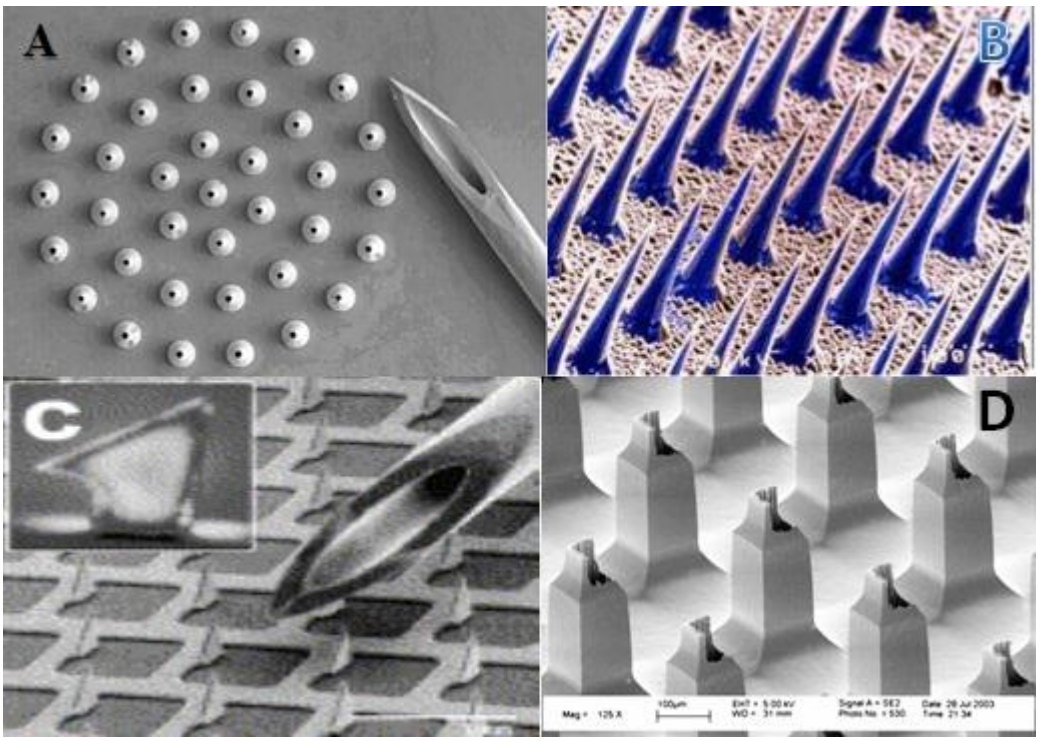

Figure 1.14 Types of microneedles A) and D) Hollow; B) solid and C) coated microneedles[186-188]

Microneedles have been one of the most sought after and extensively studied approaches to transdermal drug delivery. Their sudden rise to prominence can be attributed to the microelectronics industry that provided microfabrication tools needed to make such small structures. The first studies utilizing microneedles for transdermal drug delivery were performed in 1998.[186] Since then a lot of work has been done on microneedle-drug delivery efficacy and safety. It is generally accepted that small holes in the skin are likely to be safe and are considered to be no different to those made by hypodermic needles or accidental cuts and bruises in day-to-day

life.[189] Microneedles are considered to be reasonably pain free as they do not penetrate to the dermis where the sensory nerves are present.[186]

Microneedles are generally shorter than 1 mm in length and very easily breach the stratum corneum barrier. The main challenge microneedle researchers face is from the elasticity of the skin.[190] Hence their length, manner of insertion and the speed at which they are applied govern the shape and size of the pore formed.[191] The amount of time the pores stay open has often been an area of constant debate. While in a publication by Bal et al.[192] the authors claim a fast closure of the pores, other researchers had different opinions. Bal et al. used confocal laser scanning microscopy (CLSM) to visualise the amount of a fluorescent dye present in the pores. Visualisation using CLSM is an easy way to obtain information on geometric parameters of the pores and to monitor the behaviour of a pore and the dye over time. The authors reported a quick closure of the pores as there was a strong decrease of the dye present at the skin surface after 10-15 min.[191,192] Banks et al. utilized transepidermal water loss (TEWL) measurements after microneedle treatment and microscopic visualization to determine pore lifetime. They also measured skin permeability of NTXOL (naltrexone analogue 6-β-naltrexol) over time to determine the pore lifetime. In addition, a staining technique was developed to microscopically visualize microneedle created pores in treated guinea pig skin. Banks et al. concluded that microneedle-assisted transdermal delivery appears viable for at least 48 h after microneedle-application.[193] In a subsequent study they showed that the addition of a COX inhibitor like diclofenac can keep the microneedle pores open for up to a week.[194] It is widely accepted and proved by mathematical modelling that transport of the drug molecules after microneedle application takes place by simple diffusion.[185]

Microneedles are broadly classified into two classes.

a) Solid Microneedles
b) Hollow Microneedles

Solid microneedles (Figure 1.14) can be applied by “poke and patch” or “coat and poke” techniques. The former creates pores with the patch then being applied usually after the microneedles have been removed. The “coat and poke” technique involves insertion of microneedles, with the drug coating then dissolving off the microneedle

surface into the pores. In both cases the microneedles create micron-scale holes in the skin through which molecules can more easily be transported. The first microneedle arrays reported in the literature were etched into a silicon wafer and developed for intracellular delivery *in vitro* by Hashmi et al.[195] Shortly after this work was published, microneedles were developed for transdermal delivery applications to deliver a variety of different compounds *in vitro* and *in vivo*. Mark Prausnitz's group in 1998 was the first to use microneedles for transdermal drug delivery.[186] They used an array of solid microneedles in cadaver skin, which increased the permeability of calcein 3-fold when the microneedle were left in the skin, with the enhancement reported to occur through leakage pathways between the needles and skin. When the needles were removed skin permeability increased by 4-fold.[186]

In vivo studies by Lin et al.[196] used microneedles either alone or in combination with iontophoresis to deliver large oligodeoxynucleotides across the skin of hairless guinea pigs. Microneedle arrays were inserted and an oligonucleotide-loaded gel was applied to the skin. This design incorporated an iontophoretic electrode on top, in most of the cases. Insertion of the microneedles during iontophoresis increased transdermal flux by 100-fold relative to iontophoresis alone. Microneedle pore based delivery was higher (16.18 ± 1.84 µg) when compared to passive diffusion through intact skin (undetectable). Donnelly et al. used silicon microneedle arrays to enhance skin penetration of 5-ALA *in vitro* and *in vivo.* Microneedle treatment before the application of 5-ALA patch led to a significant increase in transdermal delivery of ALA. The authors also showed equivalent therapeutic effect with a significant dose reduction to 2.6 % w/w could be achieved compared to the 20% w/w dose currently used in clinical practise. Microneedles also allowed for shorter application times which could improve patient compliance and clinician convenience.[197]

Microneedles are often fabricated from materials that are prone to breaking, and whilst the literature shows a low incidence of metal needle fracture, brittle microneedles are a safety concern. Park et al.[198] described biodegradable polymers for microneedle fabrication and envisaged they could alleviate issues of safety as any broken needles left embedded in the skin would safely degrade and disappear. Further the disposal of polymer microneedles is also facilitated by the ability to burn, dissolve in a solvent, or mechanically destroy needles to prevent intentional or

accidental re-use.[198] Unlike metal needles the design of dissolving microneedles is governed by a number of inter-dependent material and fabrication constraints, one of which is the need for microneedles to have sufficient strength to be inserted into the skin without mechanical failure.[199]

Raphael et al.[200] introduced a novel method of fabricating arrays of multilayered dissolving nanopatches (dNPs). They achieved improved vaccine efficiency by device miniaturization using microneedles that easily penetrated the skin and upon delivery dissolved within 5 min. Successful delivery and efficient antibody generation was achieved from two vaccines, a model antigen-ovalbumin and Fluvax 2008, a commercial influenza vaccine.[200] The same group demonstrated a coating approach for similar microneedle patches and studied the delivery of a variety of molecules including OVA protein vaccine, DNA, and fluorescent dyes (Figure 14).[201] They also demonstrated that skin delivery by densely packed micro-projections invoked no delay in kinetics, compared to intramuscular injection. The results matched the kinetics achieved by intramuscular injection of liquid vaccine and the vaccines achieved peak serum antibody response within 2 weeks.[202]

Lee et al.[203] proposed a stepwise controlled drawing technique to fabricate sharp dissolving microneedles directly from maltose without moulding. This was achieved by controlling the drawing time and the viscosity of maltose at precisely the right level resulting in sharp conical microneedles of 60 mm tip diameter. After insertion into the skin *in vivo* the microneedles completely dissolved within 20 min. These dissolving microneedles were used to successfully administer the hydrophilic molecules ascorbic acid-2-glucoside and niacinamide that do not passively permeate into the skin.[203] Kommareddy et al.[204] recently described a proof of concept for delivery of unadjuvanted cell culture vaccine using dissolvable microneedle patches.[204]

The coat and poke technique has gained a lot of attention since it was first described in a patent by Cormier et al.(2002).[205] A typical coating process is expected to achieve a coating that is both uniform and reproducible. The coated drug should achieve high drug load and the coating should be controllable in thickness and coating amount. It should ideally release the drug in the skin within minutes after insertion.[206] Cormier et al. later described microneedle-enhanced delivery of desmopressin coated onto the microneedle arrays by partial immersion in aqueous

formulations containing either 24 or 40% by weight of desmopressin and 0.2 % polysorbate 20.[207] Scanning electron microscopy was used for evaluation of coating depth and thickness. An interesting observation was made regarding a significant decrease in drug delivery efficiency upon an increase in drug loading of the microneedle arrays. This behaviour could be partly explained as a product of the increased viscosity of the mixture due to increased drug concentration.

More recent work by Chen et al.[206] utilizes small microneedles (< 200 μm) coated with vaccines in 0.5% of methylcellulose and 0.5% of ovalbumin protein.[206] The method described within, details the coating process at great depth. The roles of the two main components of the coating mixture were the viscosity enhancer, methylcellulose and the surfactant, Quil-A was to serve dual purposes saving the addition of further excipients. In their later work Chen et al. further described the dry coating method. One of the biggest advantages of this coating technique is, unlike dip and coat, the jet stream used to dry the coating solution gives a very even coating and helps avoid the clogging of microneedle arrays. This is of increased value for microneedle arrays that are densely populated and are very small.[188]

Since there advent in the late 1990's various types of microneedles have been fabricated and designed.[185,186,207] Microneedle devices are very hard to standardise. This has been further exacerbated by the need of microneedle innovators to make unique devices with proprietorship in view. Hence an outcome based research methodology that could compare the efficacy of different microneedle devices is required. Gomaa et al.[208] described the effect of variables such as size, shape and microneedle array density on transepidermal water loss (TEWL). They compared microneedles of three different lengths-400 μm, 600 μm and 1000 μm. It was observed that microneedles of all sizes caused an initial sharp drop in barrier function followed by a slow incomplete recovery due to the temporary generation of micro-channels that subsequently contract due to skin elasticity.[208] Multiple insertions had a similar effect, showing a proportionate increase in TEWL with increased number of insertions. Increasing microneedle density suppressed the partial barrier recovery caused by tissue contraction. In early studies it was a common practice to leave the microneedles *in-situ*. This study showed that leaving microneedles embedded in skin reduced the initial post-insertion drop in barrier function but once the microneedles were removed the behaviour was consistent with the general trend.[208]

Bal et al.[191] described the outcomes of different sized microneedles on the permeation of fluorescein.[191] The fluorescence intensity of fluorescein was characterised as high (HIF) or low (LIF). The authors compared areas covered by both HIF and LIF after the application of three different microneedle devices. Commercially available Dermastamp® was compared to microneedle devices developed in house.

Al Qallaf et al. attempted to describe the drug penetration in skin tissues after microneedle delivery using mathematical modelling software-SKIN-CAD®.[209] They described different parameters that must be considered in designing and optimizing any microneedle system including the length of the microneedles, duration of application, surface area of the array system. A small low molecular weight model drug fentanyl was used to calculate various parameters like diffusion coefficient and elimination rate constant in both the stratum corneum and viable epidermis. Hollow microneedles were simulated which were assumed to keep the drug inflow constant.[209] In a later study similar work was done to simulate the penetration of insulin from coated microneedles.[210] This mathematical approach might help design an ideal microneedle system with the correct needle height, density and related parameters.[211] The obvious downside though, is all the calculations made were based on mathematical simulation and the predictions have not been experimentally validated in a systematic way. In their subsequent work they have added variables like the effect of metabolism of drugs taking place in the viable epidermis and compared the penetration of verapamil in skin models.[210]

1.3.4 Stratum corneum ablation

The simplest and easiest way of overcoming the skin barrier is to remove the stratum corneum as this will substantially enhance skin permeation and water loss. A number of techniques have been developed that provide a controlled removal or ablation of the stratum corneum including the application of radiofrequency energy, lasers, and formation of suction blisters.[120]

1.3.4.1 Radio frequency ablation (RF)

RF ablation is a well-known medical technology to eliminate malignant tissues by placing an electrode directly into the tissue. This energy generates movement of ions resulting in frictional heating of the tissue to produce necrosis and cell ablation.[212]

The ViaDerm system is a transdermal delivery technology that consists of a microarray of radiofrequency electrodes. (Figure 1.15) This system creates micro-channels in the epidermis by cell ablation thereby permitting drug diffusion via the micro-channels.[213] The technology has been evaluated for transdermal delivery of small hydrophilic drugs, peptides and genes.[214-216]. The ViaDerm system showed 75% more bioavailability of human growth hormone (hGH) as compared to subcutaneous injection and recently the delivery of 100 nm nanoparticles and gene therapy vectors was demonstrated.[216] It has also been reported that RF application results in 3-5 fold increase in TEWL immediately after application.[215] RF micro-channels only penetrate the outer layers of the skin thus minimizing skin trauma and unpleasant sensations.[217]

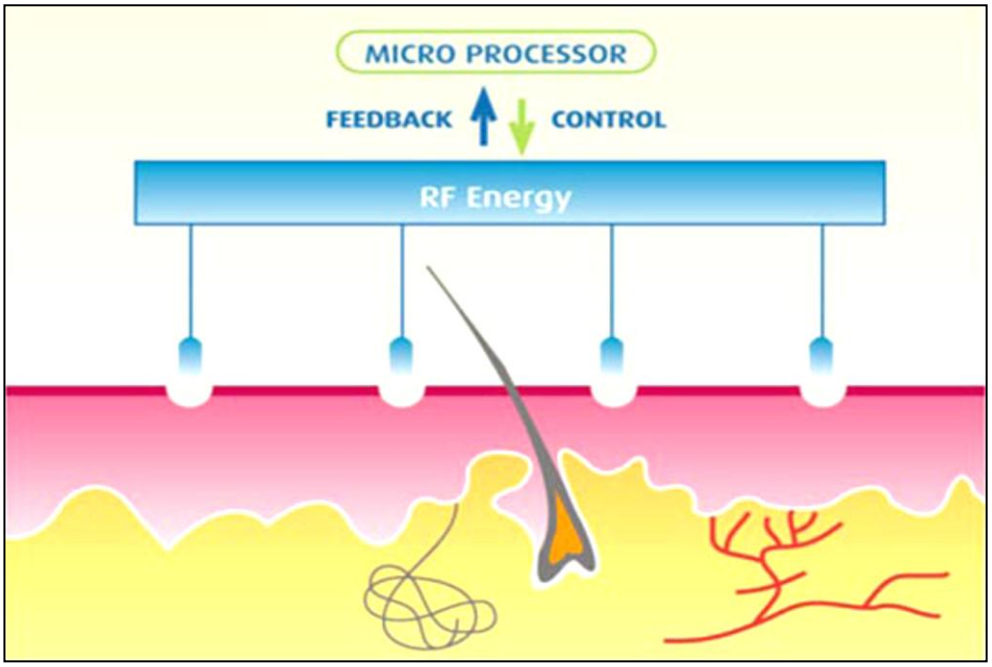

Figure 1.15 Viaderm radiofrequency thermal ablation (TransPharma Medical Ltd)

1.3.4.2 Laser ablation

A high energy laser directed at the skin surface creates pores in the skin to increase permeability to subsequently applied drugs.[3] Application of the technique, using a laser emitting at 2790 nm, to enhance drug delivery was first described by Nelson et al.[212] in 1991. They reported a 2.1 times increase in the permeability coefficient of interferon-ɣ (IFN-ɣ) across pig skin. In a more recent study, Lee et al.[218] reported successful transdermal application of polypeptides and related vaccines using an erbium: yttrium–aluminium–garnet (Er:YAG) laser. The peptide flux across skin

treated with a laser was 3–140 folds higher than that across intact skin. Molecular size, lipophilicity, and peptide sequence influenced permeation. It was also demonstrated for the first time that laser treatment with no adjuvant or penetration enhancer significantly enhanced the production of antibodies in the serum by 3-fold.[218] The technique has been further evaluated with a range of small drugs and macromolecules including insulin.[218,219,220] Pantec Biosolutions have developed P.L.E.A.S.E – Painless Laser Epidermal System, for large molecule drug delivery (www.pantecbiosolutions.com). Although this drug delivery technique may be technically feasible many questions regarding safety remain unanswered and it is likely that laser ablation would be restricted to the clinical setting with limited application.[221]

1.3.4.3 Suction blister ablation

This technique utilizes a vacuum to produce a small blister, the upper surface of which is removed to expose a pathway of low resistance for entry of small and macromolecules into the dermis.[120] The commercial product Cellpatch incorporates all the components of the process: suction device, epidermatome (to remove the blister) and drug reservoir. The device is used to deliver morphine in postoperative pain.[222] Svedman et al.[223] reported the application of the antidiuretic peptide 1-deamino-8-D-arginine vasopressin using Cellpatch with close to 100% bioavailability in healthy human subjects with recovery of the skin spot to normal after 6 weeks.[223] This technique is a multi-step process and it is unlikely to be convenient for routine use by patients or clinicians and hence may not progress further for peptide delivery.[120]

1.3.4.4 Thermal poration

Thermal methods have been used to locally heat and ablate holes in the stratum corneum thereby increasing skin permeability by formation of aqueous pathways across the stratum corneum.[185] The technology has been patented[224] and is being developed by Altea Therapeutics under the terminology of PassPort Patch (www.alteatherapeutics.com). This approach has been used to deliver conventional drugs[215] and DNA vaccines[225] to animals, and to extract interstitial fluid glucose from human subjects.[226] Badkar et al.[227] used this technology to deliver interferon α-2b through microporated skin. It was shown that interferon could not be delivered

through intact skin or even with iontophoresis, but was only delivered when these micropores were created in the skin. In another study, a 10 –100 fold greater cellular and humoral immune response was reported following topical application of an adenovirus vaccine to thermally microporated mouse skin as compared to intact skin.[225]

Methods that pierce micron-scale holes in skin, such as thermal poration and jet injection have the potential to dramatically increase transdermal delivery of small drugs and macromolecules, but more work is needed to establish safety/skin damage and cost effectiveness.[185]

1.3.5 Peptides as potential therapeutic and cosmetic agents

A number of peptides of differing molecular weights and chain lengths have been identified for their therapeutic or cosmetic potential in the skin.

1.3.5.1 Bioactive peptides as cosmeceuticals

Proteins and peptides play an important role in skin health as structural components of the skin as well as activators, regulators or inhibitors of certain biochemical processes occurring in the skin.[228] They are also important in many natural processes with relevance to skin care, such as the modulation of cell proliferation, cell migration, inflammation, angiogenesis, melanogenesis, and protein synthesis and regulation.[229] With variations in amino acid sequence, number of amino acids and derivatives thereof the array of possible peptides is almost limitless.[230] Cosmeceuticals are topically applied cosmetic products that deliver beneficial biological activity in support of cosmetic claims.[231,229] Peptides as cosmeceuticals is a fast-growing segment of the personal care industry with an increasing trend towards the use of these agents in skin care regimens for protection from radiation and oxidant damage.[232] As a result bioactive peptides that are beneficial have been increasingly used and many more are in the development pipeline.[229] There are numerous cosmeceutically active products on the market which can be broadly classified into the following categories: antioxidants, amino-peptides, growth factors, anti-inflammatories, polysaccharides and pigment lightning agents.[231] Some examples of peptides used as cosmeceuticals include copper peptides, amino-peptides, acetyl hexapeptide-3 and dimethylaminoethanol.[231]

A number of peptides play various roles in skin aging. GHK is a tripeptide that has a strong affinity for copper, so it is often called copper peptide or GHK-Cu. Copper peptides such as GHK-copper complex are included in products to improve skin firmness and texture, fine lines and hyperpigmentation. Both the tripeptide alone and the copper-tripeptide complex have been found to have beneficial effects on collagen stimulation.[233] Pal-KTTKS is a collagen peptide fragment, and there is evidence in wound healing that it may penetrate into the dermis and stimulate collagen production. Pal-KTTKS, marketed as Matrixyl (Sederna, France), is an amino acid chain (KTTKS) linked to a fatty acid (palmitoyl) to enhance its lipophilicity, and is an ingredient in a number of cosmeceuticals.[231] Pal-KTTKS was well tolerated and significantly reduced fine lines by both qualitative technical and expert grader image analysis in a 12-week, double-blind, placebo-controlled, split-face, randomized clinical study of 93 Caucasian women between 35 and 55 years of age.[234]

Acetyl hexapeptide-3 marketed as Argireline® (Lipotec, S.A.) is another popular synthetic peptide that has a botox-like effect.[235] When tested in an open label trial it showed improvement in periorbital rhytides (wrinkles on the face and near eyes) an effect that was claimed to be due to its muscle-relaxing effects.[236] Tripeptide-3 (β-Ala-Pro-Dab-NHbenzyl$_2$ AcOH), currently marketed as Syn®-Ake (Lipotec S.A.), is proposed to act similarly to Walglerin-1. Walglerin-1 (Pentapharm, Switzerland) is a neurotoxin found in the venom of the temple viper, which causes reversible antagonism of muscular nicotinic acetylcholine receptors (mnAChR) at the postsynaptic membrane decreasing muscle contraction and reducing wrinkle depth.[233] Similarly, palmitoyl hexapeptide-6, a peptide designed using an innate immunity peptide template (Grant Industries, Elmwood, NJ) stimulates fibroblast proliferation and scaffolding, collagen synthesis, and cell migration, and is currently marketed for inclusion in anti-wrinkle skin care products. Dipeptide-2 (Val-Trp) is believed to improve lymphatic circulation and is used in eye creams for dark circles and puffy eyes. The peptide's structure resembles that of the lipid content of the epidermis and is considered to be a natural moisturizing factor as it helps in the skin's healing process and prevents dermal irritation.[237]

A number of patents have been filed on the use of peptides for cosmetic products. These include a patent describing topical composition containing the tetrapeptide Arg-Ser-Arg-Lys for reducing wrinkles. This tetrapeptide is a fibroblast growth

factor derived peptide which decreases cellular activity.[238] Another patent describes the use of sirtuin 6 activating peptides, derived from highly conserved regions of human SIRT proteins, in a cosmetic composition to prevent and/or treat the cutaneous signs of aging and photo aging.[239] Carnosine (β-alanyl-L-histidine) and related naturally occurring histidine containing dipeptides such as anserine, exhibit anti-oxidative properties by quenching free radicals.[240-242] Carnosine also accelerates healing of wounds and ulcers and is reported to act as an anti-ageing peptide.[240, 242] It is speculated that the dipeptide may participate in the repair of protein isoaspartyl groups. These new observations only add to the enigma of carnosine's real *in vivo* functions and warrant further experimentation.[243]

Substantial patent activity has been found in the area of chemically modified peptides for healing, hydrating and improving skin appearance. A combination of peptides with the general sequence X-Thr-Thr-Lys-Y was reported to have activity against the formation or deterioration of wrinkles.[244] Cosmetic compositions with at least one ceramide compound and one peptide attached to a fatty acid chain have been formulated. Ceramides and their analogues have been known to protect and repair skin or hair fibres from damage caused by various agents and hair treatments by providing a barrier effect which minimizes the leakage of proteins.[245]

1.3.5.2 Bioactive peptides as dermatologicals (in skin diseases)

Bioactive peptides play an important role in maintenance of dermal integrity. Human skin is known to produce some antimicrobial peptides (AMPs) that form an innate epithelial chemical shield.[246] Many AMPs have recently been isolated such as lysozyme, RNase[247], elafin, psoriasin, dermicidin (DCD) 1L, granulysin, antileukoprotease and human cationic antimicrobial protein (hCAP18).[247,248] In addition to their antimicrobial function, endogenous peptides are also involved in extracellular matrix (ECM) remodelling and stimulation of collagen synthesis. Katayama et al.[249] identified the activities of small peptide fragments within procollagen I resulting in the identification of the sub fragment KTTKS capable of stimulating the production of both collagen and fibronectin.[249] Sederma later marketed this peptide in its lipidated form as palmitoyl pentapeptide-3 (Matrixyl) for cosmetic formulations, as noted above.[229]

Wound healing is a localised process which involves a series of specific and coordinated events such as inflammation, wound cell migration and mitosis, neovascularisation, and regeneration of the extracellular matrix (ECM).[250,251] Wound healing properties have been attributed to many endogenous and non-endogenous peptides such as cathilicidin LL-37[252], HB-107, and a derivative of cecropin B.[253] Polypeptide growth factors such as epidermal growth factor (EGF) and transforming growth factor-α (TGF-α) play a pivotal role in normal wound healing in tissues such as skin, cornea and the gastrointestinal (GI) tract.[12] Copper peptides also have a positive influence on the growth and regulation of hair follicles, and when used on wounds increase collagen disposition, tensile strength and angiogenesis in healing tissues.[254]

Another area where endo and exogenous peptides could find application is in the treatment of skin diseases such as atopic dermatitis (AD) and psoriasis. AD is a chronic inflammatory skin disease with abnormal (usually reduced) expression or processing of AMPs and patients demonstrate increased susceptibility to bacterial and viral super infection of the involved skin[255] Early treatment with microbial probiotics may be beneficial by boosting Th1 immune responses in AD. Other approaches include cytokine modulation (e.g. TNF-α inhibitors), blocking inflammatory cell recruitment by using chemokine receptor antagonist, inhibition of T cell activation, and the use of synthetic AMPs. Restoration of innate peptides to normal levels via external application could provide significant benefit.[12,229]

Psoriasis is a skin condition of unknown aetiology that is characterised by epidermal hyperplasia, vascular alterations and inflammation.[256] Genetic factors are thought to be one of the important causes for the expression of this disease. In addition, cytokines, growth factors and arachidonic acid derived mediators are potential candidates with a pathogenic role in cutaneous inflammation.[256,257] Peptides and proteins such as elafin and psoriasin are highly upregulated in psoriatic skin.[256,258] It was shown in clinical trials that the Peptide T analogue, DAPTA cleared psoriasis lesions and significantly inhibited the monocyte and lymphocyte chemotactic properties of RANTES (a beta chemokine found in increased amount in psoriatic lesions). A better understanding of the role of these peptides may provide new strategies for the treatment of diseases like psoriasis.[259]

Peptides and proteins also play an important role in melanogenesis. The synthesis and distribution of melanin contributes to skin and hair colour; however, increased levels of epidermal melanin synthesis can darken the skin and cause cosmetic problems. Melanocyte-inhibiting factor (also known as Pro-Leu-Gly-NH_2, Melanostatin, MSH release-inhibiting hormone or MIF-1) is an endogenous peptide fragment derived from cleavage of the hormone oxytocin.[260] MIF-1 has anti-depressant[261], nootropic[262] and anti-Parkinsonian effects, and has been investigated for various medical uses. The peptide crosses the blood-brain barrier easily, though it is poorly active when administered orally. In their search for active metabolites Ishihara et al.[263] isolated a microorganism from a soil sample to produce an active compound, which they designated melanostatin.

Melanostatin is a novel pseudo-tripeptide with a molecular formula of C19H25N5O5 and is structurally related to feldamycin. Melanostatin inhibited melanin formation in *Streptomyces bikiniensis* NRRLB-1049 and B16 melanoma cells. A patent filed in 2011, describes a "one-step" process for production of esters and acetylated forms of peptides such as tripeptide thyroliberin (TRH) and melanostatin (MIF), and other organic molecules. This chemical modification approach improved metabolic properties leading to increased efficiency for therapeutic and cosmetic purposes including oral, transdermal, sublingual, buccal, and topical administration.[264] The use of α-MSH (melanocyte-stimulating hormone) analogues that function as MC1-R agonists has been investigated for potential topical agents to prevent skin photo-carcinogenesis. In cultured human melanocytes, tetrapeptide α-MSH analogues, Ac-His-D-Phe-Arg-Trp-NH_2, N-pentadecanoyl and 4-phenylbutyryl-His-d-Phe-Arg-Trp-NH_2, were more potent than α-MSH in stimulating the activity of melanogenesis, reducing apoptosis and release of hydrogen peroxide, and enhancing repair of DNA photoproducts in melanocytes exposed to UV radiation.[265] Melanostatin-5 (Aqua-Dextran-Nonapeptide-1), is a new skin lightening biomimetic peptide. This peptide acts as a α-MSH antagonist thus preventing and lightening hyperpigmentation.[266] Melanostatin-5 produces noticeable skin lightening by at least 33% when formulated into a lightening product, and showed continued improvement over time.

Rigin, an immunostimulating tetrapeptide (Gly-Gln-Pro-Arg) that connects the CH_2 and CH_3 domains of human immunoglobulin G (IgG) molecule, has been shown to exhibit significant *in vitro* phagocytosis stimulating activity toward rat blood

leukocytes and *Staphylococcus aureus*.[267] Synthesis of rigin was first described in 1981 by Veretennikova et al.[268] Later Rocchi et al.[269] synthesised modified analogues of rigin with D-gluconic acid or 2-amino-2-deoxy-D-glucopyranose linked to the parent molecule through amide bonds. These compounds however where found to be ineffective *in vitro*. The down regulation of inflammatory mediators such as Interlukin-6 (IL-6) by rigin can produce increased skin firmness, smoothness, and elasticity.[229,270] Palmitoyl tripeptide (Pal-KVK) improves micro circulation, increasing the oxygen supply to tissues, strengthening and protecting the integrity of elastin and collagen in the skin by inhibiting elastase and collagenase activity. Its benefits include reduction of puffiness and dark circles around the eyes and a softening of fine lines and wrinkles.[271]

1.4 Significance

Enhanced skin delivery by the carrier conjugation approach using diketopiperazines (DKP) as proposed in this research would offer new opportunities in cosmetic and dermatological applications. CPPs have the potential to change the world of pharmaceutics as we know it today.[84] This strategy will be of particular importance for molecules with poor skin penetration profile that could offer novel therapeutics. DKPs are heterocyclic scaffolds in which diverse cargos of active molecules can be introduced and stereochemically controlled at up to four positions and DKPs can be prepared from readily available α-amino acids using very robust chemistry.[103]

Over the past few years since first described by Henry et al.[186], a variety of different microneedle designs have been fabricated using materials such as silicon, metals and polymers.[186,187] In this project fluorescent model molecules were used to look at a time correlation upon microneedle delivery. The peptides used for this were very well studied molecules with a multitude of applications. We believe that by delivering functional amounts of these peptides deep within skin we can unlock their true therapeutic potential. Consequently, we investigated microneedle facilitated delivery of melanostatin, rigin and Pal-KTTKS.

Magnetophoresis was investigated in *in vivo*, *ex vivo* and *in vitro* studies. Further, synergistic effects of microneedles with magnetophoresis were investigated. The proprietary magnets used in this PhD can be very easily developed into transdermal patches with the capacity to deliver a wide range of molecules from a suitable

reservoir. Further, we hope to throw more light on this very bleakly understood subject by undertaking mechanistic studies that can enable us to be better equipped to comment on the mechanism of magnetophoresis.

1.5 Objectives

The overall objective of this research was to investigate novel technologies for the enhanced transdermal delivery of peptides, particularly those with therapeutic or cosmetic application in skin. Despite the increasing importance of peptides and protein therapeutics and vaccines, the need to deliver them by hypodermic injection remains a major limitation.[272] Peptides are rapidly cleared from the bloodstream, can be of large molecular size and tend to undergo aggregation. Moreover peptides are vulnerable to proteolytic attack and denaturation.[1] Delivery of protein drugs through the skin is an attractive alternative to needles, but requires overcoming significant challenges.

The major objective of this research was to assess three enhancement strategies 1. Cell penetrating peptides; 2. Microneedles; and 3. Magnetophoresis for the delivery of small and high molecular weight peptides and model molecules for cosmetic and therapeutic uses. The project was divided into following parts:

- Assessment of transdermal penetration of a novel class of cell penetrating peptide-DKPs
- Assessment of the ability of DKPs to carry small therapeutic cargo, through and into human skin
- Assessment of the therapeutic activity of conjugated cargo, with the use of appropriate enzyme assays
- Assessment of transdermal penetration of model fluorescent molecules after microneedle based delivery
- Assessment of transdermal penetration of model molecules under the influence of magnetic field generated by proprietary small fixed magnets, exploration of possible synergism with the use of microneedles
- Explanation and comments on possible modes of magnetophoretic delivery in skin

Chapter 2

Permeation of Cell Penetrating Peptides and their Influence on the Permeation of Diclofenac and a Dipeptide through Human Skin

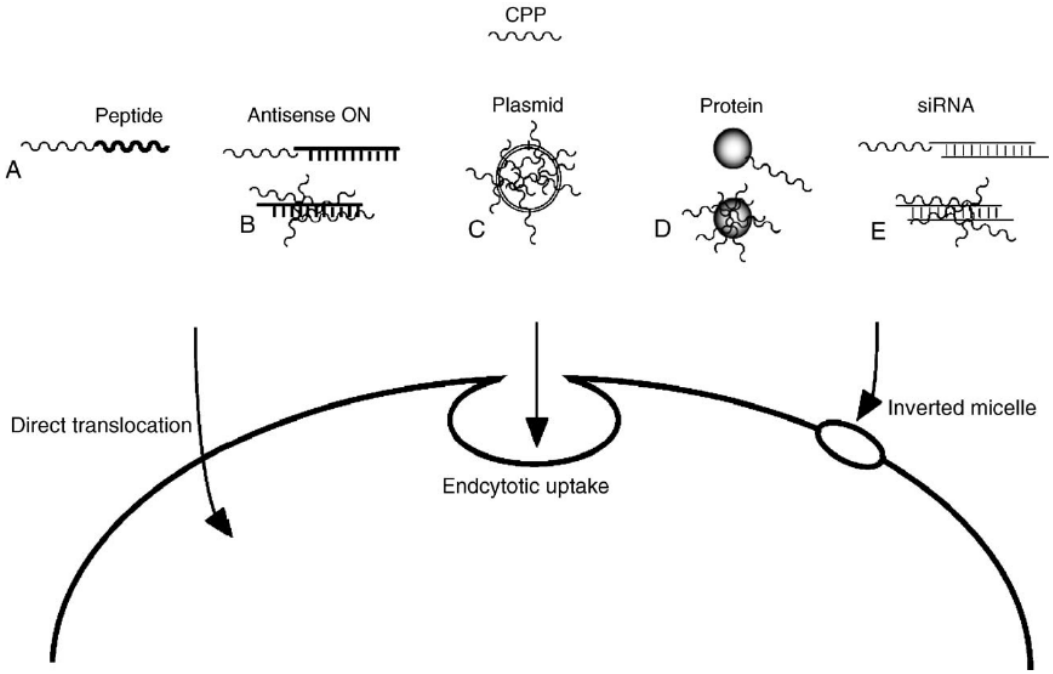

*"The peptides named **Cell Penetrating Peptides** vary greatly in size, amino acid sequence, and charge, but share the common feature that they have the ability to rapidly translocate membranes and enable delivery across it"*[74]

2.1 Introduction

Considerable research effort has been focussed on the development of skin penetration enhancement techniques primarily directed at overcoming the stratum corneum barrier. However, many of these techniques have been limited by insufficient penetration enhancement and/or induced irritancy. To date none of these approaches have been sufficiently useful in the topical/transdermal delivery of peptides and proteins, though low molecular weight drugs have been transported with some success.[273] To circumvent the problems of poor permeability, studies have been focused on improving the chemistry of these molecules, and several carrier-mediated delivery systems have recently been developed. A suitable drug carrier should [274]

- be biodegradable and biocompatible
- lack intrinsic toxicity and antigenicity
- show no accumulation in the body
- bear adequate functional groups for chemical fixation
- retain the original specificity for the target
- maintain the original activity of the delivered drug until it reaches the site of action

In this study we are going to embark upon a novel skin penetration enhancement technique- diketopiperazines (DKP) as cell penetrating peptides. Several cell penetrating peptides including HIV-1-Trans-Activator of Transcription (TAT), polyarginine and penetratin, which were initially identified for delivering drugs into the cytoplasm of cells, have been tested for penetration across the stratum corneum and a few have shown some efficacy in delivering small molecules into epidermis.[107,108,112 275]

Two strategies have been described to date; the first one requires chemical linkage between the drug and the carrier for cellular drug internalization, and the second is based on the formation of stable complexes with drugs, depending on their chemical nature.[274] In this research project I have studied both these approaches. The various mechanisms of action, uses and pharmacokinetics of cell penetrating peptides have been discussed elaborately in the first chapter. Despite enormous gaps in the

understanding of the topic, experiments continue to demonstrate the highly desirable features of cell penetrating peptides.[276]

2.2 Aims of the project

The aim of this project was to investigate the permeation and retention of cell penetrating peptides in human skin and to investigate their ability to enhance the delivery of an active molecule into the skin. The project was divided into four parts as detailed below:

1) Determination of the permeation into and through human epidermis of the cell penetrating peptides diketopiperazine (DKP) and HIV-1-Trans-Activator of Transcription (TAT).
2) Determine the influence of DKP on the skin penetration of two compounds: the non-steroidal anti-inflammatory drug, diclofenac and the dipeptide, Ala-Trp when applied as a physical admixture.
3) Conjugation of DKP with diclofenac and determination of the skin penetration and accumulation of the conjugate in human skin.
4) Determination of the skin penetration and accumulation of TAT conjugated to diclofenac.
5) Determination of the COX-2 inhibition activity of diclofenac and DKP-diclofenac conjugate using a specific enzyme assay kit.

2.3 Materials and Methods

2.3.1 Chemicals

Diketopiperazine (DKP: N-MePhe-N-MePhe; molecular weight = 359.44 g/mol) was synthesised at the University of Barcelona (in collaboration with Dr Teixidó and Prof Giralt). Alanine-Tryptophan (Ala-Trp), a model dipeptide with a molecular weight of 275.30 Da and diclofenac a model non-steroidal anti-inflammatory drug (NSAID) with a molecular weight of 318.13 Da were purchased from Sigma Aldrich (USA). TAT and TAT-diclofenac were synthesised by GLS Pharma (China). Propylene glycol (PG) and dimethyl sulphoxide (DMSO) were obtained from BDH Chemical pvt Ltd and Ajax FineChem respectively. Acetonitrile, HPLC solvent was supplied by JT Baker (USA) and phosphate buffered saline solution (PBS) was prepared

according to the United States Pharmacopoeia. COX enzyme assay kit was purchased from Cayman Ltd USA.

2.3.2 Synthesis of DKP and DKP-diclofenac

The following information describing the synthesis, purification and validation of the peptides was supplied by Professor Earnest Giralt and Dr. Meritxell Teixido's group at the University of Barcelona. A first library of 15 DKPs with distinct side chains was prepared using a solid-phase methodology (Figure 2.1, Scheme 1). For most cases, the only purification required was a de-salting step. The side chains were chosen in order to explore the effect of adding or removing a methylene group, adding a nitrogen or oxygen atom, and adding a larger aromatic ring or a hydrophobic, but not aromatic, side chain. All DKPs in this first library were characterized by HPLC, HPLC-MS, and MALDI-TOF MS. All were obtained with purity higher than 90%. The DKP selected for further skin delivery studies was DKP-2Nal-N-MePhe (Figure 2.2)

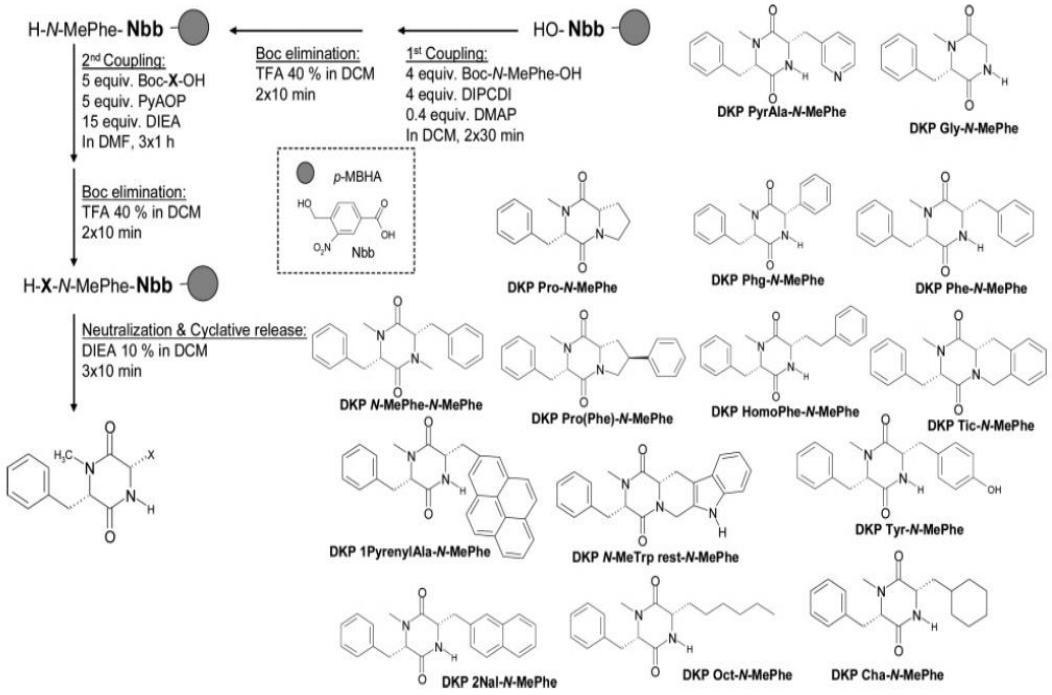

Figure 2.1 Synthesis of DKP library (scheme 1)

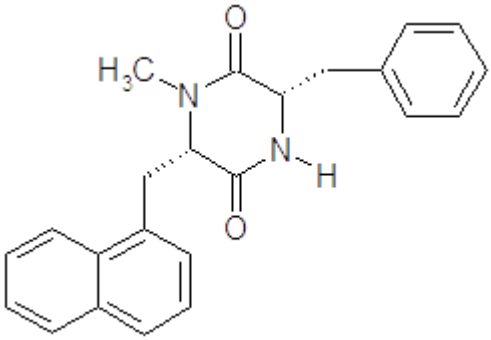

Figure 2.2 Chemical structure of DKP-2Nal-N-MePhe

The conjugation of DKP with diclofenac was carried out in a similar approach as the synthesis of DKP library (Figure 2.3, Scheme 2). The main difference was the use of Fmoc protected starting material instead of Boc protected. The synthesis was carried out to first construct the intermediate DKP-2Nal-N-MePhe, followed by a coupling reaction to add diclofenac. The purification was achieved by filtration and solvent evaporation under pressure (N_2) to yield DKP-diclofenac (Molecular weight = 652.60 g/mol) (Figure 2.4)

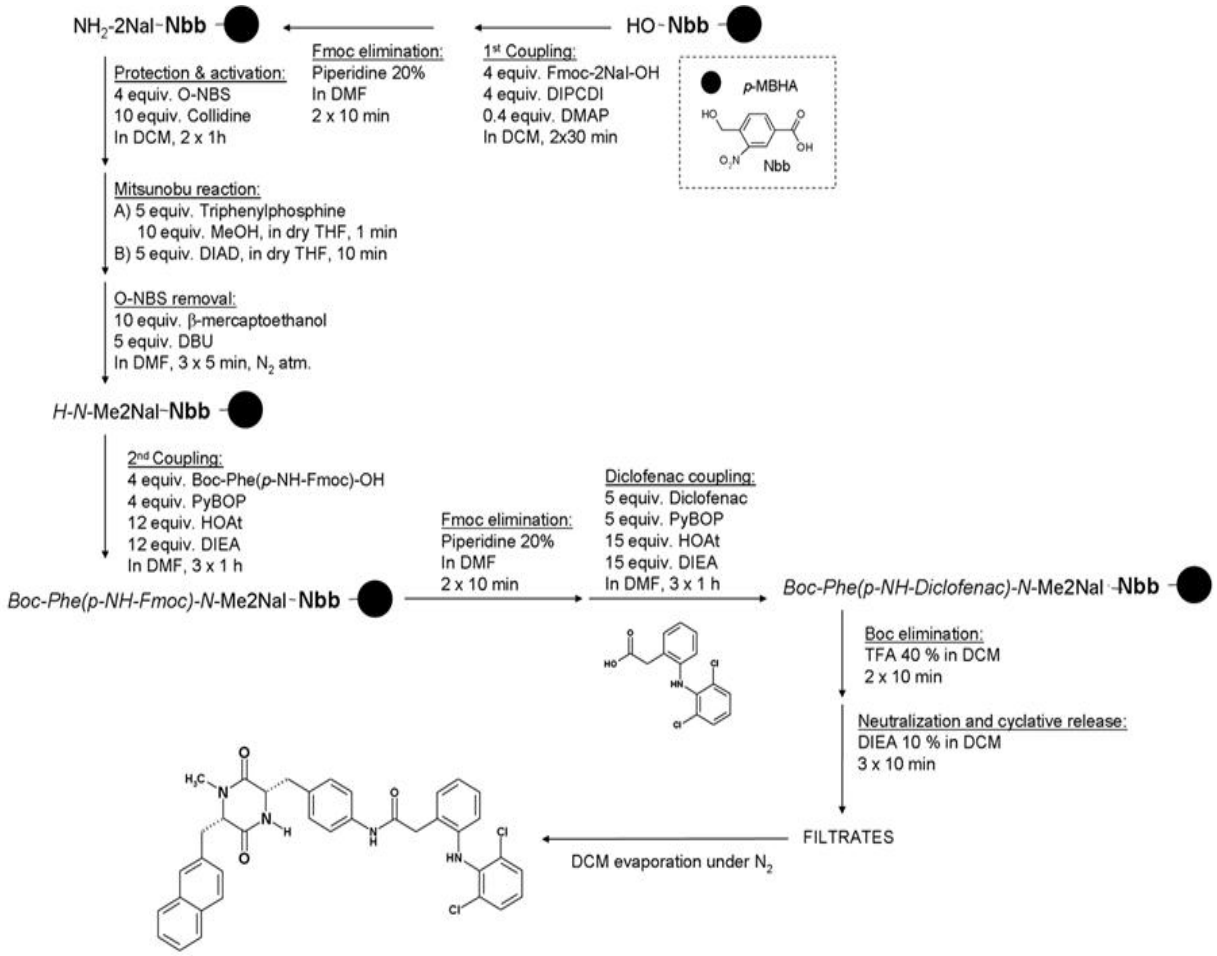

Figure 2.3 Synthesis of DKP-diclofenac (scheme 2)

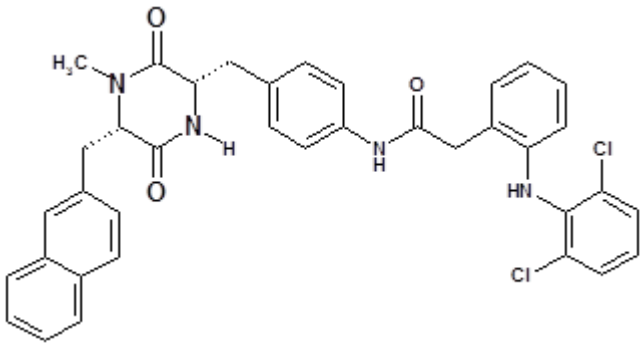

Figure 2.4 Chemical structure of DKP-diclofenac

2.3.3 Synthesis of TAT and TAT-diclofenac

Synthesis of TAT (Gly - Arg - Lys - Lys - Arg - Arg - Gln - Arg - Arg - Arg - Pro - Pro - Gln - Cys -NH_2) and TAT-diclofenac was carried out by a commercial laboratory based in China (GLS Biochem). HPLC and MS-MALDI data provided by

the suppliers was then revalidated in our laboratory. The diclofenac molecule was attached to the TAT peptide through an amide linkage at the N-terminus.

2.3.4 HPLC instrumentation and conditions

The samples obtained after *in vitro* skin permeation studies were analysed by reverse phase HPLC Agilent 1200 system which consisted of a binary pump (G1312A), autosampler (G1329A), degasser (G1379B) and photo diode array detector (G1365B). Separation was achieved on a Phenomenex Jupiter C18, 300 A column (5 μm, 4.6 mm×150 mm). Integration was undertaken using Chemstation software. The elution conditions for each of the compounds are outlined separately.

2.3.4.1 DKP

Elution was performed at ambient temperature using a mobile phase gradient with a flow rate of 1 mL/min and the wavelength of detection was 220 nm. Buffer B was 0.036% TFA in acetonitrile and Buffer A was 0.045% TFA in water. The peptide was eluted using a linear gradient protocol; Buffer B was held at 10% for 5 min followed by a linear gradient from 10 to 100% buffer B over 10 min. All samples were analysed by HPLC using injection volumes of 20 μL.

2.3.4.2 DKP-diclofenac

Elution was performed at ambient temperature using a mobile phase gradient at a flow rate of 1 mL/min and the wavelength of detection was 278 nm. Buffer B was 0.036% TFA in acetonitrile and Buffer A was 0.045% TFA in water. The peptide was eluted using a linear gradient protocol; Buffer B was held at a linear gradient from 10 to 100% buffer B over 10 min.

2.3.4.3 Ala-Trp

Elution was performed at ambient temperature using a mobile phase gradient at a flow rate of 1 mL/min and the wavelength of detection was 215 nm. Buffer A was 0.1% TFA in water and Buffer B was 0.1% TFA in acetonitrile. The dipeptide was eluted using a combination of isocratic and linear gradient protocol; Buffer B was held at 10% for 5 min followed by a linear gradient from 10 to 100% buffer B over 10 min.

2.3.4.4 Diclofenac

Elution was performed at ambient temperature using a mobile phase gradient at a flow rate of 1 mL/min and the wavelength of detection was 278 nm. Buffer A was 0.036% TFA in acetonitrile and Buffer B was 0.045% TFA in water. The peptide was eluted using a linear gradient protocol; Buffer B was held at a linear gradient from 10 to 100% over 10 min.

2.3.4.5 TAT

Elution was performed at ambient temperature using a mobile phase gradient at a flow rate of 1 mL/min and the wavelength of detection was 220 nm. Buffer A was 0.1% TFA and Buffer B was 0.1% TFA in acetonitrile. The peptide was eluted using a linear gradient protocol; Buffer B was held at a linear gradient from 10 to 100% over 22 min.

2.3.4.6 TAT-diclofenac

Elution was performed using a mobile phase gradient at a flow rate of 1 mL/min and the wavelength of detection was 220 nm. Buffer A was 0.1% TFA and Buffer B was 0.1% TFA in acetonitrile. The peptide was eluted using a linear gradient protocol; Buffer B was held at a linear gradient from 93 to 0% over 27 min.

2.3.5 HPLC analysis and validation

2.3.5.1 Linearity

A 1 mg/mL stock solution of all peptides, conjugates and models drugs was prepared by dissolving 5 mg of the compound in 5 mL of 25:75 propylene glycol (PG): phosphate buffered saline (PBS). Linear dilution was performed using PG:PBS and calibration curves were obtained using 1.95, 3.9, 7.81, 15.62, 31.25, 62.5 and 125 μg/mL for DKP; 1.56, 3.125, 6.25, 12.5, 25 and 50 μg/mL for Ala-Trp; 3.9, 7.81, 15.62, 31.25, 62.5, 125 and 250 μg/mL for DKP-Ala-Trp physical admixture; 3.9, 7.9, 15.6, 31.25, 62.5 and 125 μg/mL for diclofenac; 3.9, 7.9, 15.6, 31.25, 62.5 and 125 μg/mL for DKP-diclofenac physical admixture; 3.9, 7.81, 15.62, 31.25, 62.5, 125 and 250 μg/mL for DKP-diclofenac conjugate; 3.25, 6.5, 13, 26, 52 and 104 μg/mL for TAT; 7.81, 15.62, 31.25, 62.5, 125 and 250 μg/mL for TAT-diclofenac conjugate. Linearity (quoted as R^2) was evaluated by linear regression analysis, which was calculated by the least square regression method.

2.3.5.2 Precision

The precision of the assay was determined by injecting three standard concentrations of 1.95, 15.6 and 62.5 μg/mL DKP; 1.56, 6.25 and 50.0 μg/mL Ala-Trp; 3.9, 15.6 and 62.5 μg/mL DKP-Ala-Trp physical admixture, diclofenac, DKP-diclofenac physical admixture and DKP-diclofenac conjugate; 3.25, 13.0 and 52.0 μg/mL TAT; 7.81, 31.25 and 125 μg/mL TAT-diclofenac conjugate six times on the HPLC.

2.3.5.3 Intra-day repeatability

The intra-day repeatability was assessed by injecting 1.95 and 15.62 μg/mL DKP; 1.56 and 12.5 μg/mL Ala-Trp; 3.9 and 15.6 μg/mL DKP-Ala-Trp physical admixture, diclofenac, DKP-diclofenac physical admixture and DKP-diclofenac conjugate; 3.25 and 13.0 μg/mL TAT; 7.81 and 31.25 μg/mL TAT-diclofenac standards six times at different times in a day.

2.3.5.4 Inter-day repeatability

The inter-day repeatability was determined by injecting 1.95 and 15.62 μg/mL DKP; 1.56 and 12.5 μg/mL Ala-Trp; 3.9 and 15.6 μg/mL DKP-Ala-Trp physical admixture, diclofenac, DKP-diclofenac physical admixture and DKP-diclofenac conjugate; 3.25 and 13.0 μg/mL TAT; 7.81 and 31.25 μg/mL TAT-diclofenac conjugate standards six times on 3 different days. The intra and inter-day repeatabilities were quoted as the coefficient of variance.

2.3.5.5 Lower limit of detection (LOD)

The minimum detectable and quantifiable limits (LOD and LOQ) were measured by diluting the stock solution of DKP, Ala-Trp, diclofenac, physical admixture of Ala-Trp and diclofenac with DKP, DKP-diclofenac conjugate, TAT and TAT-diclofenac conjugate with 25:75 PG:PBS to give a concentration range from 1.56 to 250 μg/mL and then injected on the HPLC. The LOD was calculated as greater than 3 times the baseline noise level by the following formula: LOD = 3 × standard deviation of peak area of standard / slope.

2.3.5.6 Lower limit of quantification (LOQ)

The LOQ was calculated as 10 times the baseline noise level. The LOQ was calculated by the following formula: LOQ = 10 × standard deviation of peak area of standard / slope.

2.3.6 Human skin preparation

Full thickness human skin samples excised from female patients (26-48 year old female abdominal sections were used in the present study) undergoing abdominoplasty at Perth hospitals were refrigerated immediately after surgery. Sampling was approved by the Human Research Ethics Committee of Curtin University (Approval numbers HR132/2001, HR 70/2007 and HR 129/2008) and was conducted in compliance with the guidelines of the National Health and Medical Research Council of Australia. The following procedure was used to obtain epidermal sheets. The subcutaneous fat was removed by dissection, the full thickness skin then immersed in water at 60°C for 1 min, allowing the epidermis to be teased off the dermis.[277] The epidermis was placed between two sheets of Parafilm^{TM} and then onto an aluminium foil, air dried, then placed in a zip-lock bag and stored at –20°C until required. Skins from different donors were used to account for reproducibility.

2.3.7 Skin permeation experiments to determine effect of cell penetrating peptides

2.3.7.1 Skin hydration

Skin hydration can improve the delivery of drugs across the continuous stratum corneum. This was investigated by hydrating the epidermal membranes to be used in the diffusion study with phosphate buffered saline (PBS) for 0.5 h and overnight. Epidermal membranes were placed between the donor and receptor compartments of a Franz cell (Figure 2.5) and allowed to equilibrate overnight (up to 10 h) with the receptor solution (PBS pH 7.4). Before the start of the experiment, PBS was withdrawn and a fresh sample of pre-equilibrated receptor medium at 37°C was replaced in the receptor compartment.

2.3.7.2 In vitro skin diffusion studies

In vitro permeation studies across human epidermis were performed in Pyrex glass Franz-type diffusion cells (enabling permeation across skin sections of cross sectional area 1.18 cm^2; receptor volume approximately 3.5 mL: Figure 2.5). Epidermal membranes were placed between the donor and receptor compartments and allowed to equilibrate for 0.5 h or overnight with the receptor solution (PBS pH 7.4) that was stirred continuously with a magnetic stirrer bar. The receptor

compartment of the cell was immersed in a water bath at 37±0.5°C. PBS (1 mL) was placed in the donor compartment, allowed to equilibrate for 1 h or overnight and the conductivity across the epidermis was measured using a digital multimeter to determine membrane integrity. Membranes exhibiting an electrical resistance of less than 20 kΩ were rejected from the study. The PBS solution was then removed from the donor and receptor compartments and the receptor refilled with approximately 3 mL of fresh pre-warmed 25:75 PG:PBS. The donor solution, which consisted of 300 µL of either 150 µg, 300 µg or 1500 µg cell penetrating peptide (DKP or TAT), physical admixture of cell penetrating peptide and active, or conjugated cell penetrating peptides to the active in 25:75 PG:PBS, was added. Two hundred µL samples of the receptor phase were withdrawn and replaced with an equal volume of fresh pre-warmed (37°C) 25:75 PG:PBS over a 24 h period to maintain sink conditions. The active content in the samples was determined using HPLC.

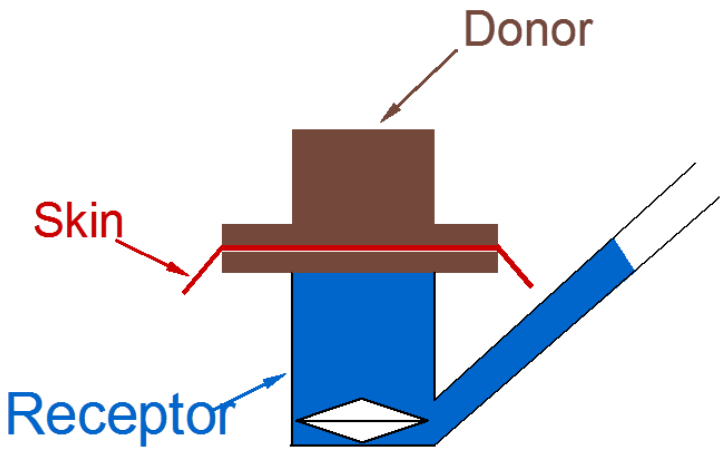

Figure 2.5 Schematic representation of skin diffusion experimental cell

At least 5 replicates were conducted for each of the cell penetrating peptides, physical admixtures and cell penetrating peptide – active conjugates. The cumulative amount of cell penetrating peptide or active permeated through the epidermis (µg/cm^2) versus time (h) was plotted. The cumulative amount was corrected for amount removed in each sample. The flux through the human epidermis was determined from the slope of the plot of cumulative amount versus time and expressed as µg/cm^2/h. Permeability coefficients (cm/h) were calculated using the following equation:

Permeability coefficient Kp (cm/h) = Flux (J) / Concentration in the donor (C)

2.3.8 Mass balance and recovery

The uptake of the each cell penetrating peptide (DKP and TAT), Ala-Trp, diclofenac and cell penetrating peptide-active conjugates in the epidermis was investigated. Propylene glycol and methanol were used as extraction solvents and the protocol for propylene glycol and methanol extraction was as follows:

The recovery of DKP, TAT, Ala-Trp, diclofenac, DKP-diclofenac conjugate and TAT-diclofenac conjugate from skin tissue was determined by spiking skin sections with the conjugates in propylene glycol. The skin sections were allowed to rest in 500 μL methanol and vortexed for 2 min. The skin section was then transferred to a second Eppendorf tube containing 500 μL methanol and vortexed for another 2 min. The skin sample was then placed in 1 mL propylene glycol for 1 h with agitation. After centrifuging each extract at 10,000 × g for 10 min, the resultant supernatants were diluted appropriately and quantified by HPLC. This extraction method using methanol and propylene glycol proved to be very efficient and was therefore used for the experimental samples.

Mass balance/recovery after the skin permeation experiments was determined by removing the donor solution from the donor compartment and appropriately diluting it to quantify the amount of active present in the donor at the end of the experiment. The donor compartment with the skin was rinsed with 300 μL PBS and the wash was collected. The receptor compartment was emptied and washed with 500 μL PBS. Samples from both washes were injected on HPLC to quantify the active present in the washes.

2.3.9 Cyclooxygenase (COX) inhibition assays

COX-2 inhibition by DKP-diclofenac conjugate and diclofenac was assessed using a COX Fluorescent Inhibitor Screening Assay Kit (700100, Cayman Chemical, USA). Cyclooxygenase is a bifunctional enzyme exhibiting both COX and peroxidise activities. COX-2 is responsible for the biosynthesis of prostaglandins under acute inflammatory conditions.[278,279] This inducible COX-2 is believed to be the target enzyme for the anti-inflammatory activity of non-steroidal anti-inflammatory drugs.[279] Diclofenac was the standard to which the conjugated DKP- diclofenac molecule was compared. The major components of the kit were COX-2 (human recombinant) enzyme, heme, arachidonic acid and the fluorimeteric substrate, ADHP

(10-acetyl-3,7-dihydroxyphenoxazine) . The assay utilizes the peroxidise component of COXs. The COX component converts arachidonic acid to a hydroxyl endoperoxide (PGG_2), and the peroxidise component reduces the endoperoxide to the corresponding alcohol (PGH_2), the precursor of prostaglandins, throboxanes and prostacyclins.[280,281] The reaction between PGG_2 and ADHP (10-acetyl-3,7-dihydroxyphenoxazine) produces the highly fluorescent compound resorufin. Resorufin fluorescence can be easily analysed with an excitation wavelength of 530-540 nm and an emission wavelength of 585-595 nm.

The activity of diclofenac and DKP-diclofenac conjugate was assessed at different concentrations from 0.000155-0.31 mM. A two minute incubation period and a fluorescence microplate reader equipped with standard fluorescein filters were used to detect the COX-2 activity.

2.3.9.1 Dilution of assay buffer

Three mL of assay buffer concentrate was diluted with 27 mL HPLC grade water. The buffer consisted of 100 mM Tris-HCl, pH 8.0. This final buffer was used in the assay and for diluting reagents.

2.3.9.2 Heme

Forty µL heme in dimethylsulfoxide (DMSO) was diluted with 960 µL of diluted assay buffer.

2.3.9.3 COX-2 (human recombinant)

Fifty µL of enzyme was diluted with 550 µL of diluted assay buffer and stored on ice. This enzyme solution was used in the assay

2.3.9.4 Arachidonic acid

One hundred µL of arachidonic acid in ethanol was transferred to another vial and 100 µL of potassium hydroxide was added. The mixture was vortexed and diluted with 800 µL of HPLC grade water to achieve a final concentration of 2 mM. A 10 µL aliquot yielded a final concentration of 100 µM in the wells.

2.3.9.5 Preparation of the fluorimeteric substrate, ADHP (10-acetyl-3,7 dihydroxyphenoxazine)

Immediately prior to assaying, the contents of the vial were dissolved in 100 µL DMSO and then 900 µL of diluted assay buffer was added.

2.3.9.6 Preparation of standard concentration of the Inhibitors

A 1 mM solution of inhibitor standards was prepared by dissolving 0.318 mg diclofenac and 0.652 mg DKP-diclofenac in the assay buffer. Further dilution was carried out with the buffer to give 0.31, 0.031, 0.0031, 0.00031 and 0.000155 mM working standard concentrations.

2.3.9.7 Reaction mixture

1) For the 100% initial activity wells, 150 µL of assay buffer, 10 µL of heme, 10 µL of fluoremetric substrate, 10 µL of COX-2 enzyme and 10 µL of solvent (the same solvent used to dissolve the inhibitor)

2) For the background wells, 160 µL of assay buffer, 10 µL of heme, 10 µL of fluorimeteric substrate and 10 µL of solvent (the same solvent used to dissolve the inhibitor) were added to the well

3) For the inhibitor wells, 150 µL of assay buffer, 10 µL of heme, 10 µL of fluorimeteric substrate, 10 µL of COX-2 enzyme and 10 µL of inhibitor (diclofenac or DKP-diclofenac) were added to the wells.

4) The reactions were initiated quickly by adding 10 µL of arachidonic acid solution to all the wells that were used.

5) The wells were incubated for 2 minutes at room temperature and were read at the appropriate wavelengths in a fluorescence microplate reader equipped with standard fluorescein filters.

6) The fluorescence intensity was measured for all samples. The fluorescence of the background wells was subtracted from the fluorescence of the 100% initial activity and the inhibitor wells.

7) The percent inhibition for each sample was determined and a graph was obtained by plotting the percent inhibition or percent initial activity as a function of the inhibitor concentration.

2.3.10 Statistical analysis

Skin permeation data consisted of cumulative measurements of the drug amount taken at various times (1 to 24 h) following active and passive treatments. A random effects regression model was used to compare the treatments at various time points, with the timings treated as categorical variables (so that no linear relationship was assumed between permeation and time). This type of regression model is equivalent to a repeated measures analysis of variance, in that it properly takes into account correlations between measurements made on the same sample at different time points. If the standard deviations of the permeations appeared to differ widely for different time periods, a logarithmic transformation was performed on the permeation before analysis.

Pairwise comparisons were calculated from the regression model by requesting certain 'contrasts' as required. Contrasts were tailored to make specific comparisons, and obtain the p-values for them. The standard errors on which the contrasts were based were estimated from the regression model which was based on all the available data. If the analysis was performed on the log-transformed data, the p-values for the pairwise comparisons were based on this analysis, but the mean permeation were quoted on the original scale (to simplify interpretation).

For the analysis of CPP and CPP conjugates retained in the skin, there were no repeated measurements, so a straightforward analysis of variance (ANOVA) was performed to compare results between treatments.

All statistical analyses were performed using the SAS version 9.2 statistical software (SAS Institute Inc, Cary, NC, USA, 2008). A p-value <0.05 was taken to indicate a statistically significant association.

2.4 Results and discussion

2.4.1 Chromatography

2.4.1.1 DKP

The current HPLC method was an adaptation of that established previously by our collaborators at the University of Barcelona with minor mobile phase changes. The method provided good selectivity and specificity and DKP eluted at approximately 6.7 min. The linearity shown by the HPLC method was 0.9993 and the precision was

0.78% for 1.95 µg/mL, 0.54% for 15.6 µg/mL and 0.47% for 62.5 µg/mL DKP. The LOD and LOQ for DKP were 173 ng and 579 ng respectively. The intra-day repeatability was 0.86% for 1.95 µg/mL and 0.56% for 15.6 µg/mL (within the acceptable criteria for intraday repeatability of RSD < 5%) and the inter-day repeatability of 1.36 % for 1.95 µg/mL and 1.03 % for 15.6 µg/mL. Thus the method was validated for detection of DKP after permeation through skin. A typical chromatogram for DKP is shown in Figure 2.6 below. The chromatogram shown below exhibits a small shoulder but it is not attributed to the degradation of DKP. The shoulder is also evident in the DKP standard synthesized and established by LCMS at University of Barcelona. The peak area of DKP for all standards, working solutions and samples was hence integrated as the entire peak including the shoulder.

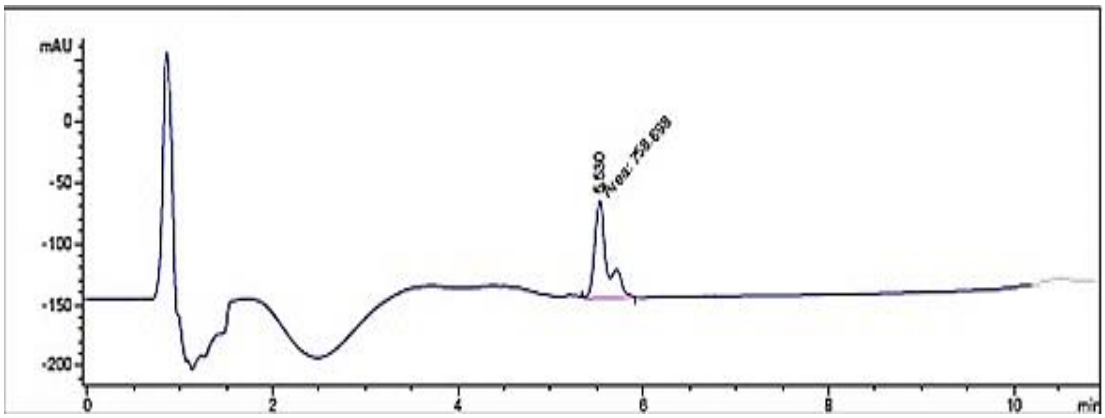

Figure 2.6 Chromatogram of 100 µg/mL standard of DKP

2.4.1.2 Ala-Trp

The method developed for Ala-Trp was a modification of the DKP method. Ala-Trp eluted at approximately 8.2 min. The linearity was 0.9999 and the precision was 0.45% for 1.56 µg/mL, 0.31% for 6.25 µg/mL and 0.24% for 50.0 µg/mL. The LOD and LOQ were 45.06 ng and 150.21 ng respectively. The intra-day repeatability was 0.61% for 1.56 µg/mL and 0.41% for 12.5 µg/mL and the inter-day repeatability was 0.60 % for 1.56 µg/mL and 0.47 % for 12.5 µg/mL. Thus the method was validated for detection of Ala-Trp after permeation through skin. A typical chromatogram for Ala-Trp is shown in Figure 2.7 below.

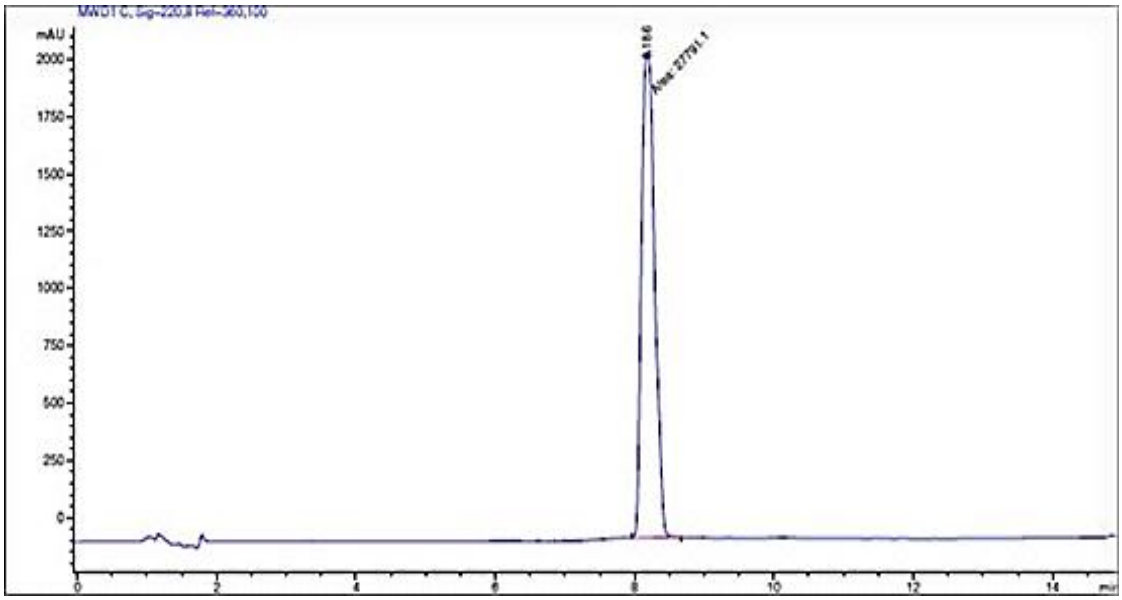

Figure 2.7 Chromatogram of 100 µg/mL standard of Ala-Trp

2.4.1.3 Diclofenac

The method developed for diclofenac was a modification of the DKP method. Diclofenac eluted at approximately 8.2 min. The linearity was 0.9994 and the precision was 0.88% for 3.9 µg/mL, 0.62% for 15.6 µg/mL and 0.34% for 62.5 µg/mL. The LOD and LOQ were 98 ng and 326.5 ng respectively. The intra-day repeatability was 0.90% for 3.9 µg/mL and 0.62% for 15.6 µg/mL and the inter-day repeatability was 0.84 % for 3.9 µg/mL and 0.74 % for 15.6 µg/mL. Thus the method was validated for detection of diclofenac after permeation through skin. A typical chromatogram for diclofenac is shown in Figure 2.8 below.

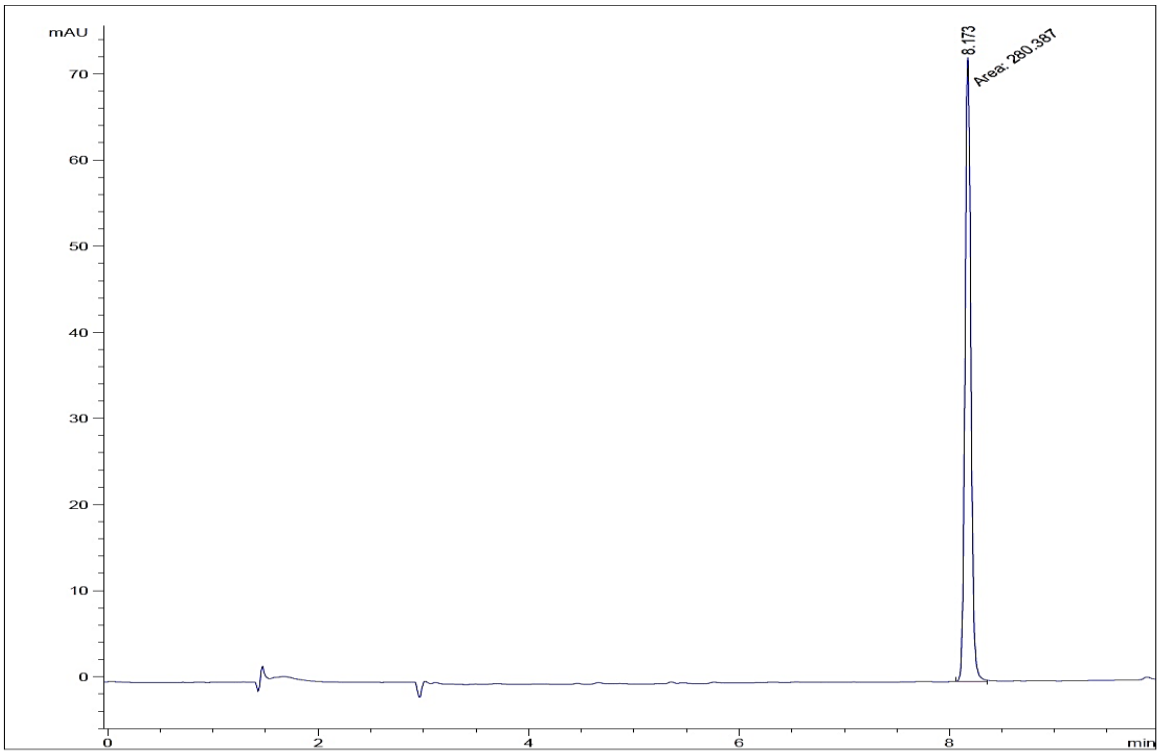

Figure 2.8 Chromatogram of 15.7 µg/mL standard of diclofenac

2.4.1.4 DKP and Ala-Trp physical mixture

The HPLC method developed for Ala-Trp enabled co-analysis of both the dipeptide and the DKP in the same run. The retention times for DKP and Ala-Trp were 11.2 min and 8.2 min respectively. The linearity shown by the HPLC method was 1.0 for DKP and 0.9993 for Ala-Trp. The precision was 0.94% and 0.95% for 3.9 µg/mL Ala-Trp and DKP respectively, 0.38% and 0.55 for 15.6 µg/mL Ala-Trp and DKP respectively and 0.11 and 0.43% for 62.5 µg/mL Ala-Trp and DKP respectively. The LOD and LOQ of Ala-Trp were 35.11 ng and 117.05 ng respectively. The LOD and LOQ of DKP in the physical admixture were 283 ng and 943 ng respectively. The intra-day repeatability was 0.82% for 3.9 µg/mL and 0.33% for 15.6 µg/mL and inter-day repeatability was 1.18 % for 3.9 µg/mL and 0.48 % for 15.6 µg/mL Ala-Trp in the physical admixture. For DKP, the intra-day repeatability was 1.11 % for 3.9 µg/mL and 0.83% for 15.6 µg/mL and inter-day repeatability was 0.86 % for 3.9 µg/mL and 0.75 % for 15.6 µg/mL. A typical chromatogram for DKP and Ala-Trp in physical admixture is shown in Figure 2.9 below.

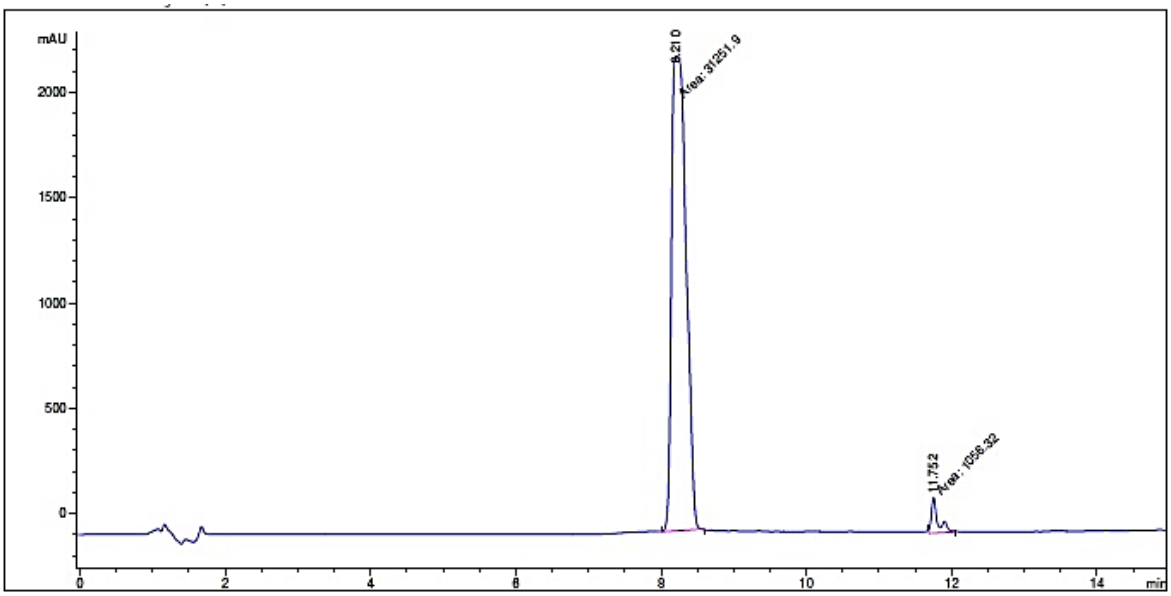

Figure 2.9 Chromatogram of 125 µg/mL standard of DKP-Ala-Trp (physical admixture)

2.4.1.5 DKP- diclofenac physical admixture

The HPLC method developed for DKP enabled the analysis of diclofenac as well as the co-analysis of both diclofenac and DKP in the same run. The retention time for DKP and diclofenac in the physical admixture were 6.7 min and 8.2 min respectively. The linearity was 0.9998 and 0.9997 for diclofenac and DKP respectively. The precision was 0.72% and 0.93% for 3.9 µg/mL diclofenac and DKP respectively, 0.59% and 0.82% for 15.6 µg/mL diclofenac and DKP respectively and 0.44% and 0.66% for 62.5 µg/mL diclofenac and DKP respectively. The LOD and LOQ of diclofenac and DKP when applied in the physical admixture were 68 ng and 228 ng, and 235.6 ng and 785.5 ng respectively. The intra-day repeatability was 0.85% for 3.9 µg/mL and 0.61% for 15.6 µg/mL and inter-day repeatability was 0.80 % for 3.9 µg/mL and 0.67 % for 15.6 µg/mL diclofenac in the physical admixture. For DKP, the method showed intra- day repeatability was 0.94 % for 3.9 µg/mL and 0.85% for 15.6 µg/mL and inter-day repeatability was 0.96 % for 3.9 µg/mL and 0.87 % for 15.6 µg/mL DKP in the physical admixture. A typical chromatogram for DKP and diclofenac applied in the physical admixture is shown in Figure 2.10 below.

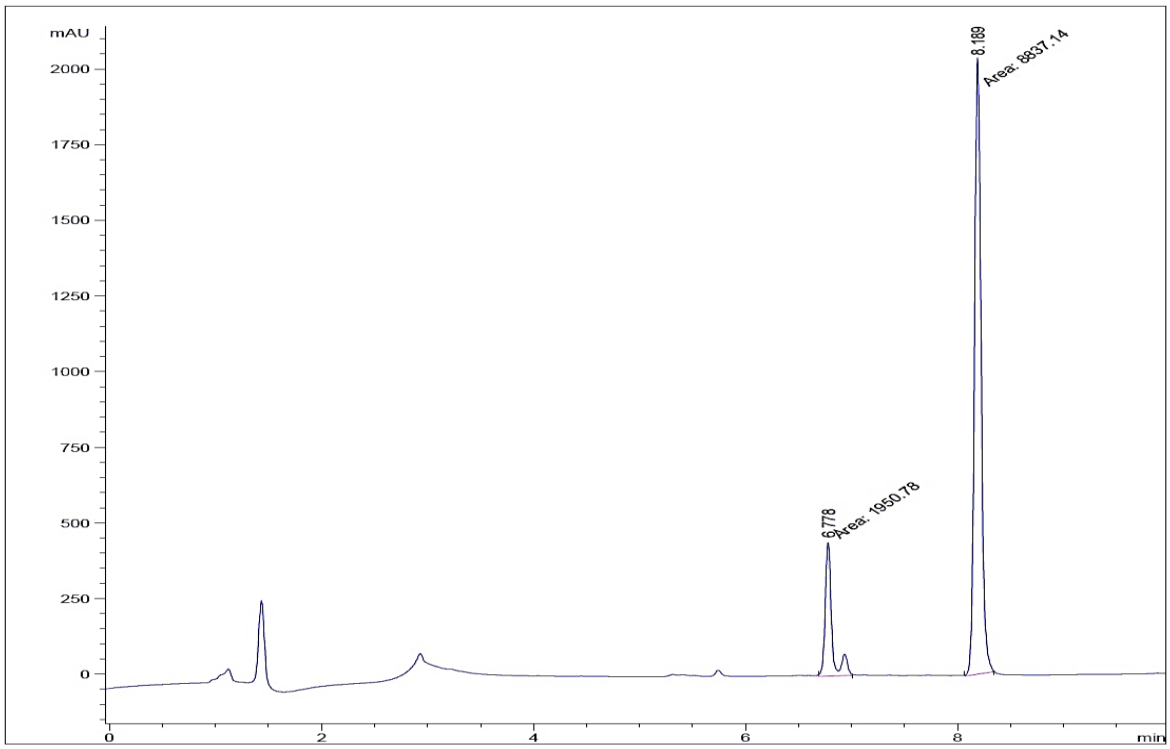

Figure 2.10 Chromatogram of 125 µg/mL standard of DKP-diclofenac (physical admixture)

2.4.1.6 TAT and TAT-diclofenac conjugate

The HPLC method for TAT and TAT-diclofenac conjugate were obtained from GLS Biochem. The method was modified to suit the system specifications in our laboratory. The retention time for TAT was 17.1 min. The linearity was 0.998 and the precision was 0.95%, 0.78% and 0.50% for 3.25 µg/mL, 13 µg/mL and 52 µg/mL TAT respectively. The LOD and LOQ of TAT were 800 ng and 2.66 µg respectively. The intra-day repeatability was 0.99% for 3.25 µg/mL and 0.82% for 13 µg/mL and inter-day repeatability was 1.04 % for 3.25 µg/mL and 0.89 % for 13 µg/mL TAT. A typical chromatogram for TAT is shown in Figure 2.11 below.

For TAT-diclofenac the retention time was 10.1 min. The linearity was 0.9997 and the precision was 0.81%, 0.73% and 0.69% for 7.81 µg/mL, 31.25 µg/mL and 125 µg/mL TAT-diclofenac respectively. The LOD and LOQ of TAT-diclofenac were 393 ng and 1.31 µg respectively. The intra-day repeatability was 0.90% for 7.81 µg/mL and 0.71% for 31.25 µg/mL and inter-day repeatability was 0.92 % for 7.81 µg/mL and 0.72 % for 31.25 µg/mL TAT-diclofenac. A typical chromatogram for TAT-diclofenac conjugate is shown in Figure 2.12 below.

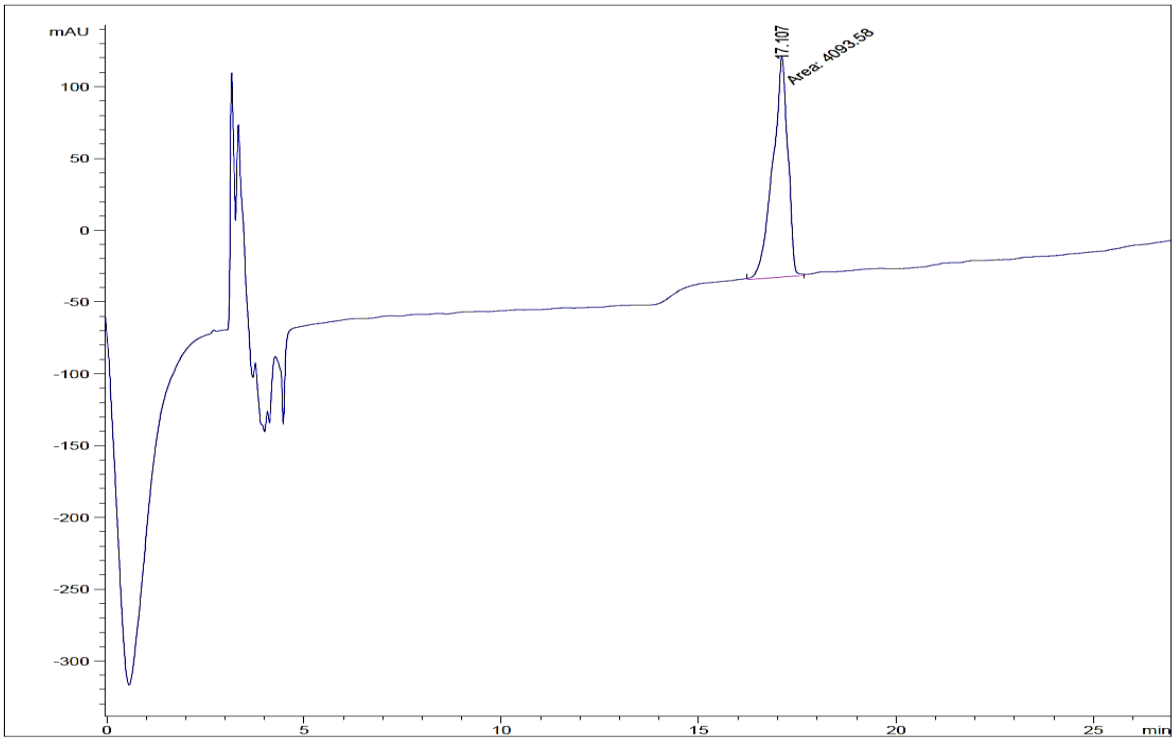

Figure 2.11 Chromatogram of 104 µg/mL standard of TAT

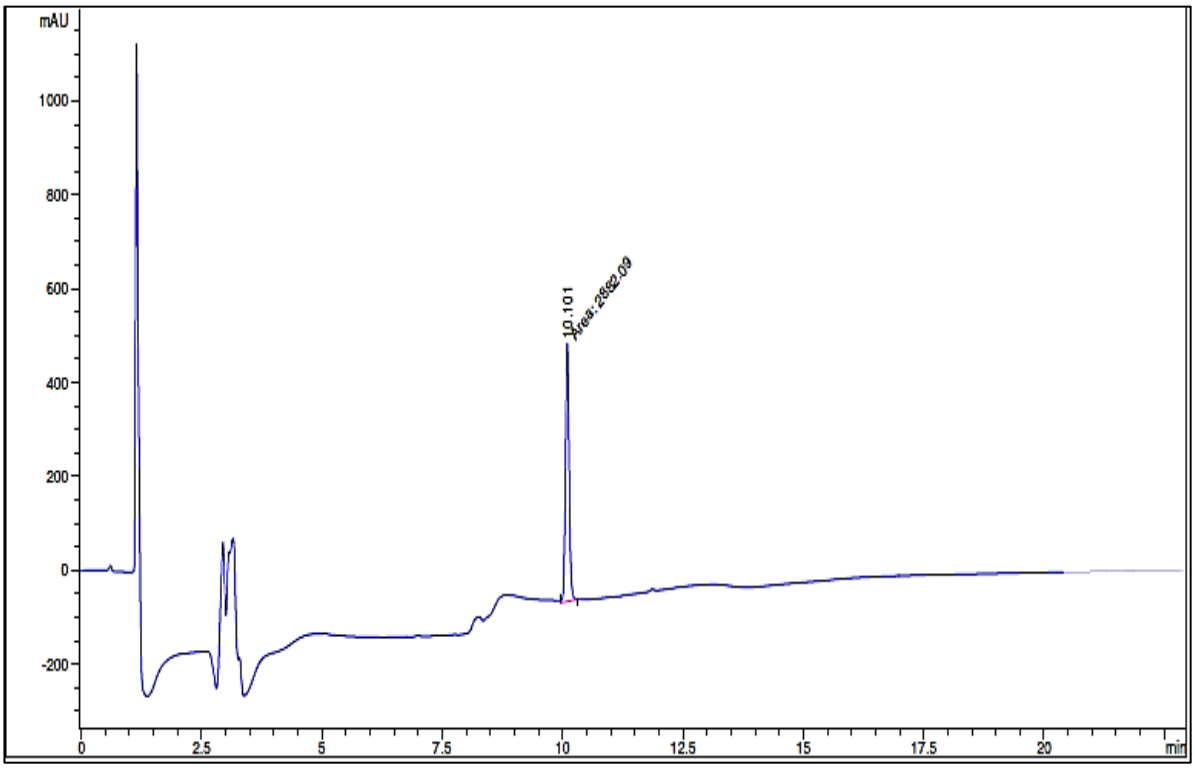

Figure 2.12 Chromatogram of 250 µg/mL standard of TAT-diclofenac conjugate

2.4.1.7 DKP-diclofenac conjugate

For DKP-diclofenac conjugate the retention time was 8.2 min. The linearity was 0.9997 and the precision was 1.16%, 1.0% and 0.65% for 3.9 µg/mL, 15.6 µg/mL and 62.5 µg/mL DKP-diclofenac respectively. The LOD and LOQ of DKP-diclofenac were 973.2 ng and 3.24 µg respectively. The intra-day repeatability was 1.31% for 3.9 µg/mL and 1.1% for 15.6 µg/mL and inter-day repeatability was 1.2 % for 3.9 µg/mL and 1.02 % for 15.6 µg/mL DKP-diclofenac conjugate. A typical chromatogram for DKP-diclofenac conjugate is shown in Figure 2.13 below.

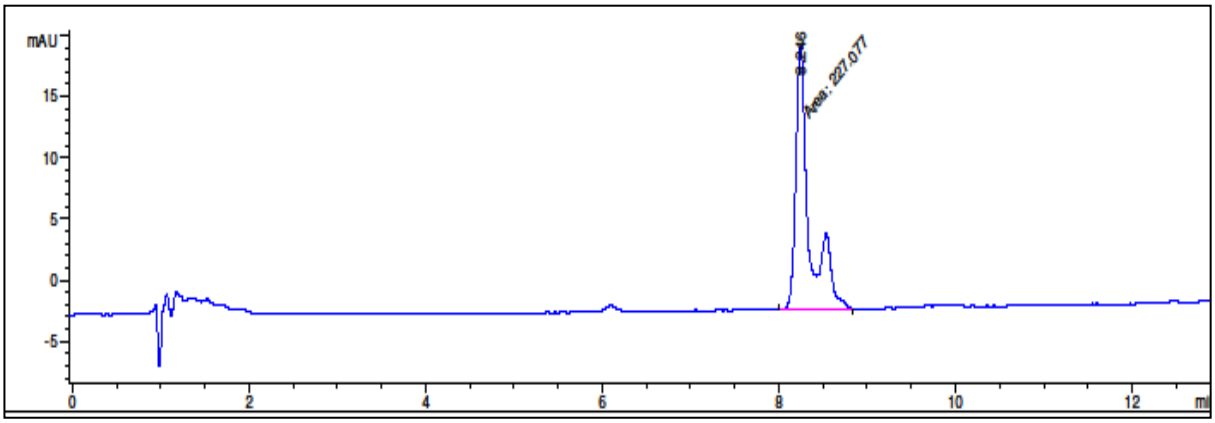

Figure 2.13 Chromatogram of 50 µg/mL standard of DKP-diclofenac conjugate

Table 2.1 HPLC summary data for analysis of cell penetrating peptides, actives, physical admixtures and conjugates

Peptide	Correlation coefficient (r^2)	Linear range (µg/mL)	Precision	Intra-day Repeatability	Inter-day Repeatability	LOD (ng)	LOQ (ng)
DKP	0.9993	1.95 - 125	0.78% at 1.95 µg/mL 0.54% at 15.6 µg/mL 0.47% at 62.5 µg/mL	0.86% at 1.95 µg/mL 0.56% at 15.6 µg/mL	1.36% at 1.95 µg/mL 1.03% at 15.6 µg/mL	173.0	579.0
Ala-Trp	0.9999	1.56- 50	0.45% at 1.56 µg/mL 0.32% at 6.25 µg/mL 0.24% at 50 µg/mL	0.61% at 1.56 µg/mL 0.41% at 12.5 µg/mL	0.60% at 1.56 µg/mL 0.47% at 12.5 µg/mL	45.1	150.2
Diclofenac	0.9994	3.9 - 125	0.88% at 3.9 µg/mL 0.62% at 15.6 µg/mL 0.34% at 62.5 µg/mL	0.90% at 3.9 µg/mL 0.62% at 15.6 µg/mL	0.84% at 3.9 µg/mL 0.74% at 15.6 µg/mL	98.0	326.5
DKP mixed with Ala-Trp	1.000	3.9 – 250	0.95% at 3.9 µg/mL 0.55% at 15.6 µg/mL 0.43% at 62.5 µg/mL	1.11% at 3.9 µg/mL 0.83% at 15.6 µg/mL	0.86% at 3.9 µg/mL 0.75% at 15.6 µg/mL	283.0	943.0
	0.9993	3.9 - 250	0.94% at 3.9 µg/mL 0.38% at 15.6 µg/mL 0.11% at 62.5 µg/mL	0.82% at 3.9 µg/mL 0.33% at 15.6 µg/mL	1.18% at 3.9 µg/mL 0.48% at 15.6 µg/mL	35.1	117.0

DKP mixed with diclofenac	0.9997 0.9998	3.9 – 125 3.9 - 125	0.93% at 3.9 µg/mL 0.82% at 15.6 µg/mL 0.66% at 62.5 µg/mL 0.72% at 3.9 µg/mL 0.59% at 15.6 µg/mL 0.44% at 62.5 µg/mL	0.94% at 3.9 µg/mL 0.85% at 15.6 µg/mL 0.85% at 3.9 µg/mL 0.61% at 15.6 µg/mL	0.96% at 3.9 µg/mL 0.87% at 15.6 µg/mL 0.80% at 3.9 µg/mL 0.67% at 15.6 µg/mL	228.0 68.0	235.6 785.5
DKP-diclofenac conjugate	0.9997	3.9 - 250	1.16% at 3.9 µg/mL 1.0% at 15.6 µg/mL 0.65% at 62.5 µg/mL	1.31% at 3.9 µg/mL 1.1% at 15.6 µg/mL	1.2% at 3.9 µg/mL 1.02% at 15.6 µg/mL	973.2	3240.0
TAT	0.9988	3.25 - 104	0.95% at 3.25 µg/mL 0.78% at 13.0 µg/mL 0.50% at 52 µg/mL	0.99% at 3.25 µg/mL 0.82% at 13.0 µg/mL	1.04 % at 3.25 µg/mL 0.89 % at 13.0 µg/mL	800.0	2660.0
TAT-diclofenac conjugate	0.9997	7.81 - 250	0.81% at 7.81 µg/mL 0.73% at 31.25 µg/mL 0.69% at 125 µg/mL	0.90% at 7.81 µg/mL 0.71% at 31.25 µg/mL	0.92% at 7.81 µg/mL 0.72% at 31.25 µg/mL	393.0	1310.0

2.4.2 Human epidermal penetration and accumulation: preliminary experiments

Preliminary investigations were carried out with DKP, diclofenac, Ala-Trp and DKP-diclofenac conjugates. It should be noted that experiments were conducted based on the availability of the peptides and conjugates. As the synthetic procedures are time consuming and expensive some compounds were available in limited quantities, therefore some experiments could not be repeated where the available compound was required for other assessment procedures. Preliminary experiments were undertaken to determine the optimal experimental protocol with respect to final donor concentration, donor vehicle, receptor vehicle and appropriate period of epidermal membrane hydration.

2.4.2.1 Choice of donor vehicle

In order to choose a suitable vehicle for the permeation experiments, a preliminary study was undertaken with DKP, Ala-Trp and diclofenac to determine the solubility in 100% propylene glycol (PG), 75:25 v/v PG:PBS and 25:75 v/v PG:PBS. The results indicated that Ala-Trp had good solubility in both 100% PG and 75:25 v/v PG: PBS mixture. The high molecular weight peptide and peptide conjugates TAT and TAT-diclofenac had optimal solubility in absolute PG with further dilution with PBS. The peptide conjugate DKP-diclofenac had similar solubility characteristics as its parent compound DKP. Considering the solubility study, 25:75 v/v PG: PBS mixture was chosen as a vehicle as it was compatible with all the compounds.

2.4.2.2 Determination of donor concentration

Donor concentration plays an important role in transdermal experimentation. For infinite dose-type studies the diclofenac concentration needs to be high enough to maintain sink conditions throughout the duration of the study. However it has been suggested that very high concentrations of lipophilic molecules can lead to aggregation and clogging of the passive transdermal channels.[282,283] Figure 2.14 is a representative graph of the cumulative amount of DKP-diclofenac (μg/cm^2) permeated in 24 h for a donor amount of 1.5 mg and 150 μg. It shows that the permeation is greater for the lower dose application. In addition to reduced permeation (2.36 μg/cm^2) with the 1.5 mg total dose, considerable variability and a longer lag time of 1.5 h was also observed. Consequently, 150 μg donor amount as

present in 300µL of 500 µg/mL was adopted for subsequent experiments. A high concentration could also lead to accumulation of the active in the superficial layers of the skin with minimal permeation across the barrier.[283]

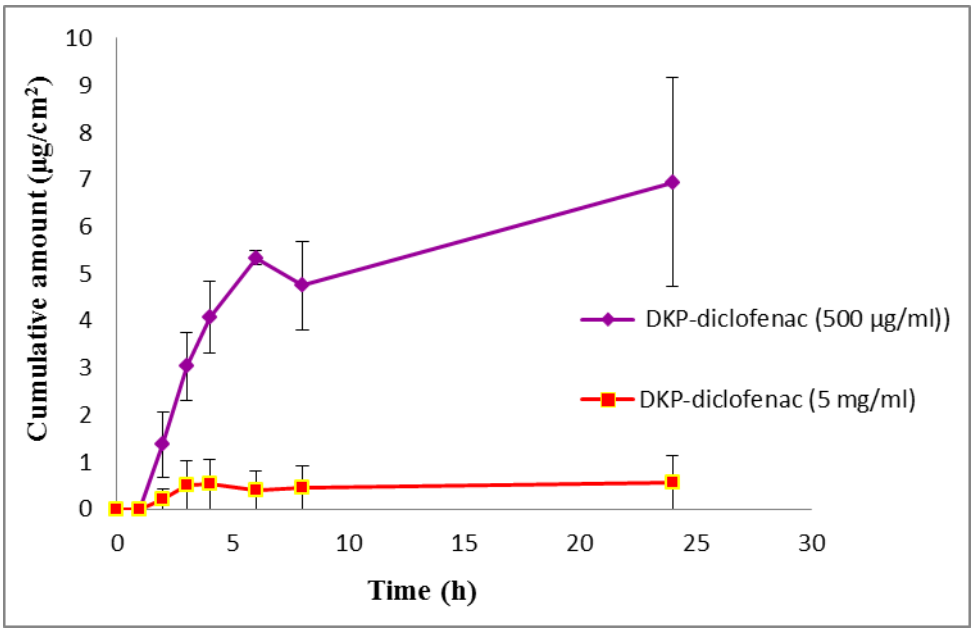

Figure 2.14 Permeation profile of cumulative amount vs. time of DKP-diclofenac conjugate (300µL donor volume i.e. 1.5 mg and 150 µg) across human epidermis. Results are expressed as mean (±SEM), n=5

2.4.2.3 Pre-hydration of epidermal membrane

Hydration of the Franz cell mounted skin prior to experimentation is common practice and has been shown to reduce variability in the experimental skin condition. Researchers have hydrated skin for times ranging from a few minutes[284], to a few hours[285,286], to longer durations like 8-10 h (overnight)[287] and observed a marked reduction in variability and loss of cells due to leakage from the membrane by overnight hydration. In this study skin was hydrated for 8-10 h (overnight) in Franz cells.

2.4.2.4 Stability of DKP/study duration of permeability experiments

Preliminary studies were conducted to establish the optimal experimental protocol with respect to duration of permeability experiment and establishing the stability of the compound when in contact with the human skin. Experiments with regular receptor sampling were carried out for 24 h, 48 h and 72 h durations. No degradation of the DKP peptide was detected on the HPLC chromatogram for receptor samples up to 72 h in contact with the skin. However it was observed that at 72 h the skin was

damaged and would not be suitable for the skin recovery studies that were one of the primary aims of our experiments. Hence for the reliable recovery of drug from the skin and to minimise variability of the experiments the duration of experiments was limited to 24 h. However, this experiment was of particular value in establishing the stability of DKP over 72 h. Figure 2.15 below shows a progressive increase in the receptor concentration of DKP from 24 h-72 h.

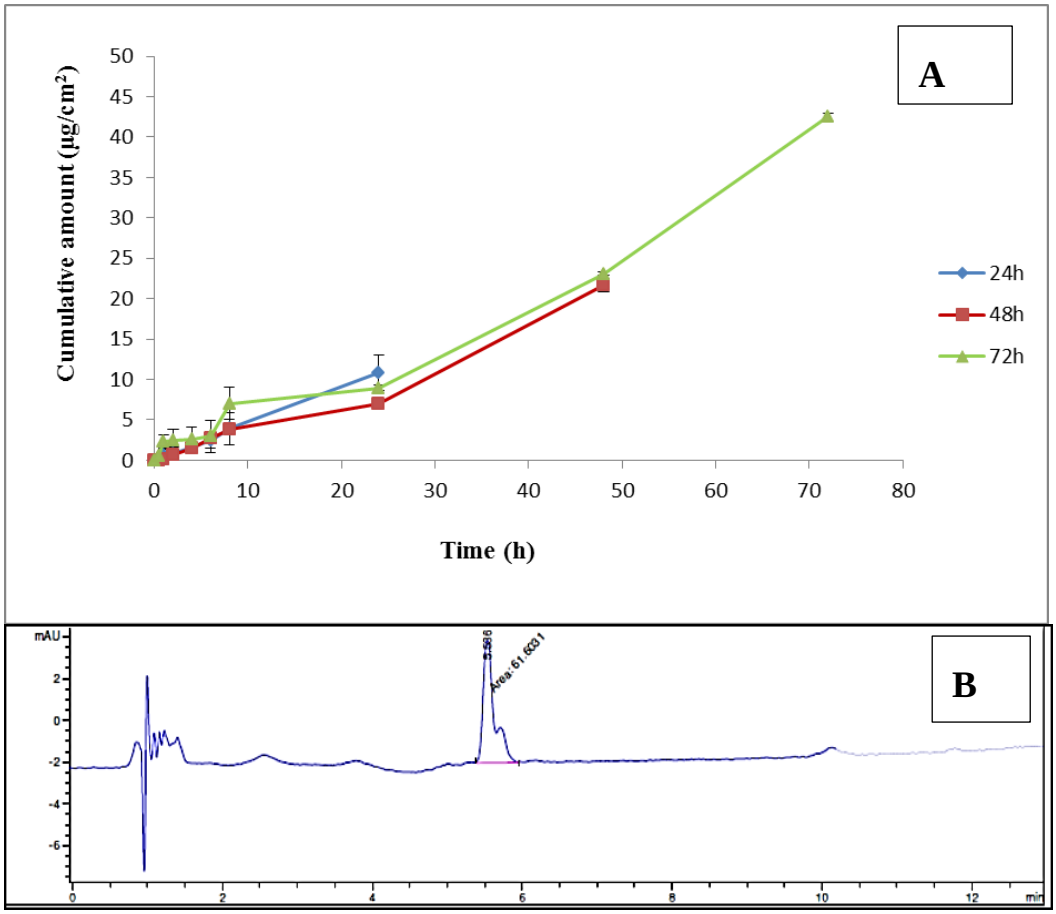

Figure 2.15 A) Cumulative amounts of DKP permeated after 24 h, 48 h and 72 h studies. B) An HPLC chromatogram of the receptor sample after 72 h study.

The structure of DKP is quite different to the cell penetrating peptides tested to date. DKP is a cyclic peptide thus providing unique properties. One of the issues in applying peptides to the skin is the ability of skin enzymes to metabolize the peptide.[288] The other issue worth considering is the stability of the cell penetrating peptides in contact to skin. Several authors have demonstrated good stability of peptides in biological tissues, including skin.[275,288] The cyclic structure of DKP confers better stability as was demonstrated when we exposed the DKP to human

epidermis at 37ºC for 72 h with only a 4% loss of DKP. Indeed diketopiperazine formation or cyclization of peptides is a common phenomenon and often found to be a result of unstable peptides forming diketopiperazines of stable conformations. Goolcharran et al.[289] determined the rates of deamination, oxidation, and diketopiperazine reactions in model peptide systems and compared them to those of recombinant human vascular endothelial growth factor (rhVEGF). The authors reported that the rate of the diketopiperazine reaction was slower in the protein (rhVEGF), which is more stable compared to the model peptides. Carpenter et al.[290] reported similar reactions leading to stable diketopiperazine formation in a tripeptide.[290] Kubo et al.[291] have similarly discussed the stable conformations of diketopiperazines.[291]

2.4.2.5 Final experimental protocol

Based on the preliminary data a final protocol for the skin permeation studies was formulated:

- Three hundred μL of a 500 μg/mL concentration of the donor for all compounds (i.e. application amount of each compound was 150 μg)
- 25:75 v/v PG:PBS for the donor vehicle and receptor medium
- Overnight (8-10 h) hydration of the epidermal membrane with the receptor medium.
- Total experiment duration of 24 h.

2.4.3 Permeation of cell penetrating peptides, admixtures of cell penetrating peptide and active, and conjugated cell penetrating peptide-actives across human epidermis *in vitro*

In this study the co-administration and conjugation of cell penetrating peptides with model and therapeutic molecules was investigated as an enhancement strategy to increase the permeation of these molecules across the human skin.

Table 2. 2 Overview of the research plan

Compound	Single ingredient control	Physical admixture	Conjugate
DKP and diclofenac	✓	✓	✓
DKP and Ala-Trp	✓	✓	×

TAT and diclofenac	✓	✖	✓

2.4.3.1 Influence of DKP on skin permeation of diclofenac and Ala-Trp

2.4.3.1.1 DKP

DKP (150 µg in 300 µL 25:75 PG:PBS) was applied to human epidermis for 24 h as per the protocol determined from preliminary experimentation. Figure 2.16 shows the cumulative amount of DKP permeated through the epidermis (µg/cm^2) versus time (h) following administration of 300 µL of 150 µg DKP in 25:75 PG:PBS. The steady-state flux (µg/cm^2/h), lag time and permeability coefficient (cm/h) are noted in Table 2.3. Over the 24 h experimental period, the cumulative amount permeated was 10.46 µg/cm^2. The transdermal flux over the 24 h period was 0.43 µg/cm^2/h and the permeability coefficient was 8.7×10^{-4} cm/h. (Table 2.3)

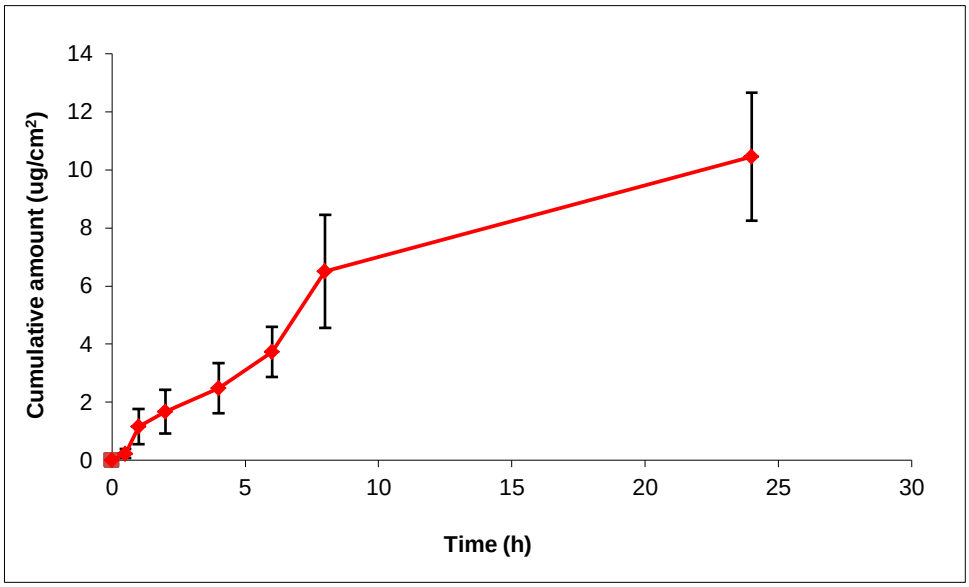

Figure 2.16 Passive permeation of DKP over 24 h, Amount in donor - 150 µg, Results are expressed as mean (±SEM: n=7).

Cell penetrating peptides, including TAT, have recently been shown to cross the stratum corneum barrier.[92] In this study we have demonstrated the skin penetration of DKP from this novel diketopiperazine class of cell penetrating peptides. DKP was previously shown to cross the blood-brain barrier by our collaborators.[99,292]

Rothbard[107] et al. reported the application of the cell penetrating peptide Peptide R7 (Polyarginine-7) for the delivery of peptides into the skin. They showed that the cell

penetrating peptide permeated into the epidermis and that the depth and intensity of skin penetration depended on the length and concentration of the active cargo peptide applied. Lopes[275] et al. conjugated the cell penetrating peptides TAT (MW: 2020) and a recent, molecular modification of TAT (YARAAARQARA) named as YARA (MW: 1668) with the peptide P20 (Heat shock protein 20 -WLRRASAPLPGLK, MW: 2005 Da). They reported rapid penetration of YARA and TAT alone in the porcine ear skin *in vitro*. They also demonstrated that combination with the chemical penetration enhancers, monoolein and oleic acid did not further enhance skin permeation of these cell penetrating peptides. However when the cell penetrating peptides were conjugated to the peptide P20, skin penetration was slow and very limited despite the high permeation of the cell penetrating peptides alone. Most of the cell penetrating peptides used in cellular and transdermal delivery to date are arginine rich[95,108,293] and questions have been raised regarding their membrane shuttling properties.[63]

DKP has been shown as a stable compound in the presence of human skin. The stability of DKP has been discussed in detail in the previous section (2.4.2.4). In contrast, TAT is prone to trans-activation and has often been methylated on the arginine amino acid. Moreover, protein transduction using TAT fusion protein systems may require denaturation of the protein before delivery to increase the accessibility of the TAT-cell penetrating peptide domain. This requirement introduces an additional delay between the time of delivery and intracellular activation of the protein.[294] The mode of transport of DKP across the skin is not very clear at this stage. Unlike TAT where the predominant mode of transport is at least partially endocytotic, DKP most likely penetrates through a rather energy independent pathway (diffusion). Endocytosis is inherently a saturation driven pathway and can easily be overwhelmed by high peptide concentrations.[295]

Diketopiperazines have been detected in a variety of natural sources and are generally considered safe. In a recent review, Huang et al. looked at activity and toxicity of DKPs.[296] Most of the reported activity of DKPs is very selective and hence they appear to be reasonably safe. Other molecules with a diketopiperazine ring at the core have been studied for toxicity by Watts et al. and were shown to be safe.[297] Specific toxicity studies are necessary to evaluate the carrier dikepiperazine used in this study.

2.4.3.1.2 Ala-Trp

Permeation profile of Ala-Trp in the current study was established at a low concentration of 500 µg/mL (150 µg) (Figure 2.17). The permeation after 24 h was 0.13 µg/cm^2 with transdermal flux of 0.01 µg/cm^2/h and permeability coefficient (K_P) of 2.0 ×10^{-5} cm/h (Table 2.3).

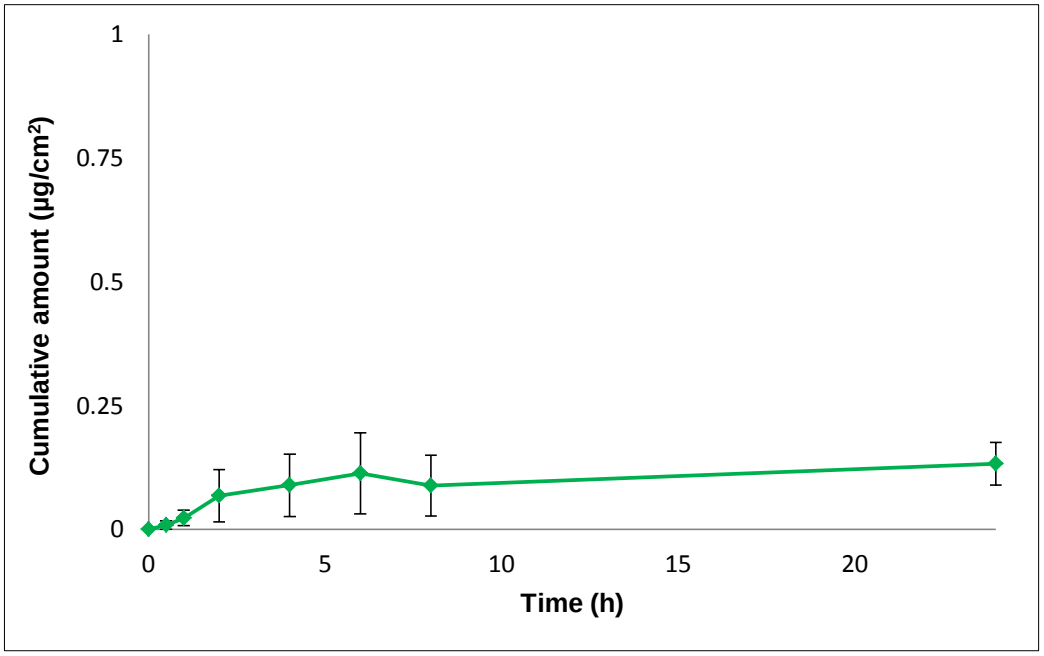

Figure 2.17 Passive permeation of Ala-Trp over 24 h, Amount in donor - 150 µg. Results are expressed as mean (±SEM: n=4).

There have been limited reports on skin penetration enhancement of dipeptides. The molecular weight of Ala-Trp (MW = 275 g/mol) would ideally fit the 500 Dalton rule,[298] however its transdermal penetration suggests that other factors are not optimal. This may be due to the highly hydrophilic nature of the drug. Altenbach et al.[299] observed no iontophoretic and passive transport of a dipeptide (Tyr-Phe) across human skin *in vitro* without the addition of an enzyme inhibitor.[299] In previous work conducted in our laboratory a novel magnetophoretic technique Dermaportation was used to enhance the transdermal permeation of Ala-Trp. Dermaportation significantly enhanced the delivery of Ala-Trp through human epidermis *in vitro* over an 8 h period (permeability coefficient: 7.7 × 10^{-4} cm/h) when compared to passive diffusion. The dipeptide was shown to be unstable on exposure to human epidermis with an increasing amount of degradation product evident in the receptor phase over

the 8 h period.[153] However, this was not observed with studies conducted during the current experiments. It can be hypothesised that the vehicle PG: PBS used in this project had a stabilising effect.

In a study, Lin et al.[300] measured the passive diffusion of Ala-Trp in porcine skin and reported a permeability coefficient of 1.39×10^{-2} cm/h. The results of this phase of the study implied that Ala-Trp would be an ideal molecule to test for penetration enhancement using an active strategy.

2.4.3.1.3 DKP-Ala-Trp (physical admixture)

Figure 2.18 shows the permeation across human epidermis of DKP and Ala-Trp applied as a physical admixture at 150 µg of each component. The cumulative amount of DKP and Ala-Trp permeated over 24 h was 10.83 and 1.19 µg/cm^2 respectively (Table 2.3). Over the 24 h experimental period, the transdermal flux of DKP in the physical admixture was 0.45 µg/cm^2/h and the permeability coefficient was 9.0×10^{-4} cm/h. The transdermal flux and permeability coefficient was found to be comparable to that for passive DKP permeation across human epidermis. The steady state flux on the other hand for Ala-Trp was 0.049 µg/cm^2/h and the permeability coefficient was 9.9×10^{-5} cm/h. An approximately 10-fold increase in the cumulative amount was observed when the dipeptide was co-administered with the cell penetrating peptide, DKP. It was interesting to note that the transport of DKP was unaffected.

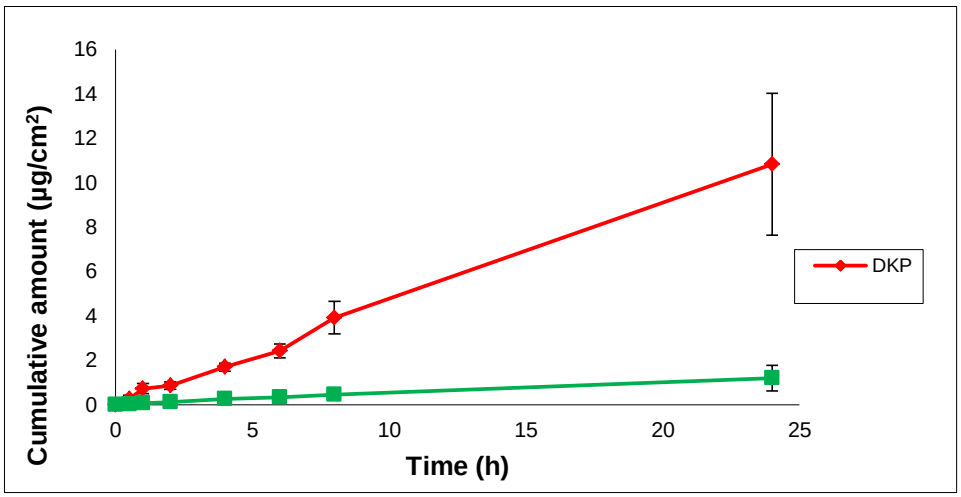

Figure 2.18 Passive permeation of DKP-Ala-Trp (physical admixture) over 24 h, Amount in donor - 150 µg, Results are expressed as mean (±SEM: n=7).

Cell penetrating peptides are known to cross membranes with a great degree of ease and when conjugated they are also known to be able to carry a reasonable payload. A study was designed to determine if they can create channels big enough to enhance transdermal transport of small hydrophilic molecules when co-administered. If so, can these channels stay open long enough to show a detectable skin permeation enhancement. An interesting viewpoint on this can be deduced from the recent work published in 2012 by Sakuma et al.[301] The authors reported that since cell penetrating peptides are highly cationic, they adsorb strongly on the membrane surface via hydrogen bond-induced formation of guanidino moieties in arginine with anionic phosphates, sulfates, and carboxylates of cellular components. Membrane-associated proteoglycans including heparan sulfate play crucial roles in the macropinocytosis of cell penetrating peptides. The process is initiated by cell activation and plasma membrane ruffling and leads to a consequential engulfment of large volumes of extracellular fluid into macropinosomes. It was hypothesised that poorly membrane-permeable molecules physically mixed with cell-penetrating peptide are incidentally internalized into cells when the cells fail to uptake the peptidyl branches in the cell penetrating peptide complex.[301]

Sakuma et al.[301] studied this mechanism by monitoring the permeation of anionic carboxyfluorescein (CF) alone and as conjugate in Caco-2 monolayer cell lines. Enhanced CF penetration of more than 5-fold was observed for the cell penetrating peptide -polymer complex (0.0123 ± 0.0026 nmol/mg to 0.213 ± 0.045 nmol/mg). Macropinocytosis was confirmed as the mechanism of uptake because the specific inhibitor [5-(N-ethyl-N-isopropyl)-amiloride; EIPA] significantly inhibited cell penetrating peptide permeation. Clearly the skin provides a more complex membrane than Caco-2 monolayers. We demonstrated a similar trend with Ala-Trp in the presence of cell penetrating peptide. When co-administered with DKP we observed a 10-fold enhancement of Ala-Trp penetration. Hence, we believe that DKP may form temporary channels by lipid bilayer rearrangements which can facilitate transport of other co-administered small molecules.

2.4.3.1.4 Diclofenac

To continue from the work described above a small therapeutic molecule, diclofenac was selected as a model, because of its low passive permeability through the skin. In

this study the cumulative amount permeated over 24 h was 4.06 µg/cm^2. (Figure 2.19). The estimated transdermal flux was calculated over 24 h as 0.173 µg/cm^2/h (Table 2.3).

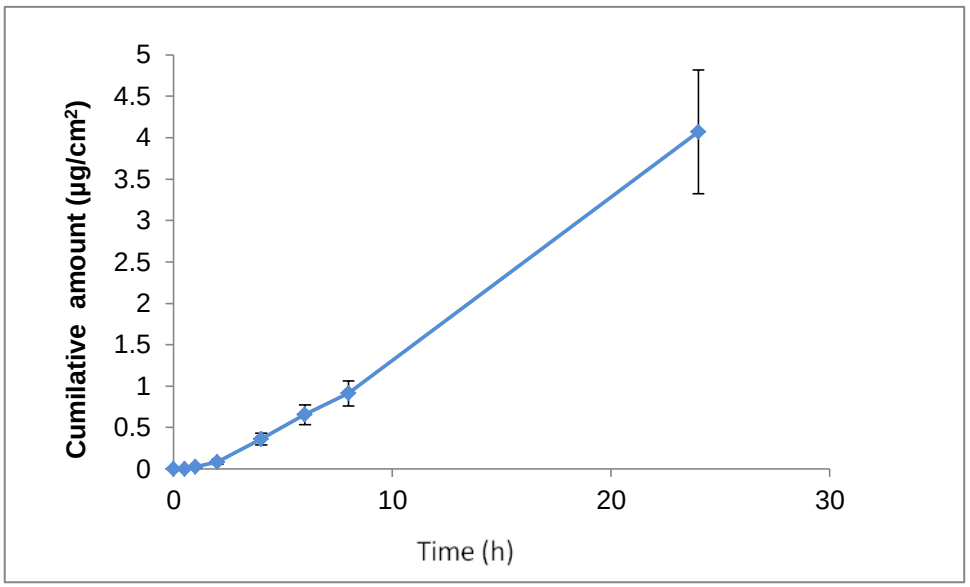

Figure 2.19 Passive permeation of diclofenac over 24 h, Amount in donor - 150 µg, Results are expressed as mean (±SEM: n=5).

Ionized diclofenac sodium faces tough resistance passing through the stratum corneum and has been used with various chemical enhancers in topical formulations to aid in its penetration.[302] Diclofenac sodium has been very well reviewed and found to be effective transdermally in randomized controlled trials.[303,304] Though diclofenac sodium has good water solubility (9 mg/mL)[305] the reported transdermal permeation has been generally low. In *in vitro* experiments Dehghanyar et al. studied the transdermal penetration of diclofenac after multiple as well as after single application at different doses and locations of human volunteer skin and reported it to be highly variable.[306] It has been recently suggested that dermal oxidative stress from UV radiation may impede absorption of topical diclofenac, although, a clinical trial in patients with sunburn did not show any significant increase or decrease in absorption measures.[307,308] It could also be inferred that the low concentrations of diclofenac in *in vitro* skin studies can be due to the presence of free radicals in excised skin. Abdulmajed et al.[309] showed that esterase activity in excised skin stored at –20 ° C is substantially lower than in freshly excised skin, which is likely to be due to deactivation of protein structure as result of freezing.[309]

2.4.3.1.5 DKP-diclofenac (physical admixture)

After successfully demonstrating an enhancement in transdermal permeation of Ala-Trp by co-administering the dipeptide with DKP, we studied the co-administration of DKP with diclofenac. The cumulative amount of DKP permeated was almost doubled and a 2-fold enhancement in the transdermal flux and permeability coefficient of diclofenac was observed. Figure 2.20 shows the permeation across human epidermis of DKP and diclofenac applied as a physical admixture at 150 µg of each component. The cumulative amount of DKP and diclofenac permeated over 24 h was 17.39 and 7.61 µg/cm^2 respectively. The estimated transdermal flux over the 24 h period for DKP and diclofenac in the mixture was 0.72 µg/cm^2/h and 0.31 µg/cm^2/h respectively. (Table 2.3) The calculated permeability coefficient was 1.4 × 10^{-3} cm/h for DKP and 6.3 × 10^{-4} cm/h for diclofenac. (Table 2.3)

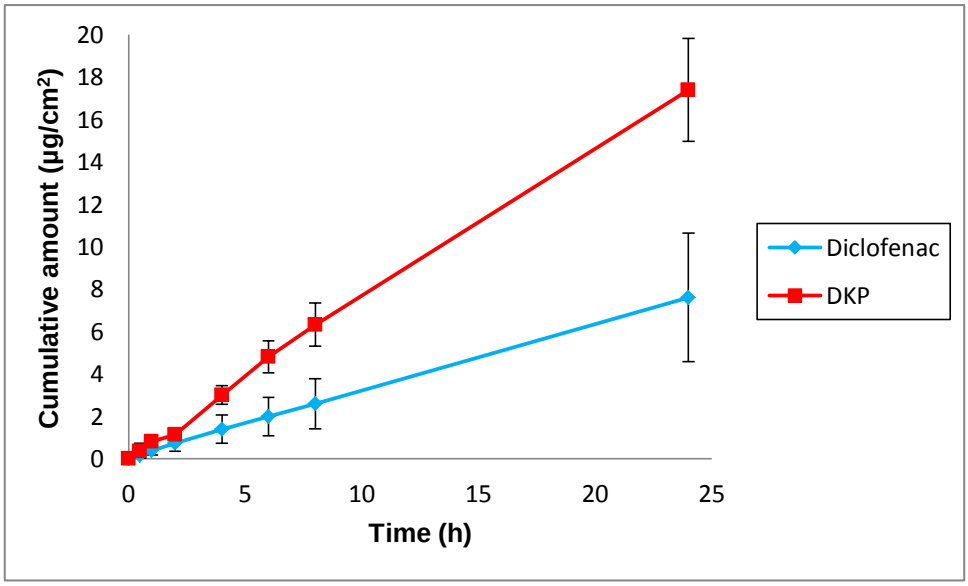

Figure 2.20 Passive permeation of DKP-diclofenac (physical admixture) over 24 h, Amount in donor - 150 µg, Results are expressed as mean (±SEM: n=5).

A similar co-administration study was conducted by Cohen-Avrahami et al.[310] Diclofenac was dissolved with and without cell penetrating peptides in reversed hexagonal (H_{II}) mesophases. Cell penetrating peptides included Penetratin, a 16 amino acid (RALARALARALRALAR) named RALA and a 9 amino acid cell penetrating peptide with sequence (RRRRRRRRR) named nona-arginine or NONA. All peptides examined were found to increase diclofenac permeation through skin. Permeation was diffusion-controlled, and the cell penetrating peptides were not involved in the diclofenac diffusion steps, out of the mesophase. The skin permeation

enhancement of these cell penetrating peptides is therefore based on their interaction with the skin.[310] To substantiate this hypothesis[311] ATR-FTIR was used to observe the lipid structure of the porcine ear skin. While the H_{II} mesophase itself had a minor effect on the lipid chain conformation, penetratin encapsulated within this carrier, triggered a transformation of lipid structure which is hexagonal in porcine skin to a more liquid transition.[311] Unlike the enhancement seen with Ala-Trp in the previous section and with diclofenac using other cell penetrating peptides, we did not observe as substantial an enhancement in the permeation of diclofenac when co-administered with DKP.

Results of this study are comparable to recent work by Lohcharoenkal et al.,[312] in which the authors observed greater permeation with a co-administration approach than with a conjugate (4.25-fold and 1.79-fold respectively) when administrating TAT for the permeation enhancement of a model green peptide.[312] When compared to the passive permeation of diclofenac in similar conditions the results were very encouraging.

2.4.3.1.6 DKP-diclofenac conjugate

Conjugation of DKP with diclofenac was successful and the conjugate was quantified by HPLC and MS. Apart from its therapeutic relevance, diclofenac was chosen due to the ease of biological activity assessment of the conjugate.

In this study we have demonstrated carrier mediated delivery of diclofenac when conjugated to DKP. Figure 2.21 shows the skin permeation of DKP-diclofenac conjugate at 150 µg across human epidermis. The cumulative amount of DKP–diclofenac conjugate permeated over 24 h was 7.82 µg/cm^2 (Table 2.3). The results indicated that upon addition of an active payload on the scaffold the permeation was comparable to that of DKP and diclofenac admixture. However, we believe that the size of this molecule must have played a role in its lower permeation when compared to DKP.

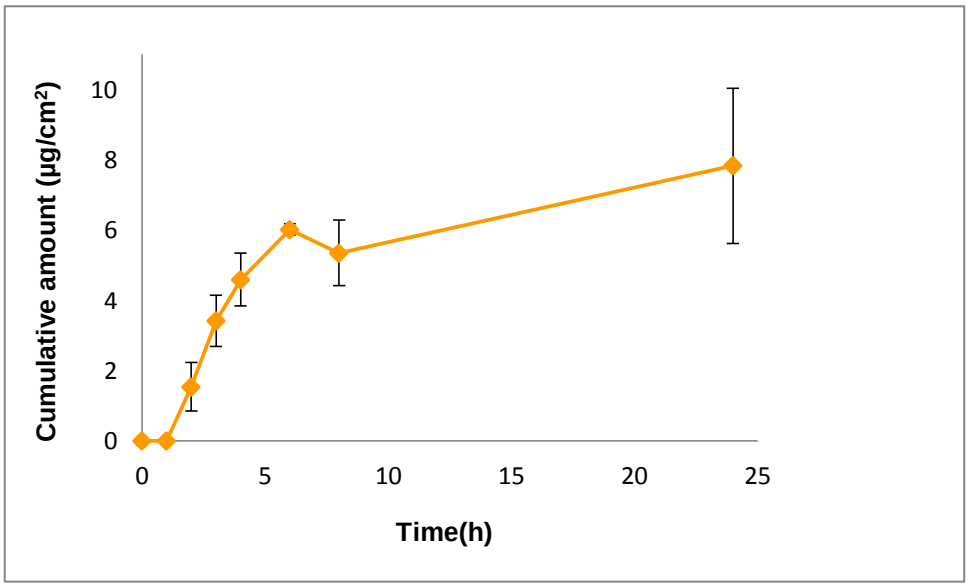

Figure 2.21 Passive permeation of DKP-diclofenac conjugate over 24 h, Amount in donor - 150 µg, Results are expressed as mean (±SEM: n=4).

The conjugate retained the COX-2 activity of diclofenac (assay results discussed in subsequent sections) and showed a marked reduction in lag time when compared to passive diclofenac. In the case of DKP-diclofenac conjugate, the cumulative amount of permeation to the receptor was 1.54 µg/cm^2 at 2 h and continued to increase linearly to 5.34 µg/cm^2 at 8 h (compared to passive permeation of 0.91 µg/cm^2 at 8 h). The transdermal flux for the conjugate was 1.21 µg/cm^2/h and the permeability coefficient was 2.4 × 10^{-3}(Table 2.3). Conjugation of diclofenac to DKP resulted in 7-fold enhancement in transdermal flux when compared to passive diclofenac permeation across human skin. The comparison between cumulative amounts of passive diclofenac and DKP-diclofenac conjugate was found to be significant ($p < 0.05$) from 4 h onwards. Given the low concentration used for this study and the small surface area studied, further simulation on a greater area would have a reasonable therapeutic potential.

COX enzyme inhibition by NSAIDs and other COX inhibitors can be assessed with a readily available assay kit. Orally administered NSAIDs can cause complications, including ulcers, GI bleeding and some renal function abnormalities.[313] Therefore, improved topical delivery of the NSAIDs would offer an appropriate solution because it would provide the patient with relief without the side effects. Percutaneous penetration can be greatly advantageous because it would preserve its high

therapeutic potency and yet avoid hepatic first-pass metabolism and considerable gastrointestinal disturbances.

Table 2.3 Summary of DKP and active drugs permeation

Compound	Cumulative amount (μg/cm^2)	Steady state flux (μg/cm^2/h)	Lag time (h)	Permeability coefficient (cm/h)
DKP	10.46	0.43	0.5	8.7×10^{-4}
Ala-Trp	0.13	0.01	2	2.0×10^{-5}
Diclofenac	4.06	0.173	1	3.46×10^{-4}
DKP-Ala-Trp admixture	DKP: 10.83 Ala-Trp: 1.19	DKP: 0.45 Ala-Trp: 0.049	DKP: 0.5 Ala-Trp: 1	DKP: 9.0×10^{-4} Ala-Trp: 9.9×10^{-5}
DKP-diclofenac admixture	DKP: 17.39 Diclofenac: 7.61	DKP: 0.72 Diclofenac: 0.31	DKP: 0.5 Diclofenac: 0.5	DKP: 1.4×10^{-3} Diclofenac: 6.3×10^{-4}
DKP-diclofenac conjugate	7.82	1.41	1	2.4×10^{-3}

2.4.3.2 Skin permeation of TAT and TAT-diclofenac conjugate

The experiments described in the sections above demonstrated that DKP could be used as a penetration enhancement technique both as a cell penetrating peptide to carry conjugated molecules to targets within the skin and as a penetration facilitator for low permeability drug molecules when applied concurrently without conjugation. At this stage a direct comparison of DKP and its conjugate DKP-diclofenac with other cell penetrating peptides was desired. TAT was selected because it has been a predominant vector used in the delivery of large molecules (e.g. proteins) making it one of the best known cell penetrating peptides. In the study, the passive permeation of TAT across human epidermis was 3.43 μg/cm^2 over 24 h (Figure 2.22). The cumulative amount of DKP at the same concentration was 3-fold higher ($p < 0.05$). The transdermal flux and permeability coefficient of DKP was 4-fold higher than that of TAT (DKP flux 0.43 μg/cm^2/h: TAT flux 0.10 μg/cm^2/h, DKP K_p 8.7×10^{-4} cm/h: TAT K_p 2.0×10^{-4} cm/h: $p < 0.05$ Table 2.3 and 2.4).

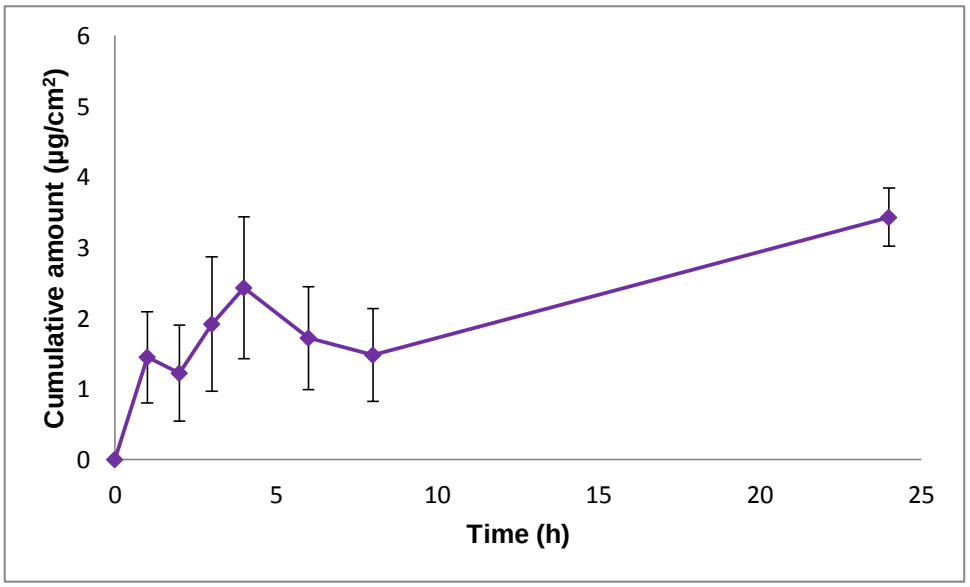

Figure 2.22 Passive permeation of TAT over 24 h, Amount in donor - 150 µg, Results are expressed as mean (±SEM: n=6).

The conjugate of diclofenac with TAT (TAT-diclofenac) was custom synthesized, to compare with DKP-diclofenac conjugate. Adding diclofenac possibly altered the skin permeability which can be seen as a 2-fold increase in penetration when compared to the passive (7.92 µg/cm^2 $p < 0.05$ at 24 h Figure 2.23). This was comparable to the permeation of DKP-diclofenac (7.82 µg/cm^2) with the same amount in the donor of 150 µg. The flux and permeability coefficient of DKP-diclofenac however, were 3.6-fold higher. (TAT-diclofenac- flux 0.33 µg/cm^2/h; K_p – 6.6×10^{-4} cm/h, $p < 0.05$)

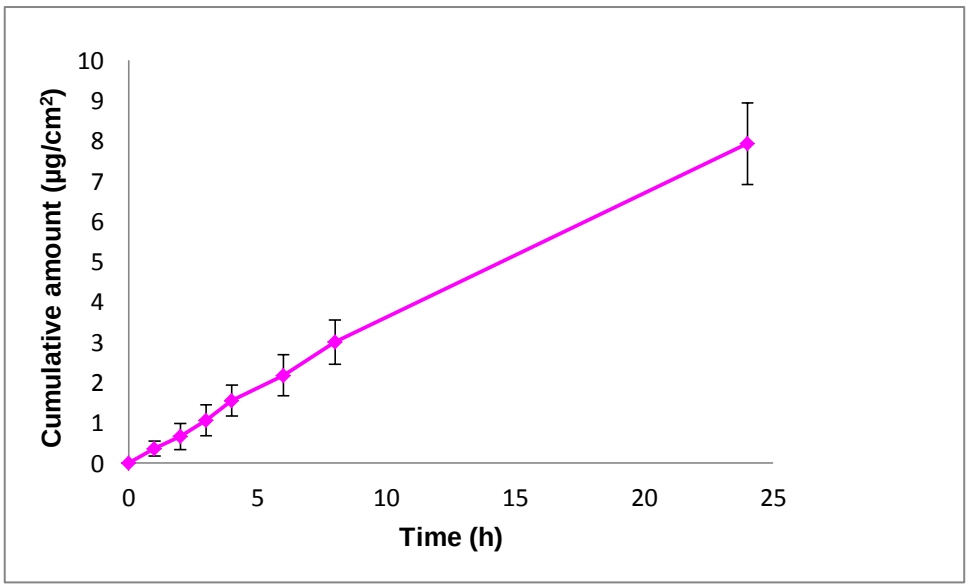

Figure 2.23 Passive permeation of TAT-diclofenac conjugate over 24 h, Amount in donor - 150 µg, Results are expressed as mean (±SEM: n=6).

Table 2.4 Summary of TAT and active compounds permeation

Compound	Cumulative amount (μg/cm^2)	Steady state flux (μg/cm^2/h)	Lag time (h)	Permeability coefficient (cm/h)
TAT	3.43	0.10	0.5	2.0×10^{-4}
TAT-diclofenac	7.92	0.33	0.5	6.6×10^{-4}

Lopes and colleagues examined permeation of TAT and other cell penetrating peptides and concluded that TAT penetrated abundantly in the skin and permeated modestly across this tissue.[275] The reported transdermal delivery of TAT-FITC (fluorescein isothiocyanate) per cm^2 porcine ear skin *in vitro* was 0.027 ± 0.009 nmol over an 8 h experiment. In the *in vitro* human epidermis model we found higher permeation of 2.0 nmol TAT at 8 h. This could be attributed to the relatively smaller size of TAT as compared to TAT conjugated to fluorescein isothiocyanate, FITC. The transdermal delivery of DKP was calculated as 29.13 nmol/cm^2 in 24 h and the transdermal delivery of DKP-diclofenac was 11.99 nmol/cm^2 in 24 h. The molecular weight of TAT is substantially higher when compared to DKP; likewise it was found from these studies that its permeation was significantly lower than DKP. To our knowledge this is the first time the carrier abilities of diketopiperazines have been tested and compared in human skin. The molecular weight and hydrophilicity of DKP make it a prime candidate for transdermal delivery.[298] Diketopiperazines as discussed previously can be very easily modified to synthesize numerous analogues which can be tailored to carry a wide range of drugs.[103] DKP can form an excellent scaffold for future transdermal delivery in addition to the reports of successful brain delivery of highly therapeutic molecules targeting a host of disease conditions.[99,106,292]

2.4.4 Recovery from and retention of cell penetrating peptide and cell penetrating peptide conjugates in the skin

Having demonstrated higher skin permeation of DKP as compared to TAT, the ability of DKP to increase the penetration when conjugated to diclofenac was evaluated. Diclofenac was conjugated with DKP and TAT and the topical and

transdermal delivery was assessed as a function of time. The cell penetrating peptides studied were able to carry the conjugated diclofenac through the skin to a similar extent though a substantial increase in the amount of DKP-diclofenac conjugate accumulated in the epidermis was observed as compared to the TAT-diclofenac conjugate. Figure 2.24 indicates the amount of DKP retained in the skin as a function of donor concentration. The amount of DKP recovered from the skin increased as the donor amount increased from 150 µg to 300 µg. A significant difference in the amount of the CPP recovered from the skin was seen when the amount of the donor was increased from 300 µg to 1500 µg ($p < 0.05$). Figure 2.25 compares the amount of DKP, diclofenac, Ala-Trp, TAT, DKP-diclofenac and TAT-diclofenac conjugates present in the skin after the skin permeation studies. The recovery of DKP, Ala-Trp, diclofenac, DKP-diclofenac conjugate, TAT and TAT-diclofenac conjugate was validated using the extraction procedure with propylene glycol and methanol. After two successive extractions with methanol followed by propylene glycol the recovery was 95%, 90%, 91%, 98% , 95%, 97% and 92% for DKP, Ala-Trp, diclofenac, DKP-diclofenac conjugate, TAT-diclofenac conjugate and TAT respectively of the theoretical concentration. The minor losses incurred in the recovery of cell penetrating peptide and cell penetrating peptide conjugates may be attributed to activity of skin enzymes, skin handling and other processes involved in the experiment.

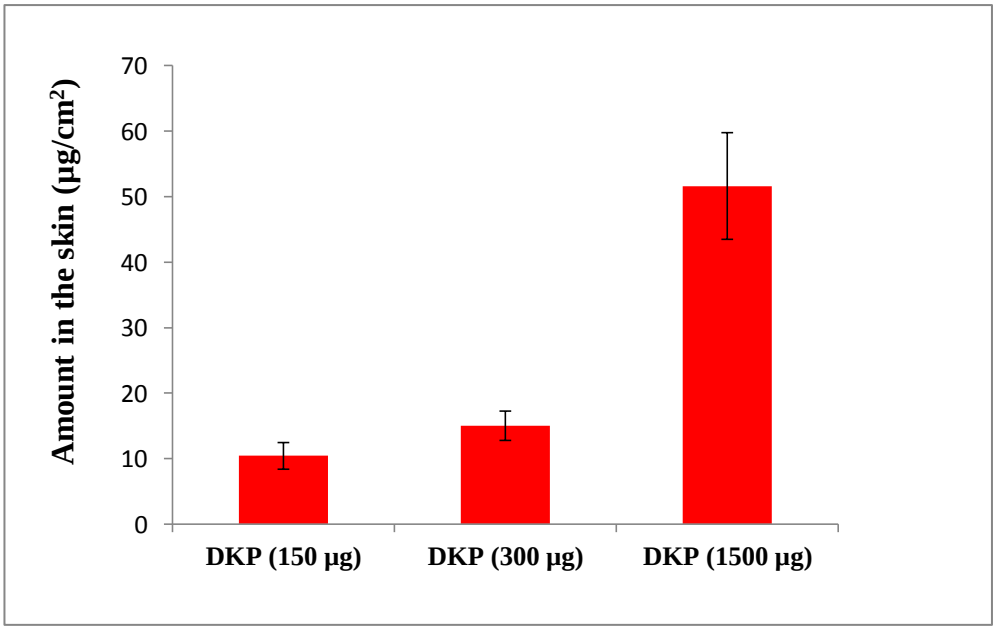

Figure 2.24 Amount of DKP in the skin after the permeation experiments (Donor amount of 150 µg, 300 µg and 1500 µg). Results are expressed as mean (±SEM: n=4)

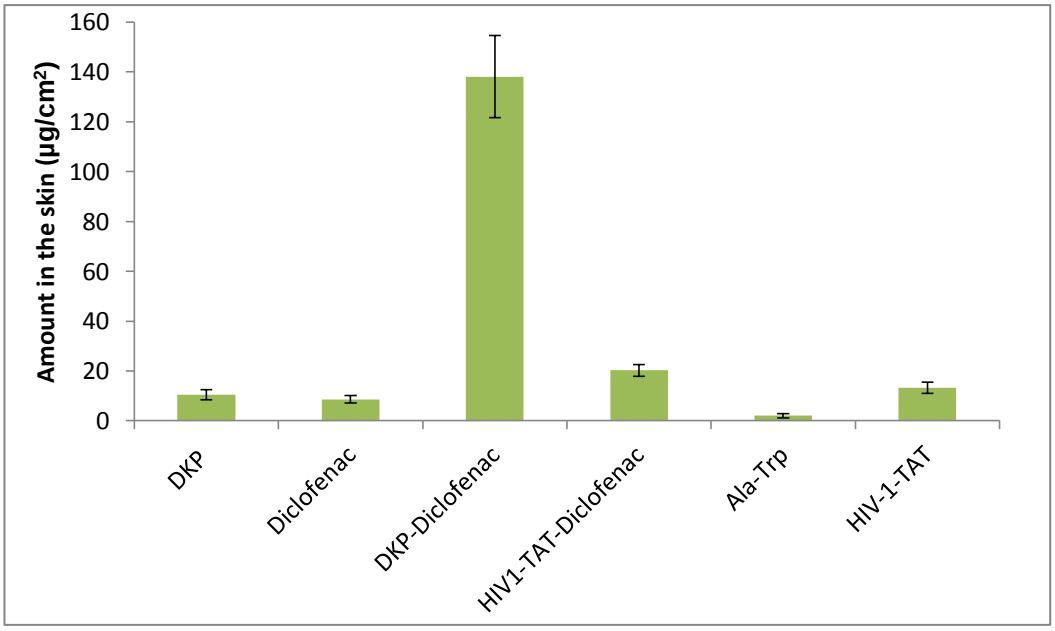

Figure 2.25 Amount of DKP, diclofenac, DKP-diclofenac conjugate, TAT-diclofenac conjugate, Ala-Trp and TAT in the skin after permeation studies (Donor amount of 150 µg). Results are expressed as mean (±SEM: n=4)

A previously reported study showed that accumulation of TAT in the skin is more than its penetration across the skin.[275] The DKP-diclofenac and TAT-diclofenac conjugate was able to permeate in the skin to a significantly higher extent as compared to diclofenac alone ($p < 0.05$). The amount of DKP-diclofenac in the skin was 7 times that of TAT-diclofenac conjugate ($p < 0.05$). We observed that a high amount of the TAT-diclofenac conjugate was recovered from the donor and hence not permeated to the lower layers of the skin. It was also found, that similar amounts of TAT and DKP were extracted from the epidermis. This comparison gives us preliminary data of the possible skin retention of DKP, a novel cell penetrating peptide as compared to TAT, a well-established cell penetrating peptide.

It has long been established that some NSAIDs have an antitumorigenic effect which may be attributable to NSAID-mediated inhibition of the cyclooxygenase pathway and specifically to reduced prostaglandin E2 synthesis.[314,315] This increase in the partitioning of DKP-diclofenac conjugate into human skin and its retention and localization in the epidermis when compared with diclofenac alone indicates the formation of a depot or reservoir of drug in the epidermis. Such localization would be extremely beneficial for the topical use of diclofenac or other NSAIDs for the topical treatment of actinic keratoses.[316] The DKP scaffold could also be used to

conjugate many drugs including corticosteroids, antifungal and antibacterial agents. This would be advantageous for the treatment of skin conditions such as psoriasis, atopic dermatitis and for targeting drugs for the treatment of skin cancers where the adverse side-effects of the drugs when delivered systemically can cause considerable problems.

2.4.5 Inhibition of Cyclooxygenase (COX) by diclofenac and DKP-diclofenac conjugate

The primary objective of this study was to assess the biological activity of the DKP-diclofenac conjugate in comparison to diclofenac**.** The COX-2 inhibitory activity of the DKP-diclofenac conjugate and diclofenac by itself was assessed at a concentration range of 0.000155-0.31 mM. The ability of the COX enzymes to digest the fluoremetric substrate ADHP (10-acetyl-3,7-dihydroxyphenoxazine) decreased as the concentration of each of the inhibitors in the reaction mixture increased (Figure 2.26). The inhibition caused by DKP-diclofenac was comparable to diclofenac: there was approximately 80% and 66% reduction in COX-2 activity with diclofenac and DKP-diclofenac at 0.31mM. DKP itself had no COX-2 inhibition.

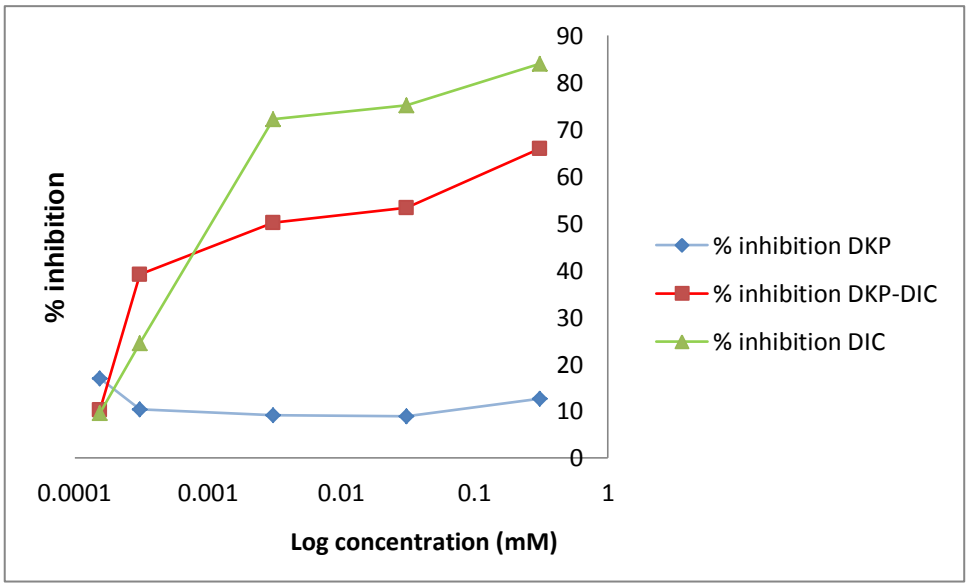

Figure 2.26 Percent inhibition of COX-2 by diclofenac and DKP-diclofenac conjugate (n=1)

In this project we have primarily assessed the capacity of DKP, unconjugated and conjugated diketopiperazines to permeate into and through the human skin. The other major aim was to analyse whether the COX-2 inhibition activity of diclofenac is retained in the DKP-diclofenac conjugate. It was concluded from this COX-2

inhibition study that the biological activity of diclofenac was not significantly affected by conjugation with DKP.

2.5 Conclusions

Skin permeation of DKP was high and consistent over different human skin donor samples. Passive permeation of Ala-Trp and diclofenac was lower than DKP. So was the passive permeation of TAT when compared to DKP at 24 h. Physical admixture of DKP with Ala-Trp increased the flux of Ala-Trp (9.15-fold). Permeation of diclofenac was enhanced 1.9-fold due to the presence of DKP in the physical admixture. Further the conjugation of DKP with diclofenac enhanced the transdermal flux 9-fold and in comparison to only 1.9-fold increased permeation of diclofenac with TAT. Amount of DKP-diclofenac present in the skin was at least 6-fold greater than TAT-diclofenac and at least 14-fold greater than diclofenac by itself.

Chapter 3

Microneedle Based Skin Penetration Studies on Fluorescent Peptides

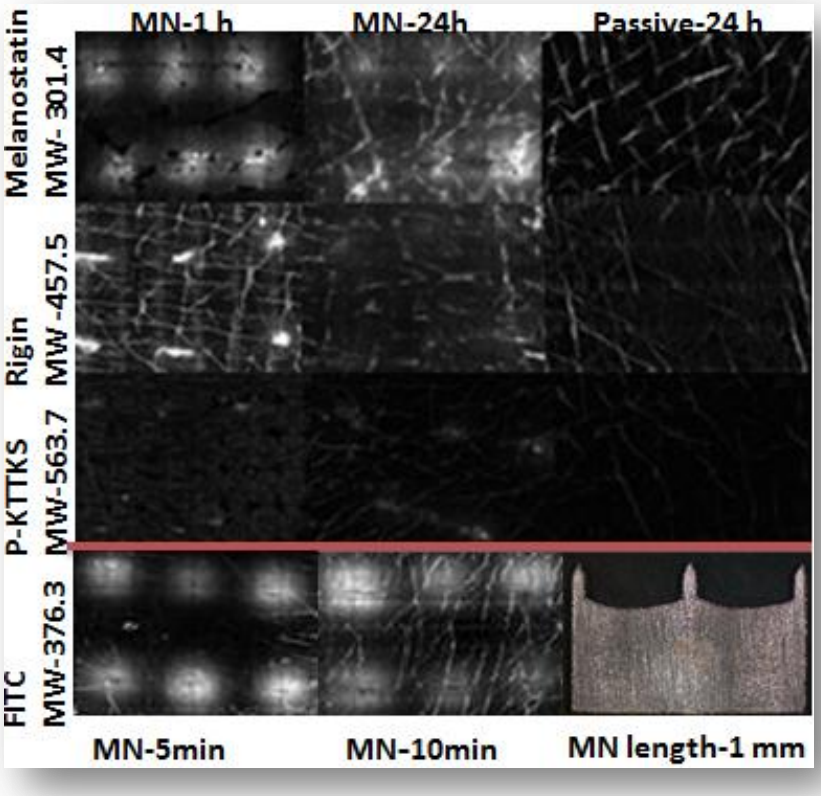

"Images play a unique role in scientific communications by delivering vast information that impacts the very reflection of the observer". [317]

3.1 Introduction

Peptides and proteins are key regulators in cellular and inter-cellular physiological processes and are potentially useful for the treatment of many diseases. Transdermal delivery has potential for the convenient and effective administration of protein and peptide drugs if the stratum corneum barrier can be overcome.[2] Microneedles (MN) have been shown to substantially enhance skin penetration and may offer a painless and effective delivery method.[5] *In vivo* confocal laser scanning microscopy is used in dermatology as an investigative tool in skin research as well as in clinical routine.[318-322] This imaging technique allows for non-invasive monitoring of the skin with microscopic resolution second only to histological analysis. Reflectance confocal microscopy (RCM) employs the reflected light after laser illumination of the tissue to obtain morphological information. This is based on the fact that light is reflected differentially according to the specific refractive indices (e.g. melanin, keratin, lipid, water, or collagen) within the skin, producing the required contrast. Similar to computerized tomography, reflectance is detected only from the focal plane via a pinhole. In this confocal manner, images of thin optical sections of horizontal tissue are gained *in vivo*, revealing cellular and even sub-cellular detail, thereby lending this technique the term reflectance confocal microscopy (RCM).[321,323]

3.2 Aims

The aim of the current study was to evaluate diffusion of fluorescent peptides after MN based delivery using fluorescence imaging and to determine distribution of the peptides within the skin strata. In particular the effect of peptide chain length (3, 4, 5 amino acid chain length) on passive and MN facilitated skin penetration was investigated. The studies were divided in two parts.

a) *Ex vivo* studies with sodium fluorescein to deduce a time co-relation on the penetration of sodium fluorescein.
b) *In vitro* studies on a series of fluorescein conjugated peptides to investigate the effect of size, peptide chain length and molecular weight on their permeation.

3.3 Materials and methods

3.3.1 Peptides and other chemicals

The fluorescent peptides were custom synthesised from Genscript USA Inc. Sodium fluorescein, laboratory solvents, propylene glycol (PG) and dimethyl sulfoxide (DMSO) were obtained from Sigma-Aldrich (Sydney, NSW Australia). Phosphate buffered saline was prepared according to United States Pharmacopeia and purified deionised Milli-Q water from Millipore (North Ryde, NSW Australia).

3.3.2 Instrumentation and techniques

3.3.2.1 Reflectance confocal microscopy and florescence imaging

Figure 3.1 VivaScope 2500

Confocal laser scanning microscopy was used to measure fluorescence in this study. The VivaScope 2500 Multilaser (Figure 3.1) used in this study provided the advantages of reflectance depiction and reliable analysis of tissue within a short time unlike conventional methods such as histology. The skin tissue did not require complex preparation and preservation procedures. The VivaScope 2500 Multilaser uses three lasers with wavelengths of 658 nm (red), 488 nm (blue) and infrared laser (830 nm or 785 nm). The device is fitted with a motorised stage (Figure 3.2) for the sample, which moves to generate a tiled image over a large area. The stage can move +/– 8.0 mm in direction of x and y totalling a complete area of 16 mm square. The

confocal microscope can image up to 9 frames per second with 1000 x 1000 pixels in an individual image.

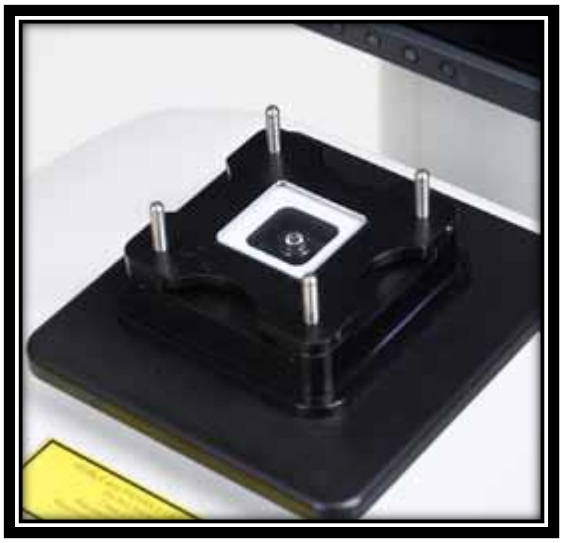

Figure 3.2 Motorised sample placement stage - VivaScope 2500.

The laser power enables imaging up to 200 μm. The VivaScope was designed as a quick and easy technique to assist physicians with the precise detection of margins between tumours and healthy tissue. For this study we have used the L1 or the blue laser to image sodium fluorescein. The confocal microscope was used with 488 nm excitation and 550 ± 88 nm emission bands to record images. Reflectance images can easily help differentiate between the different layers of the skin hence reflectance mode was used to a gain better understanding of the morphology of the skin.

3.3.2.2 Microneedles and Microneedle applicator

The microneedles used in this study were cut from a 50 μm thick 304 stainless steel sheet with the help of a LaserPro S290 laser milling machine. The microneedle arrays shown in Figure 3.3 were cut onto a single plate with 700 μm length × 250 μm width. Each plate consisted of 3 microneedles separated by a 5 mm distance. These plates were then assembled in banks of 2 with a 3 mm spacing in between. The microneedles were cut in batches with a strict quality control cut-off of 5% standard deviation. The tip of the microneedles was created at 55º forming a 250 μm long cutting surface. This method of laser cutting of microneedles was validated for consistency. A typical batch when observed for quality assurance had an average height of 703.1 ± 16.1 μm (SD = 2.25) and an average width of 257.8 ± 9.4 μm (SD = 3.64).

Figure 3.3 MN plate with three 700 µm length × 250 µm width MN.

The applicator developed for this study was designed to create an impact on the skin surface at a delivery speed of 1.5 m/s. Figure 3.4 shows a typical setup of the skin before the microneedles are applied.

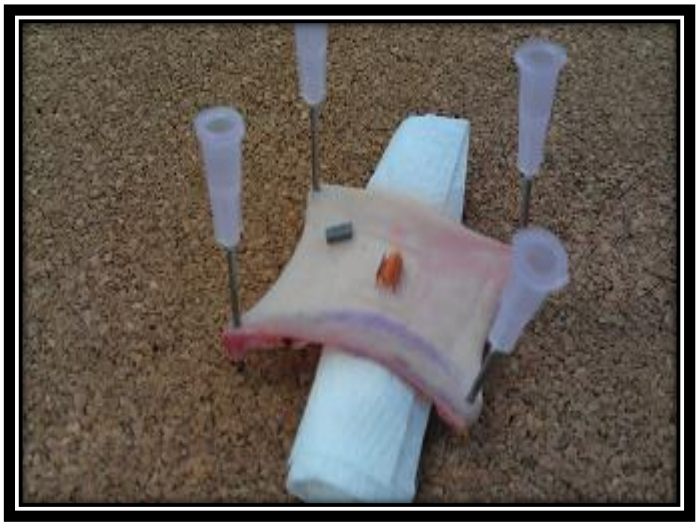

Figure 3.4 Skin setup for MN application.

The skin was moderately stretched by putting a rolled paper towel under it (figure 3.4) to allow for the proper insertion of the microneedles followed by placing the applicator on the desired location on the skin. After firmly pushing the applicator against the skin, the trigger was released to make six holes corresponding to the six microneedles. In figure 3.4 the microneedle spacers (small grey and orange blocks) have been left on the skin for explanation.

3.3.2.3 Transepidermal water loss (TEWL)

TEWL has long been used as an indicator of skin barrier integrity. Recent studies have validated the use of both open and closed chambers in the measurement of TEWL.[324] TEWL measurements in this study were performed using an AquaFlux

AF200 closed chamber evaporimeter (Biox Systems Ltd., London, UK). AquaFlux V6.2 software was used to analyse the data (Figure 3.5). TEWL readings were recorded in triplicate prior to the study and immediately after the study before imaging. Additionally on the skin groups which were applied microneedles, TEWL was measured immediately after the MN application.

Figure 3.5 AquaFlux AF200 TEWL meter.

3.3.3 Skin preparation for permeation studies

All experiments in this study were conducted on excised human skin in compliance with the guidelines of the National Health and Medical Research Council of Australia. Human skin was collected with prior approval from University of Queensland Human Ethics Committee. (2007/197) The subcutaneous fat was removed by dissection and the full thickness skin then stored at –20°C until required. Skin from different donors was used to demonstrate reproducibility of the study. Before commencing the study the skin was thawed to room temperature and carefully dabbed with clean tissue paper to remove excess moisture. The skin was then cut using a circular cutter to exact specifications to fit Franz cells with very little skin hanging over the receptor compartment.

3.3.4 Study design

3.3.4.1 Studies on sodium fluorescein

In an attempt to model the movement of the fluorescent dye after microneedle application, delivery studies were designed to determine the time taken for the dye to

move a set measure of distance away from the needle hole. Due to the proximity of the microneedle hole it was decided to study only time points prior to the overlapping of fluorescence planes. Figure 3.6 below demonstrates a typical fluorescence image taken 5 min after sodium fluorescein application.

Figure 3.6 Sodium fluorescein imaged 5 min after treatment application.

Freshly excised skin was obtained mostly on the day of the experiment or within 24 h of the experiment at the latest. *In vitro* permeation studies of sodium fluorescein across full thickness human skin were performed in Franz-type diffusion cells. The skin was mounted in the Franz cell with the stratum corneum uppermost. The receptor compartment of the cell was filled with saline, stirred with a micro stirrer and maintained at 35°C in a temperature controlled water bath. TEWL measurements were made before and after the experiment to confirm barrier integrity. All skin samples with TEWL reading above 35-40 g/m^2h were discarded. The experiments were carried out by applying the drug on either MN treated or control skin pieces. Sodium fluorescein at a concentration of 500 µg/mL was first massaged into the skin after the application of microneedles. Then a reservoir of 300 µL of sodium fluorescein solution was left in the donor compartment to provide an infinite dose.

The donor compartment was occluded with Parafilm™ and aluminium foil to avoid light and loss of hydration. The duration of the study was varied from 5 min up to 2 h. After completion of the intervention time, the excess drug was dabbed off the skin carefully, followed by imaging using confocal microscopy. Images were generated after 5, 10, 20, 40 and 120 min of drug application.

3.3.4.2 Studies on fluorescent peptides

Despite the increasing importance of protein therapeutics and vaccines, the need to deliver them by hypodermic injection remains a major limitation, due to the pain associated with it and the need for supervised application. Delivery of protein drugs through the skin is an attractive alternative to needles, but has proved elusive thus far, barring a few examples.[272] Because the primary barrier to transport through the skin is located in the upper 10-15 μm of skin and nerves are found only in deeper tissue, we used microfabrication techniques to make arrays of microneedles long enough to cross the permeability barrier with ease (700 μm) but not so long that they are painful.[325] The peptides used in this study were selected as cosmetic and therapeutic peptides with increasing chain length and increasing molecular weight. The design of the study was to observe penetration enhancement of the peptides as a function of their molecular weight or size. The experimental protocol used was similar to the sodium fluorescein studies. Fluorescein conjugated peptides melanostatin (MEL) (MW 803.92 Da), rigin (MW 959.04 Da) and palmitoyl pentapeptide (Pal-KTTKS) (MW 1191.06 Da) were first dissolved in appropriate solvents as per manufacturer's instructions. The study included eight groups each conducted in triplicate. Negative controls were solvent only and solvents post microneedle application to account for any auto fluorescence that may be encountered. Sodium fluorescein, in the amounts equivalent to that present in the peptide, was used as a positive control in both passive interventions where microneedles were not applied, and in active interventions where microneedles were applied. The last two interventions included the peptides with and without microneedles applied at a 500 μg/mL concentration. The treatment time during the study was 1 h for all interventions. For the peptides a separate 24 h time point from the same skin donor was also conducted. The replicate experiments on each peptide were conducted using skin from multiple donors.

3.3.4.3 Standard curves for sodium fluorescein and fluorescent peptides

The visual analysis of images to provide quantitative measurements such as protein concentration and the identification of specific fluorescent signals is a complicated task. It is dependent on both the methods used to acquire and analyse the data as well as the accuracy and precision of instrument functions.[317] The drawback of working with a mode of experimentation that measures luminous/fluorescent intensity is that it is not fully quantifiable in all instances. It is rather straight-forward to compare the different active and passive interventions and measure their fluorescent intensities, but correlation to their exact amounts is a desired outcome. Serial dilutions of the solutions of sodium fluorescein and the peptides were quantified. To make standard curves, images were taken at different power levels. The sample solutions were placed in a rubber ring that was stuck on a glass slide with the help of high vacuum grease. The ring was covered with a cover slip and sealed with cellophane tape on the sides. Figure 3.7 illustrates prepared samples for standard curve imaging.

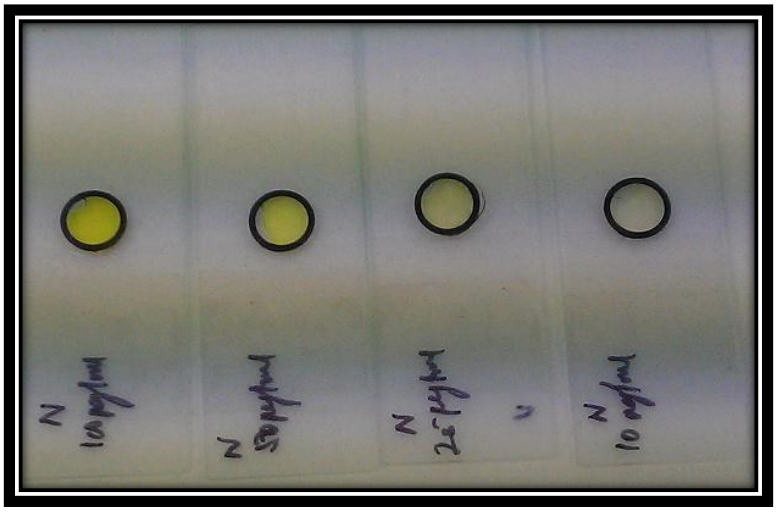

Figure 3.7 Samples prepared for standard curve.

3.3.5 Imaging and analysis of images

After completion of the treatment time the skin samples were cut to a smaller size. Before the samples were imaged with LSCM, a dermoscopic image was first taken to identify the exact location of the microneedle holes. The sample was then mounted with microscopy oil and covered with a cover slip. The VivaScope 2500 Multilaser was used for this study as it covers an area big enough to image the microneedle holes completely in one tiled image. The images were generated as cubes of tiled

images of 8×8 individual images over 20 layers. The cube was generated over 100 µm with images at a step of 5 µm. Similarly cubes were also generated from the same area (depth and location) in reflectance mode. The reflectance image in conjunction with the z-axis profile of the intensity depth was used to determine the top layer of the skin sample. The top 20 microns were designated as the stratum corneum (SC), the following 30 microns were designated as the viable epidermis (VE) and the images from below this (50 microns + deeper) were designated as the dermis (DER).[326]

Analysis of the intensity images was carried out on Image J software designed by the NIH (USA). Three different settings were used for the analysis of images from the sodium fluorescein time profile penetration experiments.

Analysis technique 1: Firstly a line plot of intensities and integrated densities (ID) on each of the layers was generated starting from the centre of each microneedle hole. Line plots were generated in all four directions on all six microneedle holes. Figure 3.8 a) illustrates a typical image with line plot drawn, b) illustrates a plot of the intensities observed.

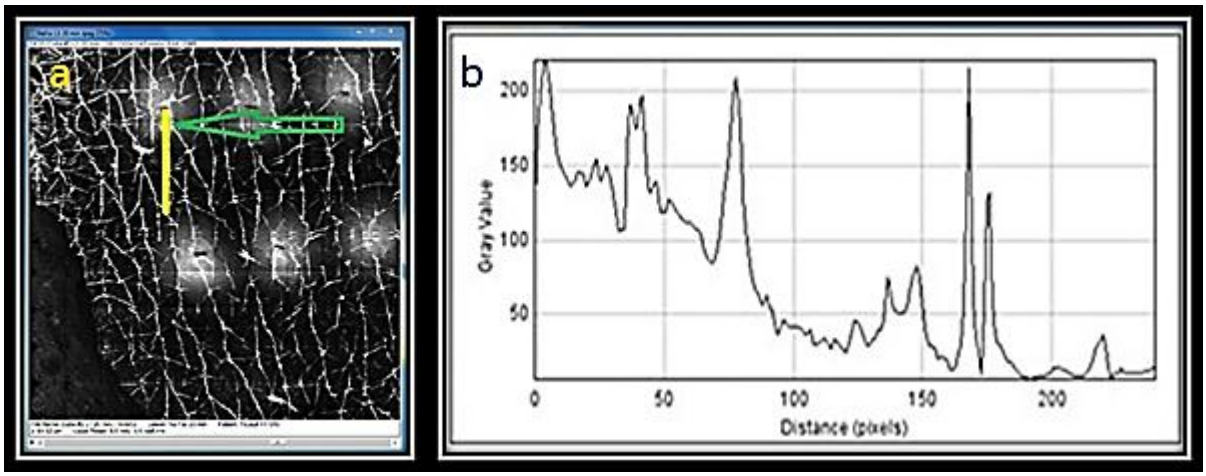

Figure 3.8 a) Image with line plot, b) Plot of the intensities measured

Analysis technique 2: The second method of analysis used modification of threshold intensity to select out the area of intensity around the microneedle hole. For all analysis a mean threshold of 54 (in arbitrary units) was used as minimum permitted intensity corresponding to the FITC or NaFsc fluorescence. The threshold was selected by visual analysis and repeated testing. Once the area of high intensity corresponding to sodium fluorescein was isolated, the size, area and integrated

density values were calculated using the ***Analyse particles*** tool on Image J. Figure 3.9 a) illustrates a high intensity area separated from the cube image by adjusting the threshold intensity, b) illustrates an outline of the area of intensity which can then be measured in either pixels or µm.

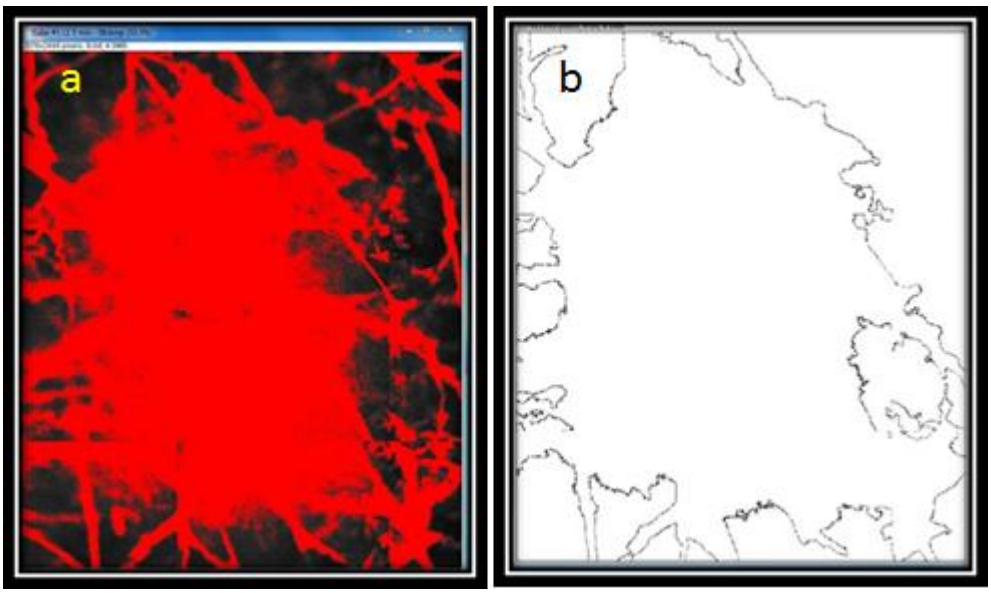

Figure 3.9 a) High intensity area, b) Outline of the area of high intensity.

Analysis technique 3: The third method of analysis used the radial profile plugin from Image J. A circular area around the microneedle hole with a predefined radius was selected, the threshold adjusted as previously described (Figure 3.10 a) and the ***Radial Profile angle*** tool from plugins was used to generate a plot (Figure 3.10 b) of integrated intensity vs. radius.

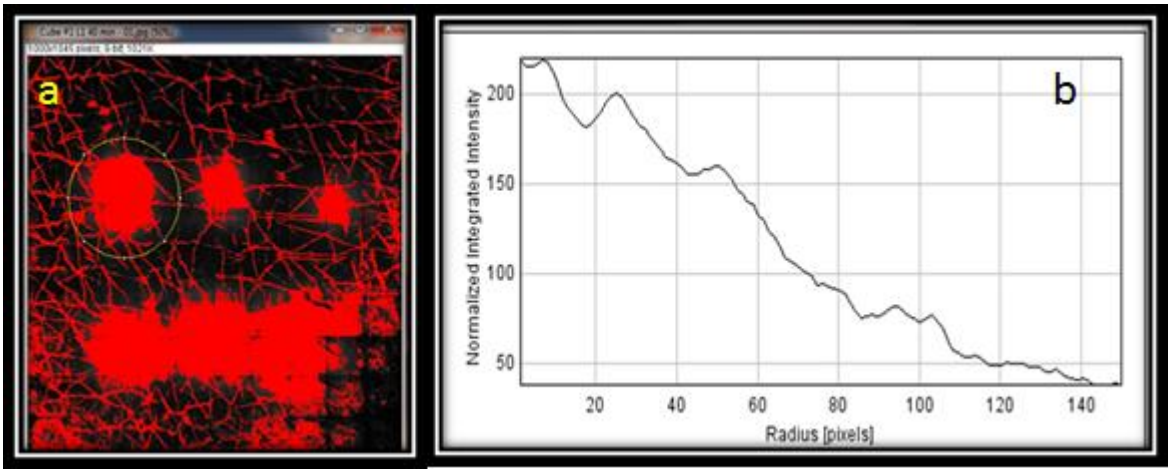

Figure 3.10 a) Circular area around the microneedle hole, b) Integrated intensity vs. radius plot.

The line plots generated from analysis technique 1 and radial profiles generated from technique 3 were compartmentalised into four different compartments of equal area (1766250 Pixels). Intensities and integrated density (ID) in these compartments were plotted against time to represent the movement of the dye from one compartment/zone to the other.

3.3.6 Statistical analysis

The skin permeation data consisted of normalised penetration area and integrated density measurements of active, passive, negative control and positive control taken at various times (1, 4 and 24 h) imaged in the skin layers, viable epidermis and dermis. A random effects regression model was used to compare the treatments at various time points, with the timings treated as categorical variables (so that no linear relationship was assumed between permeation and time). This type of regression model is equivalent to a repeated measures analysis of variance, in that it properly takes into account correlations between measurements made on the same sample at different time points. If the standard deviations of the permeation appeared to differ widely for different time periods, a logarithmic transformation was performed on the permeation before analysis.

Pairwise comparisons were calculated from the regression model by requesting certain 'contrasts' as required. Contrasts were tailored to make specific comparisons, and obtain the p-values for them. The standard errors on which the contrasts were based were estimated from the regression model which was based on all the available data. If the analysis was performed on the log-transformed data, the p-values for the pairwise comparisons were based on this analysis, but the mean permeations were quoted on the original scale (to simplify interpretation).

All statistical analyses were performed using the SAS version 9.2 statistical software (SAS Institute Inc, Cary, NC, USA, 2008). A p-value <0.05 was taken to indicate a statistically significant association.

3.4 Results and Discussion

3.4.1 Preliminary studies

3.4.1.1 Preliminary studies on sodium fluorescein

Time profiling studies on NaFsc were conducted to gain information about the kinetics of drug diffusion post microneedle (MN) application. We hypothesised that MN based delivery will follow different kinetics in different layers of the skin (SC, VE and DER) that can be statistically verified. To optimise the experimental protocol for the time based study we conducted numerous pilot studies and examined different variables.

3.4.1.1.1 Effect of concentration of Sodium fluorescein (NaFsc) on its lateral diffusion

Solutions of NaFsc were prepared in water with concentrations of 500 µg/mL and 1 mg/mL. The 1 mg/mL solution gave an intensity signal which was very strong and in some cases was giving results which were to the maximum threshold intensity (254). A very high intensity image makes it difficult to quantify and isolate the area around the MN. On reduction of the concentration to 500 µg/mL the pictures were of reasonable contrast and detail with minimal photo bleaching. The area of penetration around the MN was measurable and fluorescence was observed up to 200 µm deep. Passive administration of NaFsc at 500 µg/mL permeated to the shallow layers of the skin and was concentrated in the skin furrows. Figure 3.11 (a) shows a 500 µg/mL NaFsc image from the passive treatment in viable epidermis, (b) shows a 500 µg/mL NaFsc image from the active MN treated skin in viable epidermis.

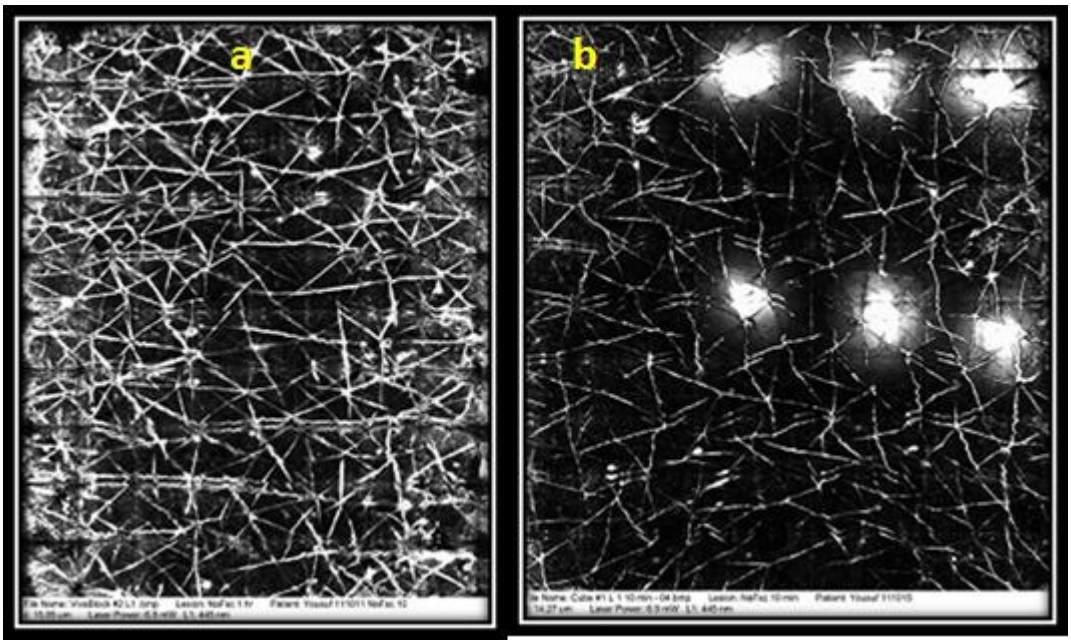

Figure 3. 11 a) NaFsc diffusion (passive) in viable epidermis, b) NaFsc diffusion (active-MN) in viable epidermis.

3.4.1.1.2 Effect of time

To observe a time correlation of penetration after MN application we conducted pilot studies on times ranging from 5 min to 8 h. Due to the highly hydrophilic nature of NaFsc its penetration after the stratum corneum is breached is extremely fast.[191] It was observed that the movement of the fluorescent peptides was much slower when compared to NaFsc. Therefore at the longer time points studied, NaFsc showed rapid movement of the bright fluorescent area away from the MN hole and towards the periphery of the skin sample. In all time points over 1 h the highest intensity fluorescent area was not observed around the microneedle holes. The fluorescence was of much lighter intensity but the area of fluorescence was vastly increased, encircling all the holes and distinction of fluorescence from the fluorescent drug present around individual MN holes was not feasible. Figure 3.12 shows a 4 h image of NaFsc after MN application.

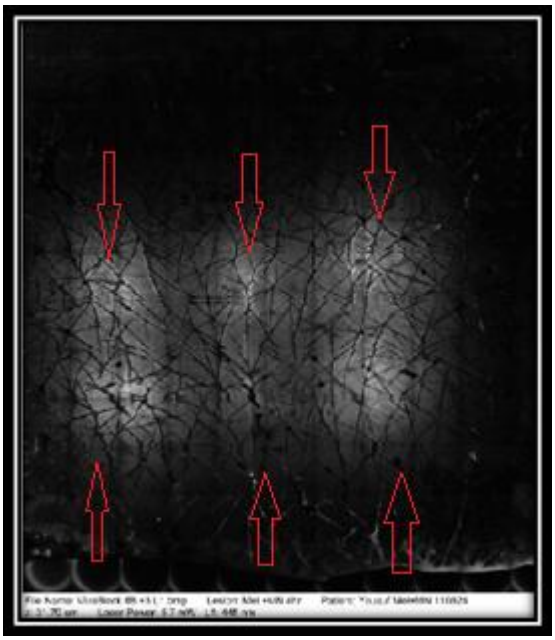

Figure 3.12 NaFsc at 4 h after MN application.

3.4.1.1.3 RCM settings- Auto power control

The VivaScope 2500 provides a tunable range to adjust laser power and gain.[321-323] However automatic image control allows the VivaScope to automatically optimize the laser power so that the image is displayed with the proper illumination. Reflectance confocal microscopy has been extensively used in the field of dermatology and there are more than 150 publications where RCM has been used.[327] However, confocal microscopy is not optimal for quantitative measurements when using a single power setting. It has been shown that epidermal scattering and absorption limit the penetration depth of light, both in the acceptable laser excitation powers as well as the emitted fluorescence.[328] In the automatically adjusted laser power used for this study, the reflectance mode laser power ranged between 0.4 and 1.2 milliwatts (mW) and in fluorescence mode, the laser power ranged between 4 and 6.9 mW.

3.4.1.1.4 Effect of microneedle size/ design and impact velocity of the applicator

For this project we have used multiple MN designs and some have been shown in Figure 3.13 (a) 1 mm row of 3 MN, (b) 700 µm row of 5 MN, (c) 1 mm polymer row of 3 MN, (d) 700 µm row of 3 MN. The MN designs were governed by various factors such as ease of piercing into the skin, strength of the MN, reproducibility of puncture and area of fluorescence after MN application.[209,325,329,330] The 1 mm MN

were discontinued after the pilot stages, as they were deemed to be slightly longer than the generally required length to sufficiently pierce the skin. Moreover the polymer (epoxy) microneedles fabricated in the lab using Polydimethylsiloxane (PDMS) moulds were found to be brittle and posed a risk of breaking on application. In a study conducted on human volunteers by Gill et al.[325] 30% of subjects reported both the 480 μm and the 700 μm long microneedles as completely painless, whereas 0% and 10% reported the 960 μm and 1450 μm long microneedles painless, respectively.[325] The 700 μm row of 5 MN was equally effective in strength and reproducibility to the 700 μm row of 3 MN which were ultimately selected for the studies. However, due to the proximity of needles to each other the zone of florescence penetration plane was not accurately measureable. Hence the MN plate with a row of 5 MN was replaced by the 3 MN plate and the distance between the needles set as 2.1 mm. The tip of the microneedles was angled at 55º. Two plates of these microneedles were arranged in the applicator with the help of spacers totalling 6 MN per array. The study by Gill et al. also showed that MN arrays containing 5 to 50 microneedles were completely painless as reported by a significant number of test subjects; however there was no significant correlation found with pain and the microneedle tip angle.[325]

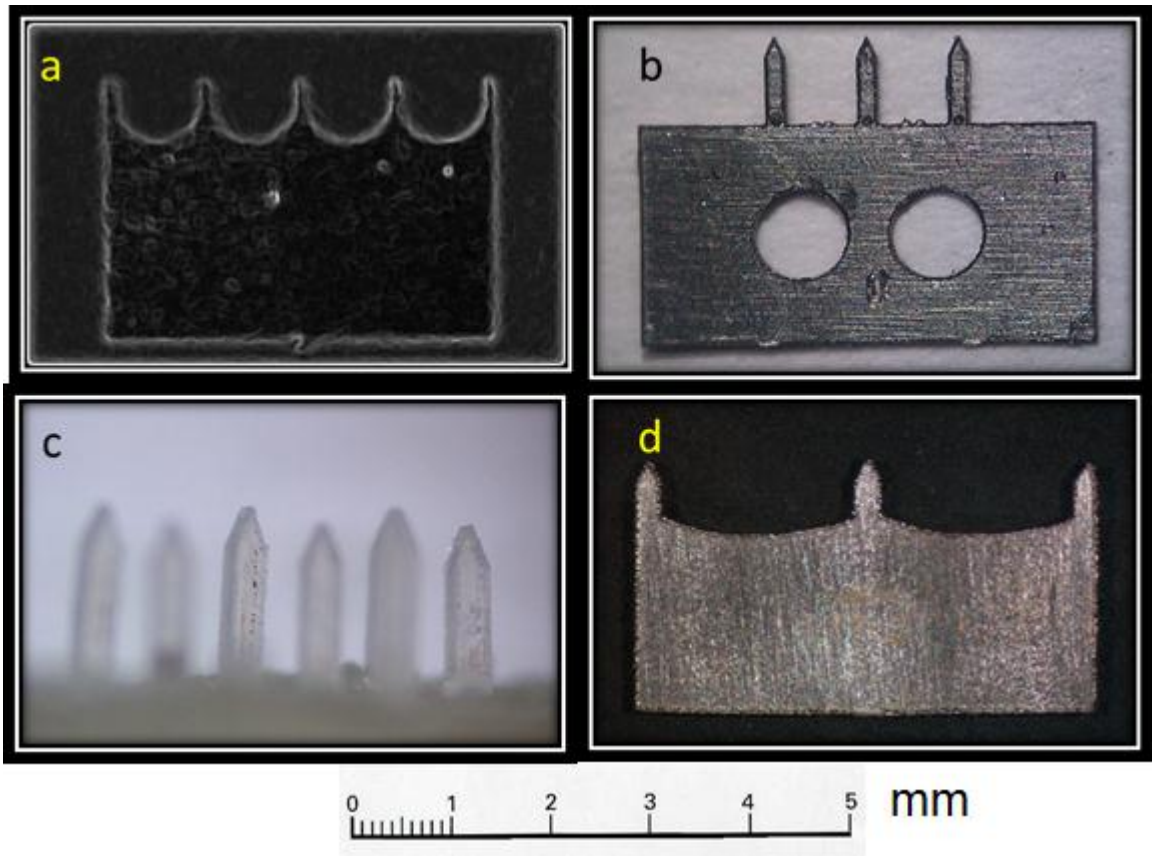

Figure 3.13 a) Stainless steel MN plate with a row of 5 MN, b) Stainless steel MN plate with a row of 3 1mm MN, c) Cured epoxy adhesive MN plate with a row of 3 MN, d)) Stainless steel MN plate with a row of 3 MN

The strength and speed at which the MNs are applied not only governs the optimal piercing of the skin but also the shape and size of the pores/conduits formed.[191, 208,329] Verbaan et al.[331] showed that a higher piercing velocity resulted in a higher transport rate of dyes after MN application. The authors have been granted a patent on an electronically operated MN applicator which can insert MN at a piercing velocity of 1 to 3 m/s.[331] For this study we used a spring loaded mechanical applicator which inserted the MNs with 1.5 m/s piercing velocity.

3.4.1.2 Preliminary studies on fluorescent peptides

3.4.1.2.1 Effect of concentration

The peptides used in this study were applied at a concentration of 500 µg/mL as the preliminary studies with NaFsc were used as a yardstick to decide various transposable parameters. However, for these studies NaFsc was used as a positive control and it was decided by careful consideration that NaFsc should not be used at a 500 µg/mL concentration. Firstly, NaFsc has considerably better transport

properties then the peptides in the study. Moreover, the amount of fluorescein present in the peptides is a molar ratio, and hence substantially lower. Therefore, NaFsc equivalents were calculated for all 3 peptides: the amount of NaFsc used was 310 µg/mL, 261 µg/mL and 163 µg/mL for melanostatin, rigin and palmitoyl pentapeptide (Pal-KTTKS) respectively.

3.4.1.2.2 Effect of time

Pilot studies were conducted with treatment times of 1 h, 2 h, 3 h, 4 h, 8 h and 24 h in an attempt to effect maximum penetration of the peptides with minimum damage to the skin. After numerous attempts to optimise the study duration, the studies on the peptides were conducted for 1 h. This was mainly due the markedly high lateral penetration of NaFsc (positive control) after MN based delivery. Figure 3.12 shows a 4h NaFsc treatment. However, for the peptides a 24 h sample point was carried out in expectation of a greater degree of penetration both passively (without MN) and actively (with MN). Peptides are highly prone to lipid binding and their partitioning from the transdermal lipids can be time consuming.[272,332] The peptides used in this study are primarily cosmetic peptides and a longer duration of intervention before they can show the desired effects is generally more tolerable then for therapeutic molecules.[12,333,334]

3.4.1.2.3 Effect of vehicle for peptide dissolution

The peptides were dissolved according to the solubility studies completed by the synthetic laboratory (Genscript USA). Melanostatin was soluble in water at pH 10; ammonia solution was used to adjust the pH. Rigin was soluble in water at pH 7. However, with Pal-KTTKS, the ideal solvent after solubility test was found to be DMSO. DMSO has been used as a very potent chemical penetration enhancer and at higher concentrations can lead to cornification of the skin.[335] Moreover, the outcome of our studies was entirely dependent on the ability to image the various layers of the skin with good contrast and quality. This was not possible as the morphology of the skin was severely altered. Figure 3.14 shows images from the viable epidermis taken during a pilot study with (a) Water as solvent and (b) DMSO as solvent. The disintegration of cellular structure and disappearance of furrows is clearly visible from the images where DMSO was used as a solvent.

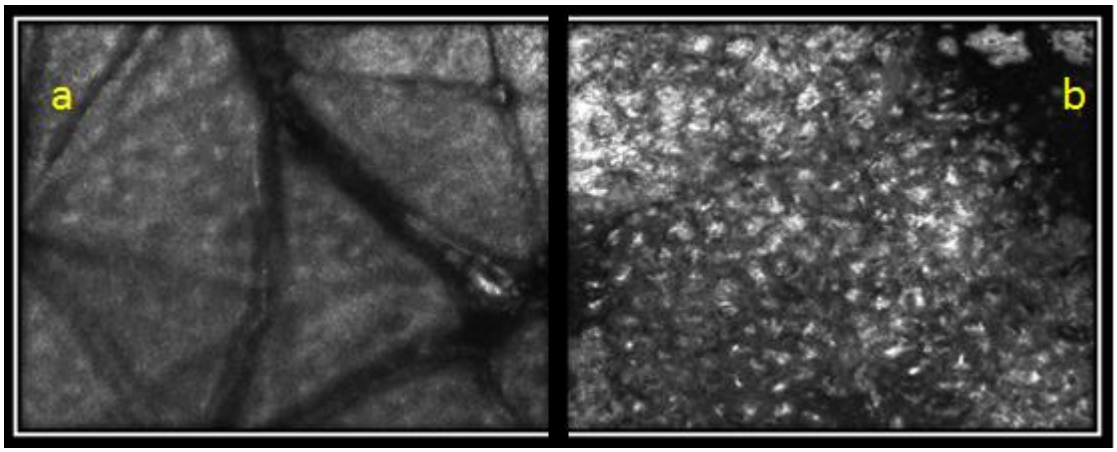

Figure 3.14 Images from the viable epidermis taken during a pilot study a) Water as solvent b) DMSO as solvent

For Pal-KTTKS and later on for all the controls 25:75 PG: Water was used as the solvent. Though propylene glycol is a mild penetration enhancer,[153,336] it does not affect the imaging quality. The penetration enhancement effect of PG however was not observed during our studies.

3.4.2 Imaging protocol for MN based delivery studies

The skin samples were cut into a desirable size to expose only the MN applied area. The immersion gel was placed between the objective lens and the glass slide, whereas the excised skin was covered with a coverslip using microscopy immersion oil. The reflectance mode was used to locate the top of the skin, the objective was moved up by 5-10 microns and this was set as the Zero depth. This was followed by a switch to fluorescence mode where the 'Z' position was moved to 40-50 μm from Zero depth. A complete '*Viva block*' was captured which basically is one layer of the cube at a given depth. This was done to make sure all six needle holes and their fluorescence planes were imaged in the block. Imaging was performed to capture cubes of composite maps. The composite maps were a series of full field (750 × 750 μm) images in a single, horizontal plane that are automatically captured and "stitched" together to form a composite image that ranged from 4 × 4 mm to 8 × 8 mm square. This mosaic of images essentially "cuts" an optical section into the specimen close to its surface. Sequential stacks of images were captured as long as image quality and resolution were maintained, to a maximum depth of 200 μm. Individual full field images and stacks of area containing the MN holes were

captured as needed. The complete imaging process took 20–40 minutes, although initial images were obtained in less than five minutes.

The *'Z'* stack images of the individual MN hole were used only for illustration purpose and better understanding of the morphology. No analysis was carried out using these pictures. Figure 3.15 (a) shows a *'Z'* stack image of MN hole in reflectance mode and (b) *'Z'* stack image in fluorescence mode. The VivaScope 2500 is capable of imaging with good clarity up to 300 μm, for this study cubes and stacks were produced with a 200 μm depth.

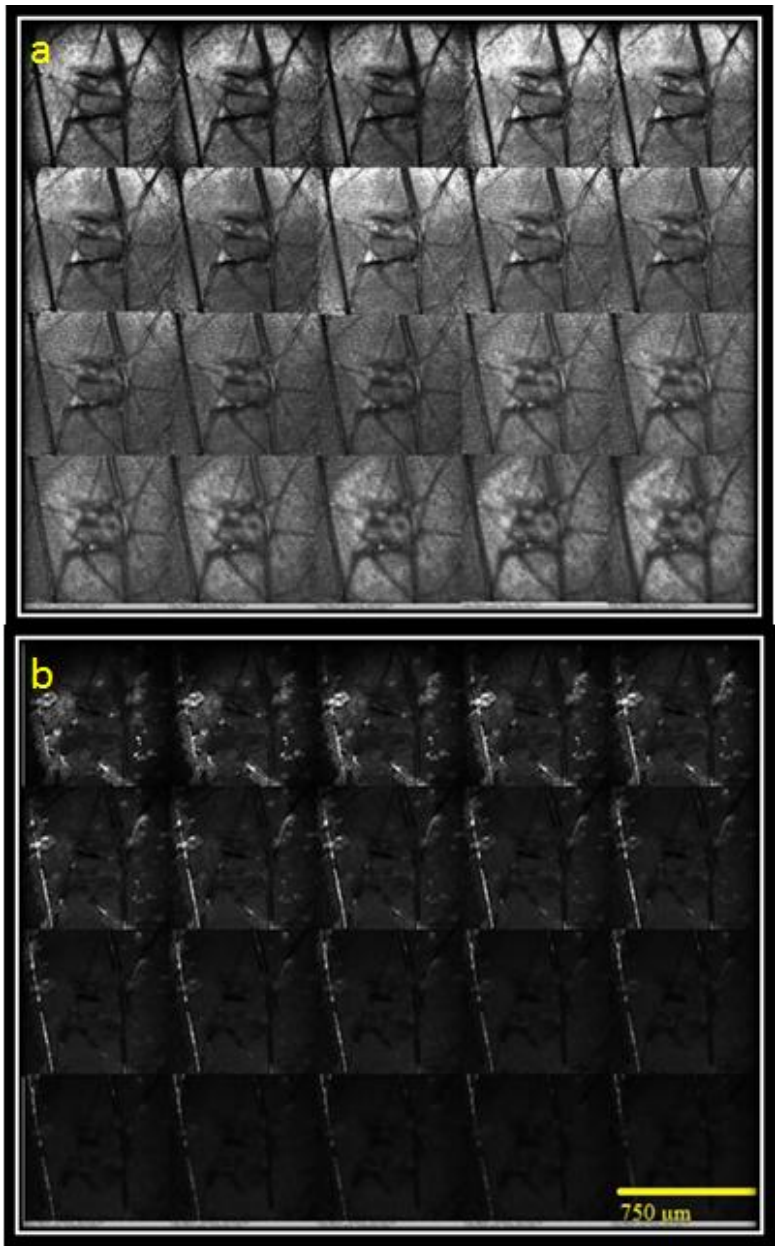

Figure3.15 a) 'Z' stack image of MN hole in reflectance mode and b) 'Z' stack image in fluorescence mode

Transverse sections of skin are often used in dermoscopic evaluation.[337] In this study we have used cryosectioning in the pilot stages to locate MN holes and look at lateral penetration from the MN holes. However, cube images of the VivaScope are a very reliable and quick way to gain the same information in one place. Though sectioning can provide more detailed information, it is a time consuming and arduous task. The confocal optical section thickness compares very well to the typically 5 μm thin sections that are prepared for conventional histopathology using skin freezing followed by fixing. With Reflectance confocal microscopy, skin can be imaged either *in vivo* or *ex vivo* without any processing.[338]

3.4.3 MN based delivery studies on Sodium Fluorescein (NaFsc)

Fluorescent molecules are the easiest way of studying not only the histology of skin and morphology of live and excised tissue; they are also a very useful tool in exploring effectiveness and feasibility of novel skin penetration technologies. Fluorescent molecules like sodium fluorescein (NaFsc) have been used to study transdermal penetration enhancement for a very long time.[339,340] In this study we aimed to evaluate the effectiveness of the MN fabricated and designed *in-house*. It was also envisaged to develop a working transdermal delivery model from the MN based delivery of NaFsc. This model would be able to better characterise the diffusion of molecules from the MN hole in sink conditions. Various parameters like transdermal flux and permeability coefficients would ideally drive towards better optimization of MN design and provide useful information on the expected flow properties of a host of other therapeutic molecules. A time based compartmentalisation of NaFsc in the various layers of the skin such as stratum corneum (SC), viable epidermis (VE) and the dermis (DER), along with the movement of the dye from the centre of the MN hole to the periphery of the fluorescent aura can be studied in sink conditions. Hence in this study, the lateral and depth penetration of NaFsc was studied over a series of short to medium durations.

The data analysis was carried out using methods 2 and 3 described in section 3.3.5 Figures below show the penetration of NaFsc in stratum corneum (SC), viable epidermis and dermis in the three replicates produced in different skin donors: Figure 3.16 donor 1, Figure 3.17 donor 2 and Figure 3.18 donor 3. The replicates show a

degree of variability within the skin donor group that varied from 27 to 54 year old females.

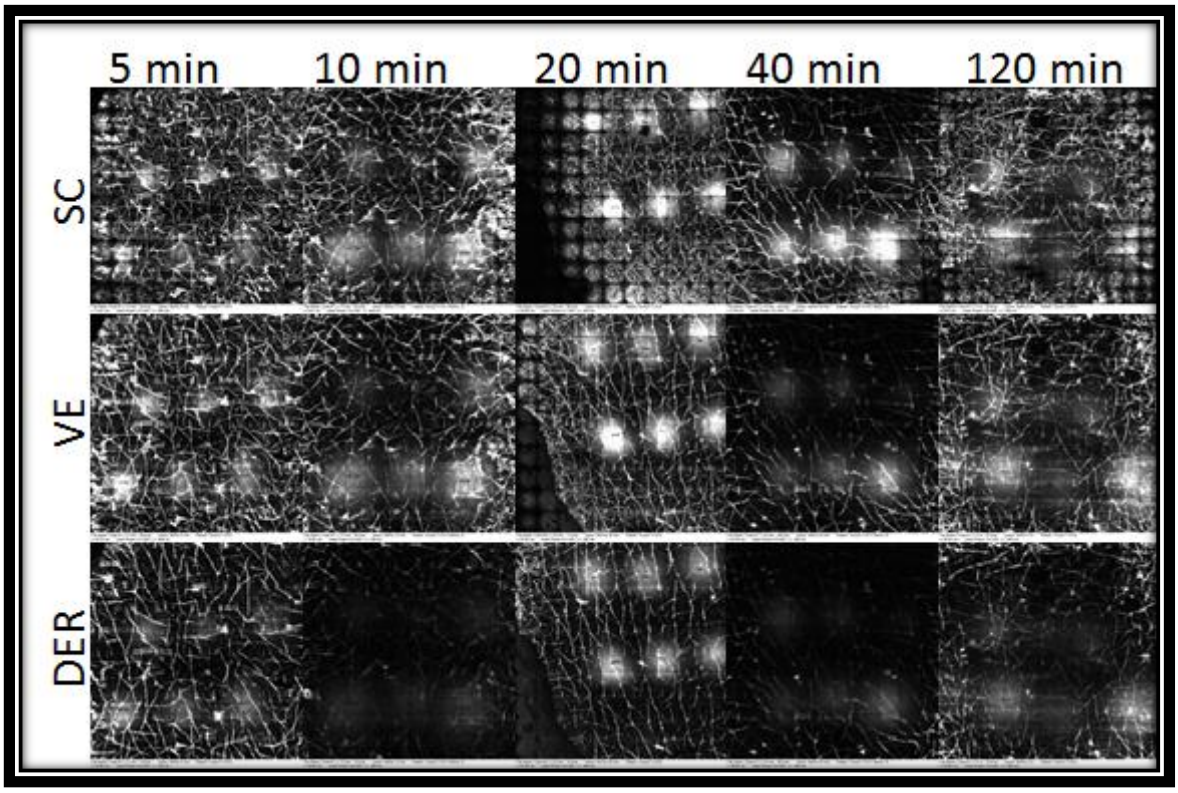

Figure 3.16 Penetration of NaFsc in stratum corneum, viable epidermis and dermis from 5-120 min after microneedle mediated skin delivery (Donor 1)

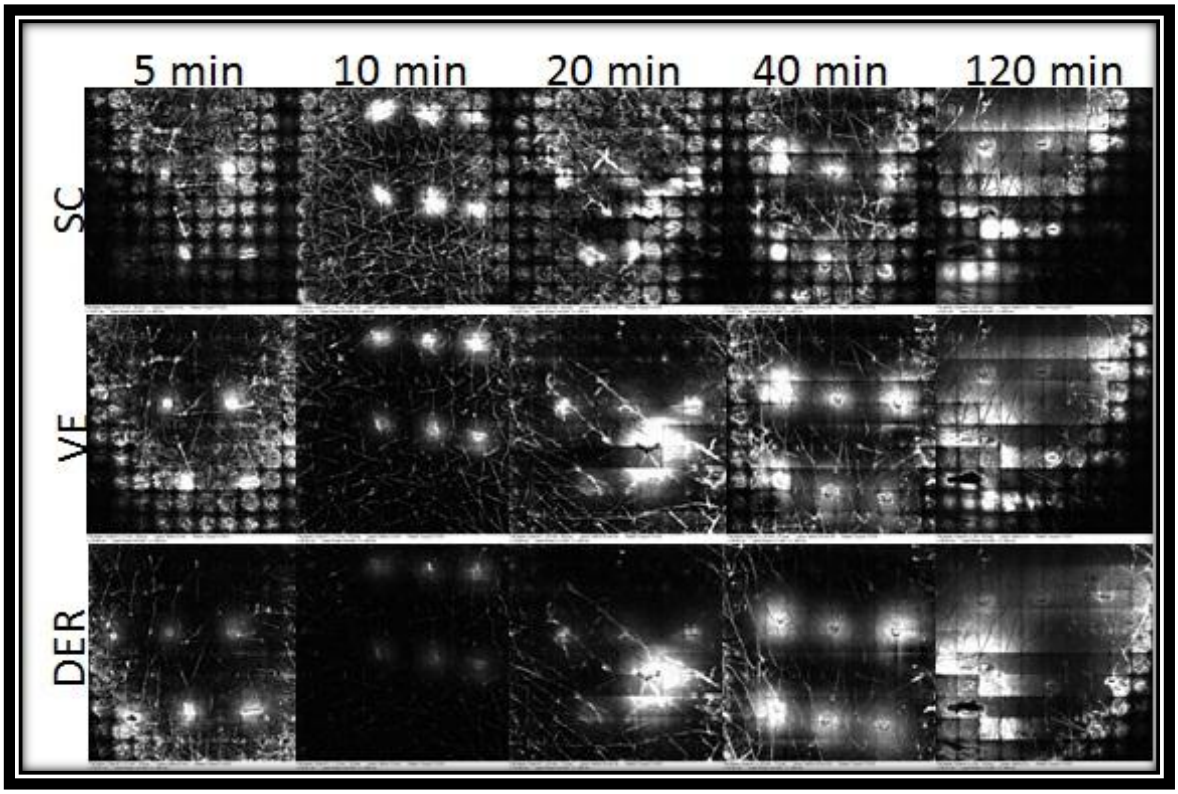

Figure 3.17 Penetration of NaFsc in stratum corneum, viable epidermis and dermis from 5-120 min after microneedle mediated skin delivery (Donor 2)

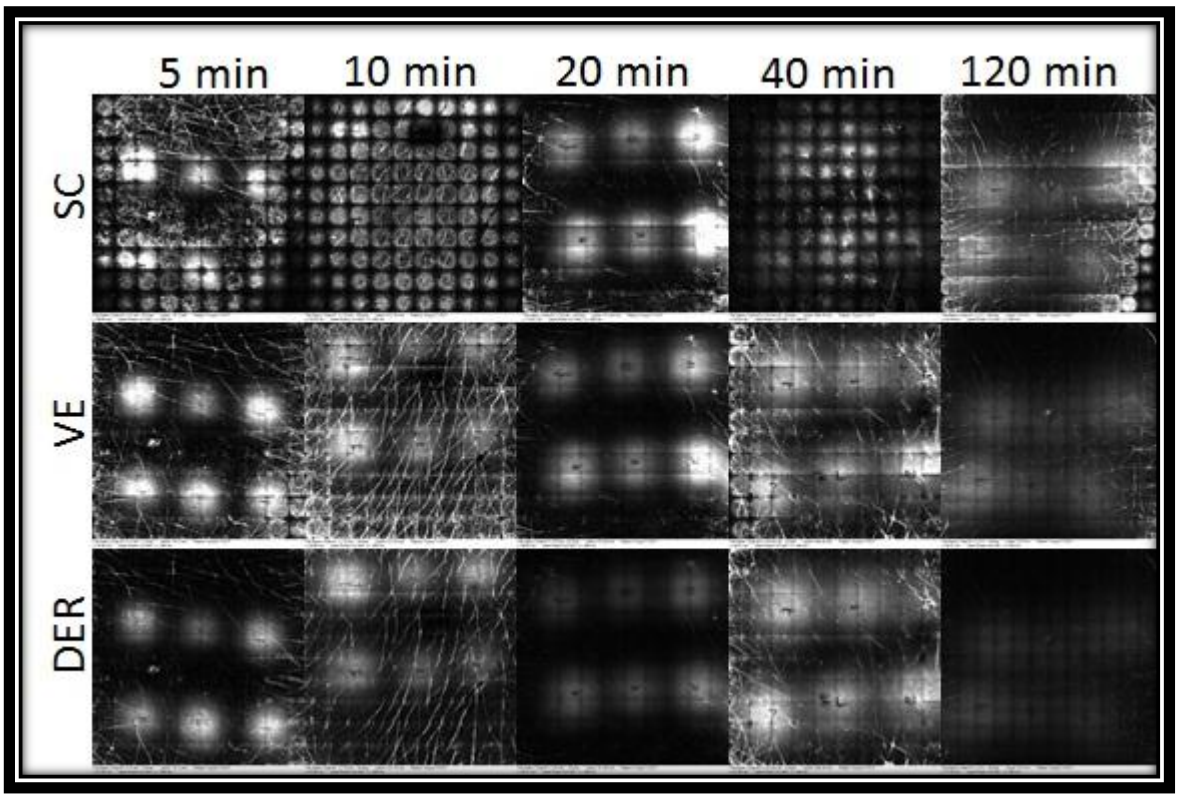

Figure 3.18 Penetration of NaFsc in stratum corneum, viable epidermis and dermis from 5-120 min after microneedle mediated skin delivery (Donor 3)

Using the second method of analysis and selecting out the area of intensity around the microneedle hole by modifying of the threshold intensity, the total area of penetration was calculated. These calculations were based on the average fluorescence intensity between 54 and 255. The merit of doing this was the ability to select out only an area of even fluorescence surrounding the MN holes. Establishing the threshold to eliminate noise or background was carried out by subtracting the threshold from the image.[341] Bal et al.[191] categorised pixel intensity into three different classes: the class with the highest pixel intensity between 230 and 255 AU was referred to as high intensity fluorescence (HIF); the class with pixel intensity between 230 and 14 AU was referred to as low intensity fluorescence (LIF) and the class with pixel intensity values below 14 AU was regarded as background. The Figure 3.19 below shows an image from the 40 min time in our study (a) the area selected in at intensity range of 54-255 AU. Conversely in (b) selected at intensity threshold range of 14-255 AU the entire image was selected as the zone of penetration.

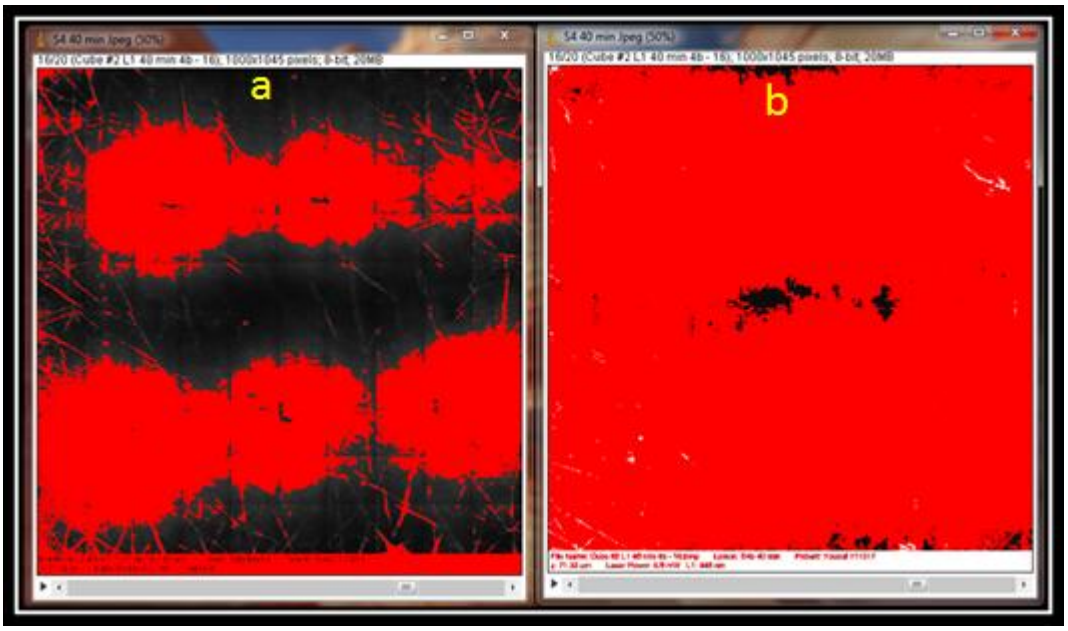

Figure 3.19 Image from the 40 min time point a) selected intensity threshold range of 54-255 AU b) selected intensity threshold range of 14-255 AU.

The concentration of NaFsc used in our study was a quarter of the concentration used by Bal et al. (Bal et al. 2 mg/mL vs. our study 500 µg/mL). At 500 µg/mL the area of penetration from the MN used in this study was 3.47 mm radially from the centre of MN. This area gradually increased to 5.2 mm by 120 min of NaFsc application. The

results in Figure 3.20 show an increase in area of penetration as the time period was increased and the area of penetration in the VE and DER increased gradually.

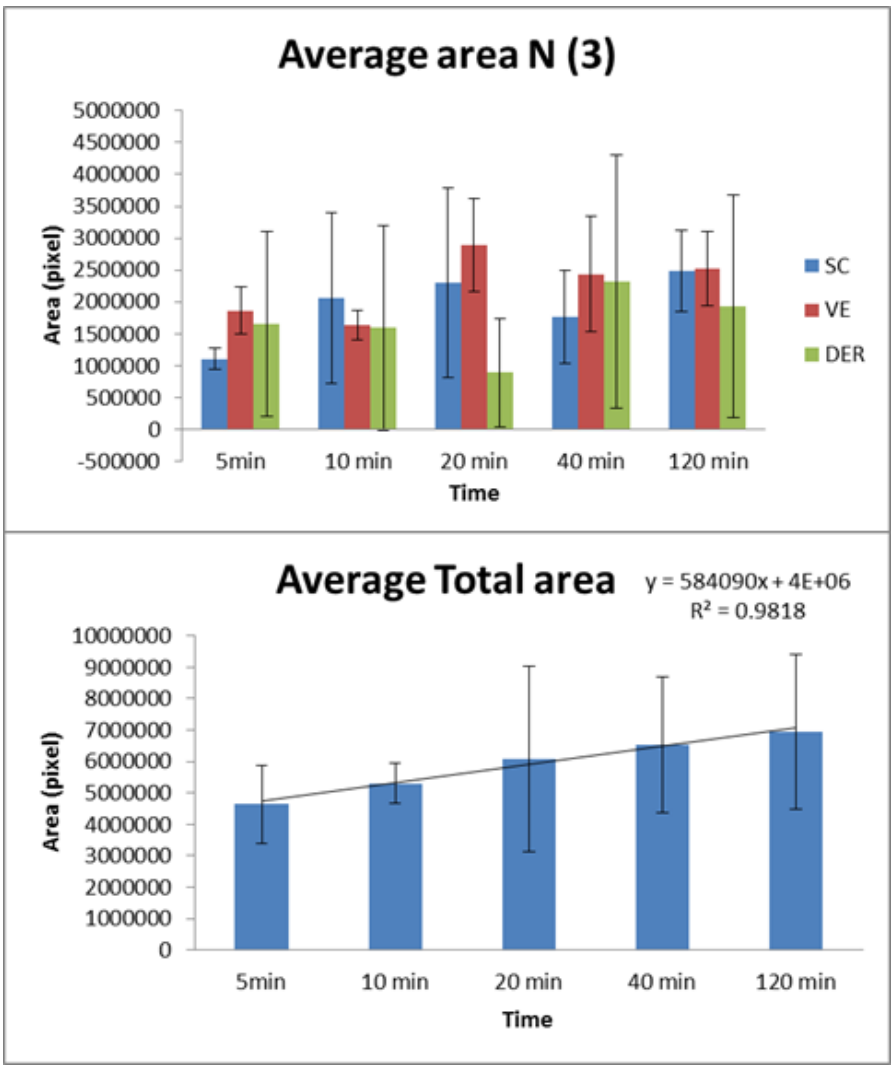

Figure 3.20 Average area of NaFsc penetration in skin strata (n=3, results expressed as mean ± SD)

Figure 3.21 below shows a 3D view of the area of penetration around one of the MN holes after 5 min time point. Images are shown in a series from the DER to the top of the SC across 60 µm. The axis 'x' and 'y' are planner and 'z' is the axial depth adding the third dimension.

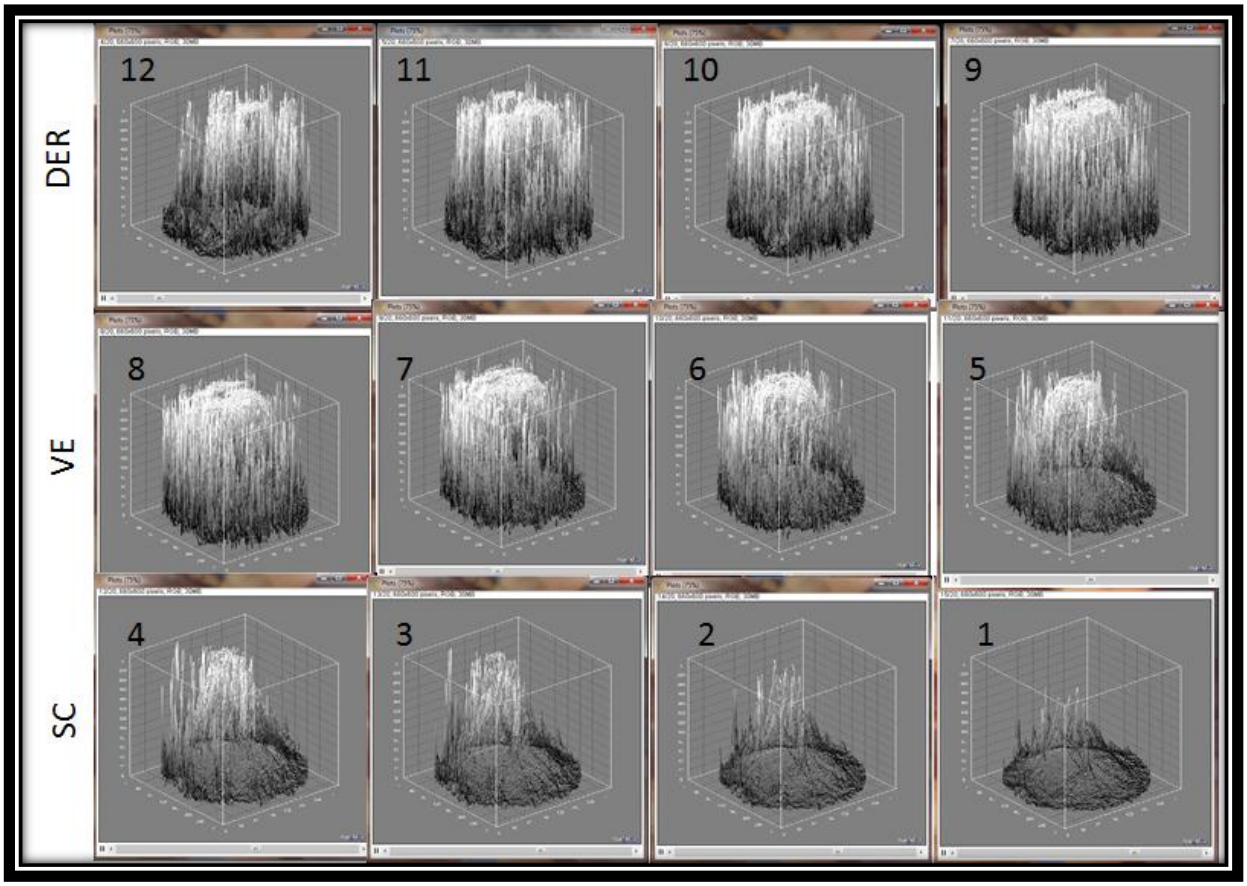

Figure 3.21 3D view of the area of penetration-5 min

In the next method integrated density (ID) values were calculated in a series of compartments/zones (Z) starting from Z1, the closest to the MN hole. Integrated density is the sum of the values of the pixels in the image or selection. This is equivalent to the product of area and mean grey value (MGV). Circular sections of the complete penetration zone were divided into 4 compartments of identical area (1766250 pixels). Concentric circles of radius 750 pixels, 1060.65 pixels, 1299.03 pixels and 1500 pixels were drawn. Figure 3.22 illustrates the zoning of the fluorescent planes.

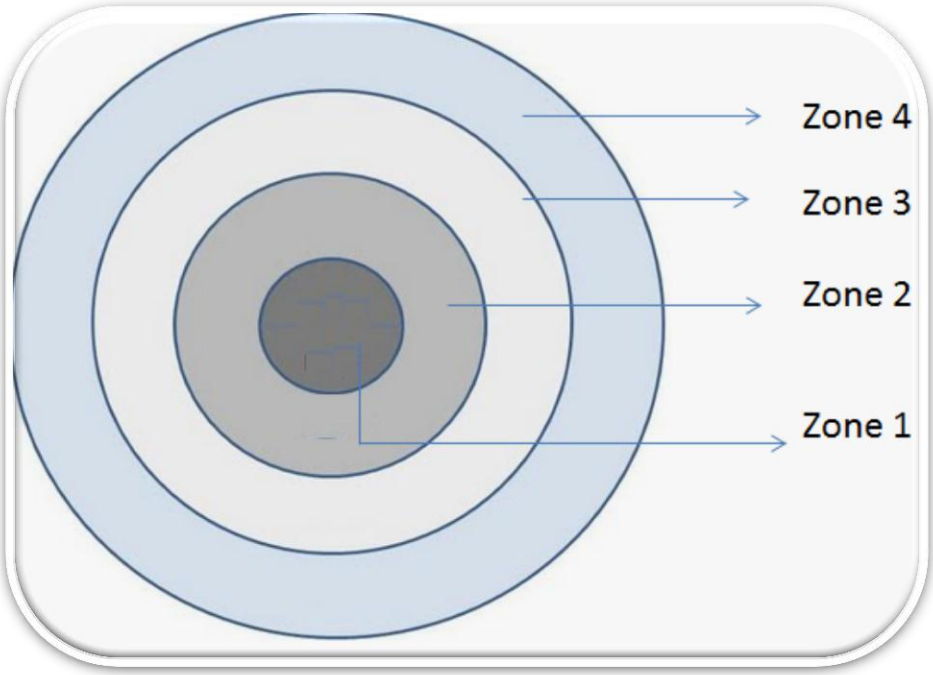

Figure 3.22 Fluorescence plane divided in 4 Zones

The analysis showed a decrease in the average integrated density in the zone closest to the MN hole and a gradual increase in the ID in the zones away from the MN holes. Figure 3.23 shows the average ID in all layers of the skin a) Stratum corneum (SC) b) Viable epidermis (VE) c) Dermis (DER) and d) Total ID of the fluorescence in different lateral zones. The ID in zone 1 at 5 min was 50% more than that of the ID in zone 1 at 120 min (Z1 5 min 12266756 – Z1 120 min 8385689). The data from the previous area analysis show an increase in the penetration area, hence the decrease in ID. The results in the VE were more obvious where there was a 3 fold decrease in the ID from 5 to 120 min (Z1 5 min VE 15621369 – Z1 120 min VE 5343177)

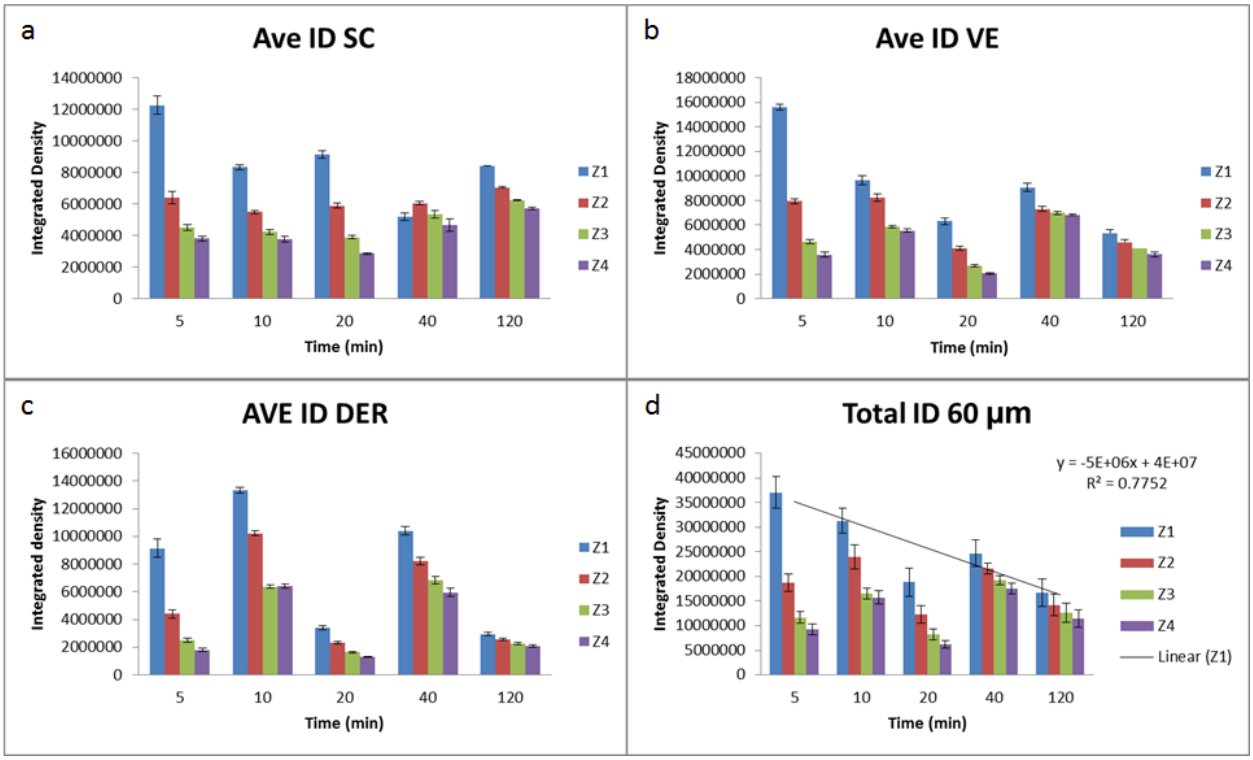

Figure 3.23 Average integrated density in all layers of the skin a) Stratum corneum (SC) b) Viable epidermis (VE) c) Dermis (DER) and d) Total ID (n= 4, results are expressed as mean ± SD)

Radial profile angle tool from Image J downloadable ***Plug-ins*** was used in the final analysis (as described section 3.3.5) to generate intensity profiles from the centre of the needle hole to a radius of 1500 pixels or 1129 µm. Intensity numbers were generated on the entire 60 µm depth from the top of stratum corneum to the top part of dermis. To improve the consistency in the analysis 20 µm each was denoted as SC, VE and DER. The intensities in these 20 µm (4 images) were averaged. The average intensities were then separated to accommodate four penetration zones (compartments) C1, C2, C3 and C4 starting from the centre of the microneedle hole. The penetration zones are expressed as '*ZONES*' in the previous section and as '*COMPARTMENTS*' here. It was hypothesised that in sink conditions as time increases the drug (model dye NaFsc) will move away from the microneedle hole towards the periphery or the C4. Figure 3.24 shows the average intensity in the three layers of the skin across the four compartments. As expected, there was a 1.5 times increase in the intensity in C4 from 5 min to 120 min in the stratum corneum. The movement away from the needle hole was also consistent in the other layers of the skin as well with 1.4 and 1.7 times increase in the viable epidermis and dermis

respectively. The average intensity representing the total amount of drug in each compartment can be seen in the figure to move from the centre of the MN hole to the peripheral compartments. Towards the 120 min mark the average intensities were almost similar in all the four compartments.

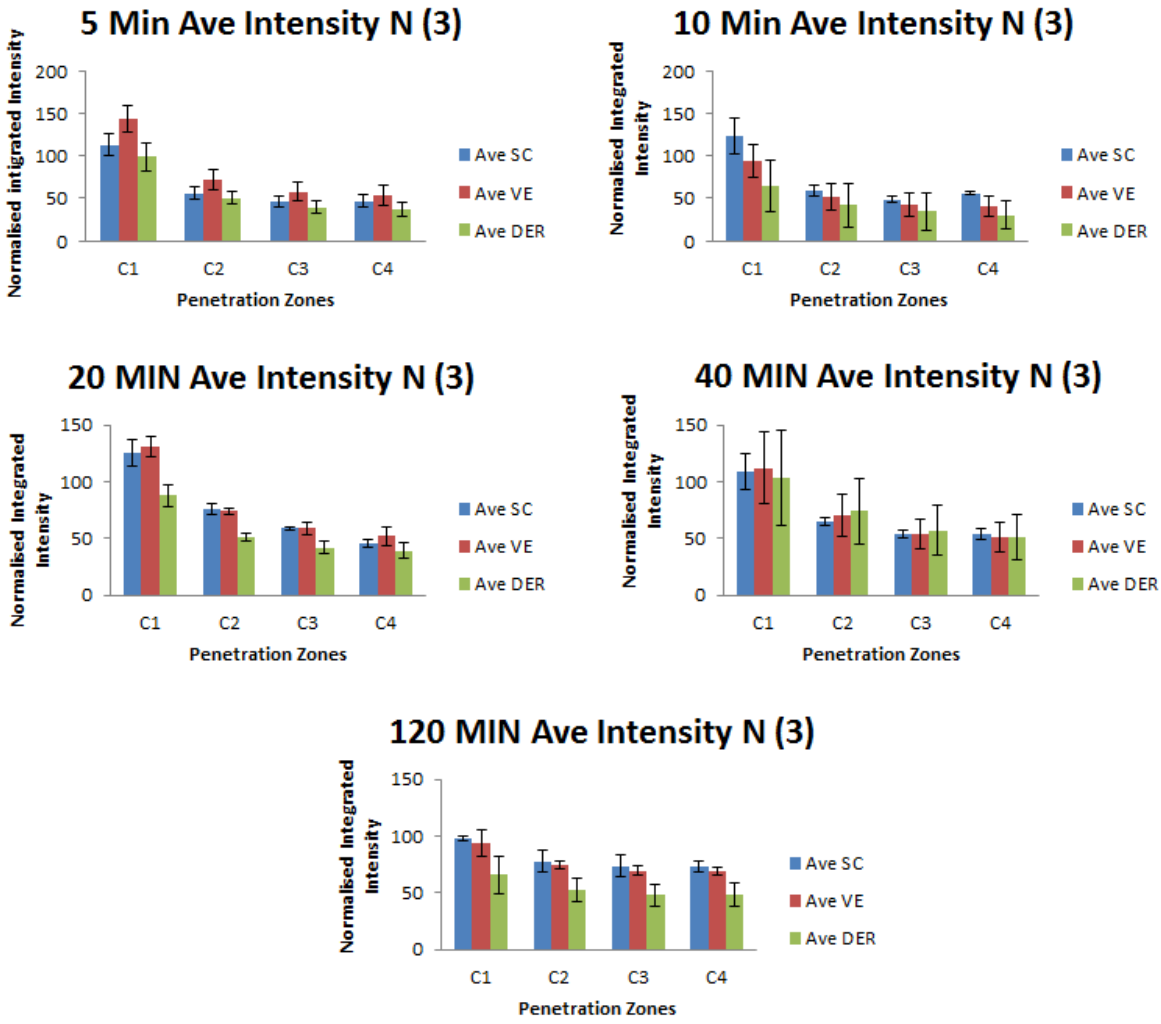

Figure 3.24 Average intensity in the three layers of the skin across the four compartments (n=3, results are expressed as mean ± SEM)

3.4.4 Standard curves and fluorescence quantification of NaFsc and fluorescent peptides

Measurements in fluorescence microscopy may be discussed in the context of three major criteria: (1) intensity which is usually expressed as a function of spectral frequency, (2) spatial analysis which is three dimensional where x, y are planer and z is the depth, and (3) temporal.[317] The studies in the previous section describe the

entire three measurement criterion. In this section we tried to draw a parallel between these measurements and the actual concentration of the fluorescent entity. For this we measured the fluorescence intensity in a known volume (50 μL) of a series of standard samples. The intensity values were plotted against concentration at 5 different power levels. The standard curves were generated in triplicate and a plot of the average values is illustrated in Figure 3.25 below. The purpose of a standard curve apart from the ability to work out concentrations of NaFsc and peptides was to standardise the imaging process. As previously described, all the images taken during this study were done with automated power and gain control feature in VivaScope 2500. To normalise the difference in power at which each cube of image was captured, a standard curve would be ideal. However, the intensity values corresponding to the standard solutions of NaFsc were not entirely reflective of the intensity values from a deeper axial area.

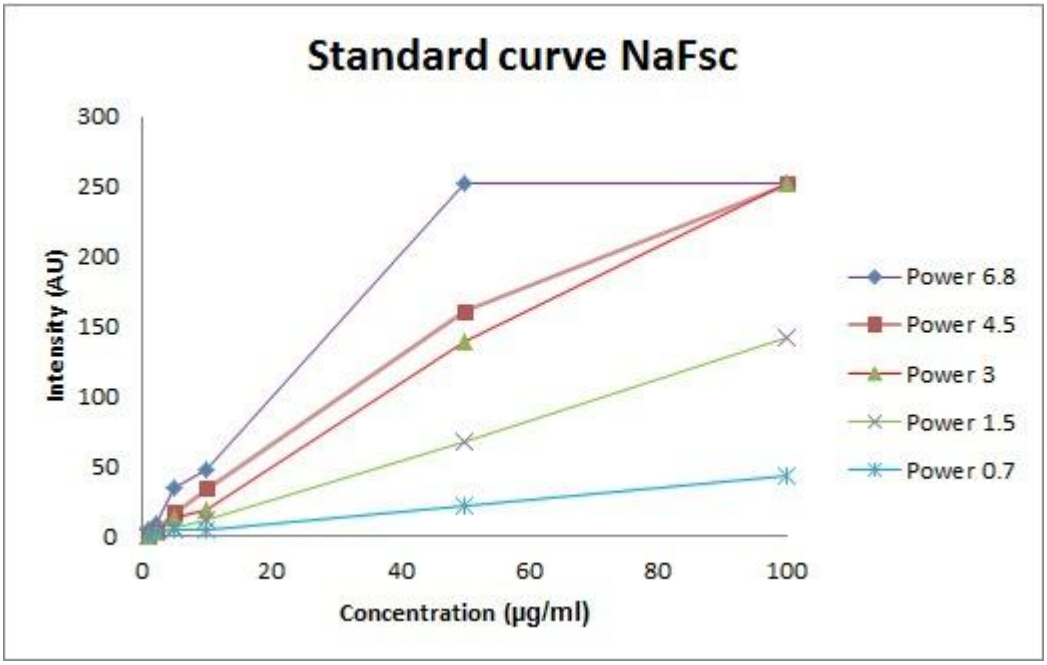

Figure 3.25 Standard curves of NaFsc at different power levels

Boi et al. described a method that can be used to evaluate the DNA content or the concentration of any protein, marked by an appropriate fluorescent dye, in single cells or in a tissue.[342] The method involved simple measuring of the total intensity in all the imaged layers/ optical sections and summing the intensities. The total intensity over the thick optical section would then correspond to the total amount of fluorochrome/fluorophore in the sample.[343] The researchers used mathematical

calculations to deduce the correct size of the optical section that should be imaged for accurate measurement capacity. The system described in Boi et al.'s research was not reproducible within our laboratory; however the technical intricacies regarding avoiding sources of error such as photo bleaching were very valuable. Most recent studies using fluorescent molecules have either quoted intensity values as an outcome[191] or used tape stripping and fluorimeteric analysis[275, 344-346] to quantify the amount of drug permeated. Fluorescence quantification by virtue of a standard curve will be pursued in the future as the group gains access to more knowhow and infrastructure. For the completion of this research however, intensity values combined with analysis of area of penetration and integrated density (ID) will be used as outcome measures.

3.4.5 MN based delivery studies on fluorescent peptides

Transdermal delivery studies using fluorescently tagged peptides have been described frequently.[112,133,272,275,347-349] Microneedles have been used for safe and effective administration of a range of large and poorly permeable molecules.[5,51,190,193,194,201,204,207,350,351] In this study we have aimed to investigate the permeability of peptides of increasing chain length and molecular weight, using fluorescence microscopy after MN based delivery. Microneedles used in this study showed marked enhancement in penetration of the peptides across the full thickness excised human skin when compared to no MN used.

3.4.5.1 Melanostatin

In this section and the subsequent sections on rigin and pal-KTTKS the names of the native peptides has been used but the description provided is that of the fluorescently conjugated peptides. This has been done to keep the discussion relevant to the peptides as primary targets of this investigation.

Melanostatin is a tripeptide (Pro-Leu-Gly) with theoretical molecular weight 803.92 Da post conjugation with FITC on the N-terminal. The log P of melanostatin was -0.485. Hence, it was expected that post breaching of the stratum corneum with MN, this peptide would permeate very well. As was expected the small size, combined with hydrophilicity, helped melanostatin permeate to a great degree in all the layers of the skin. To understand the study better, images from the different sampling arms are shown below. Figure 3.26 shows the experimental images in the order imaged in

the study. It is clear from visual analysis that negative controls (solvent and solvent with MN) showed no fluorescence and positive controls (NaFsc and NaFsc with MN) showed the most fluorescence. Active (MEL MN) and passive interventions (MEL) at 1 h and 24 h showed fluorescence in between the range.

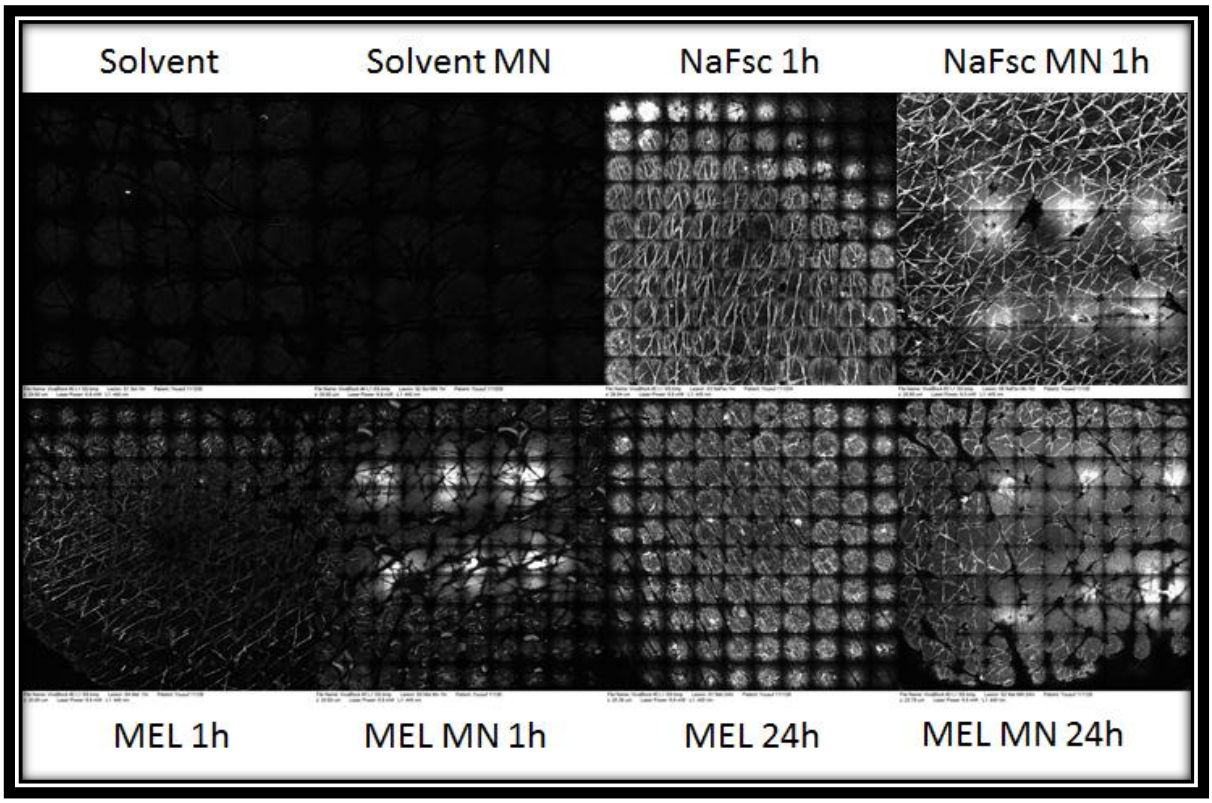

Figure 3.26 Mosaic images of the 8 study groups

Figure 3.27 below shows the penetration of melanostatin at 1 and 24 h.

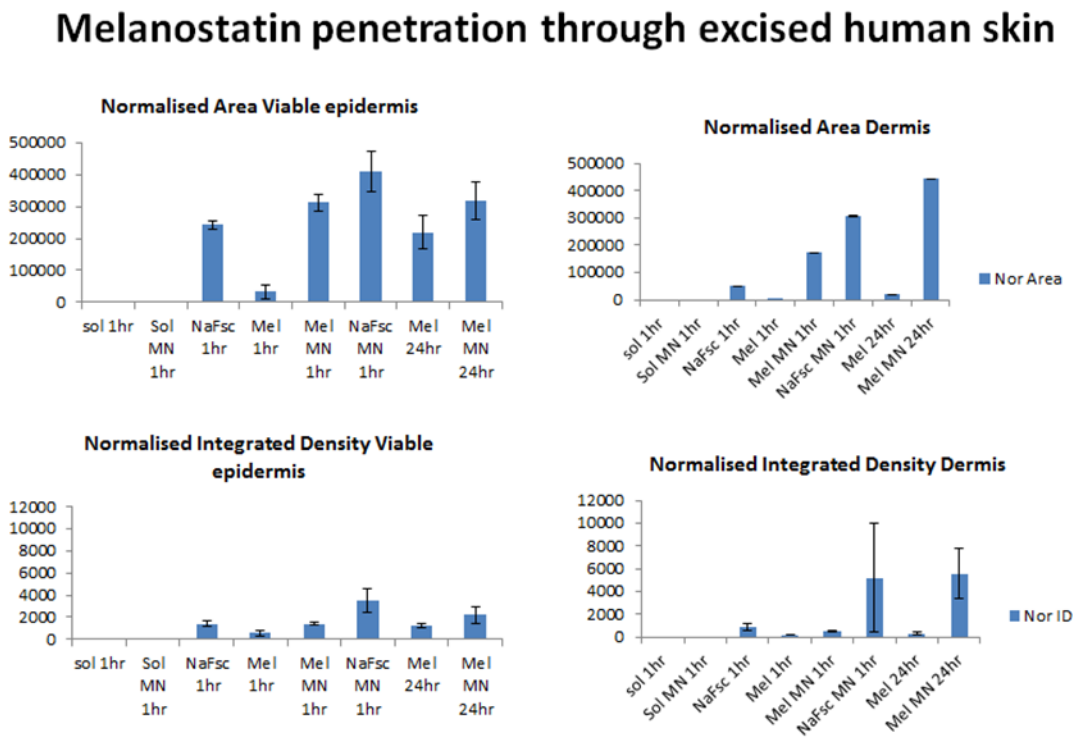

Figure 3.27 Melanostatin penetration at 1 and 24 h (n=3, results expressed as ± SEM)

At 1 h melanostatin showed a 10-fold enhancement in penetration area in the viable epidermis with the use of MN (Area 311848 pixels) when compared to without MN (Area 32641 pixels). This was found to be statistically significant ($p < 0.05$) At the same time point the integrated density was enhanced 2.6-fold. (ID without MN-549, ID with MN-1410) With the increment of time to 24 h, enhancements of 50% and 80% were seen in the area and ID respectively ($p < 0.05$). The results improved with increasing depth. MN showed a 132-fold increase in the total area of penetration in the dermis (without MN: 1308; with MN: 173361). This was highly significant in the regression model analysis ($p < 0.0001$). At 24 h the comparison was similar, a 22-fold increase in area was seen in the dermis (without MN:19386; with MN: 443623). This was accompanied with a 19-fold increase in ID (without MN: 289; with MN: 5582). Despite its bigger size and lower hydrophilicity compared to NaFsc, melanostatin showed appreciable penetration in similar conditions and concentration. NaFsc was clearly penetrating to a greater degree at the 1 h time point, but over 24 h melanostatin reached the same amount of penetration/diffusion (NaFsc 1 h with MN: 5204; MEL 24 h with MN: 5582). This comparison was not statistically significant. Without the barrier perturbation of the MN, NaFsc permeated 3-fold higher than

MEL (NaFsc 1 h without MN: 853; MEL 24 h without MN: 289). Figure 3.28 shows the 1 h and 24 h penetration of melanostatin passively and actively after MN based delivery in three different skin donors.

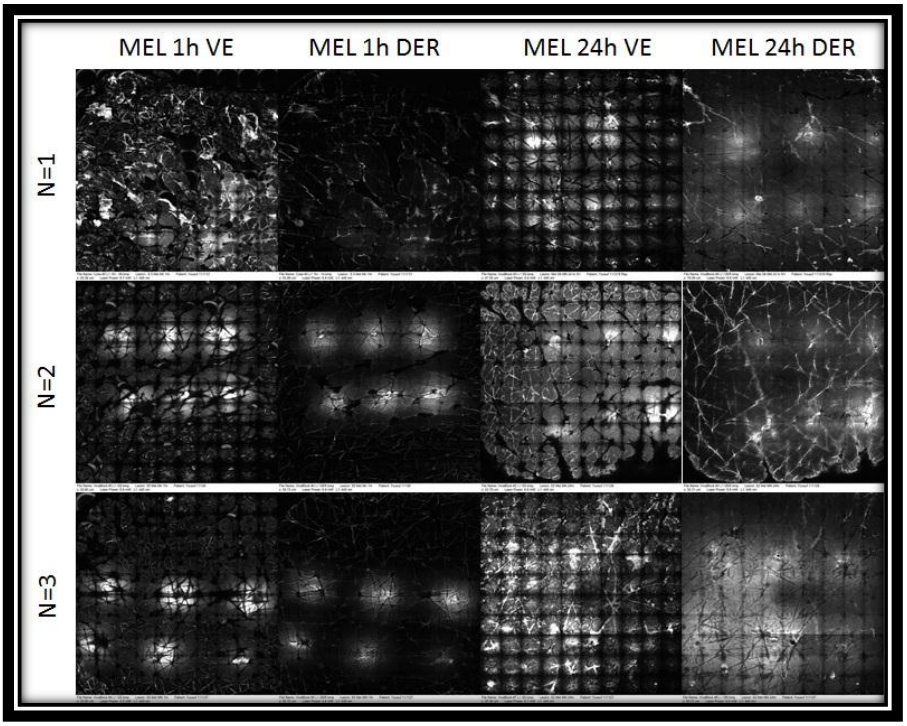

Figure 3.28 1 h and 24 h penetration of melanostatin after MN based delivery in three different skin donors

Melanostatin is a melanin synthesis inhibitor, which was identified and its structure was elucidated by Ishihara et al.[263] Numerous researchers have worked on the structure and activity of melanostatin[352,353,354] but work relating to its biological activity has not been published in great detail. Transdermal delivery of melanostatin for non-cosmeceutical use has not been reported. Melanostatin and its analogues have also been studied for their antidepressive activity[355-357] and researchers have also modified the -Leu-Gly- sequence to include a beta-lactam ring and found it to be very active biologically.[358] Several studies have shown that melanostatin potentiates the behavioural effects of L-Dopa and facilitates morphine dependence.[359] It is, therefore, under development for Parkinson's disease therapy.[360] Another example of melanostatin use was shown in a patent on the interactions of the neurologic-endocrine-immune complex in malignant melanomas. Treatment with melanostatin was based on the hypothesis that neuroendocrine suppression of MSH would enhance the effectiveness of immune modulation.[361] The reported usage of melanostatin in research has been predominantly parenteral including subcutaneous.

Though Ripka et al. have stated in the patent that it can be formulated in transdermal dosage forms, it has not been reported as yet.[361] In this project I have demonstrated the capability to delivery melanostatin to all the layers of epidermis and also to the dermis. This outcome can be of great relevance to the current knowledge base. Along with the CNS effects, one particularly important role of melanostatin is in specific hyperpigmentary problems such as post inflammatory hyperpigmentation (PIH), solar lentigos, and melasma.[362,363] Other examples where melanostatin could play a definite role include freckles and red patches due to hyperactive melanocytes that start in infancy, particularly in fair skin and areas of the Chloasma, also known as pregnancy mask. For complicated and uncomplicated skin disease states involving the hyperactivity of melanocytes, MN based delivery as shown here can be of clinical value upon further development. Atrium owns the rights to a melanostatin sequence based nona-peptide Melanostatine 5 which is marketed for skin lightening in cosmetic products.[266] The use of invasive techniques such as Derma Roller, cosmetic facial surgery and semi invasive techniques such as microneedles is not very uncommon is cosmetic dermatology. Hence, MN based delivery of melanostatin could be suitable for cosmetic purposes.

3.4.5.2 Rigin

Rigin is a tetrapeptide (Gly-Gln-Pro-Arg) with molecular weight 959.04 Da post conjugation with FITC on the N-terminus. The log P of the native peptide Rigin was -2.887. Rigin had good water solubility and hence was also expected to permeate well. However the results were contrary to this prediction and may be associated with the higher molecular weight. The Figure 3.29 below shows a mosaic of 1 h images of rigin with and without MN. The zone of penetration and hence separation of the penetration area post MN application was not clear. Figure 3.30 shows 1 h and 24 h images from rigin treated skin after MN application.

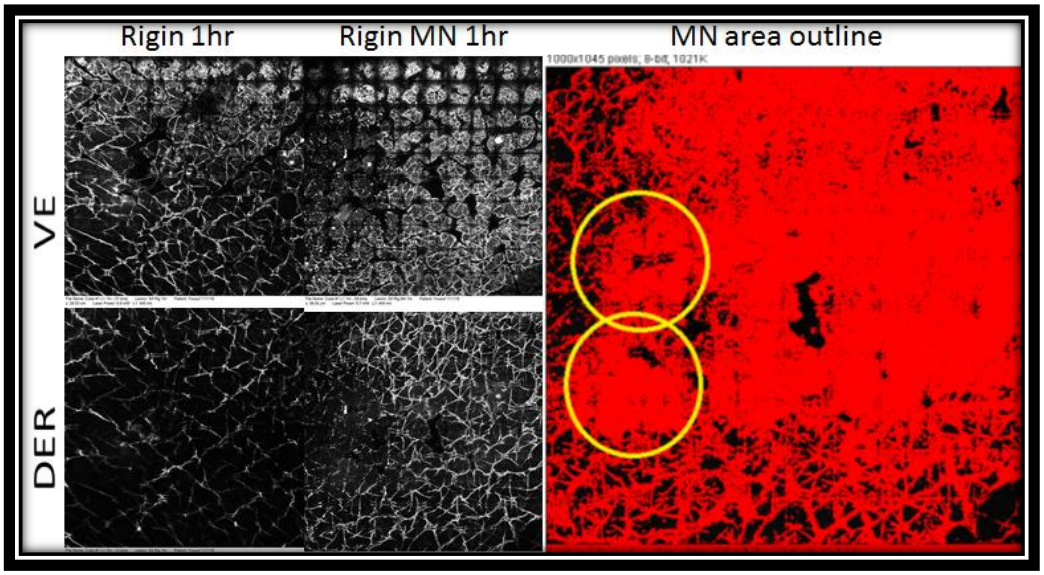

Figure 3.29 Images of rigin with and without MN at 1 h

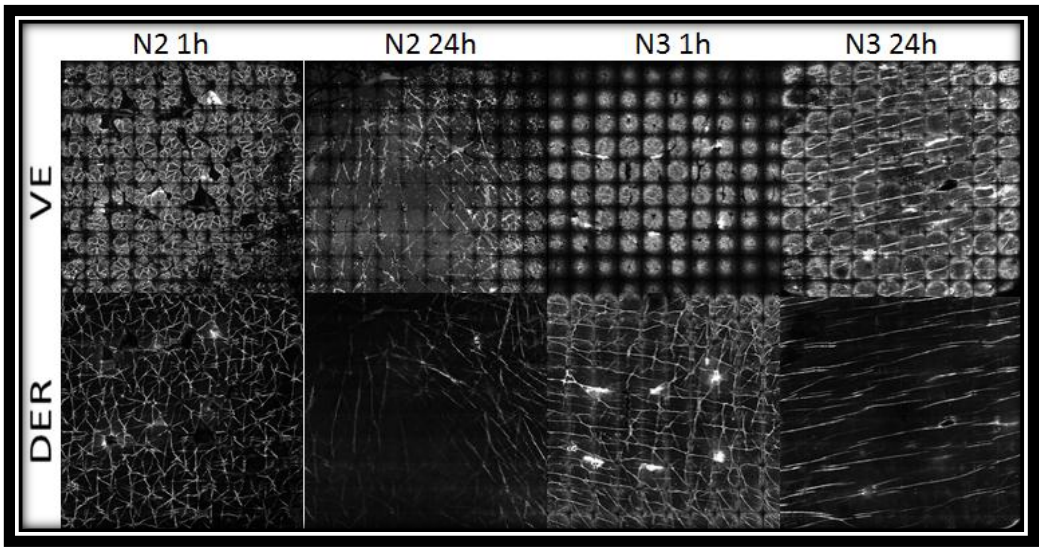

Figure 3.30 Images from rigin treated skin after MN application

The permeability results of rigin showed a longer lag time due to its higher molecular weight (Figure 3.31). Rigin with MN showed a 1.8-fold increase in the area (Rigin 1 h with MN: 314847; Rigin 1 h without MN: 173020) and 1.7-fold increase in the ID in the viable epidermis at 1 h ($p < 0.05$). At 24 h the penetration areas were identical (Rigin 24 h with MN: 294090; Rigin 24 h without MN: 290515). The results were similar in comparison in the dermis though the area was 6-fold less than that in the viable epidermis. These results suggest that not only was the lateral penetration of rigin lower; its axial penetration was substantially reduced. After MN treatment, rigin penetrated better than both rigin without MN and NaFsc without MN. In this study I have shown that the MN can deliver the molecule down to the dermis, from

there it is the optimisation of drug characteristics like hydrophilicity, partitioning and protein binding that will enhance its lateral diffusion.

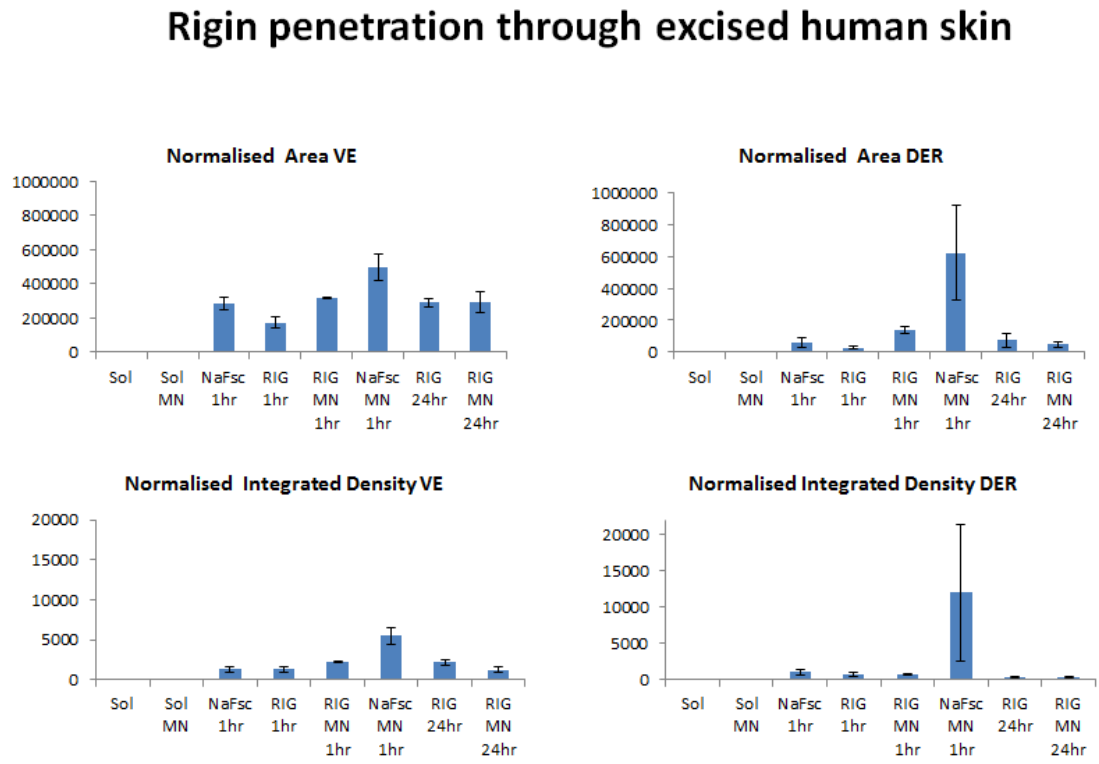

Figure 3.31 Penetration of rigin through human skin (n=3, results are expressed as ± SEM)

Rigin (Gly–Gln–Pro–Arg) is a tetrapeptide originated from immunoglobulin g (IgG), which is found to be immunostimulatory.[268,364] Immunoglobulins, interferons, interleukins, growth factors, and other biologically active proteins and peptides like rigin are the precursors of tetins.[270] Rigin is very similar in structure and action to tuftsin another tetrapeptide which has been widely researched for its immunomodulatory effects in a range of disease conditions including parasitic infections, AIDS, cancer and other autoimmune diseases.[365-368] Rigin though has not been as extensively studied.

The chemistry of rigin has been studied well because of its similarities to tuftsin. Ashish et al. conducted the conformational analysis of rigin both theoretically and experimentally and found considerable similarity of spatial arrangement of tuftstin and rigin[369] and Kumar et al. examined for its secondary structure preferences.[267] Martinez et al. synthesised a decapeptide containing in its sequence the subunits of rigin and found it to have immunomodulatory effects.[370] In a chemistry and activity

defining research Rocchi et al. studied binding of rigin to receptors and found it to bind to receptors that are unrelated to the tuftsin receptors.[269] Apart from the above mentioned therapeutic potentials rigin is currently been marketed by Sederma™ as Palmitoyl tetrapeptide-7 in their product Matrixyl® 3000 and Matrixyl® synthe'6™. It is promoted as an enhancer of skin elasticity via interleukin (IL)-6 reduction. Rigin is also marketed by Microneedle therapy system (MTS™) as MTS VitaPep Serum in conjunction with a microneedle roller MTS-ROLLER™ as a part of the MTS Anti-Aging Complex™.[371] Though the MTS-ROLLER™ has been used to stimulate the skin to produce new collagen formation and not transdermal delivery of the active formulations, in my project I have shown that MN can deliver rigin into the viable epidermis. The ability of rigin to down-regulate IL-6 in resting and inflamed cells was compared with dehydroepiandrosterone (DHEA) *in vitro*, and the two actives were comparable. Marketing materials related to rigin indicate that this reduction in IL-6 can produce increased skin smoothness, firmness, and elasticity.[229,362] In commercial cosmeceutical products rigin has been used at a dosage of 3% w/w as a part of the formulation. In the studies I have conducted, rigin at 0.05% was able to penetrate into the viable epidermis and dermis after MN based delivery within 1 h. Moreover, after 24 h the penetration area of rigin passively (without MN) in the VE was 290515 pixels. Perhaps the reports of rigin's *in vivo* activity in the light of the penetration results shown in this project hold true and the use of MN would further increase its suitability for cosmetic purposes.

3.4.5.3 Pal-KTTKS

The last peptide studied in this project was the palmitoylated pentapeptide (Pal-KTTKS/PAL-KTTKS; Pal-Lys-Thr-Thr-Lys-Ser). The molecular weight post palmitoylation and conjugation of FITC was 1191.06 Da and the log P of this native peptide was theoretically calculated as 3.32. This lipophilic peptide was not soluble in water and was hence expected to travel poorly in the dermis and epidermis laterally after MN treatment. The results showed no change in penetration area in the viable epidermis over 1 h (Pal-KTTKS 1 h with MN: 33268; Pal-KTTKS 1 h without MN: 33702). However, in the dermis a statistically significant enhancement was seen with the MN (Pal-KTTKS 1 h with MN: 2473; Pal-KTTKS 1 h without MN: 319; $p < 0.05$). Over 24 h the passive permeation of Pal-KTTKS in the VE was greater to the MN based permeation (Pal-KTTKS 24 h with MN: 44693; Pal-KTTKS 24 h

without MN: 116577). We presumed that lipophilic Pal-KTTKS, penetrated better passively in the viable epidermis. In the hydrophilic dermis however, the effect of better lipophilicity may have little effect. The penetration area analysis in the dermis conformed this. There was a 6-fold enhancement in the area of permeation post MN treatment (Pal-KTTKS 24 h with MN: 31755; Pal-KTTKS 24 h without MN: 5389; $p < 0.05$) Figure 3.32 shows Pal-KTTKS penetration over 24 h; figure 3.33 shows 1 h and 24 h images from Pal-KTTKS treated skin after MN application

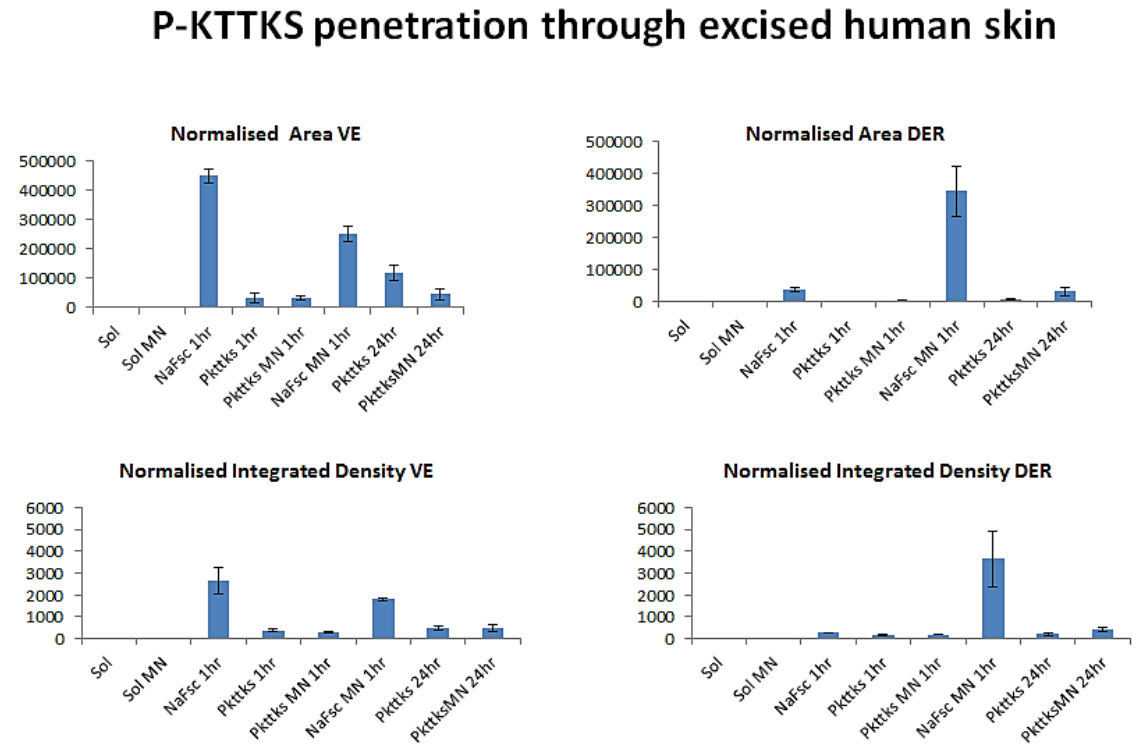

Figure 3.32 Pal-KTTKS penetration after MN application in excised human skin over 24 h (n=3, results expressed as mean ± SEM)

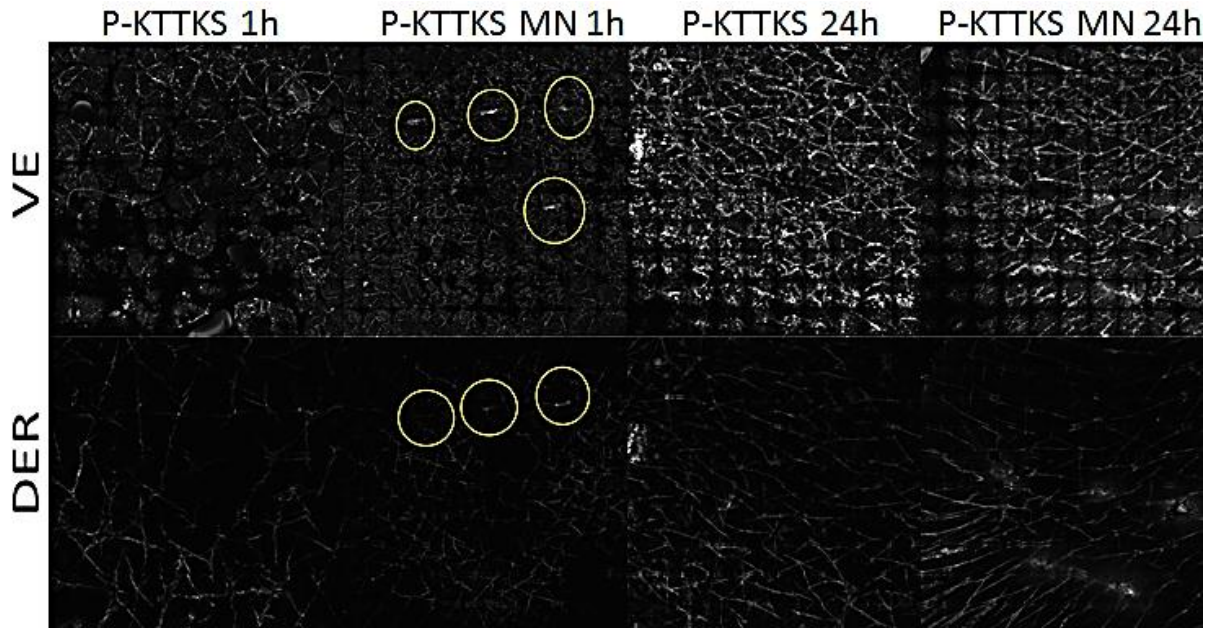

Figure 3.33 Images from Pal-KTTKS treated skin after MN application (n=3, results expressed as ± SEM)

Of the three peptides studied here palmitoyl pentapeptide or Pal-KTTKS is the most popular in cosmeceutical circles. Work by a group at the University of Tennessee in 1993 identifying the activities of small peptide fragments within procollagen I resulted in the identification of KTTKS, a sub fragment within the carboxy-terminal propeptide (residues 197-241) capable of stimulating the production of both collagen and fibronectin.[249] This peptide fragment dramatically augmented extracellular matrix (ECM) production in sub confluent fibroblasts.[233] It also stimulated type I and type III collagens and fibronectin production in a dose and time-dependent manner with no effect on total protein synthesis or on the ratio of secreted proteins to cell-associated proteins. Osborne[372] et al. showed a robust result for this peptide in reducing bumpy texture and fine wrinkles compared with other baseline and comparators.[372] Fu et al. conducted a long-term clinical study comparing a cosmetic anti-ageing regimen including Pal-KTTKS, against a recognized prescription topical treatment for improving the appearance of facial wrinkling.[373]

In a study by Robinson et al. on 93 Caucasian female volunteers, Pal-KTTKS had significantly better scores than placebo for expert grader assessment and subject self-assessment of age hyperpigmented spots.[234] In another study Kaczvinsky et al. studied effects of cosmetic products containing Pal-KTTKS using 3-D imaging and concluded that four weeks of treatment showed improvement in the smoothness of

periorbital skin and reduced the apparent depth of larger wrinkles.[374] Though there are numerous newsletters and promotional material highlighting *in vivo* case studies showing tremendous benefits from Pal-KTTKS, transdermal delivery studies have not been conducted to support that these peptides actually go in the skin. Abu samah et al. conducted a review on topically applied KTTKS and remarked that "indeed, KTTKS and palmitoyl-KTTKS are unusual in that no supporting *in vitro* data has ever been published supporting their successful transcutaneous delivery".[375] The positive results of passive permeation of Pal-KTTKS in the VE as shown above (Fig 3.32) are very encouraging. Hence, we presume that the penetration enhancement role of MN which now can be seen predominantly in the dermis would be more distinct if the pentapeptide was not palmitoylated.

3.5 Future directions

Peptides possess enormous potential for the treatment of various diseases. In contrast to youthful skin, mature skin undergoes well-established clinical and microscopic changes, particularly after menopause. In particular, dermal thinning, loss of dermal collagen and decreased lipid production are complicated by the effects of life-long sun exposure.[376] It is well-accepted that cosmeceuticals are topically applied products that are more than merely cosmetic, yet they are not true drugs that have undergone rigorous placebo controlled studies for safety and efficacy before they can be marketed.[377] Peptides and proteins, frequently used in anti-aging regimens, are categorized into four groups: signal peptides, enzyme-inhibitor peptides, neurotransmitter- inhibitor peptides and carrier peptides.[378] The peptides studied in this project have a multitude of therapeutic actions and have been researched for potential clinical uses. The success of MN to enhance transdermal penetration and intradermal accumulation of peptides in the skin opens new opportunities. In future studies, other non-invasive transdermal delivery techniques can be used synergistically with the microneedles used in this project. One potential synergistic technology is Magnetophoresis which is described in the next chapter. In the course of this project the group has applied and successfully achieved animal and human ethics approvals for the use of microneedles in various research projects. It will be a future direction of the group to apply for further ethics approvals to pursue advanced work on the fluorescently labelled peptides *in vivo*. In particular the tetrapeptide rigin and pentapeptide Pal-KTTKS have tremendous potential for *in*

vitro and *in vivo* transdermal delivery studies. These peptides are either precursors or fragments of naturally and endogenously occurring proteins and polypeptides and hence there use for *in vivo* research would hold key to unlocking further potential.

3.6 Conclusions

Development of effective and functional delivery systems for new active pharmaceutical and cosmeceutical ingredients is a challenging task.[379] In this chapter I have demonstrated that microneedles are an effective way of delivering large and complex pharmaceutically active molecules deep into the skin. Confocal laser scanning microscopy (CLSM) has provided a significant tool to visualize skin structure and the localization of fluorescent molecules within the skin tissue.[380] CLSM has rendered it possible to visualise and quantify the penetration of the peptides studied in this project in a fast and efficient manner. The rationale for selection of the peptides in this research was a broad classification into an established transdermal stream and relatively smaller size. The project was designed to study peptides with similar biological activity and increasing chain length. It is a particularly difficult task to find peptides of increasing chain length which fall in the same therapeutic class. Moreover, it was a deliberate effort to work on peptides which act within the skin rather than systemic peptides. The peptides melanostatin, rigin and Pal-KTTKS are, as described in the sections before of a reasonable size (3, 4 and 5 amino acid). In addition to a large number of other potential actions especially for melanostatin and rigin, their role as cosmeceuticals is of increasing importance.

Chapter 4

Effect of low field strength magnets on the skin permeation of peptides and small molecules. Assessment of potential synergistic enhancement with microneedle pretreatment.

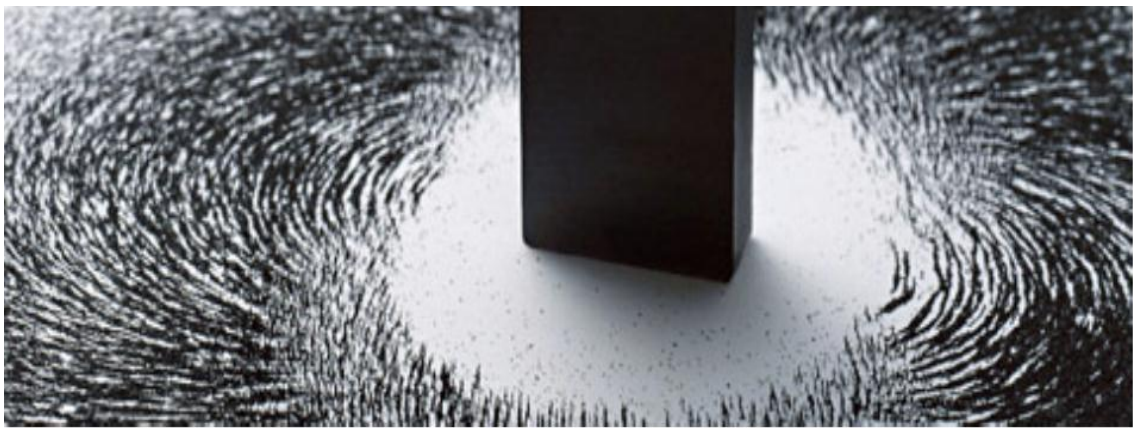

Diamagnetism occurs because the external magnetic field alters the orbital velocity of electrons around their nuclei, thus changing the magnetic dipole moment. [152]

4.1 Introduction

Magnetophoresis is the enhancement of drug permeation across biological barriers by application of an alternating or a fixed magnetic field.[6] Although some mechanistic studies have been reported,[7, 154] the precise mechanism of penetration enhancement is not yet clear. It has been postulated that magnetophoresis may act on diamagnetic drugs or can fluidize the skin lipids. It is also possible that magnetophoresis can act by both mechanisms. The effect on the active molecule may be attributed to the diamagnetic properties of the molecules,[152] whilst the effect on the skin may be through perturbation of skin lipids due to the stationary magnetic fields.[7, 381]

ETP (enhanced transdermal polymer) magnets and Dermaportation, an alternating magnetic field electromagnetic coil system, were provided as a gift from OBJ Ltd, a Perth based biotechnology firm. To investigate the potential diamagnetic effect of ETP on small molecules, experiments were conducted on a non-membrane model that showed predictable resistance. The agar gel based model provided easy study of the movement of dye molecules, presumably following first order kinetics. This was advantageous when compared to skin, where compartmentalisation and complex kinetics make it very unpredictable and there is the potential for interaction of the magnetic field with the skin barrier structure. Experiments were then conducted *in vitro*, across human epidermis with diclofenac sodium in a carbopol gel formulation. In this study Dermaportation was compared to ETP and passive permeation of diclofenac sodium. Finally, to assess whether magnetophoresis using ETP had any membrane perturbation effect, experiments were carried out *in vivo* on human volunteers with a model small molecule, curcumin, which facilitated skin visualisation.

Further, the successful enhancement of transdermal permeation and intradermal accumulation of peptides achieved with microneedles (Chapter 3) prompted me to explore the synergistic potential of skin pretreatment with microneedles with magnetophoresis. Although transdermal permeation enhancers have been individually shown to enhance drug transport, their combinations can be significantly more effective.[382] Consequently microneedles have been used in conjunction with

other transdermal delivery techniques like iontophoresis[383], electrophoresis[384], nanoparticles[52] and chemical enhancers.[385]

In this chapter by utilising different skin and non-skin models I aim to elucidate and comment on the mechanism of magnetophoretic drug delivery alone and in combination with microneedle pretreatment.

4.2 Aims

The aims of this study were:

1. To assess the permeation of a dye (brilliant blue) through a non-membrane agar gel model.
2. To study the penetration enhancement effects of ETP on diclofenac sodium across human epidermis *in vitro* and to compare the skin permeation achieved with ETP magnets to that with Dermaportation.
3. To examine the penetration enhancing effects of 2 fixed magnetic arrays (ETP008 and ETP012) on *in vivo* permeation of Curcumin by multi photon tomography/ microscopy.
4. To investigate the permeation and distribution of a model tripeptide across full thickness human skin *ex vivo*. To assess effects of ETP magnets on peptide permeation and to explore the possible synergistic effects on skin diffusion of the peptide with microneedles.

4.3 Materials and Methods

4.3.1 Chemicals

Melanostatin, a tripeptide conjugated to FITC (MW = 803.92) was purchased from Genscript, USA. Curcumin and diclofenac sodium, model small molecules with a molecular weight of 368.38 and 318.13 respectively were purchased from Sigma Aldrich (USA). HPLC grade acetonitrile was supplied by JT Baker (USA) and all other chemicals including brilliant blue dye and carbopol were of analytical grade and were purchased from Sigma Aldrich (Australia). Phosphate buffered saline solution (PBS) was prepared according to the United States Pharmacopoeia.

4.3.2 Instrumentation

4.3.2.1 Magnetic film arrays (ETP)

Magnetic film array material consisted of 35 mm × 35 mm sections of unpowered flexible array matrix ETP (008 and 012), a proprietary enhanced transdermal delivery array film developed by OBJ Ltd (Perth, WA, Australia) was a gift from the company. The magnetic film arrays are thin flexible polymer matrix containing multiple magnetic elements arranged to produce complex 3-dimensional magnetic gradients. The material has a peak magnetic field strength of 40 mT. However, the arrangement and distribution of alternating poles across the surface of the material results in a total magnetic gradient of 2 T/m^2. Figure 4.1 illustrates the magnetic fields using a metal dust polymer strip: a) ETP 008 magnetic field and b) ETP 012 magnetic field.

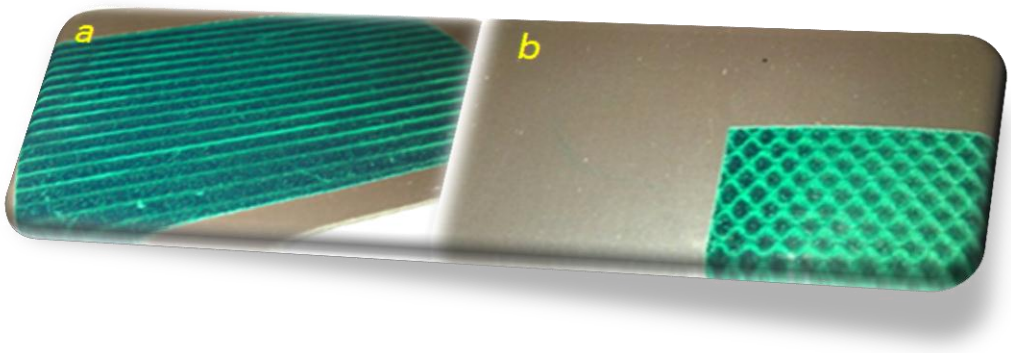

Figure 4.1 a) ETP 008 magnetic field and b) ETP 012 magnetic field as observed on a metal dust polymer strip

4.3.2.2 Microneedles and Microneedle applicator

The microneedle arrays were cut using laser etcher (LaserPro 5290) onto a single plate of 50 μm stainless steel with a 700 μm length × 250 μm width. Each plate consisted of 3 microneedles separated by a 5 mm distance. These plates were then assembled in banks of 2 with 3 mm spacing. The applicator used in this study had an impact velocity of 1.5 m/s. Figure 4.2 shows a microneedle plate on a fingertip.

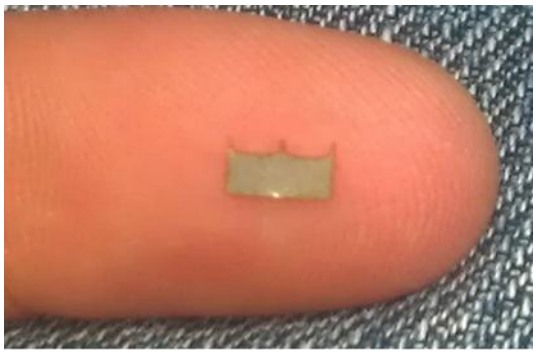

Figure 4.2 A microneedle plate on finger tip

4.3.2.3 Reflectance confocal microscopy and imaging parameters

RCM (VivaScope 2500) has been described in chapter 3 section 3.3.2.1. For this study we used L1 (454 nm) to image the FITC conjugated fluorescent peptide melanostatin. The confocal microscope was used with 488 nm excitation and 550 ± 88 nm emission bands to record images. Reflectance mode was first used for orientation.

4.3.2.4 UV spectrophotometry

Fluorimeteric analysis of dye samples was performed in a UV-Vis spectrophotometer (UV mini-1240) that allows for full spectral data acquisition over the wavelength range of 190 nm to 1100 nm. Linear dilution was performed with water and calibration curves were obtained at 5×10^{-3}, 2.5×10^{-3}, 1.25×10^{-3}, 6.25×10^{-4}, 3.125×10^{-4}, 1.5625×10^{-4}, 7.8125×10^{-5} and 3.90×10^{-5} μg/mL of the dye solution.

4.3.2.5 HPLC instrumentation and conditions

High performance liquid chromatography was used for analysis of samples obtained in the *in vitro* skin diffusion studies undertaken with diclofenac in carbopol gel. The samples were analysed by reverse phase HPLC Agilent 1100 system which consisted of a quaternary pump (G1311A), autosampler (G1313A), degasser (G1312A) and photo diode array detector (G1321A). Separation was achieved on a Phenomenex Jupiter C18, 300A column (5 μm, 4.6mm×150mm). Integration was undertaken using Chemstation software B.03.01. Elution was performed at ambient temperature using a mobile phase gradient at a flow rate of 1 mL/min and the wavelength of detection was 278 nm. Buffer B was 0.036% TFA in acetonitrile and Buffer A was 0.045% TFA in water. The peptide was eluted using a linear gradient protocol;

Buffer B was held at a linear gradient from 10 to 100% over 10 min. All samples were analysed by HPLC using injection volumes of 20 μL.

4.3.2.6 HPLC analysis and validation

4.3.2.6.1 Linearity

A 1 mg/mL stock solution of diclofenac sodium was prepared by dissolving 5 mg of the compound in 5 mL water. Linear dilution was performed and calibration curves were obtained using 3.9, 7.80, 15.75, 31.5, 63.0 and 126 μg/mL for diclofenac sodium. Linearity (quoted as R^2) was evaluated by linear regression analysis, which was calculated by the least square regression method.

4.3.2.6.2 Precision, Intra and Inter-day repeatability

The precision of the assay was determined by injecting three standard concentrations of 7.80, 15.75 and 63.0 μg/mL diclofenac six times on the HPLC. The intra-day repeatability was assessed by injecting 3.90 and 15.75 μg/mL diclofenac standards six times at different times in a day. The inter-day repeatability was determined by injecting 3.90 and 15.75 μg/mL diclofenac standards six times on 3 different days. The intra- and inter-day repeatabilities were quoted as the coefficient of variance.

4.3.2.6.3 Lower limit of detection (LOD)

The minimum detectable and quantifiable limits (LOD and LOQ) were measured by diluting the stock solution of diclofenac to give a concentration range from 3.9 to126 μg/mL and then injected on the HPLC. The LOD was calculated as greater than 3 times the baseline noise level by the following formula: LOD = 3 × SD of peak area of standard / slope.

4.3.2.6.4 Lower limit of quantification (LOQ)

The LOQ was calculated as 10 times the baseline noise level by the following formula:

LOQ = 10 × SD of peak area of standard / slope.

4.3.2.7 Multi photon tomography

Multiphoton images for the *in vivo* experiments were collected on a DermaInspect system (JenLab GmbH, Jena, Germany) with an ultra-short pulsed mode-locked 80 MHz Titanium Sapphire MaiTai laser (Spectra Physics, Mountain View, CA, USA)

which has a tuning range of 710 – 920 nm with an 85 femtosecond pulse width. The tomography system had an integrated time correlated single photon counting (TCSPC Becker and Hickl, Berlin, Germany) 830 detector to enable fluorescence-lifetime imaging microscopy (FLIM) measurements. Figure 4.3 illustrates the schematics of a MPT system. The excitation wavelength was 740 nm, and the average incident optical power was 23 mW. Treated skin was optically sectioned using MPT-FLIM with a 740 nm excitation wavelength from just above the stratum corneum to below the dermis (total 100 μm) in 5 μm increments using a Zeiss Plan-Neoflour oil-immersion 40X objective lens, resulting in an image size of 210×210 μm^2.

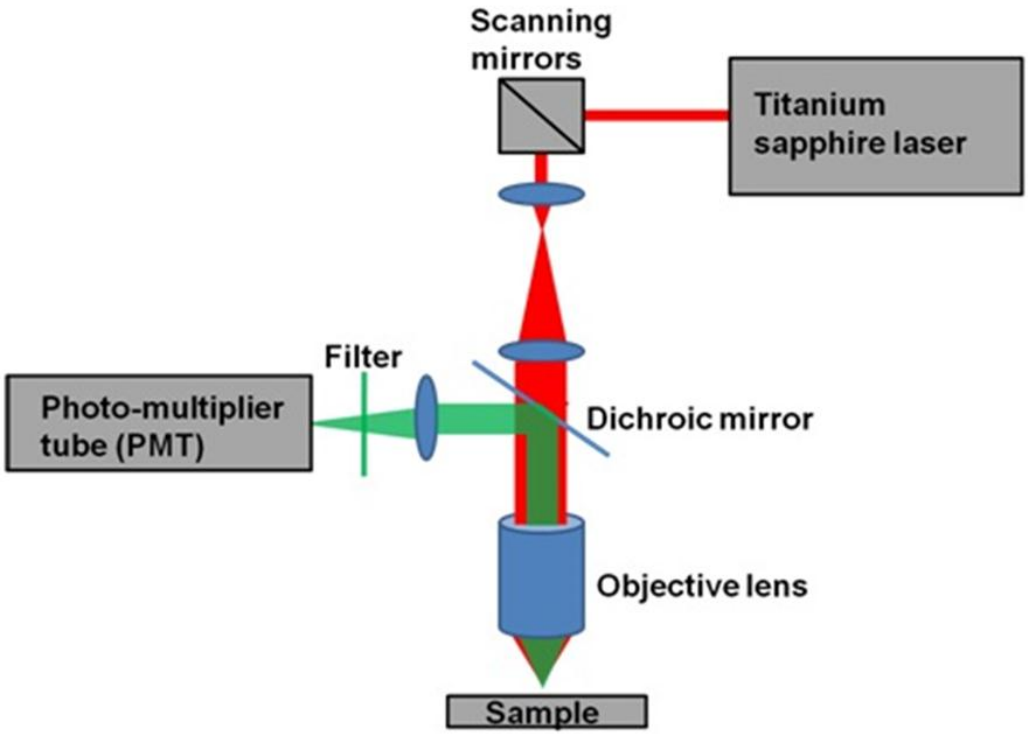

Figure 4.3 Schematic showing a typical MPT set-up

4.3.3 Study design

The scheme below shows an overview of the various models used and experiments conducted to investigate the possible skin permeation enhancement effect of magnetophoresis.

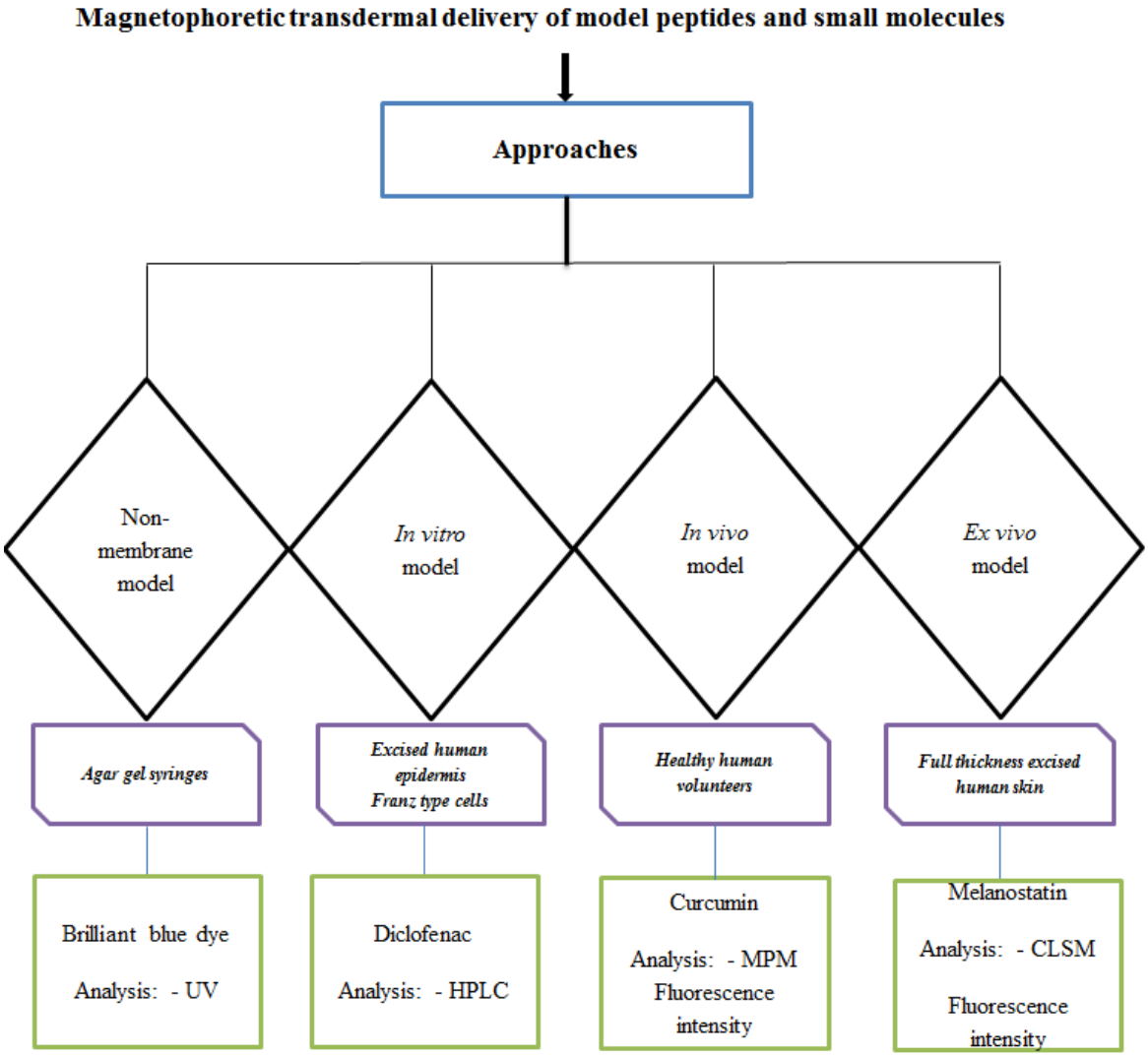

Figure 4.4 Overview of experimentation

4.3.3.1 Studies on permeation of brilliant blue dye in Agar gel syringes

A 0.8% agar gel was prepared by dissolving 0.8 g agar in 100 mL water and by gentle warming to 60 ºC. The warm agar gel was then poured into a 20 mL syringe that had its top cut. The plunger of the syringe was moved up with the agar still in liquid form to make a donor well on the top end of the syringe. The agar was then allowed to solidify. Brilliant blue dye solution was placed in the donor well. An ETP magnet or dummy non-magnetic film was then lowered into place on top of the donor solution so that it was in contact with the solution but not submerged in it. The experimental set-up is shown below in Figure 4.5. The experiments were carried out for 2 hours after which the excess dye was removed. The plunger was moved up to bring the agar gel to the surface, from where it was cut into discs of equal height

using a thin wire. Each agar disc was weighed and dissolved in 10 mL of water. The absorbance of the solution was measured at 630 nm using a UV/Vis. The experiments were conducted in quadruplicates.

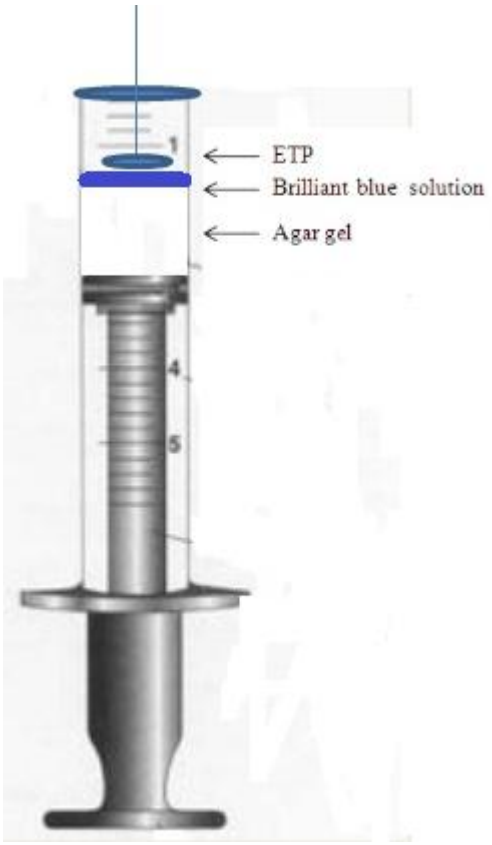

Figure 4.5 Study setup for Agar gel pilot studies

4.3.3.2 Studies on permeation of diclofenac gel through human skin

4.3.3.2.1 Preparation of diclofenac gel

A 0.5% carbopol gel was prepared and homogenised with 250 mg of diclofenac sodium per 50 g of gel. The gel formulation allowed for the ETP magnets to be placed with ease, without being in touch with the skin.

4.3.3.2.2 Human skin preparation

Full thickness human skin samples excised from patients (30-50 year old female abdominal sections) undergoing abdominoplasty were refrigerated immediately after surgery. Sampling was approved by the Human Research Ethics Committee of Curtin University (Approval numbers HR132/2001, HR 70/2007 and HR 129/2008) and was conducted in compliance with the guidelines of the National Health and Medical Research Council of Australia. The following procedure was used to obtain

epidermal sheets. The subcutaneous fat was removed by dissection, the full thickness skin then immersed in water at 60 °C for 1 min, allowing the epidermis to be lifted off the dermis.[277] The epidermis was placed onto aluminium foil, air dried, then placed in a sealed bag and stored at –20 °C until required.

4.3.3.2.3 Skin permeation of diclofenac sodium across human skin

In vitro permeation studies across human epidermis were performed in Pyrex glass Franz-type diffusion cells (enabling permeation across skin sections of cross sectional area 1.18 cm^2; receptor volume approximately 3.5 mL). Epidermal membrane was placed between the donor and receptor compartments and allowed to equilibrate for 1 h with the receptor solution (PBS pH 7.4) which was stirred continuously with a magnetic stirrer bar. The receptor compartment of the cell was immersed in a water bath at 37 ± 0.5 °C. PBS (1 mL) was placed in the donor compartment, allowed to equilibrate for 1 h and the conductivity and resistance across the epidermis was measured using a digital multimeter to determine membrane integrity. Membranes exhibiting an electrical resistance of less than 20 kΩ were rejected from the study. The PBS solutions were then removed from the donor and receptor compartments and the receptor refilled with approximately 3 mL of fresh pre-warmed PBS. The donor consisted of 1 g of 0.5% diclofenac sodium in a carbopol gel. Two hundred μL samples of the receptor phase were withdrawn and replaced with an equal volume of fresh pre-warmed (37 °C) PBS over a 6 h period to maintain sink conditions. The diclofenac content in the samples was determined using HPLC.

Sections of magnetic film array (ETP 012) were cut to a size suitable for insertion into the donor compartment of the Franz-type cell and suspended on the surface of the gel, while passive cells had a non-magnetic polymer film of similar dimensions and material placed on the gel surface. (Figure 4.6)

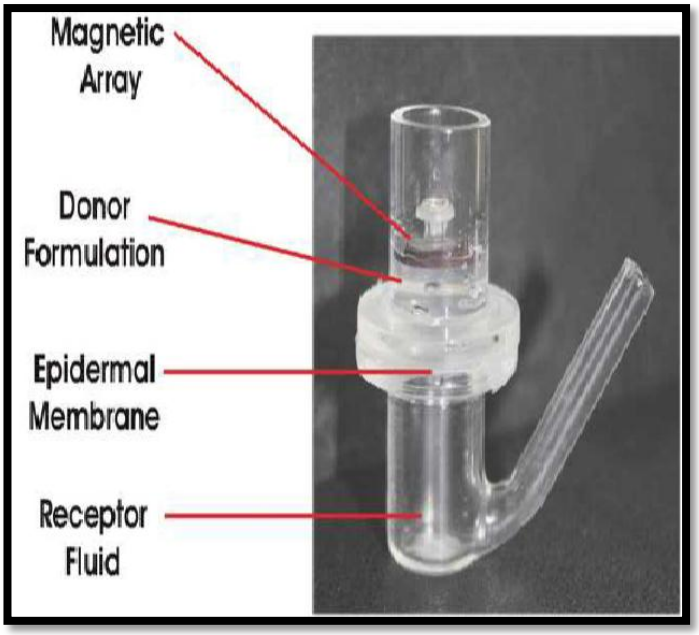

Figure 4.6 Set-up for diclofenac gel studies

In the Dermaportation cells, the Dermaportation coils were added to the exterior of the donor compartment and energy applied for 6 h, whilst other cells had no external Dermaportation energy applied. All cells were also occluded by sealing the top of the donor compartment of the cell with Parafilm^{TM}. After 6 h the donor and receptor fluids were recovered, the cell disassembled and the skin epidermal membrane examined for obvious tears (any cells with torn membranes were rejected). At least 6 replicates were conducted for ETP, Dermaportation and for passive diffusion experiments.

4.3.3.2.4 Data Analysis

The cumulative amount of drug permeated through the epidermis (μg/cm^2) versus time (h) was plotted. The flux of diclofenac sodium through the human epidermis was determined from the slope of the plot of cumulative amount versus time and expressed as μg/cm^2/h. Permeability coefficients (cm/h) were calculated for diclofenac in all the study arms.

4.3.3.3 Studies on permeation of Curcumin through human volunteer skin

For *in vivo* transdermal delivery studies, Curcumin in mineral oil was used as a model fluorescent molecule which could be easily imaged. Curcumin has molecular formula of $C_{21}H_{20}O_6$ and a molecular weight of 368.38. The structure of curcumin (a) and its fluorescence spectrum (b) is described below Figure 4.7.

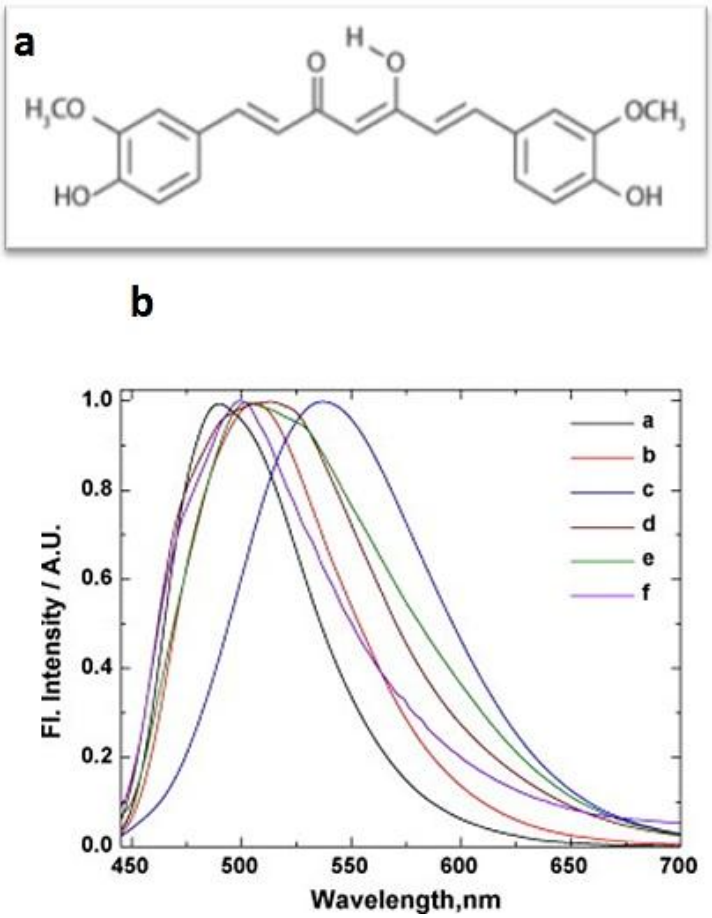

Figure 4.7 a) Structure and b) fluorescence spectrum of curcumin in different solvents[386]

The *in vivo* penetration experiments were carried out on healthy human volunteers, with approval of Princess Alexandra Hospital Research Committee Approval No. 2007/197, administrated by the University of Queensland Human Ethics Committee. The intervention was carried out by applying the curcumin and occluding the spot on the forearm with either the magnet or dummy material, followed by imaging. Three spots were located on the forearm, marked and cleaned on each hand of the volunteers (described in Figure 4.8 a). An initial measure of the Trans Epidermal Water Loss (TEWL) was recorded, which was used to include a correction factor for the variability in the different skin conditions within the same subject as well as inter-subject variability.

The skin spots selected for tape stripping were then stripped 20 times to remove approximately 5 µm of the stratum corneum. Tape stripped skin served as a positive control as the removal of stratum corneum was expected to have a much bigger permeation enhancing effect when compared to the active interventions of

magnetophoresis assisted delivery. The tape stripped spots were measured for TEWL after stripping to account for the increased permeability, before the application of curcumin in mineral oil formulation. Negative controls consisting of mineral oil only and mineral oil with ETP magnets were used to account for the auto fluorescence encountered. The effect of tape stripping on fluorescence was assessed by applying only mineral oil to a separate tape stripped spot.

Curcumin in mineral oil was then applied to the skin passively where the skin spot was occluded with a dummy non-magnetic occlusive strip. Curcumin was also applied actively, occluded with the ETP magnets. The experiments were designed to ensure that each spot with curcumin was isolated to avoid accidental contamination of the negative control spots. Figures 4.8 a) and b) show a volunteer during the study.

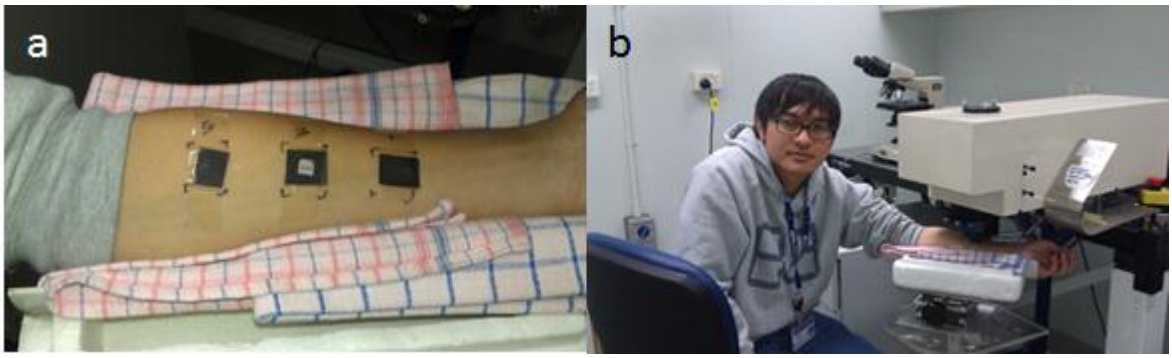

Figure 4.8 a) Volunteer arm with ETP treatment b) Volunteer during the MPT imaging

The skin delivery experiments were carried out with a 1 h treatment time. After completion of the treatment duration, *Z*-Stack images were generated to a depth of 100 µm with each layer in the stack being 5 µm apart.

The multi photon tomography (MPT) imaging was carried out on a DermInspect system (JenLab GmbH, Jena, Germany). All the fluorescence data was then analysed using SPC image and Image J software. For the calculation and quantification of fluorescence intensity, intensity images were transformed from the grey scale images originally generated by the MPT and intensity was calculated in the appropriate 740 nm channel 3. The fluorescence intensities in the study arms was then plotted against depth and compared. Other more accurate measures like fluorescence lifetime analysis were carried out at the pilot stages of experimentation. The fluorescence lifetime analysis is used to generate the amount of protein bound (τ_1), unbound (τ_2) drug and the metabolic ratio a_1/a_2. These values are characteristic of an individual

molecule and are generally used to separate the fluorescence signal of an externally applied substance from the auto fluorescence. For this study the curcumin signal was gathered from a dedicated channel (C3) and hence the lifetime data was not used.

4.3.3.4 Studies on florescent tagged melanostatin

The study was designed to investigate the penetration enhancement effects in the peptide as a function of the combined effect of the microneedle and the magnets. The experimental protocol was similar to the studies described in Chapter 3 (Section 3.4.5.1). The peptide was first dissolved in water. The study arms were:

- A negative control - solvent with magnet post MN application to account for any auto fluorescence encountered
- Peptide with magnet and no MN
- Peptide with magnet post MN application
- Peptide with a non-magnetic occlusive strip made of the same material as the ETP magnets (DUMMY) and no MN
- Peptide with DUMMY post MN application

The treatment duration of the study was 1 h for all interventions. Different skin donors were used for carrying out the replicates on each peptide. Figure 4.9 below shows the experimental set-up. The peptide, which has also been described in the previous chapter, melanostatin, a tripeptide (Pro-Leu-Gly) with molecular weight 803.92 when conjugated with FITC and a log P of -0.485 (native peptide only) was selected based on its favourable penetration profile. Previously melanostatin showed good penetration both passively as well as with the aid of microneedles. It was hence expected that magnetophoresis would further enhance its penetration beyond the effect of microneedles themselves. Moreover, of particular interest to us was the stratum corneum (SC) breaching capacity of magnetophoresis where no MNs were used. ETP magnet, ETP 012 was used with and without MN; dummy non-magnetic strips were used as controls to demonstrate that there was no penetration enhancement due to the material itself or due to simple occlusion with any non-magnetic substance. After the completion of the treatment duration of 1 h, images were captured with the VivaScope 2500. For the analysis of the RCM images, image

J software was used as per the methods described in Chapter 3 section 3.3.5.

Figure 4.9 Set-up for studies on Melanostatin

4.3.4 Statistical analysis

Skin permeation data from the *in vitro* study consisted of cumulative amount measurements of passive, ETP and Dermaportation taken at various times (1 to 24 h). A random effects regression model was used to compare the treatments at various time points, with the timings treated as categorical variables (so that no linear relationship was assumed between permeation and time). This type of regression model is equivalent to a repeated measures analysis of variance, in that it properly takes into account correlations between measurements made on the same sample at different time points. If the standard deviations of the permeation appeared to differ widely for different time periods, a logarithmic transformation was performed on the permeation before analysis.

Pairwise comparisons were calculated from the regression model by requesting certain 'contrasts' as required. Contrasts were tailored to make specific comparisons, and obtain the p-values for them. The standard errors on which the contrasts were based were estimated from the regression model which was based on all the available data. If the analysis was performed on the log-transformed data, the p-values for the pairwise comparisons were based on this analysis, but the mean permeation was quoted on the original scale (to simplify interpretation).

For the analysis of area and integrated density in the *ex vivo* study, there were no repeated measurements, so a straightforward analysis of variance (ANOVA) was performed to compare results between treatments.

The data for the *in vivo* study consisted of 6 different exposures applied to each of 6 different subjects. The data were then observed at different skin depths varying from 5 to 55 µm. All the data was fitted into a single (random effects) regression model similar to the *in vitro* study.

All statistical analyses were performed using the SAS version 9.2 statistical software (SAS Institute Inc, Cary, NC, USA, 2008). A p-value <0.05 was taken to indicate a statistically significant association.

4.4 Results and Discussion

4.4.1 Studies on agar gel

In the initial pilot studies, the ETP 012 magnets (cumulative amount - 3.40 µg/mL) showed a 33% increase in permeation when compared to the dummy magnets (cumulative amount - 2.40 µg/mL). Figure 4.10 below shows the results obtained after the permeation of brilliant blue in the agar gel (n=4).

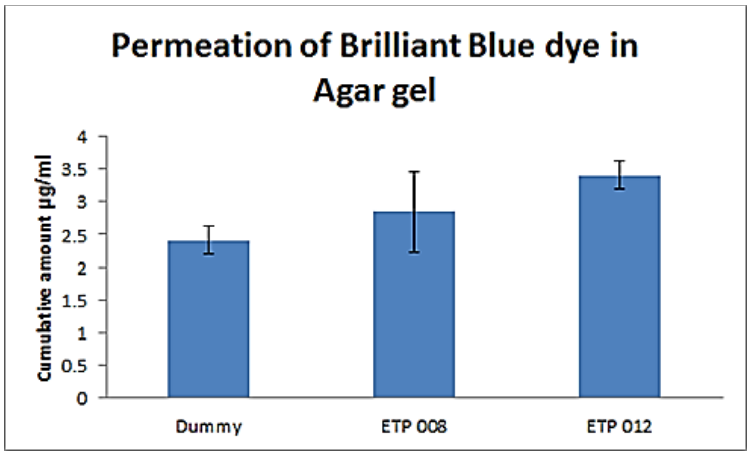

Figure 4.10 Permeation of Brilliant blue dye in the agar gel (n=4). Results are expressed as mean ± SEM

The agar gel syringe model followed the studies described by Schantz et al.[387] and Lauffer et al.[388] At completion of the 2 h application time, the agar gel was pushed up out of the syringe and discs were cut and weighed. This protocol was reasonably reproducible with the weight of the agar discs being within 10% of the 1 g mean weight. The agar disc was then dissolved in 10 mL of water in bottles that were

labelled according to their distance from the top of the syringe. Absorbance was measured at 630 nm and corrected for the weight difference. Linearity was conducted on a series of standard dye solutions. The observed linearity of the standards was 0.99. Though these study results did not show a statistically significant penetration enhancement, the positive trend combined with results of previous studies from our group[7,153,157] provided with an impetus to continue the work further.

This experimental set up is prone to some technical flaws. Schantz et al. had reported that if the gel is pulled away from the wall of the syringe after it is set, erratic results might be obtained because of the solution containing the solute creeping into the capillary space created. We countered this problem by moving the gel into the desired position to create a donor chamber by moving the plunger of the syringe while the gel was still in a liquid state. A problem we encountered was that the surface layer of the gel that was in contact with air was more "hardened" and thus more resistant to diffusion that the bulk of the agar gel. To prevent this problem Schantz et al. had cut of the top part of the hardened gel while the gel was still at the tip of the syringe and lowered the plunger after the gel was formed. However, as we had allowed the gel to solidify below the syringe surface it was not possible to simply remove the surface. Therefore, the pouring of the agar was accurately timed throughout all replicates to make this model consistent.

4.4.2 In vitro studies on excised human skin/ Magnetophoretic delivery of diclofenac sodium in carbopol gel formulation.

4.4.2.1 *Chromatography*

Diclofenac sodium was analysed by UV detection using HPLC. The active eluted without any interfering peaks at a retention time of 8.2 min. The linearity obtained by the HPLC method was 1.0 over the range of the calibration curve (1.9-125.0 μg/mL) for diclofenac sodium standard solutions. Figure 4.11 shows a typical HPLC chromatogram of diclofenac sodium at 31.25 μg/mL.

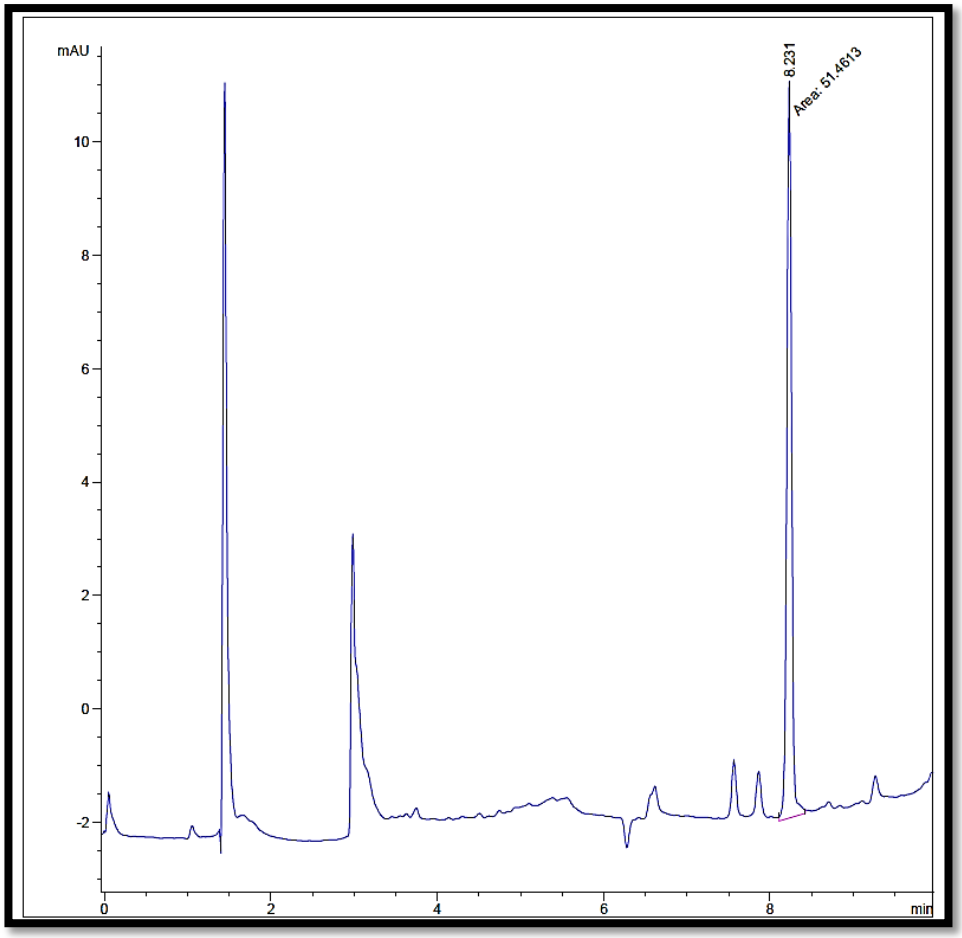

Figure 4.11 HPLC chromatogram of diclofenac sodium at 31.25 µg/mL

A calibration curve was obtained by plotting the peak area versus concentration of standards injected. The CV for precision, determined from the relative standard deviation (n = 5), was 0.75% for 3.9 µg/mL, 0.65% for 15.75 µg/mL and 0.57% for 63.0 µg/mL diclofenac sodium standard solutions in PBS. The intra-day variation was 0.78% and 0.69% and the inter-day variation was 0.96% and 0.73% at 3.9 and 15.75 µg/mL of diclofenac sodium standard solutions in PBS, respectively. These are within the acceptable criteria for intra and inter-day repeatability of R.S.D < 2%.

The limit of detection (LOD), calculated as greater than three times the baseline noise level in the assay, was 90 ng/mL. The limit of quantitation (LOQ), calculated as greater than 10 times the baseline noise level in the assay, was 300 ng/mL.

4.4.2.2 Permeation of diclofenac sodium through human epidermis with ETP and Dermaportation

HPLC analysis of samples post treatment with diclofenac passively and in the presence of ETP magnets and Dermaportation electromagnets showed there was a

substantial increase in mean cumulative permeation of diclofenac over 6 h for ETP application (34.17 ± 8.12 μg/cm^2) as compared with passive application (14.47 ± 3.27 μg/cm^2) and Dermaportation (16.5 ± 7.01 μg/cm^2). All permeation parameters were enhanced by magnetic application (ETP), the enhancement was statistically significant ($p < 0.05$) from 4h onwards when compared to both passive and Dermaportation. The steady state flux increased from 0.0398 to 0.0943 μg/cm^2/h by administration of diclofenac sodium with ETP (Table 4.1). Dermaportation did not have a substantial effect on diclofenac sodium delivery across the epidermis.

Table 4.1 Skin permeation results for diclofenac sodium post magnetophoretic treatment (n=8)

Parameters	**Treatment**		
	Passive	ETP	Dermaportation
Mean cumulative permeation (μg/cm^2)	14.47 ± 3.27	34.17 ± 8.12	16.50 ± 7.01
Steady state flux (μg/cm^2/h)	0.0398	0.0943	0.0451
Permeability coefficient (cm/h)	7.9×10^{-6}	19×10^{-6}	9.0×10^{-6}

The *in vitro* permeation profiles of diclofenac sodium across human epidermis are presented in Figure 4.12. A comparison of the cumulative amount of diclofenac sodium penetrating the epidermis to the receptor solution versus time was plotted for passive, magnetic array enhanced applications and Dermaportation (Figure 4.12) As observed from the preliminary agar gel study, ETP magnets have demonstrated an ability to push drug molecules across membranes and gels due to diamagnetic properties of the drugs. Hence in this study, we tried to compare the diamagnetic repulsion of the ETP magnets to that of a pulsating electro-magnet.

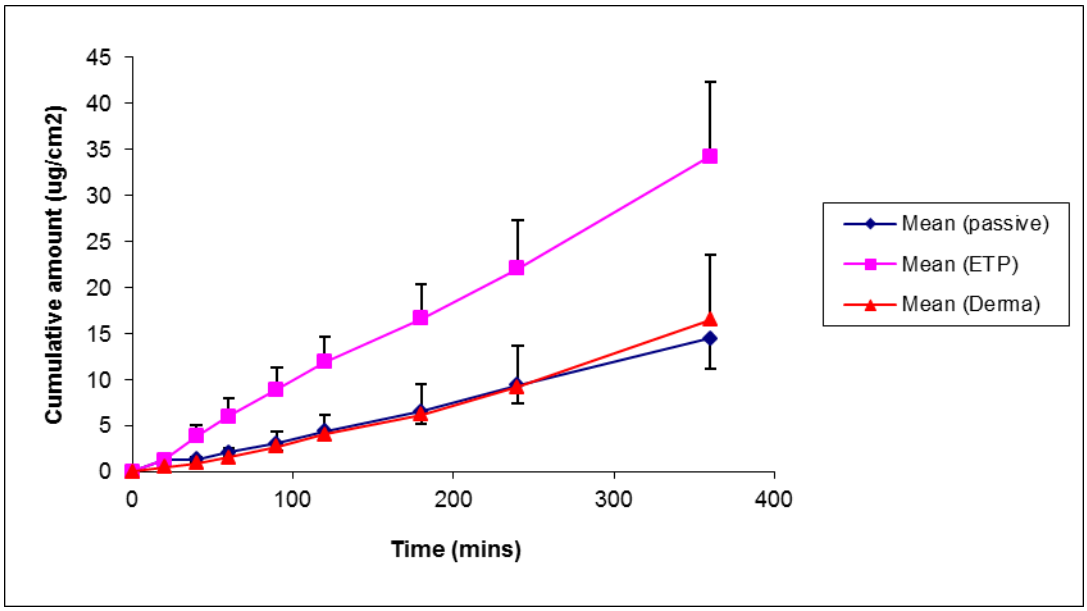

Figure 4.12 Skin permeation of diclofenac sodium. Results are expressed as mean ±SEM (n=8)

Benson et al. investigated the effect of magnetic film array technology on the skin permeation of urea *in vitro* and its effect on skin hydration *in vivo*. They found that under active occlusion (ETP 008), the epidermal thickness (as a measure of hydration) as determined by optical coherence tomography (OCT) increased by 16 and 11% at 30 and 60 min, respectively. They concluded that administration with this novel magnetic film array technology provided enhanced skin penetration of urea and thus increased epidermal hydration when compared with administration under an occlusive film only. OCT measurements also revealed that the changes in the epidermal properties maximise after about 30 min and then stabilise or even decrease over longer periods of time. In our study a linear increase in diclofenac permeation was observed after 30 min until the termination of the experiment.

We have previously demonstrated enhanced skin penetration of 5-aminolevulinic acid, a dipeptide and naltrexone hydrochloride by a pulsed electromagnetic field.[153,156,157] In a preliminary investigation undertaken by our group to elucidate the mechanism of magnetic enhanced delivery, 10 nm gold nanoparticles were applied to human epidermis with and without electromagnetic fields.[381] Multiphoton microscopy with fluorescent lifetime imaging showed skin permeation of the nanoparticles with the pulsed electromagnetic field with no evidence of passive permeation. It was thus hypothesized that the magnetic energy may induce channels within the stratum corneum of at least 10 nm in diameter.

The precise mechanism of skin permeation enhancement may vary with the magnetic field characteristics.[7] Biological and therapeutic effects of electromagnetic fields and inductive effects on biological tissues have been widely reported, for example, enhancement of healing of venous ulcers and bone fractures and effects on a range of cellular functions.[146,299]

The standard Dermaportation system (DP1001) generates a specific pattern of energy pulses that have been shown to induce transdermal flux increases during field exposure of a number of small molecules, such as 5-aminolevulinic acid,[157] lidocaine hydrochloride[159] and a model dipeptide Ala-Trp.[153] It is proposed that the Dermaportation energy influences both the molecular movement of drug molecules in the epidermis and the ordered structure of the stratum corneum lipid bilayers. The precise mechanism of enhancement is an area of continuing investigation. Dermaportation was not used for subsequent studies as it failed to show a positive skin permeation enhancement effect, when compared to ETP magnets.

4.4.3 In vivo studies on a model fluorescent compound (Curcumin)

Figure 4.13 below presents the effects of tape stripping and magnetic array on the skin penetration of curcumin, expressed as mean intensity versus depth. As anticipated, tape stripping had the most profound effect on skin penetration and served as an effective positive control for the study. ETP 008 demonstrated enhanced curcumin penetration in the upper part of the skin. As the depth increased the effect of the magnets reduced and the intensity observed was similar to the auto fluorescence encountered in the negative controls. Overall the penetration of curcumin in the top layer of the skin was 1.4 times greater due to ETP 008 magnets when compared to the dummy non-magnetic strips.

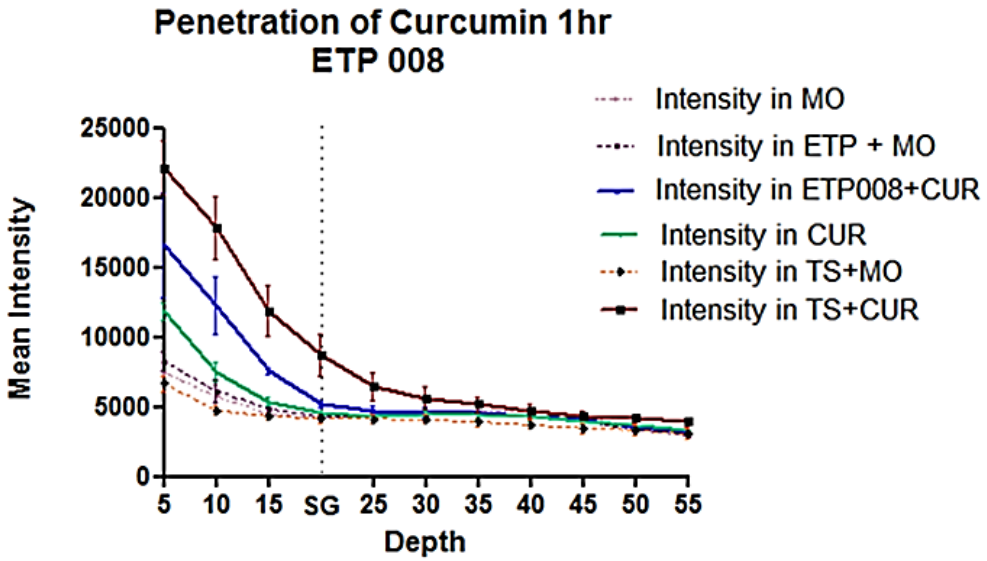

Figure 4.13 ETP 008 induced skin penetration enhancement of curcumin

The results of the ETP 012 studies are presented below in Figure 4.14 Similar to ETP 008, ETP 012 showed enhanced penetration of curcumin in the top parts of the skin. The penetration of curcumin was enhanced by 1.5 times. ETP 012 showed enhanced penetration to deeper distance in the skin. (ETP 008: 20 µm; ETP 012: 30 µm; $p < 0.05$)

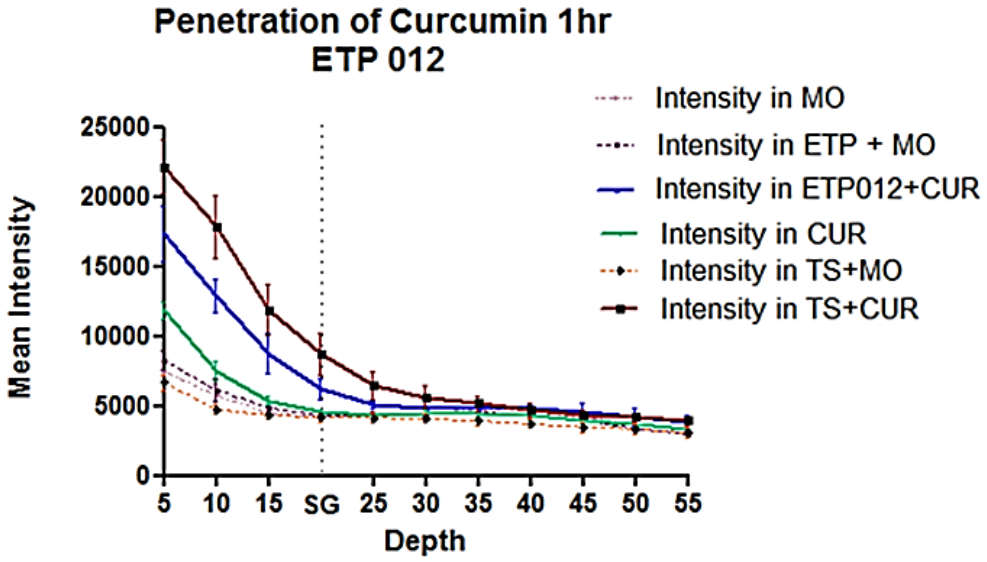

Figure 4.14 ETP 012 induced skin penetration enhancement of curcumin

The studies conducted and described in this chapter were designed to examine magnetophoresis as a penetration enhancement technique in its own right as well as a potential synergistic skin penetration enhancement technology with microneedles. To

understand the mechanism of magnetophoretic drug delivery work done by Murthy's group and previous work by our group are of utmost importance. As these are the only available sources for such work across skin (both human and non-human).

The potential to increase diffusion or flow within the applied solvent possibly due to an interaction between the magnetic field and the diamagnetic properties of the molecules was investigated in agar gel, excised human epidermis and excised human full thickness skin. The former was chosen as a simple system, whereas in the skin the magnetic fields may also influence the skin structure. I have also attempted to look at differences in the skin lipid structure with the help of ATR-FTIR by applying ETP magnets to excised human skin mounted on an ATR-FTIR crystal (data not presented). The results of this preliminary study did not show any noticeable change to the primary and secondary structure of the skin. This is in agreement with Murthy et al.[154] who examined the effect of more powerful magnets (30, 150 and 300 mT compared to ETP 5-40 mT) on skin using ATR-FTIR and reported no changes to the skin structure. It is unclear if ATR-FTIR is the best system for these measurements and Raman spectroscopy may be a better analytical tool. In this study I attempted to gain more knowledge on the possible mechanism of the ETP magnets, by conducting studies on human volunteers. I expected that any effect of the magnets on skin structure would be better observed *in vivo*. The solvent mineral oil showed the least fluorescence with and without ETP magnets. It was also hypothesised that the removal of stratum corneum by tape stripping (TS) would increase the trans epidermal water loss (TEWL) reading and hence would enhance skin permeability to extraneously applied drug, curcumin (CUR). The results of TEWL before and after the study are presented in the figures below (Figure 4.15 and Figure 4.16). Tape stripping increased the TEWL by 3-6 times in all the subjects ($p < 0.05$). The reading after the study suggested further that the skin permeability remained high for a long duration.

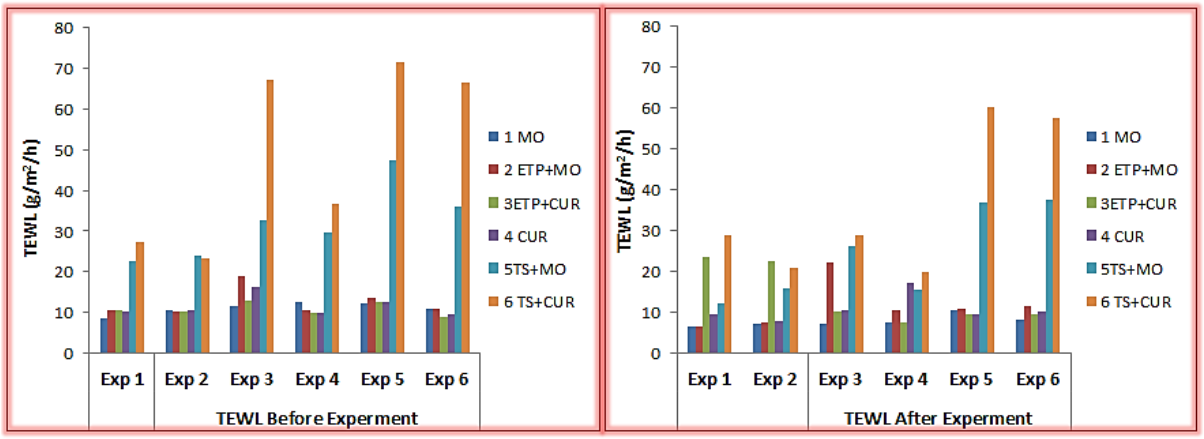

Figure 4.15 TEWL readings before and after the treatment

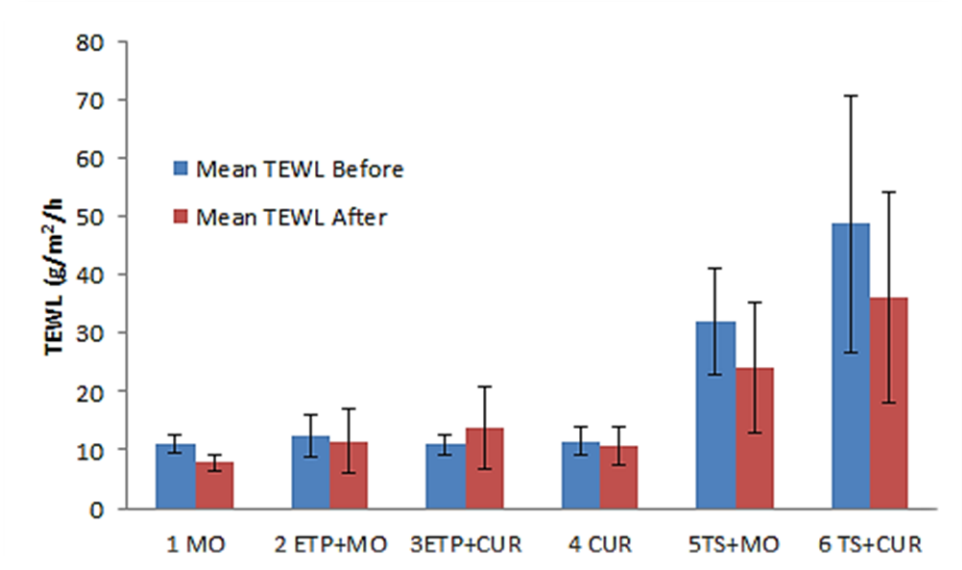

Figure 4.16 Average TEWL across subjects (n=6). Results are expressed as mean ± SD

Figures 4.17 and 4.18 below show pseudo coloured images from channel 1 and channel 3 of the different sample points. Curcumin fluorescence can be observed in C 3 as bright orange colouration.

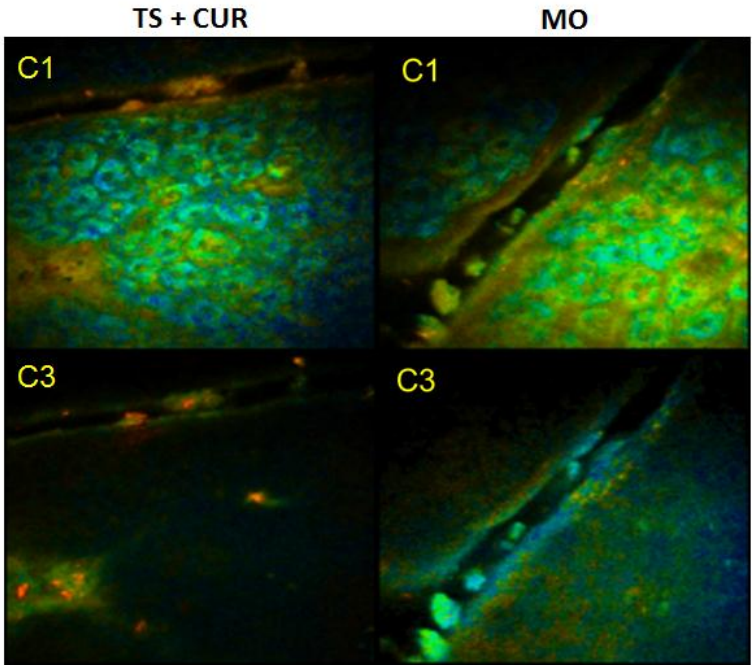

Figure 4.17 Pseudo coloured images from channel 1 and channel 3 –Negative control (MO) and positive control (TS + CUR)

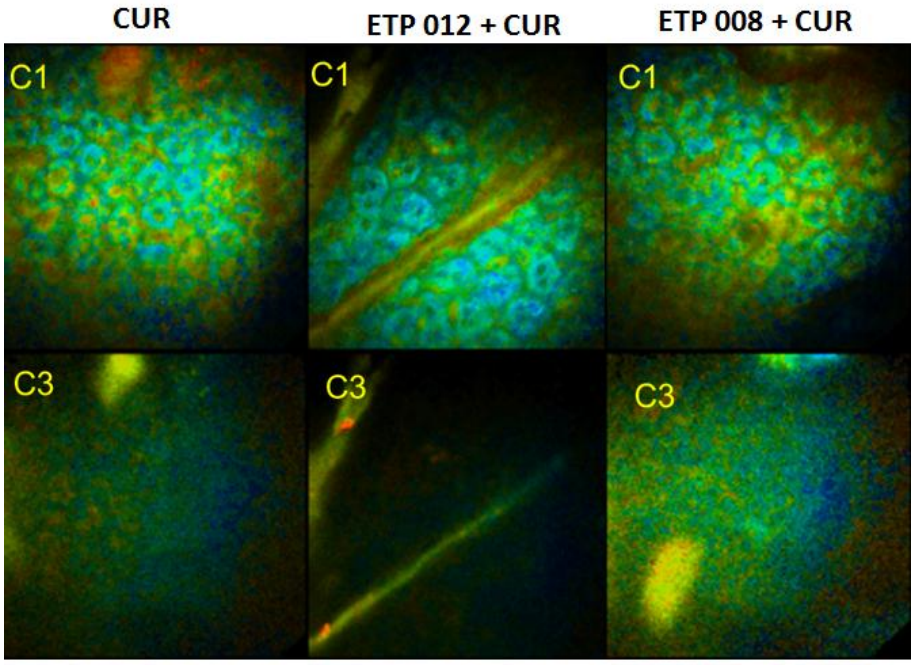

Figure 4.18 Pseudo coloured images from channel 1 and channel 3 – Passive (CUR) and active treatments (ETP 008, ETP 012)

The premise that all cells produce a certain degree of autofluorescence, lead us to evaluate the effects of the magnets with a correction for the autofluorescence. Following the above described procedures form section 4.3.3.3, background fluorescence of the corresponding treatment arms was subtracted from all the

curcumin containing interventions. The resulting net intensity (δ) was graphed (Figure 4.19). Both magnets showed twice the intensity of that observed with curcumin and dummies (ETP 008 -8050; ETP 012 – 8950; Dummy – 4055). Tape stripping however, was by far, the most effective intervention in enhancing the skin permeation of curcumin. (TS – 15890)

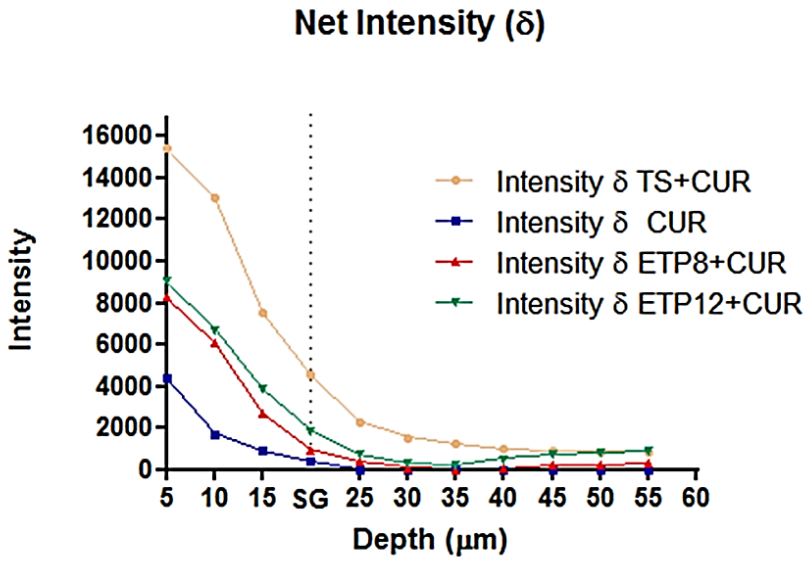

Figure 4.19 Net fluorescence intensity (δ) of curcumin following treatment with ETP 008, ETP 012 and tape stripping

4.4.4 Ex-vivo studies on a fluorescent peptide (Melanostatin)

Average penetration area and average integrated density, calculated using image J were used to assess the penetration of melanostatin. Figure 4.20 shows the penetration of melanostatin after 1 h post treatment with MN and ETP magnets. In the absence of the MN the area of penetration was significantly low and the fluorescence was mostly accumulated in the skin furrows. The fluorescent intensity too was lower than that for the skin samples with MN treatment. However, both the indicators were significantly higher when compared to the negative control (MN + ETP + Solvent). The average penetration area of melanostatin with MN and ETP 012 was 1.48 times greater than that observed with MN and dummy non-magnetic strips (MN dummy: 103052 ± 37546 pixels; MN ETP 012: 153058 ± 48963 pixels; $p < 0.05$). This result was an average across all the three measured skin layers (SC, VE, and DER, Table 4.2). The area of penetration was larger and the measured intensity was greater in all three layers (Table 4.2). The most profound effect of the ETP

magnets when used in conjunction with the MN was seen in the dermis where the integrated density was 2.42 times higher than the ID of MN with dummy. The area of penetration as well was greater by a factor of 4.63 times in the dermis. The ETP 012 magnets showed 7.12 times greater area of penetration when compared to dummy strips (Dummy-1091 vs. ETP012- 7775) when no MN were used, this comparison was statistically significant ($p < 0.05$). The average intensity of the penetration area represented by integrated density was also enhanced by 2.8 times (Dummy-133 vs. ETP012- 368) demonstrating that the ETP 012 magnets had the ability to transport the peptide across the SC, without the MN.

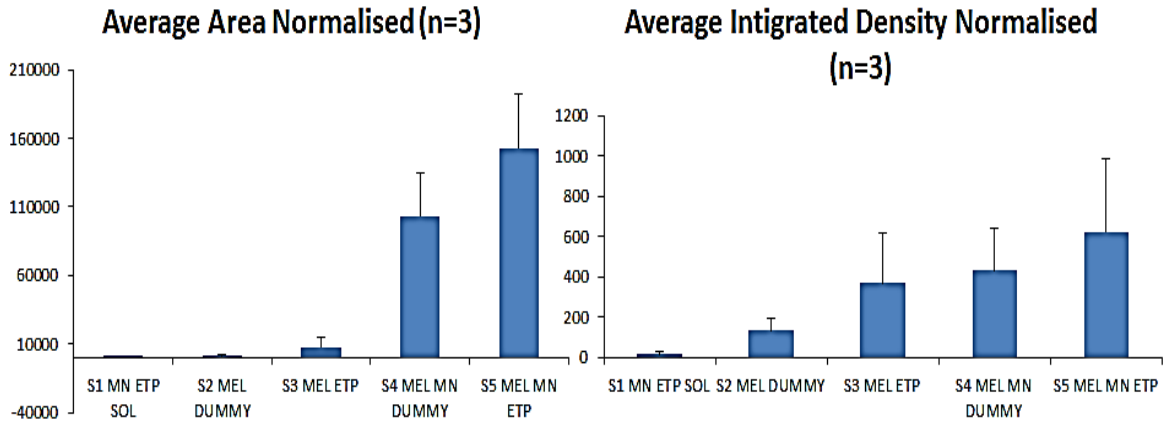

Figure 4.20 Average penetration area and average integrated density of melanostatin after 1 h post treatment with MN and ETP magnets

Table 4.2 Penetration area and fluorescence integrated density of melanostatin after MN and ETP treatment

	MEL MN DUMMY		MEL MN ETP	
	Nor Area (pixels)	Nor ID	Nor Area (pixels)	Nor ID
SC	91743	531	97273	629
VE	191637	657	242548	987
DER	25777	107	119355	260
AVERAGE	103052	432	153059	625

It was observed that topical peptide application results in accumulation in the skin furrows. The average width of the furrows measured in pixels and the average intensity of the fluorescence signal present in the furrows was calculated in image J (Figure 4.21). The difference in penetration and accumulation within the furrows of ETP treated and dummy treated skin samples were investigated. Figure 4.21 shows an example of the skin sample images showing the line profile of each of ETP and dummy treated skin samples. The cut-off intensity of 54 has been used as the lower threshold limit for all the analysis in chapter 3 as it is a positive indication of FITC fluorescence and not auto-fluorescence. To measure the width of the furrows, consecutive pixels with intensity above 32/pixels was used (Figure 4.21). The average width of furrow fluorescence in the ETP 012 treated skin sample was 2.4 times that observed in dummy strip treated skin (Dummy: 8.6 ± 5.47; ETP012: 20.6 ± 15.2 pixels). Further, the average intensity of fluorescence in these furrows was 1.2 times that of the dummy strips (Dummy: 52.3 ± 12.4; ETP012: 67.3 ± 21.5). Such an analysis of the fluorescent drug particles in the skin furrows has previously been reported with other topical products like sunscreens and heavy metal nano-particles.[41,389,390] Accumulation of drugs in the skin furrows can be advantageous, as it can act like a reservoir for drugs in solution. Form the furrows the drug can be taken up into the skin over time. Though the furrows contribute to only 0.1% of the total skin surface, once accumulated in the furrows, the drug is transported into the skin.[391,392]

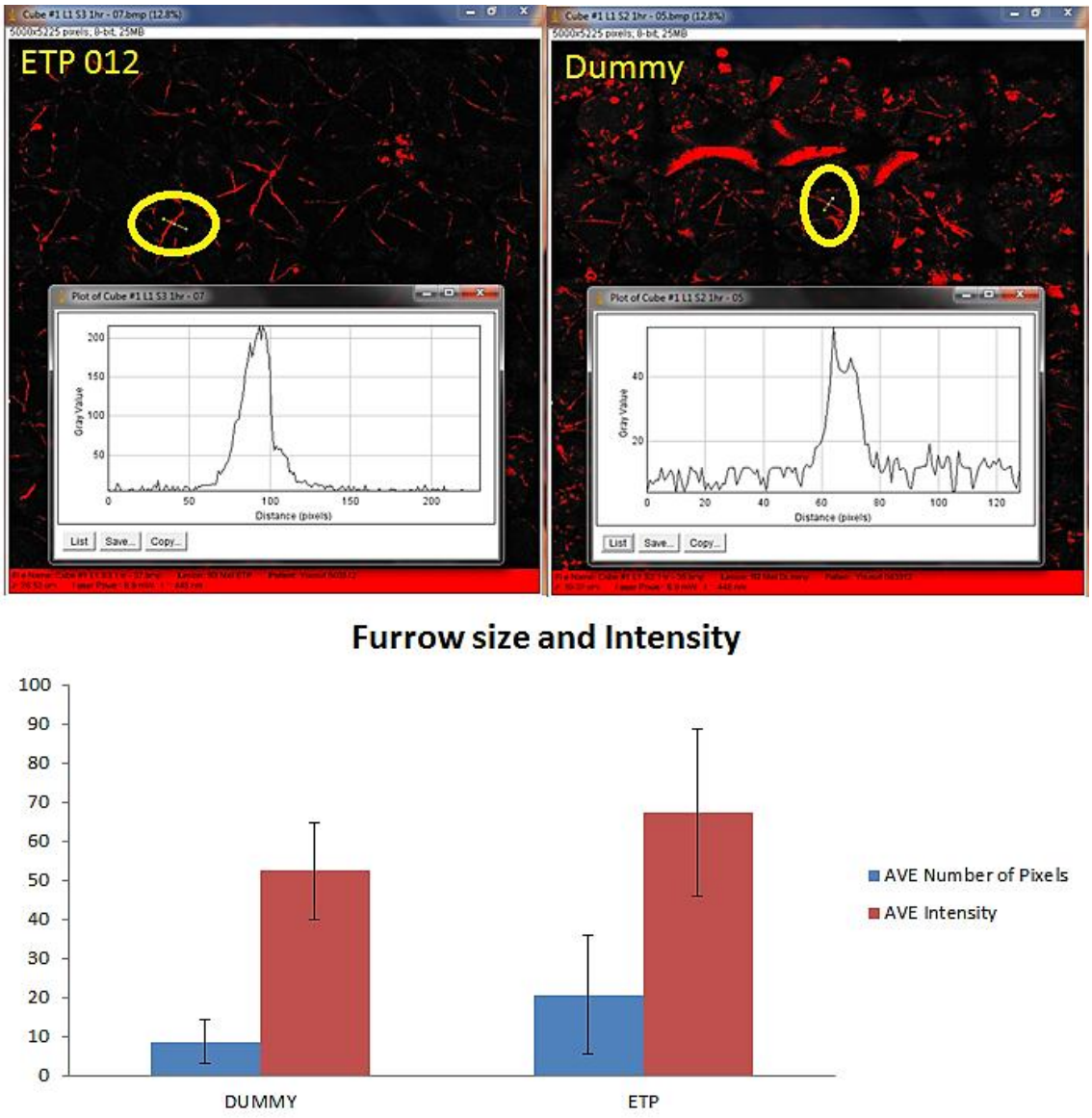

Figure 4.21 Width and fluorescence intensity signal analysis within skin furrows (mean ± SD, n=3)

4.5 Conclusions and future directions

Though the magnets used in this project are of very weak field strength, they have shown to increase the permeation of a number of molecules here. In this project I have demonstrated a 33% increase in the permeation of a dye through an agar gel based model, a 200% increase in mean cumulative permeation of diclofenac sodium (gel formulation) through human epidermis *in vitro* and a 10 fold higher permeability coefficient when compared to passive diffusion. I have also demonstrated that the results of the *in vitro* studies were fully reproducible in an *in vivo* set-up. In the studies on human volunteers a 200% increase in the curcumin net intensity was

observed when compared to dummy non-magnetic strips of similar material. Further, the ETP magnets also showed an average 500-600% increase in the permeation of a tripeptide through full thickness human skin *ex vivo*. The ETP magnets can hence be of great value as transdermal permeation enhancers. Moreover, these ETP magnets have potential to be easily formulated into non-invasive transdermal patches. ETP magnets can also be used in synergistic combination with microneedles, especially dissolvable hollow microneedles to deliver drugs and vaccines transdermally through a reservoir patch. Further studies are required to understand the optimal performance of the magnets and their mechanism of transdermal delivery enhancement. Successful transformation of this technique can provide an inexpensive transdermal delivery system which can be used without the need of elaborate procedures and expert supervision.

Chapter 5

Summary and future directions

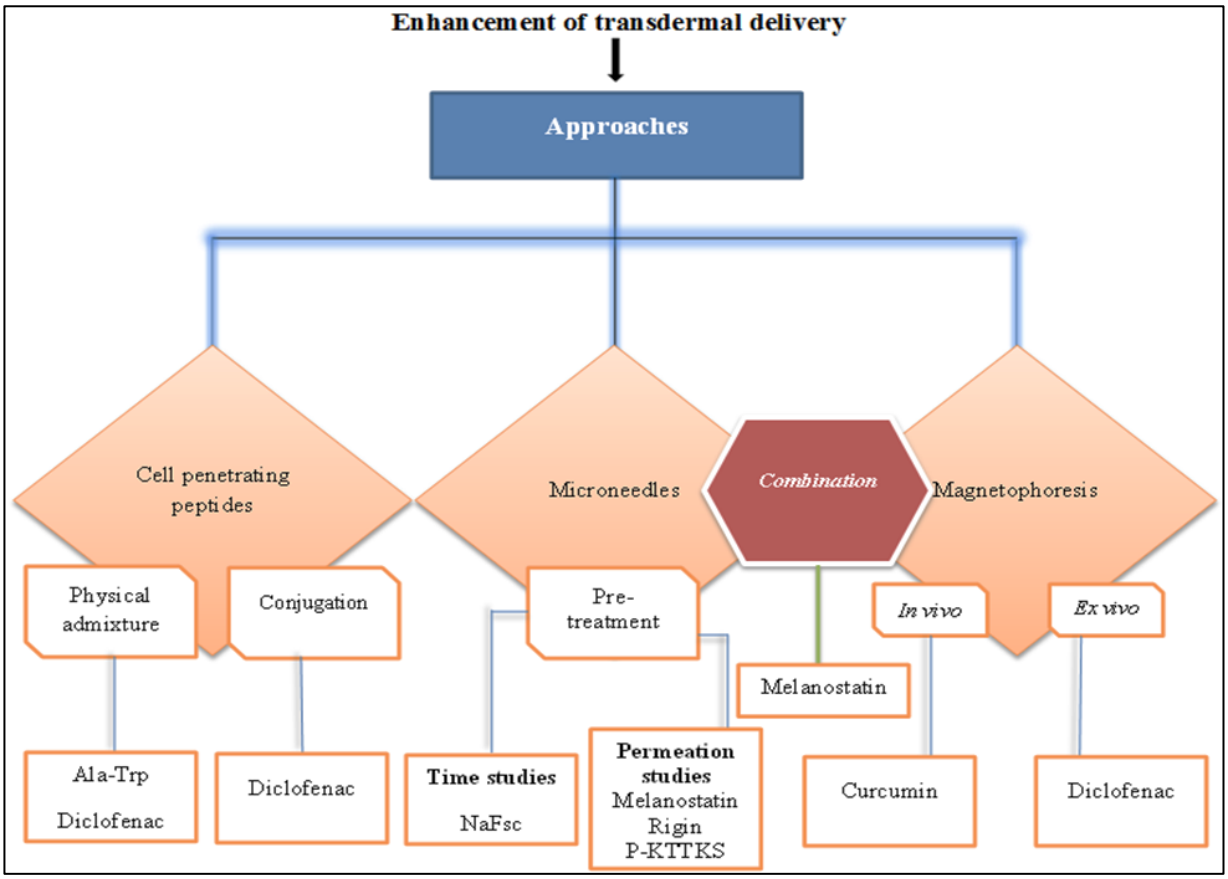

Figure 5.1 Skin penetration enhancement strategies used in this project

Development of effective and functional delivery systems for new active pharmaceutical and cosmeceutical products is a challenging task and a long term goal of drug delivery research.[379] In this PhD project efforts have been made to advance the science through three different methods. These approaches are highlighted in Figure 5.1 above.

Chapter 2 describes the use of ***Cell penetrating peptides***, in particular diketopiperazine (DKP) in penetration enhancement of a small dipeptide (Ala-Trp) and diclofenac. The physical admixture of these molecules with DKP enhanced their permeation across human epidermis *in vitro* by 9.15-fold and 1.9-fold respectively. These results were consistent with previous findings.[310,311] Proteins and peptide delivery with the use of CPPs has gained a lot of attention. The major obstacles for *in vivo* clinical applications of peptides is their poor permeability through plasma membrane and their sensitivity to enzymatic degradation.[92] Conjugation of DKP with diclofenac enhanced the transdermal flux of diclofenac 9-fold and significantly enhanced drug deposition into the skin (14-fold compared to passive diclofenac). A comparison with the well-established cell penetrating peptide TAT showed that DKP enhanced the permeation of diclofenac through the skin and the deposition of diclofenac in the skin, 5-fold and 6-fold greater than TAT respectively. Enzyme assay results demonstrated COX inhibition by the DKP-diclofenac conjugate, showing it retained its anti-inflammatory activity. Further work needs to be undertaken to better understand the mode of skin penetration of the diketopiperazine based cell penetrating peptides. Fluorescence tagging of DKP would be of particular value for investigating its route of skin penetration. This information will be invaluable in optimization and accurate selection of the most suitable drugs for skin delivery using the DKP platform. The strategies used to deliver these peptides across the skin so as to ensure they are made available to the site of action in a non-invasive manner will govern the success of this approach.

Chapter 3 demonstrated the enhanced delivery of three peptides by ***Microneedle*** pre-treatment of the skin. Confocal laser scanning microscopy (CLSM) in conjunction to the reflectance mode available in the VivaScope 2500 rendered it possible to visualise and quantify the penetration of the peptides studied in this project in a rapid and efficient manner. The peptides selected for these studies were 3, 4 and 5 amino acids in length (melanostatin, rigin and palmitoyl pentapeptide). Melanostatin and

rigin are fairly water-soluble peptides whereas palmitoyl pentapeptide has the peptide conjugated to a lipophilic group that is designed to enhance stratum corneum permeability. The stratum corneum is generally regarded as relatively impermeable to hydrophilic molecules and hence preferentially permeable to reasonably lipophilic solutes. However it has recently been suggested that the skin permeability of highly hydrophilic drugs is generally under-predicted by 2–6 orders of magnitude.[393] In this study, all peptides showed enhanced penetration with the microneedle pretreatment, although the enhancement varied considerably between the peptides. Melanostatin showed a 10-fold enhancement in penetration area in the viable epidermis at 1 h and a 22-fold increase in area in the dermis with microneedle pretreatment. Melanostatin is currently used in specific hyperpigmentary problems such as post inflammatory hyperpigmentation, solar lentigos, and melasma.[362,363] Our research clearly shows that microneedle pretreatment is a useful method to enhance delivery and potentially improve clinical outcomes for these conditions.

Rigin showed a 1.8-fold increase in the area at 1 h and no difference at 24 h with microneedle pretreatment. Sederma™ markets rigin as Palmitoyl tetrapeptide-7 in their product Matrixyl® 3000 and Matrixyl® synthe'6™. It is promoted as an enhancer of skin elasticity via interleukin (IL)-6 reduction. For the studies on rigin in this project the parent molecule was used rather than the palmitoylated tetrapeptide to manage the size of the molecule. To our knowledge skin permeation studies on these peptides have not been published and the manuscript prepared on this project could be the first publication reporting passive (without MN) and MN based skin delivery.

Palmitoyl pentapeptide or Pal-KTTKS is a frequently used peptide in the cosmeceutical industry. At 1 h post administration there was no difference in penetration area in the viable epidermis with the use of microneedles, but over 24 h the passive permeation of Pal-KTTKS was increased 2.6-fold with microneedle pretreatment. Figure 5.2 below shows the comparative assessment of skin penetration area of all the peptides.

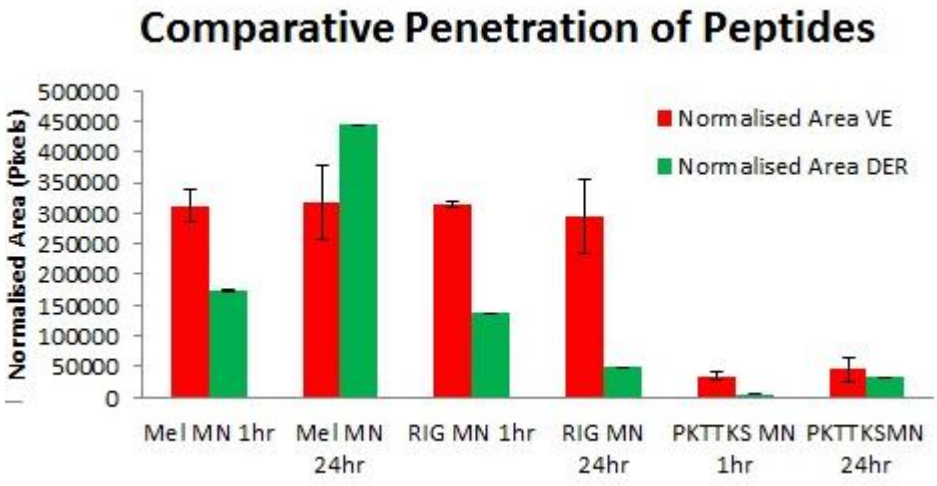

Figure 5.2 Comparison of penetration area of peptides after microneedle (MN) based application. Mean ±SEM (n=3)

Pretreatment with a microneedle patch is not very uncommon and has been used indiscriminately for various transdermal drugs. 3M in 2011 have launched a stand-alone microneedle based pretreatment device. 3M calls it, its "Microchannel Skin System," and it consists of a sterile, single-use patch with hundreds of microneedles that create "micro channels" to administer the drug.[394] Currently available only for dermatologists, through dedicated dealers, this device is touted to be made available for the patients in the near future. However, debate regarding safety and efficacy is bound to stretch far and long.

Figure 5.3 3M - Microchannel Skin System

Successful application of microneedles depends on the applicator device that facilitates microneedle insertion and possible infusion of drugs into the skin, skin recovery and regeneration after microneedle insertion. Other important factors

include drug efficacy, safety, stability during manufacturing and patient outcomes such as lack of pain, skin irritation and skin infection.[395] In order to get a particular design of microneedles approved to be marketed for transdermal drug delivery, it is very important to properly choose the type of microneedle (e.g., hollow, solid, geometry, material, density, length). Furthermore, to obtain sufficient and reproducible penetration and a possibility of self-administration by the patient, the right microneedle application devices must be used. Therefore, new microneedle-based products for transdermal drug delivery usually need to be a complete package for each type of drug.[396] Microneedles have been shown to enhance the skin diffusion of various drugs including peptides and vaccines.[5, 186, 187, 199-201, 350, 395] In this project microneedles were used to enhance skin diffusion and penetration of small peptides. Further work needs to be undertaken to compare different microneedle designs before an optimised model can be generated.

Chapter 4 describes the novel skin penetration enhancement technique of ***Magnetophoresis***. Magnetophoresis is a recently introduced technique to be used in transdermal delivery that involves the application of a magnetic field to the skin. Previous research by our group and Murthy's group has shown skin delivery of various molecules with the use of fixed and pulsating magnets.[6,7,153-155,157,381] The influence of magnetic field strength on diffusion flux was determined by Murthy et al. and reported to increase with an increase in the applied field strength.[6]

The magnets used in this project are of comparatively weak field strength but were found to significantly enhance skin penetration alone and in combination with microneedles. A series of experiments was designed to assess magnetophoresis compared to passive permeation. In the first study, ETP 012 showed a 2.4-fold increase in diclofenac permeation *in vitro* across human epidermis when compared to passive treatment. In the studies on human volunteers we also showed a 200% increase in the net fluorescence intensity generated by curcumin when compared to passive (dummy non-magnetic strips of similar material). When investigated for their use in combination with microneedles, the magnetic film array (ETP 012) showed a 5-fold increase in skin diffusion of melanostatin in full thickness human skin *ex vivo* when compared to microneedles alone. In CLSM generated image analysis, in addition to the increase in area and fluorescence intensity, the average width of furrow fluorescence in the ETP 012 treated skin sample was 2.4 times that observed

for microneedle pretreatment alone. These experiments suggest that magnetophoresis is worthy of further investigation as a stand-alone enhancement technology and may also be useful in driving drug into the skin via pores generated by microneedles. The small field magnets used in this project are a unique and non-invasive skin delivery approach. Further work needs to be undertaken to better understand the mode of action of these magnets.

Overall, it can be concluded that all three approaches to enhance transdermal delivery that were investigated in this project have shown improved permeation and diffusion of peptides and small drugs after topical application.

Chapter 6

References

1. Amsden BG, Goosen MFA. Transdermal delivery of peptide and protein drugs: an overview. Bioengineering, Food and Natural products. 1995; 41(8):1972-1997.

2. Benson HAE, Watkinson AC. Topical and Transdermal Drug Delivery: Principles and Practice. New Jersey: John Wiley & Sons; 2012.

3. Benson HAE, Namjoshi S. Proteins and peptides: Strategies for delivery to and across the skin. Journal of Pharmaceutical Sciences. 2008; 97(9):3591-10.

4. Hällbrink M, Florén A, Elmquist A, Pooga M, Bartfai T, Langel Ü. Cargo delivery kinetics of cell-penetrating peptides. Biochimica et Biophysica Acta (BBA) - Biomembranes. 2001; 1515(2):101-109.

5. Prow TW, Chen X, Prow NA, Fernando GJP, Tan CSE, Raphael AP, et al. Nanopatch-targeted skin vaccination against west nile virus and chikungunya virus in mice. Small. 2010; 6(16):1776-1784.

6. Murthy SN. Magnetophoresis: an approach to enhance transdermal drug diffusion. Pharmazie. 1999; 54(5):377-409.

7. Benson HAE, Krishnan G, Edwards J, Liew YM, Wallace VP. Enhanced skin permeation and hydration by magnetic field array: preliminary in-vitro and in-vivo assessment. Journal of Pharmacy and Pharmacology. 2010; 62(6):696-701.

8. Bolzinger M-A, Briançon S, Pelletier J, Chevalier Y. Penetration of drugs through skin, a complex rate-controlling membrane. Current Opinion in Colloid & Interface Science. 2012; 17(3):156-165.

9. Troy D, editor. Principals of Drug Discovery. Fifth edition ed: Lippincott Williams and Wilkins; 2002.

10. Banga AK, Chien YW. Systemic delivery of therapeutic peptides and proteins. International Journal of Pharmaceutics. 1988; 48(1-3):15-50.

11. Siddiqui, Chien YW. Non-parental administration of peptide and protein drugs. Critical Reviews in Therapeutic Drug Carrier Systems. 1987; 3(3):195.

12. Namjoshi S, Caccetta R, Benson HAE. Skin peptides: biological activity and therapeutic opportunities. Journal of Pharmaceutical Sciences. 2008; 97(7):2524-42.

13. Williams AC. Structure and function of human skin. In: Transdermal and Topical Drug delivery: Pharmaceutical Press; 2003.

14. Mills PC, Cross SE. Transdermal drug delivery: Basic principles for the veterinarian. The Veterinary Journal. 2006; 172(2):218-233.

15. Wilkes GL, Brown IA, Wildnauer RH. The biomechanical properties of skin. CRC Critical Reviews in Bioengineering. 1973; 62:453 - 495.

16. Holbrook KA, Odland GF. Regional differences in the thickness (cell layers) of the human stratum corneum : An ultrastructural analysis. The Journal of Investigative Dermatology. 1974; 62:415 - 422.

17. Benson HAE. Transdermal drug delivery:Penetration enhancement techniques. Current Drug Delivery. 2005; 2(1):23 - 33.

18. Barry BW. Novel mechanisms and devices to enable successful transdermal drug delivery. European Journal of Pharmaceutical Sciences. 2001; 14:101 - 114.

19. Swartzendruber D, Wertz P, Madison K, Downing D. Evidence that the corneocyte has a chemically bound lipid envelope. Journal of Investigative Dermatology. 1987; 88:709 - 713.

20. Potts RO, Francoeur ML. The influence of stratum corneum morphology on water permeability. The Journal of Investigative Dermatology. 1991; 96:495 - 499.

21. Bouwstra JA, Gooris GS, spek Vd, Bras JA. Structural investigations of human stratum corneum by small-angle X-Ray scattering. Journal of Investigative Dermatology. 1991; 97:1005 - 1012.

22. Anderson RL, Cassidy JM. Variations in physical dimensions and chemical composition of human stratum corneum. The Journal of Investigative Dermatology. 1973; 61:30 - 32.

23. Senti G. Epicutaneous allergen administration: Is this the future of allergen-specific immunotherapy? Allergy. 2011; 66(6):798-809.

24. Hata M, Tokura Y, Takigawa M, Sato M, Shioya Y, Fujikura Y, et al. Assessment of epidermal barrier function by photoacoustic spectrometry in relation to its importance in the pathogenesis of atopic dermatitis. Laboratory Investigation. 2012; 82(11):1451-1461.

25. Watanabe M, Tagami H, Horii I, Takahashi M, Kligman AM. Functional analyses of the superficial stratum corneum in atopic xerosis. Archives of Dermatology. 1991; 127(11):1689-1692.

26. Wertz PW. Stratum Corneum : Biological and Biochemical Considerations. In: Hadgraft J, guy RH, editors. Transdermal drug delivery : developmental issues and research initiatives. New York: Marcel Dekker Inc; 1989. p. 1 - 22.

27. Barry BW. Drug delivery routes in skin : a novel approach. Advanced Drug Delivery Reviews. 2002; 54(Suppl 1):S 31 - S 40.

28. Trommer H, Neubert RHH. Overcoming the stratum corneum: The modulation of skin penetration. Skin Pharmacology and Physiology. 2006; 19(2):106-121.

29. Williams AC. Theoretical aspects of transdermal drug delivery. In: Transdermal and Topical drug delivery. London: Pharmaceutical Press; 2003. p. 26-49.

30. Sloan KB. Prodrugs: Topical and ocular drug delivery. Marcel Dekker Inc: New York; 1992.

31. Williams A. Chemical modulation of topical and transdermal permeation. In: Transdermal and topical drug delivery: Pharmaceutical Press; 2003.

32. Megwa SA, Cross SE, Benson HA, Roberts MS. Ion-pair formation as a strategy to enhance topical delivery of salicylic acid. Journal of Pharmacy and Pharmacology. 2000; 52(8):919-28.

33. Larsen SW. Kinetics of degradation and oil solubility of ester prodrugs of a model dipeptide (Gly-Phe). European Journal of Pharmaceutical Sciences. 2004; 22(5):399-408.

34. Touitou E, Dayan N, Bergelson L, Godin B, Eliaz M. Ethosomes — novel vesicular carriers for enhanced delivery: characterization and skin penetration properties. Journal of Controlled Release. 2000; 65(3):403-418.

35. Gupta PN. Non invasive vaccine delivery in transferosomes, niosomes and liposomes: a comparative study. International Journal of Pharmaceutics. 2005; 293(1-2):73-82.

36. Benson HAE. Transfersomes for transdermal drug delivery. Expert Opinion on drug Delivery. 2006; 3(6):727-737.

37. Manconi M. Niosomes as carriers for tretinoin III. A study into the in vitro cutaneous delivery of vesicle-incorporated tretinoin International Journal of Pharmaceutics. 2006; 311(1-2):11-19.

38. Arruebo M, Fernández-Pacheco R, Ibarra MR, Santamaría J. Magnetic nanoparticles for drug delivery. Nanotoday 2007; 2(3):22-32.

39. Soares AF, Carvalho RdA, Veiga F. Oral administration of peptides and proteins: nanoparticles and cyclodextrins as biocompatible delivery systems. Nanomedicine. 2007; 2(2):183-202.

40. Robertson TA, Sanchez WY, Roberts MS. Are commercially available nanoparticles safe when applied to the skin? Journal of Biomedical Nanotechnology. 2010; 6(5):452-468.

41. Prow TW, Grice JE, Lin LL, Faye R, Butler M, Becker W, et al. Nanoparticles and microparticles for skin drug delivery. Advanced Drug Delivery Reviews. 2011; 63(6):470-491.

42. Webster TJ. Safety of Nanoparticles: From Manufacturing to Medical Applications. Springer; 2008.

43. Nohynek GJ, Lademann J, Ribaud C, Roberts MS. Grey Goo on the Skin? Nanotechnology, Cosmetic and Sunscreen Safety. Critical Reviews in Toxicology. 2007; 37(3):251-277.

44. Müller RH, Radtke M, Wissing SA. Solid lipid nanoparticles (SLN) and nanostructured lipid carriers (NLC) in cosmetic and dermatological preparations. Advanced Drug Delivery Reviews. 2002; 54:S131-S155.

45. Wissing SA, Muller RH. Cosmetic applications for solid lipid nanoparticles (SLN). International Journal of Pharmaceutics. 2003(254);65 - 68.

46. Malavolta L. Peptides: Important tools for the treatment of central nervous system disorders. Neuropeptides. 2011; 45(5):309-316.

47. Lucke A, Fustella E, Teßmar J, Gazzaniga A, Göpferich A. The effect of poly(ethylene glycol)–poly(d,l-lactic acid) diblock copolymers on peptide acylation. Journal of Controlled Release. 2002; 80(1-3):157-168.

48. Fraysse-Ailhas C, Graff-Meyer A, Rigler P, Mittelhozer C, Raman S, Aebi U, et al. Peptide nanoparticles for drug delivery applications. European Cells and Materials. 2007; 14(3):115.

49. Gareth A H. Nanostructure-mediated drug delivery. Nanomedicine: Nanotechnology, Biology and Medicine. 2005; 1(1):22-30.

50. Lee P-W, Peng S-F, Su C-J, Mi F-L, Chen H-L, Wei M-C, et al. The use of biodegradable polymeric nanoparticles in combination with a low-pressure gene gun for transdermal DNA delivery. Biomaterials. 2008; 29(6):742-751.

51. Coulman SA, Anstey A, Gateley C, Morrissey A, McLoughlin P, Allender C, et al. Microneedle mediated delivery of nanoparticles into human skin. International Journal of Pharmaceutics. 2009; 366(1-2):190-200.

52. Lee SH. Nanoparticle popsicle: Transdermal delivery of nanoparticles using polymeric microneedle array. Korean Journal of Chemical Engineering. 2011; 28(9):1913-1917.

53. Ali M, Manolios N. Peptide delivery systems. Letters in Peptide Science. 2002; 8:289–294.

54. Setoh K, Murukami M, Araki N, Fujita T, Yamamoto A, Muranishi S. Improvement of transdermal delivery of tetragastrin by lipophilic modification with fatty acids Journal of Pharmacy and Pharmacology. 1995; 47(10):808-811.

55. Toth I, Danton M, Flinn N, Gibbons WA. A combined adjuvant and carrier system for enhancing synthetic peptides immunogenicity utilising lipidic amino acids. Tetrahedron Letters. 1993; 34(24):3925-3928.

56. Staffan T, Hashimoto K, Malkinson J, Lazorova L, Toth I, Artursson P. A new principal for tight junction modulation based on occludin peptides. Molecular Pharmacology. 2003; 64(6):1530-1540.

57. Yamamoto A, Setoh K, Murakami M, Shironoshita M, Kobayashi T, Fujimoto K, et al. Enhanced transdermal delivery of phenylalanyl-glycine by

chemical modification with various fatty acids. International Journal of Pharmaceutics. 2003; 250(1):119-128.

58. Fujita T, Fujita T, Morikawa K, Tanaka H, Iemura O, Yamamoto A, et al. Improvement of intestinal absorption of human calcitonin by chemical modification with fatty acids: Synergistic effects of acylation and absorption enhancers. International Journal of Pharmaceutics. 1996; 134(1-2):47-57.

59. Linter K, Peschard O. Biologically active peptides: From a laboratory bench curiosity to a functional skin care product International Journal of Cosmetic Science. 2000; 22:207-218.

60. Frankel AD, Pabo CO. Cellular uptake of the tat protein from human immunodeficiency virus. Cell. 1988; 55(6):1189-1193.

61. Green M, Loewenstein PM. Autonomous functional domains of chemically synthesized human immunodeficiency virus tat trans-activator protein. Cell. 1988; 55(6):1179-1188.

62. André Z. Thermodynamic studies and binding mechanisms of cell-penetrating peptides with lipids and glycosaminoglycans. Advanced Drug Delivery Reviews. 2008; 60(4–5):580-597.

63. Zorko M, Langel Ü. Cell-penetrating peptides: mechanism and kinetics of cargo delivery. Advanced Drug Delivery Reviews. 2005; 57(4):529-545.

64. Dietz GPH, Bδhr M. Delivery of bioactive molecules into the cell: The trojan horse approach. Molecular and Cellular Neuroscience. 2004; 27(2):85-131.

65. Madani F, Lindberg S, Langel, Futaki S, Slund A. Mechanisms of cellular uptake of cell-penetrating peptides. Journal of Biophysics. 2011.

66. Hansen M, Kilk K, Langel Ü. Predicting cell-penetrating peptides. Advanced Drug Delivery Reviews. 2008; 60(4–5):572-579.

67. Sandberg M, Eriksson L, Jonsson J, Sjöström M, Wold S. New chemical descriptors relevant for the design of biologically active peptides. A multivariate characterization of 87 amino acids. Journal of Medicinal Chemistry. 1998; 41(14):2481-2491.

68. Lundberg P, Langel Ü. A brief introduction to cell-penetrating peptides. Journal of Molecular Recognition. 2003; 16(5):227-233.

69. Alain P. Protein and peptide transduction, twenty years later a happy birthday. Advanced Drug Delivery Reviews. 2008; 60(4–5):448-451.

70. Arwyn T J. Gateways and tools for drug delivery: Endocytic pathways and the cellular dynamics of cell penetrating peptides. International Journal of Pharmaceutics. 2008; 354(1–2):34-38.

71. Tyagi M, Rusnati M, Presta M, Giacca M. Internalization of HIV-1 tat requires cell surface heparan sulfate proteoglycans. Journal of Biological Chemistry. 2001; 276(5):3254-3261.

72. Wender PA. The design, synthesis, and evaluation of molecules that enable or enhance cellular uptake: Peptoid molecular transporters. Proceedings of the National Academy of Sciences of the United States of America. 2000; 97(24):13003-13008.

73. Magzoub M, Gräslund A. Cell-penetrating peptides: small from inception to application. Quarterly Reviews of Biophysics. 2004; 37(02):147-195.

74. Järver P, Langel Ü. Cell-penetrating peptides—A brief introduction. Biochimica et Biophysica Acta (BBA) - Biomembranes. 2006; 1758(3):260-263.

75. Pooga M. Cell penetration by transportan. The FASEB Journal. 1998; 12(1):67-77.

76. Vladimir P T. Multifunctional nanocarriers. Advanced Drug Delivery Reviews. 2006; 58(14):1532-1555.

77. Bárány-Wallje E, Keller S, Serowy S, Geibel S, Pohl P, Bienert M, et al. A critical reassessment of renetratin translocation across lipid membranes. Biophysical journal. 2005; 89(4):2513-2521.

78. Saar K, Lindgren M, Hansen M, Eiríksdóttir E, Jiang Y, Rosenthal-Aizman K, et al. Cell-penetrating peptides: A comparative membrane toxicity study. Analytical Biochemistry. 2005; 345(1):55-65.

79. Vivès E, Brodin P, Lebleu B. A truncated HIV-1 tat protein basic domain rapidly translocates through the plasma membrane and accumulates in the cell nucleus. Journal of Biological Chemistry. 1997; 272(25):16010-16017.

80. Vivès E, Schmidt J, Pèlegrin A. Cell-penetrating and cell-targeting peptides in drug delivery. Biochimica et Biophysica Acta (BBA) - Reviews on Cancer. 2008; 1786(2):126-138.

81. Cardozo AK, Buchillier V, Mathieu M, Chen J, Ortis F, Ladrière L, et al. Cell-permeable peptides induce dose- and length-dependent cytotoxic effects. Biochimica et Biophysica Acta (BBA) - Biomembranes. 2007; 1768(9):2222-2234.

82. Tréhin R, Merkle HP. Chances and pitfalls of cell penetrating peptides for cellular drug delivery. European Journal of Pharmaceutics and Biopharmaceutics. 2004; 58(2):209-223.

83. Brooks NA, Pouniotis DS, Tang C-K, Apostolopoulos V, Pietersz GA. Cell-penetrating peptides: Application in vaccine delivery. Biochimica et Biophysica Acta (BBA) - Reviews on Cancer. 2010; 1805(1):25-34.

84. Räägel H, Pooga M. Chapter 10 - Peptide and Protein Delivery with Cell-penetrating Peptides. In: Chris Van Der W, editor. Peptide and Protein Delivery. Boston: Academic Press; 2011. p. 221-246.

85. Sugahara KN, Teesalu T, Karmali PP, Kotamraju VR, Agemy L, Greenwald DR, et al. Coadministration of a tumor-penetrating peptide enhances the efficacy of cancer drugs. Science. 2010; 328(5981):1031-1035.

86. Chugh A, Eudes F, Shim Y-S. Cell-penetrating peptides: Nanocarrier for macromolecule delivery in living cells. IUBMB Life. 2010; 62(3):183-193.

87. Järver P, Mäger I, Langel Ü. In vivo biodistribution and efficacy of peptide mediated delivery. Trends in Pharmacological Sciences. 2010; 31(11):528-535.

88. Laakkonen P, Åkerman ME, Biliran H, Yang M, Ferrer F, Karpanen T, et al. Antitumor activity of a homing peptide that targets tumor lymphatics and tumor cells. Proceedings of the National Academy of Sciences of the United States of America. 2004; 101(25):9381-9386.

89. Gius DR, Ezhevsky SA, Becker-Hapak M, Nagahara H, Wei MC, Dowdy SF. Transduced p16INK4a peptides Inhibit hypophosphorylation of the retinoblastoma protein and cell cycle progression prior to activation of Cdk2 complexes in late G1. Cancer Research. 1999; 59(11):2577-2580.

90. Ward B, Seal BL, Brophy CM, Panitch A. Design of a bioactive cell-penetrating peptide: when a transduction domain does more than transduce. Journal of Peptide Science. 2009; 15(10):668-674.

91. Temsamani J, Vidal P. The use of cell-penetrating peptides for drug delivery. Drug Discovery Today. 2004; 9(23):1012-1019.

92. Margus H, Padari K, Pooga M. Cell-penetrating peptides as versatile vehicles for oligonucleotide delivery. Molecular Therapy. 2012.

93. Mäe M, Langel Ü. Cell-penetrating peptides as vectors for peptide, protein and oligonucleotide delivery. Current Opinion in Pharmacology. 2006; 6(5):509-514.

94. Räägel H, Säälik P, Pooga M. Peptide-mediated protein delivery—Which pathways are penetrable? Biochimica et Biophysica Acta (BBA) - Biomembranes. 2010; 1798(12):2240-2248.

95. Mark A L. Peptide-mediated cell delivery: application in protein target validation. Current Opinion in Pharmacology. 2002; 2(5):587-594.

96. Myou S, Zhu X, Myo S, Boetticher E, Meliton AY, Liu J, et al. Blockade of airway inflammation and hyperresponsiveness by HIV-TAT-dominant negative Ras. The Journal of Immunology. 2003; 171(8):4379-4384.

97. Fujimoto K, Hosotani R, Miyamoto Y, Doi R, Koshiba T, Otaka A, et al. Inhibition of pRb phosphorylation and cell cycle progression by an antennapedia-p16INK4A fusion peptide in pancreatic cancer cells. Cancer letters. 2000; 159(2):151-158.

98. Snyder EL, Meade BR, Saenz CC, Dowdy SF. Treatment of terminal peritoneal carcinomatosis by a transducible p53-activating peptide. PLoS Biology. 2004; 2(2):e36.

99. Teixidó M, Zurita E, Malakoutikhah M, Tarragó T, Giralt E. Diketopiperazines as a sool for the study of transport across the Blood−Brain Barrier (BBB) and their potential yse as BBB-shuttles. Journal of the American Chemical Society. 2007 [cited 2012/01/14]; 129(38):11802-11813.

100. William M P. Blood–brain barrier delivery. Drug Discovery Today. 2007; 12(1–2):54-61.

101. Kumar P, Wu H, McBride JL, Jung K-E, Hee Kim M, Davidson BL, et al. Transvascular delivery of small interfering RNA to the central nervous system. Nature [10.1038/nature05901]. 2007; 448(7149):39-43.

102. Rousselle C, Clair P, Lefauconnier J-M, Kaczorek M, Scherrmann J-M, Temsamani J. New advances in the transport of doxorubicin through the Blood-Brain Barrier by a peptide vector-mediated strategy. Molecular Pharmacology. 2000; 57(4):679-686.

103. Fischer PM. Diketopiperazines in peptide and combinatorial chemistry. Journal of Peptide Science. 2003; 9(1):9-35.

104. Bolognesi ML, Ai Tran HN, Staderini M, Monaco A, López-Cobeñas A, Bongarzone S, et al. Discovery of a class of diketopiperazines as antiprion compounds. ChemMedChem. 2010; 5(8):1324-1334.

105. Martins MB, Carvalho I. Diketopiperazines: biological activity and synthesis. Tetrahedron. 2007; 63(40):9923-9932.

106. Malakoutikhah M, Teixidó M, Giralt E. Toward an optimal Blood−Brain Barrier shuttle by synthesis and evaluation of peptide libraries. Journal of Medicinal Chemistry. 2008 [cited 2012/01/14]; 51(16):4881-4889.

107. Rothbard JB, Garlington S, Lin Q, Kirschberg T, Kreider E, McGrane PL, et al. Conjugation of arginine oligomers to cyclosporin A facilitates topical delivery and inhibition of inflammation. Nature Medicine. 2000; 6(11):1253-1257.

108. Hou Y-W, Chan M-H, Hsu H-R, Liu BR, Chen C-P, Chen H-H, et al. Transdermal delivery of proteins mediated by non-covalently associated arginine-rich intracellular delivery peptides. Experimental Dermatology. 2007; 16(12):999-1006.

109. Jin LH, Bahn JH, Eum WS, Kwon HY, Jang SH, Han KH, et al. Transduction of human catalase mediated by an HIV-1 TAT protein basic domain and arginine-rich peptides into mammalian cells. Free Radical Biology and Medicine. 2001; 31(11):1509-1519.

110. Wender PA, Rothbard JB, Jessop TC, Kreider EL, Wylie BL. Oligocarbamate molecular transporters: design, synthesis and biological evaluation of a new class of

transporters for drug delivery. Journal of the American Chemical Society. 2002 [cited 2012/01/19]; 124(45):13382-13383.

111. Lim JM, Chang MY, Park SG, Kang NG, Song YS, Lee YH, et al. Penetration enhancement in mouse skin and lipolysis in adipocytes by TAT-GKH, a new cosmetic ingredient. Journal of Cosmetic Sciences. 2003; 54(5):483-91.

112. Hsu T, Mitragotri S. Delivery of siRNA and other macromolecules into skin and cells using a peptide enhancer. Proceedings of the National Academy of Sciences. 2011.

113. Lee JN. The effects of depilatory agents as penetration enhancers on human stratum corneum structures. Journal of investigative dermatology. 2008; 128(9):2240-2247.

114. Tsai TH. Multiphoton microscopy in dermatological imaging. Journal of Dermatological Science. 2009; 56(1):1-8.

115. Kumar R, Philip A. Modified transdermal technologies: Breaking the barriers of drug permeation via the skin. Tropical Journal of Pharmaceutical Research. 2007; 6(1):633-644.

116. Magnusson BM, Runn P. Effect of penetration enhancers on the permeation of the thyrotropin releasing hormone analogue pGlu-3-methyl-His- Pro amide through human epidermis. International Journal of Pharmaceutics. 1999; 178(2):149-159.

117. Kanikkannan N, Kandimalla K, Lamba S, Singh M. Structure-activity relationship of chemical penetration enhancers in transdermal drug delivery. Current Medicinal Chemistry. 2000; 6:593-608.

118. Wang Y, Thakur R, Fan Q, Michniak B. Transdermal iontophoresis: combination strategies to improve transdermal iontophoretic drug delivery. European Journal of Pharmaceutics and Biopharmaceutics. 2005; 60(2):179-191.

119. Michael J P. The role of electroosmotic flow in transdermal iontophoresis. Advanced Drug Delivery Reviews. 2001; 46(1-3):281-305.

120. Schuetz YB, Naik A, Guy RH, Kalia YN. Emerging strategies for the transdermal delivery of peptide and protein drugs. Expert Opinion on Drug Delivery. 2005; 2(3):533-548.

121. Naik A, Kalia YN, Guy RH. Transdermal drug delivery: overcoming the skin's barrier function. Pharmaceutical Science & Technology Today. 2000; 3(9):318-326.

122. Hirvonen J, Kalia YN, Guy RH. Transdermal delivery of peptides by iontophoresis. Nature Biotechnology. 1996; 14(13):1710-1713.

123. Schuetz YB, Naik A, Guy RH, Kalia YN. Effect of amino acid sequence on transdermal iontophoretic peptide delivery. European Journal of Pharmaceutical Sciences. 2005; 26(5):429–437.

124. Kochhar C, Imanidis G. In vitro transdermal iontophoretic delivery of leuprolide under constant current application. Journal of Controlled Release. 2004; 98(1):25-35.

125. Robert Meyer B, Kreis W, Eschbach J, Omara V, Rosen S, Sibalis D. Transdermal versus subcutaneous leuprolide: A comparison of acute pharmacodynamic effect. Clinical Pharmacology and Therapeutics. 1990; 48(4):340-345.

126. Green PG. Iontophoretic delivery of peptide drugs. Journal of Controlled Release. 1996; 41:33-48.

127. Banga AK, Chien YW. Hydrogel-based iontotherapeutic delivery devices for transdermal delivery of peptide/protein drugs. Pharmaceutical Research. 1993; 10(5):697-702.

128. Pillai O, Kumar N, Dey CS, Borkute S, Nagalingam S, RPanchagnula. Transdermal iontophoresis of insulin. Part 1: A study on the issues associated with the use of platinum electrodes on rat skin. Journal of Pharmacy and Pharmacology. 2003; 55(11):1505-13.

129. Tokumoto S, Higo N, Sugibayashi K. Effect of electroporation and pH on the iontophoretic transdermal delivery of human insulin. International Journal of Pharmaceutics. 2006; 326(1-2):13-19.

130. Bhatia KS, Singh J. Effect of linolenic acid/ethanol or limonene/ethanol and iontophoresis on the in vitro percutaneous absorption of LHRH and ultrastructure of human epidermis. International Journal of Pharmaceutics. 1999; 180(2):235-250.

131. Boinpally RR, Zhou SL, Devraj G, Anne PK, Poondru S, Jasti BR. Iontophoresis of lecithin vesicles of cyclosporin A. International Journal of Pharmaceutics. 2004; 274(1-2):185-190.

132. Williams A, editor. Physical and Technological Modulation of Topical and Transdermal Drug Delivery. London: Pharmaceutical Press; 2003.

133. Vanbever R, De Morre N, Préat V. Transdermal delivery of fentanyl by electroporation II. Mechanisms involved in drug transport. Pharmaceutical Research. 1996; 13(9):1360-1366.

134. Prausnitz MR, Bose VG, Langer R, Weaver JC. Electroporation of mammalian skin: A mechanism to enhance transdermal drug delivery. Proceedings of the Natural Academy of Sciences of the United States of America. 1993; 70(22):10504–10508.

135. Edwards DA, Prausnitz MR, Langer R, Weaver JC. Analysis of enhanced transdermal transport by skin electroporation. Journal of Controlled Release. 1995; 34(3):211-221.

136. Prausnitz MR, Edelman ER, Gimm JA, Langer R, Weaver JC. Transdermal delivery of heparin by skin electroporation. Biotechnology (NY). 1995; 13:1205-1209.

137. Regnier V, Doan TL, Préat V. Parameters controlling topical delivery of oligonucleotides by electroporation. Journal of Drug Targeting. 1998; 5(4):275-289.

138. Vanbever R, Boulange´ EL, Pre´at V. Transdermal delivery of fentanyl by electroporation I. Influence of electrical factors. Pharmaceutical Research. 1996; 13:559-565.

139. Gaudy C, Richard MA, Folchetti G, Bonerandi JJ, Grob JJ. Randomized controlled study of electrochemotherapy in the local treatment of skin metastases of melanoma. Journal of Cutaneous Medicine and Surgery. 2006; 10:115-121.

140. Lombry C, Dujardin N, Préat V. Transdermal delivery of macromolecules using skin electroporation. Pharmaceutical Research. 2000; 17(1):32-37.

141. Wang S, Kara M, Krishnan TR. Transdermal delivery of cyclosporin-A using electroporation. Journal of Controlled Release. 1998; 50(1-3):61-70.

142. Sen A, Daly ME, Hui SW. Transdermal insulin delivery using lipid enhanced electroporation. Biochimica et Biophysica Acta (BBA) - Biomembranes. 2002; 1564(1):5-8.

143. Medi BM, Singh J. Electronically facilitated transdermal delivery of human parathyroid hormone (1–34). International Journal of Pharmaceutics. 2003; 263(1-2):25-33.

144. Vanbever R, Preat V. In vivo efficacy and safety of skin electroporation. Advanced Drug Delivery Reviews. 1999; 35:77 - 88.

145. Philpott WH, Kalita DK, Goldberg B. Innerself [In: A Brief History of Magnet Therapy. 2000. Tiburon, CA, USA.:

146. Mooney V. A randomized double-blind prospective study of the efficacy of pulsed electromagnetic fields for interbody lumbar fusions. Spine. 1990; 15(7):708-12.

147. Simko M, Mattsson MO. Extremely low frequency electromagnetic fields as effectors of cellular responses in vitro: possible immune cell activation. J Cell Biochem. 2004; 93(1):83-92.

148. Santini JT, Cima MJ, Langer R. A controlled-release microchip. Nature. 1999; 397(28):335-338.

149. Nishijima S, Mishima F, Terada T, Takeda S. A study on magnetically targeted drug delivery system using superconducting magnet. Physica C: Superconductivity. 2007; 463–465(1):1311-1314.

150. Grief AD, Richardson G. Mathematical modelling of magnetically targeted drug delivery. Journal of Magnetism and Magnetic Materials. 2005; 293(1):455-463.

151. Huang W-C, Hu S-H, Liu K-H, Chen S-Y, Liu D-M. A flexible drug delivery chip for the magnetically-controlled release of anti-epileptic drugs. Journal of Controlled Release. 2009; 139(3):221-228.

152. In: Diamagnetism. Wikipedia.

153. Namjoshi S, Chen Y, Edwards J, Benson HAE. Enhanced transdermal delivery of a dipeptide by dermaportation. Biopolymers Peptide Science. 2008; 90(5):655-662.

154. Murthy SN, Sammeta SM, Bowers C. Magnetophoresis for enhancing transdermal drug delivery: Mechanistic studies and patch design. Journal of Controlled Release. 2010; 148(2):197-203.

155. Sammeta SM, Repka MA, Narasimha Murthy S. Magnetophoresis in combination with chemical enhancers for transdermal drug delivery. Drug Development and Industrial Pharmacy. 2011; 37(9):1076-1082.

156. Krishnan G. Enhanced skin permeation of naltrexone by pulsed electromagnetic fields in human skin in vitro. Journal of Pharmaceutical Sciences. 2010; 99(6):2724-2731.

157. Namjoshi S, Caccetta R, Edwards J, Benson HAE. Liquid chromatography assay for 5-aminolevulinic acid: Application to in vitro assessment of skin penetration via Dermaportation. Journal of Chromatography B. 2007; 852(1-2):49-55.

158. Benson HAE, Caccetta R, Eijkenboom M. 8th World Congress on Inflammation [2007]. Copenhagen, Denmark:

159. Benson HAE, Caccetta R, Namjoshi S, Edwards J, Eijkenboom M. World Congress on Pain [2005]. Sydney:

160. Mitragotri S, Blankschtein D, Langer R. Ultrasound-mediated transdermal protein delivery. Science. 1995; 269(5225):850-853.

161. Pitt WG, Husseini GA, Staples BJ. Ultrasonic drug delivery—A general review. Expert Opinion on drug Delivery. 2004; 1(1):37-56.

162. Mitragotri S. A mechanistic study of ultrasonically-enhanced transdermal drug delivery. Journal of Pharmaceutical Sciences. 1995; 84(6):697-706.

163. Cross SE, Roberts MS. Physical enhancement of transdermal drug application: is delivery technology keeping up with pharmaceutical development? Current drug delivery. 2004; 1(1):81-92.

164. Gaertner W. Frequency dependence of ultrasonic cavitation. The Journal of the Acoustical Society of America. 1954; 26(6):977-980.

165. Alvarez-Roman R, Merino G, Kalia YN, Naik A, Guy RH. Skin permeability enhancement by low frequency sonophoresis: Lipid extraction and transport pathways. Journal of Pharmaceutical Sciences. 2003; 92(6):1138-46.

166. Tezel A, Sens A, Mitragotri S. Description of transdermal transport of hydrophilic solutes during low-frequency sonophoresis based on a modified porous pathway model. Journal of Pharmaceutical Sciences. 2003; 92(2):381-393.

167. Liu H, Li S, Pan W, Wang Y, Han F, Yao H. Investigation into the potential of low-frequency ultrasound facilitated topical delivery of Cyclosporin A. International Journal of Pharmaceutics. 2006; 326(1-2):32-38.

168. Le L, Kost J, Mitragotri S. Combined effect of low-frequency ultrasound and iontophoresis: applications for transdermal heparin delivery. Pharmaceutical Research. 2000; 17(9):1151-1154.

169. Brown MB, Traynor MJ, Martin GP, Akomeah FK. Transdermal Drug Delivery Systems: Skin Perturbation Devices Totowa, NJ: Humana Press; 2008.

170. Schramm J, Mitragotri S. Transdermal drug delivery by jet injectors: energetics of jet formation and penetration. Pharmaceutical Research. 2002; 19(11):1673-1679.

171. Sarno MJ. Clinical immunogenicity of measles, mumps and rubella vaccine delivered by the Injex jet injector: comparison with standard syringe injection. The Pediatric Infectious Disease Journal. 2000; 19(9):839-42.

172. Jackson L. Safety and immunogenicity of varying dosages of trivalent inactivated influenza vaccine administered by needle-free jet injectors. Vaccine. 2001; 19(32):4703-4709.

173. Resman E. The application of insulin using the jet injector DG-77. Acta Diabetologica Latina. 1985; 22(2):119-125.

174. Dean H. Powder and particle-mediated approaches for delivery of DNA and protein vaccines into the epidermis. Comparative Immunology, Microbiology and Infectious Diseases. 2003; 26(5-6):373-388.

175. Kendall M. Engineering of needle-free physical methods to target epidermal cells for DNA vaccination. Vaccine. 2006; 24(21):4651-4656.

176. Doukas A. Physical characteristics and biological effects of laser-induced stress waves. Ultrasound in Medicine & Biology. 1996; 22(2):151-164.

177. Haar T. Biological effects of ultrasound in clinical applications. New York: VCH Publishers; 1988.

178. Doukas AG, McAuliffe DJ, Lee S, Venugopalan V, Flotte TJ. Physical factors involved in stress-wave-induced cell injury: the effect of stress gradient. Ultrasound in Medicine & Biology. 1995; 21(7):961-967.

179. Lee S, Anderson T, Zhang H, Flotte TJ, Doukas AG. Alteration of cell membrane by stress waves in vitro. Ultrasound in Medicine & Biology. 1996; 22(9):1285-1293.

180. Lee S, Kollias N, McAuliffe DJ, Flotte TJ, Doukas AG. Topical drug delivery in humans with a single photomechanical wave. Pharmaceutical Research. 1999; 16(11):1717-1721.

181. Lee S, McAuliffe DJ, Flotte TJ, Kollias N, Doukas AG. Photomechanical transcutaneous Delivery of macromolecules. Journal of Investigative Dermatology. 1998; 111(6):925-929.

182. Lee S, McAuliffe DJ, Mulholland SE, Doukas AG. Photomechanical transdermal delivery of insulin in vivo. Lasers in Surgery and Medicine. 2001; 28(3):282-285.

183. Doukas AG, Kollias N. Transdermal drug delivery with a pressure wave. Advanced Drug Delivery Reviews. 2004; 56(5):559-579.

184. Gerstel MS, Place VA, inventors; Drug delivery device. United States of America. U.S. Patent 3,964,482. June 22, 1976.

185. Prausnitz M. Current status and future potential of transdermal drug delivery. Nature reviews. Drug discovery. 2004; 3(2):115-24.

186. Henry S, McAllister DV, Allen MG, Prausnitz MR. Microfabricated Microneedles : A novel approach to transdermal drug delivery. Journal of Pharmaceutical Sciences. 1998; 87(8):922 - 925.

187. Prausnitz MR. Microneedles for transdermal drug delivery. Advanced Drug Delivery Reviews. 2004; 56(5):581 - 587.

188. Chen X. Dry-coated microprojection array patches for targeted delivery of immunotherapeutics to the skin. Journal of Controlled Release. 2009; 139(3):212-220.

189. Champion RH, Burton JL, Burns T, Breathnach SM, Burns DA. Textbook of Dermatology. John Wiley & Sons, Limited; 1998.

190. Martanto W, Moore JS, Couse T, Prausnitz MR. Mechanism of fluid infusion during microneedle insertion and retraction. Journal of Controlled Release. 2006; 112(3):357-361.

191. Bal SM, Kruithof AC, Zwier R, Dietz E, Bouwstra JA, Lademann J, et al. Influence of microneedle shape on the transport of a fluorescent dye into human skin in vivo. Journal of Controlled Release. 2010; 147(2):218-224.

192. Bal S, Kruithof AC, Liebl H, Tomerius M, Bouwstra J, Lademann J, et al. In vivo visualization of microneedle conduits in human skin using laser scanning microscopy. Laser Physics Letters. 2010; 7(3):242-246.

193. Banks SL, Pinninti RR, Gill HS, Paudel KS, Crooks PA, Brogden NK, et al. Transdermal delivery of naltrexol and skin permeability lifetime after microneedle treatment in hairless guinea pigs. Journal of Pharmaceutical Sciences. 2010; 99(7):3072-3080.

194. Banks S, Paudel K, Brogden N, Loftin C, Stinchcomb A. Diclofenac enables prolonged delivery of naltrexone through microneedle-treated skin. Pharmaceutical Research. 2011; 28(5):1211-1219.

195. Hashmi S. Genetic transformation of nematodes using arrays of micromechanical piercing structures. BioTechniques. 1995; 19(5):766-770.

196. Lin W. Transdermal delivery of antisense oligonucleotides with microprojection patch (Macroflux®) technology. Pharmaceutical Research. 2001; 18(12):1789-1793.

197. Donnelly RF, Morrow DIJ, McCarron PA, Woolfson AD, Morrissey A, Juzenas P, et al. Microneedle-mediated intradermal delivery of 5-aminolevulinic acid: Potential for enhanced topical photodynamic therapy. Journal of Controlled Release. 2008; 129(3):154-162.

198. Park J-H, Allen MG, Prausnitz MR. Biodegradable polymer microneedles: Fabrication, mechanics and transdermal drug delivery. Journal of Controlled Release. 2005; 104(1):51-66.

199. Lee JW, Park J-H, Prausnitz MR. Dissolving microneedles for transdermal drug delivery. Biomaterials. 2008; 29(13):2113-2124.

200. Raphael AP, Prow TW, Crichton ML, Chen X, Fernando GJP, Kendall MAF. Targeted, needle-free vaccinations in skin using multilayered, densely-packed dissolving microprojection arrays. Small. 2010; 6(16):1785-1793.

201. Chen X, Corbett HJ, Yukiko SR, Raphael AP, Fairmaid EJ, Prow TW, et al. Site-selectively coated, densely-packed microprojection array patches for targeted delivery of vaccines to skin. Advanced Functional Materials. 2011; 21(3):464-473.

202. Chen X, Fernando GJP, Raphael AP, Yukiko SR, Fairmaid EJ, Primiero CA, et al. Rapid kinetics to peak serum antibodies is achieved following influenza vaccination by dry-coated densely packed microprojections to skin. Journal of Controlled Release. 2011; 158(1):78-84.

203. Lee K, Lee CY, Jung H. Dissolving microneedles for transdermal drug administration prepared by stepwise controlled drawing of maltose. Biomaterials. 2011; 32(11):3134-3140.

204. Kommareddy S, Baudner BC, Oh S, Kwon S-y, Singh M, O'Hagan DT. Dissolvable microneedle patches for the delivery of cell-culture-derived influenza vaccine antigens. Journal of Pharmaceutical Sciences. 2012; 101(3):1021-1027.

205. Michel C, Peter D. Macroflux Technology for Transdermal Delivery of Therapeutic Proteins and Vaccines. In: Modified-Release Drug Delivery Technology: Informa Healthcare; 2002. p. 589-598.

206. Chen X Novel coating of micro-nanoprojection patches for targeted vaccine delivery to skin. International Conference on Nanoscience and Nanotechnology; 2008 p. 105-108.

207. Cormier M, Johnson B, Ameri M, Nyam K, Libiran L, Zhang DD, et al. Transdermal delivery of desmopressin using a coated microneedle array patch system. Journal of Controlled Release. 2004; 97(3):503-511.

208. Gomaa YA. Effects of microneedle length, density, insertion time and multiple applications on human skin barrier function: Assessments by transepidermal water loss. Toxicology In Vitro. 2010; 24(7):1971-1978.

209. Al Qallaf B. Modelling transdermal delivery of high molecular weight drugs from microneedle systems. Philosophical transactions - Royal Society. Mathematical, Physical and engineering sciences. 2007; 365(1861):2951-2967.

210. Al-Qallaf B, Moriy D, Olatunjiz L, Das DB, Cuiyy Z. Transdermal drug delivery by microneedles: Does skin metabolism matter? International Journal of Chemical Reactor Engineering. 2009; 7:1-23.

211. Mitragotri S, Anissimov YG, Bunge AL, Frasch HF, Guy RH, Hadgraft J, et al. Mathematical models of skin permeability: An overview. International Journal of Pharmaceutics. 2011; 418(1):115-129.

212. Nelson JS, McCullough JL, Glenn TC, Wright WH, Liaw LH, Jacques SL. Mid-infrared laser ablation of stratum corneum enhances in vitro percutaneous transport of drugs. Journal of Investigative Dermatology. 1991; 97(5):874-879.

213. Furness G. Global overview of the active transdermal drug delivery market Drug Development and Delivery. 2003; 4(3).

214. Birchall J. Cutaneous gene expression of plasmid DNA in excised human skin following delivery via microchannels created by radio frequency ablation. International Journal of Pharmaceutics. 2006; 312(1-2):15-23.

215. Sintov A. Radiofrequency-driven skin microchanneling as a new way for electrically assisted transdermal delivery of hydrophilic drugs. Journal of Controlled Release. 2003; 89(2):311-320.

216. Levin G. Transdermal delivery of human growth hormone through RF-microchannels. Pharmaceutical Research. 2005; 22(4):550-5.

217. Levin G. Advances in radio-frequency transdermal drug delivery.(Transdermal Delivery). Pharmaceutical Technology. 2008; 32(4):s12.

218. Lee W-R. Erbium:YAG laser enhances transdermal peptide delivery and skin vaccination. Journal of Controlled Release. 2008; 128(3):200-208.

219. Lee W-R. Skin pretreatment with an Er:YAG laser promotes the transdermal delivery of three narcotic analgesics. Lasers in Medical Science. 2007; 22(4):271.

220. Fang J-Y. Transdermal delivery of macromolecules by erbium:YAG laser. Journal of Controlled Release. 2004; 100(1):75-85.

221. Noel H, James D. Minimally Invasive Systems for Transdermal Drug Delivery. In: Transdermal Drug Delivery Systems: Informa Healthcare; 2002.

222. Westerling D. Transdermal administration of morphine to healthy subjects. British Journal of Clinical Pharmacology. 1994; 37(6):571-6.

223. Svedman PS, Svedman. Administration of antidiuretic peptide (DDAVP) by way of suction de-epithelialised skin. Lancet. 1991; 337(8756):1506-1509.

224. Eppstein J, inventor; Altea Therapeutics Corporation, assignee. Apparatus for microporation of biological membranes using thin film tissue interface devices. US. 2010.

225. Bramson J, Dayball K, Evelegh C, Wan YH, Page D, Smith A. Enabling topical immunization via microporation: a novel method for pain-free and needle-free delivery of adenovirus-based vaccines. Gene Therapy. 2003; 10(3):251-260.

226. Gebhart S. Glucose sensing in transdermal body fluid collected under continuous vacuum pressure via micropores in the stratum corneum. Diabetes Technology & Therapeutics. 2003; 5(2):159-66.

227. Badkar AV, Smith AM, Eppstein JA, Banga AK. Transdermal delivery of interferon alpha-2B using microporation and iontophoresis in hairless rats. Pharmaceutical Research. 2007; 24(7):1389–1395.

228. Heidl M. Peptides for prolonging youth. Advances in experimental medicine and biology. 2009; 611:263-264.

229. Zhang L, Falla TJ. Cosmeceuticals and peptides. Clinics in Dermatology [doi: 10.1016/j.clindermatol.2009.05.013]. 2009; 27(5):485-494.

230. Donald L B. Common cosmeceuticals. Clinics in Dermatology [doi: 10.1016/j.clindermatol.2009.05.006]. 2009; 27(5):435-445.

231. Choi CM, Berson DS. Cosmeceuticals. Seminars in Cutaneous Medicine and Surgery. 2006; 25:163-168.

232. Brandt FS, Cazzaniga A, Hann M. Cosmeceuticals: Current Trends and Market Analysis. Seminars in Cutaneous Medicine and Surgery [doi: 10.1016/j.sder.2011.05.006]. 2011; 30(3):141-143.

233. Lupo MP, Cole AL. Cosmeceutical peptides. Dermatologic Surgery. 2007; 20(5):343-349.

234. Robinson LR, Fitzgerald NC, Doughty DG. Topical palmitoyl pentapeptide provides improvement in photoaged human facial skin. International Journal of Cosmetic Science. 2005; 27:155–160.

235. Vleugels RA. Cosmeceuticals: From topical antioxidants to peptides. The Dermatology Report. 2008; 2(1).

236. Katyama K, Armendariz-Borunda J, Rachow R. A pentapeptide from Type I procollgen promotes extracellular matrix production. Journal of Biological Chemistry. 1993; 268:9941-9944.

237. Dipeptide - 2. [05/08/09]. Available from: http://www.truthinaging.com/ingredients/dipeptide-2/.

238. Bascom CC, inventor; The Procter and Gamble Company, assignee. Compositions for treating wrinkles comprising a peptide. United States patent 5492894. 1993 June 25.

239. Farra CD, Domloge N, Botto J-M, inventors; Novel sirtuin 6 activating peptides and cosmetic or pharmaceutical composition containing them. USA patent 20110318284. 2011.

240. Quinn PJ, Boldyrev AA, Formazuyk VE. Carnosine: Its properties, functions and potential therapeutic applications. Molecular aspects of Medicine. 1992; 13:379-444.

241. Kansci G, Genot C, Meynier A, Gandemer G. The antioxidant activity of carnosine and its consequences on the volatile profiles of liposomes during iron/ascorbate induced phospholipid oxidation. Food Chemistry. 1997; 60(2):165-175.

242. Hipkiss AR. Carnosine, a protective, anti-ageing peptide? The International Journal of Biochemistry and Cell Biology. 1998; 30:863-868.

243. Alan R H. On the enigma of carnosine's anti-ageing actions. Experimental Gerontology. 2009; 44(4):237-242.

244. Linter K, inventor; Sederma, assignee. Cosmetic or dermopharmaceutical use of peptides for healing, hydrating and improving skin appearance during natural or induced ageing (Heliodermia, Pollution). France. 2003.

245. Martin DC, inventor; L'Oreal Paris, assignee. Cosmetic compositions containing a lipid ceramide compund and a peptide having a fatty chain and their uses. France. 1998.

246. Niyonsaba F, Ogawa H. Protective roles of the skin against infection: Implication of naturally occurring human antimicrobial agents [beta]-defensins, cathelicidin LL-37 and lysozyme. Journal of Dermatological Science. 2005; 40:157-168.

247. Harder J, Schroder JM. Psoriatic scales: A promising source for the isolation of human skin derived antimicrobial proteins. Journal of Leukocyte Biology. 2005; 77:476–486.

248. Marks R. The stratum corneum barrier - the final frontier. Journal of Nutrition. 2004.

249. Katayama K, Armendariz-Borunda J, Raghow R, Kang AH, Seyer JM. A pentapeptide from type I procollagen promotes extracellular matrix production. Journal of Biological Chemistry. 1993; 268(14):9941-9944.

250. Schultz G. EGF and TGF-alpha in wound healing and repair. Journal of Cellular Biochemistry. 1991; 45(4):346-52.

251. Meyer-Ingold W. Wound therapy: Growth factors as agents to promote healing. Trends in Biotechnology. 1993; 11(9):387–392.

252. Braff MH. Structure-function relationships among human cathelicidin peptides: Dissociation of antimicrobial properties from host immunostimulatory activities. The Journal of Immunology. 2005; 174(7):4271-4278.

253. Lee PHA. HB-107, a nonbacteriostatic fragment of the antimicrobial peptide cecropin B, accelerates murine wound repair. Wound Repair and Regeneration. 2004; 12(3):351-358.

254. Carraway JH. Using Aldara, copper peptide, and niacinamide for skin care Aesthetic Surgery Journal. 2004; 24(1):83-84

255. Leung DYM, Boguniewicz M, Howell MD, Nomura I, Hamid Q. New insights into atopic dermatitis. Journal of Clinical Investigation. 2004; 113(5):651-657.

256. Madsen P, Rasmussen HH, Leffers H, Honore B, Dejgaard K, Olsen E, et al. Molecular cloning, occurrence, and expression of a novel partially secreted protein "psoriasin" that is highly up-regulated in psoriatic skin. Journal of Investigative Dermatology. 1991; 97(4):701-712.

257. Ruzicka T, Simmet T, Peskar B, Ring J. Skin levels of arachidonic acid—Derived inflammatory mediators and histamine in atopic dermatitis and psoriasis. Journal of Investigative Dermatology. 1986; 86(2):105–108.

258. Nonomura K, Yamanish K, Yasuno H. Upregulation of elafin/SKALP gene expression in psoriatic epidermis. Journal of Investigative Dermatology. 1994; 103(1):88–91.

259. Harder J, Schröder J-M. RNase 7, a novel innate immune defense antimicrobial protein of healthy human skin. Journal of Biological Chemistry. 2002; 277(48):46779-46784.

260. Taleisnik S. Regulation of Formation and Proposed Structure of the Factor Inhibiting the Release of Melanocyte-Stimulating Hormone. Proceedings of the National Academy of Sciences of the United States of America. 1971; 68(7):1428-1433.

261. Pignatiello. MIF-1 is active in a chronic stress animal model of depression. Pharmacology, Biochemistry and Behavior. 1989; 32(3):737-742.

262. Stratton L. Increased acquisition of a complex appetitive task after MSH and MIF. Pharmacology, Biochemistry and Behavior. 1975; 3(5):901-904.

263. Ishihara Y. Melanostatin, a new melanin synthesis inhibitor. Production, isolation, chemical properties, structure and biological activity. The Journal of Antibiotics. 1991; 44(1):25-32.

264. Skinner KK, inventor; Methods and compositions for improved uptake of biological molecules US. 2010.

265. Abdel Malek Z. Melanoma prevention strategy based on using tetrapeptide alpha-MSH analogs that protect human melanocytes from UV-induced DNA damage and cytotoxicity. The FASEB Journal. 2006; 20(9):1561-3.

266. Dhatt S. Rebuilding the dermal matrix with this new in-demand ingredient in skin care products. Aesthetic Trends and Technologies. 2006:17-20.

267. Kumar N, Kishore R. Determination of an unusual secondary structural element in the immunostimulating tetrapeptide rigin in aqueous environments: insights via MD simulations, 1H NMR and CD spectroscopic studies. Journal of Peptide Science. 2010; 16(9):456-464.

268. Veretennikova NI, Chipens GI, Nikiforovich GV, Betinsh YR. Rigin, another phagocytosis-stimulating tertrapeptide isolated from human IgG: confirmations of a hypothesis. International Journal of Peptide and Protein Research. 1981; 17(4):430-435.

269. Rocchi R, Biondi L, Cavaggion F, Filira F, Gobbo M, Dagan S, et al. Synthesis and biological activity of tuftsin and rigin derivatives containing monosaccharides or monosaccharide derivatives. International Journal of Peptide and Protein Research. 1987; 29(2):262-275.

270. Navolotskaya EV, Zargarova TA, Lepikhova TN, Turobov VI, Nurieva RI, Malkova NV, et al. Study of immunosuppressive activity of a synthetic decapeptide corresponding to an ACTH-Like sequence of human immunoglobulin G1. Biochemistry. 1999; 64(7):906-913.

271. In: Syn^{R}-Coll : Pentapharm Ltd Engelgasse : Basel

272. Prausnitz MR. A peptide chaperone for transdermal drug delivery. Nature Biotechnology. 2006; 24(4):416-417.

273. van der Maaden K, Jiskoot W, Bouwstra J. Microneedle technologies for (trans)dermal drug and vaccine delivery. Journal of Controlled Release. (0).

274. Morris MC, Deshayes S, Heitz F, Divita G. Cell-penetrating peptides: from molecular mechanisms to therapeutics. Biology of the Cell. 2008; 100(4):201-217.

275. Lopes LB. Comparative study of the skin penetration of protein transduction domains and a conjugated peptide. Pharmaceutical Research. 2005; 22(5):750-757.

276. Sebbage V. Cell-penetrating peptides and their therapeutic applications. Bioscience Horizons. 2009; 2(1):64-72.

277. Christophers E, Kligman AM. Visualisation of the cell layers of the stratum corneum. Journal of Investigative Dermatology. 1964; 42:407-409.

278. Xie WL, Chipman JG, Robertson DL, Erikson RL, Simmons DL. Expression of a mitogen-responsive gene encoding prostaglandin synthase is regulated by mRNA splicing. Proceedings of the National Academy of Sciences. 1991; 88(7):2692-2696.

279. Blobaum AL, Marnett LJ. Structural and functional basis of cyclooxygenase inhibition. Journal of Medicinal Chemistry. 2007; 50(7):1425-1441.

280. Nugteren DH, Hazelhof E. Isolation and properties of intermediates in prostaglandin biosynthesis. Biochimica et Biophysica Acta (BBA) - Lipids and Lipid Metabolism. 1973; 326(3):448-461.

281. Hamberg M, Samuelsson B. Detection and Isolation of an Endoperoxide Intermediate in Prostaglandin Biosynthesis. Proceedings of the National Academy of Sciences. 1973; 70(3):899-903.

282. Lu MF, Lee D, Carlson R, Rao GS, Hui HW, Adjei L, et al. The effects of formulation variables on iontophoretic transdermal delivery of leuprolide to humans. Drug Development and Industrial Pharmacy. 1993; 19(13):1557-1571.

283. Badkar AV, Banga AK. Electrically enhanced transdermal delivery of a macromolecule. Journal of Pharmacy and Pharmacology. 2002; 54(7):907-912.

284. Christensen JM, Chuong MC, Le H, Pham L, Bendas E. Hydrocortisone diffusion through synthetic membrane, mouse skin, and Epiderm™ cultured skin. Archives of Drug Information. 2011; 4(1):10-21.

285. Aguzzi C, Rossi S, Bagnasco M, Lanata L, Sandri G, Bona F, et al. Penetration and distribution of thiocolchicoside through human skin: comparison between a commercial foam and a drug solution. AAPS PharmSciTech. 2008; 9(4):1185-1190.

286. Mueller B, Anissimov YG, Roberts MS. Unexpected clobetasol propionate profile in human stratum corneum after topical application in vitro. Pharmaceutical Research. 2003; 20(11):1835-1837.

287. Dragicevic-Curic N, Scheglmann D, Albrecht V, Fahr A. Temoporfin-loaded invasomes: Development, characterization and in vitro skin penetration studies. Journal of Controlled Release. 2008; 127(1):59-69.

288. Lee VHL. Penetration and enzymatic barriers to peptide and protein absorption. Advanced Drug Delivery Reviews. 1989; 4(2):171-207.

289. Goolcharran C, Jones AJS, Borchardt RT. Comparison of the rates of deamidation, diketopiperazine formation, and oxidation in recombinant human vascular endothelial growth factor and model peptides. AAPS Pharmsci. 2000; 2(1):1-6.

290. Carpenter KA, Weltrowska G, Wilkes BC, Schmidt R, Schiller PW. Spontaneous Diketopiperazine formation via end-to-end cyclization of a nonactivated linear tripeptide: An unusual chemical reaction. Journal of the American Chemical Society. 1994; 116(19):8450-8458.

291. Kubo A, Takahashi K, Arai T. Diketopiperazines containing L-proline from Streptomyces lavendulae and their stereochemistry in solution. Cellular and Molecular Life Sciences. 1977; 33(1):12-13.

292. Teixidó M, Mohammed Y, Benson H, Giralt E. European Peptide Symposium [In: Across the skin barrier, a comparative transport study of a diketopiperazine-based shuttle. 2010. Copenhagen]

293. Jones SW, Christison R, Bundell K, Voyce CJ, Brockbank SMV, Newham P, et al. Characterisation of cell-penetrating peptide-mediated peptide delivery. British Journal of Pharmacology. 2005; 145(8):1093-1102.

294. Morris MC, Depollier J, Mery J, Heitz F, Divita G. A peptide carrier for the delivery of biologically active proteins into mammalian cells. Nature Biotechnology. 2001; 19(12):1173-1176.

295. Boisseau S, Mabrouk K, Ram N, Garmy N, Collin V, Tadmouri A, et al. Cell penetration properties of maurocalcine, a natural venom peptide active on the intracellular ryanodine receptor. Biochimica et Biophysica Acta (BBA) - Biomembranes. 2006; 1758(3):308-319.

296. Huang R, Zhou X, Xu T, Yang X, Liu Y. Diketopiperazines from marine organisms. Chemistry & Biodiversity. 2010; 7(12):2809-2829.

297. Watts KR, Ratnam J, Ang K-H, Tenney K, Compton JE, McKerrow J, et al. Assessing the trypanocidal potential of natural and semi-synthetic diketopiperazines from two deep water marine-derived fungi. Bioorganic & Medicinal Chemistry. 2010; 18(7):2566-2574.

298. Bos J. The 500 dalton rule for the skin penetration of chemical compounds and drugs. Experimental Dermatology. 2000; 9(3):165-169.

299. Altenbach M, Schnyder N, Zimmermann C, Imanidis G. Cutaneous metabolism of a dipeptide influences the iontophoretic flux of a concomitant uncharged permeant. International Journal of Pharmaceutics. 2006; 307(2):308-317.

300. Lin R-Y, Hsu C-W, Chen W-Y. A method to predict the transdermal permeability of amino acids and dipeptides through porcine skin. Journal of Controlled Release. 1996; 38(2-3):229-234.

301. Sakuma S, Suita M, Yamamoto T, Masaoka Y, Kataoka M, Yamashita S, et al. Performance of cell-penetrating peptide-linked polymers physically mixed with poorly membrane-permeable molecules on cell membranes. European Journal of Pharmaceutics and Biopharmaceutics. 2012; 81(1):64-73.

302. Nokhodchi A, Sharabiani K, Rashidi MR, Ghafourian T. The effect of terpene concentrations on the skin penetration of diclofenac sodium. International Journal of Pharmaceutics. 2007; 335(1–2):97-105.

303. Galer BS, Rowbotham M, Perander J, Devers A, Friedman E. Topical diclofenac patch relieves minor sports injury pain: results of a multicenter controlled clinical trial. Journal of Pain and Symptom Management. 2000; 19(4):287-294.

304. Rainsford KD, Kean WF, Ehrlich GE. Review of the pharmaceutical properties and clinical effects of the topical NSAID formulation, diclofenac epolamine. Current Medical Research and Opinion. 2008; 24(10):2967-2992.

305. Donnelly RF, Pascuet E, Ma C, Vaillancourt R. Stability of diclofenac sodium oral suspensions packaged in amber polyvinyl chloride bottles. The Canadian Journal of Hospital Pharmacy. 2010; 63(1).

306. Dehghanyar P, Mayer BX, Namiranian K, Mascher H, Mller M, Brunner M. Topical skin penetration of diclofenac after single- and multiple-dose application.

International Journal of Clinical Pharmacology and Therapeutics. 2004; 42(7):353-359.

307. Rojo-Vergara C, López-Alarcón C, Alvarez-Figueroa MJ. Transdermal penetration of diclofenac in the presence of AAPH-derived peroxyl radicals. Drug Development and Industrial Pharmacy. 2009; 35(8):976-980.

308. Magnette JL, Kienzler JL, Sallin D, Ménart C, Nollevaux F, Knops A. Diclofenac systemic exposure is not increased when topical diclofenac is applied to ultraviolet-induced erythema. European Journal of Clinical Pharmacology. 2004; 60(8):591-594.

309. Abdulmajed K, McGuigan C, Heard CM. Topical delivery of retinyl ascorbate co-drug. 5. In vitro degradation studies. Skin Pharmacology and Physiology. 2006; 19(5):248-258.

310. Cohen-Avrahami M, Libster D, Aserin A, Garti N. Sodium diclofenac and cell-penetrating peptides embedded in HII mesophases: Physical characterization and delivery. The Journal of Physical Chemistry B. 2011; 115(34):10189-10197.

311. Cohen-Avrahami M, Libster D, Aserin A, Garti N. Penetratin-induced transdermal delivery from HII mesophases of sodium diclofenac. Journal of Controlled Release. 2012; (0).

312. Lohcharoenkal W, Manosaroi A, Götz F, Werner RG, Manosroi W, Manosaroi J. Potent enhancement of GFP uptake into HT-29 cells and rat skin permeation by coincubation with tat peptide. Journal of Pharmaceutical Sciences. 2011; 100(11):4766-4773.

313. Drugs & Medications - diclofenac sodium oral. 2012 [updated 25th Feb]. Available from: http://www.webmd.com/drugs/mono-4049-DICLOFENAC+SODIUM+ENTERIC-COATED+TABLET+-+ORAL.aspx?drugid=4284&drugname=diclofenac+sodium+oral.

314. Panje WR. Regression of head and neck carcinoma with a prostaglandin-synthesis inhibitor. Archives of Otolaryngology. 1981; 107(11):658-663.

315. Braun DP, Taylor SG, Harris JE. Modulation of immunity in cancer patients by prostaglandin antagonists. Progress in Clinical and Biological Research. 1989; 288:439-48.

316. Brown MB, Jones SA. Hyaluronic acid: a unique topical vehicle for the localized delivery of drugs to the skin. Journal of the European Academy of Dermatology and Venereology. 2005; 19(3):308-318.

317. Garsha K. Quantitative Fluorescence Microscopy: Considerations and Controls Standardization and Quality Assurance in Fluorescence Measurements II. In: Resch-Genger U, editor.: Springer Berlin Heidelberg; 2008. p. 55-88.

318. Pirard GE. In vivo confocal microscopy: a new paradigm in dermatology. Dermatology. 1993; 186(1):4-5.

319. Branzan A, Landthaler M, Szeimies R-M. In vivo confocal scanning laser microscopy in dermatology. Lasers in Medical Science. 2007; 22(2):73-82.

320. Skvara H, Kittler H, Schmid JA, Plut U, Jonak C. In vivo fluorescence confocal microscopy: indocyanine green enhances the contrast of epidermal and dermal structures. Journal of Biomedical Optics. 2011; 16(9):096010.

321. Rajadhyaksha M, Gonzalez S, Zavislan JM, Anderson RR, Webb RH. In vivo confocal scanning laser microscopy of human skin II: Advances in instrumentation and comparison with histology. Journal of Investigative Dermatology. 1999; 113(3):293-303.

322. Jonak C, Skvara H, Kunstfeld R, Trautinger F, Schmid JA. Intradermal indocyanine green for In Vivo fluorescence laser scanning microscopy of human skin: A pilot study. PLoS ONE. 2011; 6(8):23972.

323. Rajadhyaksha M, Grossman M, Esterowitz D, Webb RH, Anderson RR. In vivo confocal scanning laser microscopy of human skin: Melanin provides strong contrast. Journal of Investigative Dermatology. 1995; 104(6):946-952.

324. Elkeeb R, Hui X, Chan H, Tian L, Maibach HI. Correlation of transepidermal water loss with skin barrier properties in vitro: comparison of three evaporimeters. Skin Research and Technology. 2010; 16(1):9-15.

325. Gill H, Denson D, Burris B, Prausnitz M. Effect of microneedle design on pain in human volunteers. The Clinical Journal of Pain. 2008; 24(7):585-594.

326. Sauermann K, Clemann S, Jaspers S, Gambichler T, Altmeyer P, Hoffmann K, et al. Age related changes of human skin investigated with histometric

measurements by confocal laser scanning microscopy in vivo. Skin Research and Technology. 2002; 8(1):52-56.

327. Wurm EMT, Soyer HP. The Confocal Story Reflectance Confocal Microscopy for Skin Diseases. In: Hofmann-Wellenhof R, Pellacani G, Malvehy J, Soyer HP, editors.: Springer Berlin Heidelberg; 2012. p. 3-5.

328. Mortensen LJ, Glazowski CE, Zavislan JM, DeLouise LA. Near-IR fluorescence and reflectance confocal microscopy for imaging of quantum dots in mammalian skin. Biomedical Optics Express. 2011; 2(6):1610-1625.

329. Yan G, Warner KS, Zhang J, Sharma S, Gale BK. Evaluation needle length and density of microneedle arrays in the pretreatment of skin for transdermal drug delivery. International Journal of Pharmaceutics. 2010; 391(1–2):7-12.

330. Carey JB, Pearson FE, Vrdoljak A, McGrath MG, Crean AM, Walsh PT, et al. Microneedle array design determines the induction of protective memory CD8 T Cell responses induced by a recombinant live malaria vaccine in mice. PLoS ONE. 2011; 6(7):22442.

331. Verbaan FJ, Bal SM, van den Berg DJ, Dijksman JA, van Hecke M, Verpoorten H, et al. Improved piercing of microneedle arrays in dermatomed human skin by an impact insertion method. Journal of Controlled Release. 2008; 128(1):80-88.

332. Cullander C, Guy RH. (D) Routes of delivery: Case studies: (6) Transdermal delivery of peptides and proteins. Advanced Drug Delivery Reviews. 1992; 8(2–3):291-329.

333. Priya B, Rashmi T, Bozena M. Transdermal iontophoresis. Expert Opinion on Drug Delivery. 2006; 3(1):127-138.

334. Langer R. New methods of drug delivery. Science. 1990; 249(4976):1527-1533.

335. Montes LF, Day JL, Wand CJ, Kennedy L. Ultrastructural changes in the horny layer following local application of dimethyl sulfoxide. The Journal of Investigative Dermatology. 1967; 48(2):184-196.

336. Benson HA, Prankerd RJ. Optimisation of drug delivery: transdermal drug delivery. Australian Journal of Hospital Pharmacy. 1997; 27:441 - 448.

337. Rezze G, Scramim A, Neves R, Landman G. Structural correlations between dermoscopic features of cutaneous melanomas and histopathology using transverse sections. The American Journal of Dermatopathology. 2006; 28(1):13-20.

338. Rajadhyaksha M, Menaker G, Flotte T, Dwyer PJ, Gonzalez S. Confocal examination of nonmelanoma cancers in thick skin excisions to potentially guide Mohs micrographic surgery without frozen histopathology. 2001; 117(5):1137-1143.

339. Meuwissen MEMJ, Janssen J, Cullander C, Junginger HE, Bouwstra JA. A cross-section device to improve visualization of fluorescent probe penetration into the skin by confocal laser scanning microscopy. Pharmaceutical Research. 1998; 15(2):352-356.

340. Zellmer S, Pfeil W, Lasch J. Interaction of phosphatidylcholine liposomes with the human stratum corneum. Biochimica et Biophysica Acta (BBA) - Biomembranes. 1995; 1237(2):176-182.

341. Hibbs AR, MacDonald G, Garsha K. Practical Confocal Microscopy

Handbook Of Biological Confocal Microscopy. In: Pawley JB, editor.: Springer US; 2006. p. 650-671.

342. Boi S, Fascio U. A method of quantitative measurement of fluorescence intensity by confocal laser scanning microscopy. Journal of Computer-Assisted Microscopy. 1998; 10(4):163-166.

343. Zucker RM, Price OT. Statistical evaluation of confocal microscopy images. Cytometry. 2001; 44(4):295-308.

344. Patzelt A, Richter H, Buettemeyer R, Huber HJR, Blume-Peytavi U, Sterry W, et al. Differential stripping demonstrates a significant reduction of the hair follicle reservoir in vitro compared to in vivo. European Journal of Pharmaceutics and Biopharmaceutics. 2008; 70(1):234-238.

345. Teichmann A. Differential stripping: Determination of the amount of topically applied substances penetrated into the hair follicles. Journal of Investigative Dermatology. 2005; 125(2):264-269.

346. Voegeli R, Heiland J, Doppler S, Rawlings AV, Schreier T. Efficient and simple quantification of stratum corneum proteins on tape strippings by infrared densitometry. Skin Research and Technology. 2007; 13(3):242-251.

347. Uchida T, Kanazawa T, Takashima Y, Okada H. Development of an efficient transdermal delivery system of small interfering RNA using functional peptides, Tat and AT-1002. Chemical & Pharmaceutical Bulletin. 2011; 59(2):196-201.

348. Chen Y, Shen Y, Guo X, Zhang C, Yang W, Ma M, et al. Transdermal protein delivery by a coadministered peptide identified via phage display. Nature Biotechnology. 2006; 24(4):455-460.

349. Desai P, Patlolla RR, Singh M. Interaction of nanoparticles and cell-penetrating peptides with skin for transdermal drug delivery. Molecular Membrane Biology. 2010; 27(7):247-259.

350. Martanto W, Davis SP, Holiday NR, Wang J, Gill HS, Prausnitz MR. Transdermal delivery of insulin using microneedles in vivo. Pharmaceutical Research. 2004; 21(6):947-952.

351. Sivamani RK, Stoeber B, Wu GC, Zhai H, Liepmann D, Maibach H. Clinical microneedle injection of methyl nicotinate:stratum corneum penetration. Skin Research and Technology. 2005; 11:152 - 156.

352. Ralston E, De Coen JL, Walter R. Tertiary structure of H-Pro-Leu-Gly-NH2, the factor that inhibits release of melanocyte stimulating hormone, derived by conformational energy calculations. Proceedings of the National Academy of Sciences of the United States of America. 1974; 71(4):1142-1144.

353. Lee JH, Lim SK, Huh SH, Lee D, Lee W. Solution structures of the melanocyte-stimulating hormones by two-dimensional NMR spectroscopy and dynamical simulated-annealing calculations. European Journal of Biochemistry. 1998; 257(1):31-40.

354. Sasidhar YU, Dhingra MM, Saran A. Conformational preference of Leu side chain in melanostatin in DMSO. Indian Journal of Biochemistry and Biophysics. 1990; 27(2):69-75.

355. Shapiro I, Gorbatiuk VI, Kabanov VM, Mazurov AA, Andronati SA, Lobasiuk BA, et al. [Conformational properties of biologically active melanostatin analogs]. Bioorganicheskaĭa khimiĭa. 1990; 16(12):1607-1617.

356. Voronina TA, Markina NV, Kalinina TS, Kabanov VM, Mazurov AA, Andronati SA. Anti-amnestic and antidepressant activity of melanostatin analogs. Pharmaceutical Chemistry Journal. 1992; 26(9):753-756.

357. Val'dman AV, Kozlovskaya MM, Klusha VE, Svirskis SV. The psychopharmacological spectrum of melanostatin. Bulletin of Experimental Biology and Medicine. 1980; 89(6):780-783.

358. Valle G, Crisma M, Toniolo C, Yu KL, Johnson RL. Crystal-state structural analysis of two gamma-lactam-restricted analogs of Pro-Leu-Gly-NH_2. International Journal of Peptide & Protein Research. 1989; 33(3):181-190.

359. Bjrkman S, Castensson S, Sievertsson H. Tripeptide analogues of melanocyte-stimulating hormone release-inhibiting hormone (Pro-Leu-Gly-NH2) as inhibitors of oxotremorine-induced tremor. Journal of Medicinal Chemistry. 1979; 22(8):931-935.

360. Hennemann J, Schatton W, Lyssy RH. Parkinsonism Treatment. In: Ullmann's Encyclopedia of Industrial Chemistry: Wiley-VCH Verlag GmbH & Co. KGaA; 2000.

361. Ripka JFJ, FL), inventor; Bio-Logic Research and Development Corporation (Jacksonville, FL), assignee. Compositions for enhancing immune function. United States. 1999.

362. Fields K, Falla TJ, Rodan K, Bush L. Bioactive peptides: signaling the future. Journal of Cosmetic Dermatology. 2009; 8:8-13.

363. Ortonne J-P, Bissett DL. Latest insights into skin hyperpigmentation. Journal of Investigative Dermatology Symposium. 2007; 13(1):10-14.

364. Dutta RC, Puri A, Anand N. Immunomodulatory potential of hydrophobic analogs of Rigin and their role in providing protection against Plasmodium berghei infection in mice. International Immunopharmacology. 2001; 1(5):843-855.

365. Najjar VA. Preface. Molecular and Cellular Biochemistry. 1983; 53-54(1):7-7.

366. Siemion IZ, Kluczyk A. Tuftsin: On the 30-year anniversary of Victor Najjar’s discovery. Peptides. 1999; 20(5):645-674.

367. Nishioka K, Babcock GF, Phillips JH, Banks RA, Amoscato AA. In Vivo and in Vitro antitumor activities of tuftsin. Annals of the New York Academy of Sciences. 1983; 419(1):234-241.

368. Corazza GR, Ginaldi L, Profeta V, Quaglino D, Zoli G, Gasbarrini G, et al. Tuftsin deficiency in AIDS. The Lancet. 1991; 337(8732):12-13.

369. Ashish, Grover A, Kishore R. Characterization of a novel type VII β-turn conformation for a bio-active tetrapeptide rigin. European Journal of Biochemistry. 2000; 267(5):1455-1463.

370. Martinez J, Winternitz F. New synthetic and natural tuftsin-related compounds and evaluation of their phagocytosis-stimulating activity. Annals of the New York Academy of Sciences. 1983; 419(1):23-34.

371. MTS Clinical Resolution Laboratory I. In: MTS Anti-Aging Complex™. 2011

372. Osborne R, inventor; Personal care compositions. US patent 20070020220. 2006.

373. Fu JJJ, Hillebrand GG, Raleigh P, Li J, Marmor MJ, Bertucci V, et al. A randomized, controlled comparative study of the wrinkle reduction benefits of a cosmetic niacinamide/peptide/retinyl propionate product regimen vs. a prescription 0.02% tretinoin product regimen. British Journal of Dermatology. 2010; 162(3):647-654.

374. Kaczvinsky J, Griffiths CEM, Schnicker M, Li J. Efficacy of anti-aging products for periorbital wrinkles as measured by 3-D imaging. Journal of Cosmetic Dermatology. 2009; 8(3):228-233.

375. Abu Samah NH, Heard CM. Topically applied KTTKS: a review. International Journal of Cosmetic Science. 2011; 33(6):483-490.

376. Bergstrom K. Beyond tretinoin: cosmeceuticals for aging skin. Journal of Drugs in Dermatology. 2009; 8(7):674-677.

377. Reszko A, Berson D, Lupo M. Cosmeceuticals: practical applications. Dermatologic clinics. 2009; 27(4):401-416.

378. Gorouhi F, Maibach HI. Role of topical peptides in preventing or treating aged skin. International Journal of Cosmetic Science. 2009; 31(5):327-345.

379. Bariya SH, Gohel MC, Mehta TA, Sharma OP. Microneedles: an emerging transdermal drug delivery system. Journal of Pharmacy and Pharmacology. 2012; 64(1):11-29.

380. Alvarez-Román R, Naik A, Kalia YN, Fessi H, Guy RH. Visualization of skin penetration using confocal laser scanning microscopy. European Journal of Pharmaceutics and Biopharmaceutics. 2004; 58(2):301-316.

381. Krishnan G, Edwards J, Chen Y, Benson HAE. Magnetic enhanced delivery creates transient epidermal pores. Perth: OBJ Ltd; 2010. Available from: http://www.obj.com.au/wp-content/uploads/Epidermal-Pore-Formation-by-Magnetic-Fields.pdf.

382. Mitragotri S. Synergistic effect of enhancers for transdermal drug delivery. Pharmaceutical Research. 2000; 17(11):1354-1359.

383. Vemulapalli V, Yang Y, Friden PM, Banga AK. Synergistic effect of iontophoresis and soluble microneedles for transdermal delivery of methotrexate. Journal of Pharmacy and Pharmacology. 2008; 60(1):27-33.

384. Garland MJ, Caffarel–Salvador E, Migalska K, Woolfson AD, Donnelly RF. Dissolving polymeric microneedle arrays for electrically assisted transdermal drug delivery. Journal of Controlled Release. 2012; (1).

385. Wermeling DP, Banks SL, Hudson DA, Gill HS, Gupta J, Prausnitz MR, et al. Microneedles permit transdermal delivery of a skin-impermeant medication to humans. Proceedings of the National Academy of Sciences. 2008; 105(6):2058-2063.

386. Priyadarsini KI. Photophysics, photochemistry and photobiology of curcumin: Studies from organic solutions, bio-mimetics and living cells. Journal of Photochemistry and Photobiology C: Photochemistry Reviews. 2009; 10(2):81-95.

387. Schantz EJ, Lauffer MA. Diffusion measurements in agar gel. Biochemistry. 1962; 1(4):658-663.

388. Lauffer MA. Theory of diffusion in gels. Biophysical Journal. 1961; 1(3):205-213.

389. Labouta H, Liu D, Lin L, Butler M, Grice J, Raphael A, et al. Gold nanoparticle penetration and reduced metabolism in human skin by toluene. Pharmaceutical Research. 2011; 28(11):2931-2944.

390. Lin L, Grice J, Butler M, Zvyagin A, Becker W, Robertson T, et al. Time-correlated single photon counting for simultaneous monitoring of zinc oxide nanoparticles and NAD(P)H in intact and barrier-disrupted volunteer skin. Pharmaceutical Research. 2011; 28(11):2920-2930.

391. Yow HN, Wu X, Routh AF, Guy RH. Dye diffusion from microcapsules with different shell thickness into mammalian skin. European Journal of Pharmaceutics and Biopharmaceutics. 2009; 72(1):62-68.

392. Moser K, Kriwet K, Naik A, Kalia YN, Guy RH. Passive skin penetration enhancement and its quantification in vitro. European Journal of Pharmaceutics and Biopharmaceutics. 2001; 52(2):103 - 112.

393. Chen L, Han L, Lian G. Recent advances in predicting skin permeability of hydrophilic solutes. Advanced Drug Delivery Reviews. 2012.

394. Smartplanet ACPw. Business / Smart Takes [In: 3M's new drug delivery system: disposable microneedles. 2011]

395. Kim Y-C, Park J-H, Prausnitz MR. Microneedles for drug and vaccine delivery. Advanced Drug Delivery Reviews. 2012.

396. van der Maaden K, Jiskoot W, Bouwstra J. Microneedle technologies for (trans)dermal drug and vaccine delivery. Journal of Controlled Release. 2012; 161(2):645-655.